SCHOOL OF CHEMICAL ENGINEERING

AND ADVANCED MATERIALS

Control of Detergent Properties in a Spray Dryer Process

Mark Jonathan Crosby

March 2017

Table of Contents

Abstract

This research details the building, implementation and validation of models designed for the control of specific powder detergent properties in a spray dryer process. Findings are reported in two sections; the control of moisture content, particle size distribution (PSD) and bulk density properties; the development of a process model for the online estimation and simulation of the process. The project was completed at Procter & Gamble's Newcastle Innovation Centre, using a mixed flow spray dryer for the case study.

Moisture content can be controlled using a soft sensor to enable estimation of this parameter at a higher sampling frequency than manual measurements of the powder. The proposed empirical model proved to be the most successful approach compared to heat and mass balances. Each model required adjustment of a parameter following the first manual measurement of moisture in a batch run.

Control of PSD can be achieved through analysis of droplet size distribution. The dominant influence on the final PSD is the atomization of the slurry, which can be manipulated through changes to the ratio of air and slurry flow to the nozzle. However, numerous sources of variability necessitate continuous amendments to the atomizing air flow rate to maintain the PSD at the required target value. The use of an automatic cascade loop control strategy facilitated manipulation of the air flow to the nozzle, improving control of PSD considerably, halving the response time and reducing variability of mean particle size.

Control of bulk density is dependent on an understanding of the key factors that determine the final density of the powder. The density model proposed incorporates statistics for the impact of packing, air entrapment and drying. The model details the limits of the rate of air injection into the slurry, its influence on density control and provides explanations for density changes during the process.

Separate studies demonstrate the influence of each property on process conditions in each compartment of the mixed flow spray dryer. A model linking these properties to the process conditions has been formulated to provide optimal control strategies for the process. The spray drier involves 3 compartments; a spray chamber, an inner fluid bed and an outer fluid bed. Computational fluid dynamics are used to estimate flow properties and residence times of the chamber and a CSTR model is used to model the fluid beds. The constant drying rate curve (CDRC) and reactor engineering approach (REA) drying models have been implemented and fitted using historical data. A sigmoidal model approach to the CDRC has been included to enable a smoother transition between the constant and falling rate periods. Simulation of the process and online estimations of the powder's properties were assessed. In each batch, the CDRC model provided the most accurate representation of the process. The CDRC model is recommended for control of the spray drying process and in simulation studies.

Acknowledgements

First of all, I would like to thank my industrial supervisor Luis Martin de Juan for his supervision and guidance throughout my engineering doctorate. He has been a vital component in producing this thesis and has been a superb mentor and friend.

A special thank you is reserved for my mother who helped review my thesis. There help was vital in producing the final draft of this thesis when academic support was lacking due to their other commitments and changes in role. Thank you so much for your help and support.

I am very grateful to Elaine Martin and Gary Montague for their academic supervision. Our correspondence throughout the degree has helped me further develop my ideas and schedule my work load. I am also grateful to Adam Harvey who provided support from the university after Gary and Elaine changed roles.

I thank all of the operators, especially Tony Meenaghan with which I produced all of the experimental data for my thesis. I would also like to thank the modelling team at Procter & Gamble along with the multiscale understanding centre.

At this point I would like to thank the EPSRC for their funding of this project. I would also like to thank Procter & Gamble for their support and belief in me. They have dedicated a lot of time and resources to ensure the completion of this thesis.

I sincerely thank my friends and family for their love, encouragement and support. This would have never been possible without them and I could not ask for anything more.

Nomenclature

A, B, C, a, b, n	Constants
A	Surface Area (m^2)
Ar	Archimedes number
C_p	Specific heat (*J/kg K*)
D_v	Vapour diffusion coefficient (m^2/s)
d_L	Diameter of liquid nozzle tip(*mm*)
d_p	Particle diameter(*μm*)
D	Diameter (*m*)
D_{eff}	Effective Diffusion coefficient (m^2/s)
$D_{3,2}$	Sauter mean diameter (*μm*)
$D_{V,10}$	10th percentile volume diameter (*μm*)
$D_{V,50}$	Median diameter(*μm*)
$D_{V,90}$	90th percentile volume diameter (*μm*)
e	Efficiency of air entrainment
E_v	Activation energy(*J/mol*)
F(s)	Laplace Process function
f	Relative drying rate fraction
H_A	Specific Humidity of the Air (*kg of water/kg of air*)

H_{BED}	Heiglt of Fluid bed
h_C	Heat transfer coefficient (W/m^2K)
k_g	Mass transfer coefficient (m/s)
K_D	Thermal conductivity ($W/m\ K$)
K_V	Apparent reaction frequency (kg/m^3)
m	Mass (kg)
N	Drying rate (kg/s)
N_P	Pump Speed (rpm)
Nu	Nusselt number
Oh	Ohnesorge number
p	Partial pressure (Pa)
P	Pressure (Bar)
Pr	Prandlt number
Q	Volumetric flow rate (m^3/s)
r	Radius (m)
Re	Reynolds number
R_{CDF}	Rosin-Rammler cumulative distribution function
Sc	Schmidt number
Sh	Sherwood number

SPAN	Span of Distribution
T	Temperature (K)
t	Time (s)
V_p	Relative velocity (m/s)
We	Weber number
X	Moisture content ($\%$)
μ	Viscosity($kg.s/m^2$)
ρ	Density(kg/m^3)
$P_{v,s}$	Vapour concentration at the surface
$P_{v,sat}$	Vapour concentration at saturation
$\rho_{v,\infty}$	Bulk vapour concentration
σ	Surface tension(N/m)
λ	Latent heat of vaporization (J/kg)
ψ	Relative humidity ($\%$)
ϕ	Characteristic moisture content
τ	Residence time (s)
Θ	Plug flow residence time (s)
Φ_s	Sphericity coefficient

Subscripts

A	Air
$Chamber$	Drying Chamber
Cr	Critical
d	Dry material
dev	Deviation in Variable
emp	Empirical
eq	Equilibrium
f	fraction
G	Gas
i	Stream number or initial
IFB	Inner fluid bed
L	Liquid
$Manual$	Manual Input of parameter
mf	Minimum Fluidization
$Online$	Online measurement of parameter
OFB	Outer fluid bed
ref	Reference Temperature

S	Saturation
$Solids$	Solid content
T	Total
W	Water
WB	Wet Bulb

Acronyms

CDRC	Characteristic Drying Rate Curve
CFD	Computational Fluid Dynamics
CSTR	Continuously Stirred Tank Reactor
MPS	Mean Particle Size
P & G	Procter & Gamble
PFR	Plug Flow Reactor
PID	Proportion, Intergral, Derivative
PLC	Programmable Logic Controller
PSD	Particle Size Distribution
R & D	Research and Development
REA	Reactor Engineering Approach
RMSE	Root Mean Squared Error
SIG	Sigmoidal model approach
SMD	Sauter Mean Diameter
SMM	Slurry Mixed Moisture Content

Related Publications

Crosby, M.J. et al., 2015. Particle size control of detergents in mixed flow spray dryers. *The Journal of Engineering*, pp.1–6. Available at: http://digital-library.theiet.org/content/journals/10.1049/joe.2014.0250.

1. INTRODUCTION

1 Spray Drying

Spray drying is a process used to produce a dry powdered product, such as a detergent, from a liquid feed. The liquid feed is introduced into a spray dryer via an atomization device to produce a spray of droplets. These droplets are then dried by a hot air stream entering the spray dryer concurrently or counter currently to the spray direction. Spray dryers can vary in size and shape depending on the application, atomization device and air flow direction. There are numerous applications for spray dryers, as powders are commonly manufactured for use in the detergent, food, pharmaceutical, and many other industries.

2 Background

Procter & Gamble (P&G) utilise spray dryers to produce detergent powder. The dry laundry business is steadily increasing in volume, mainly in developing markets where capacity is set to double in the next 10 years. There is an ongoing need to develop smarter ways to increase plant capacity via optimization of current operations. This objective may be achieved by reducing:

- Reblend streams of out of specification and start up products
- Product reliability losses due to out of specification products
- Time taken to reach target specification between batches

At the same time, formulations of detergents are evolving towards narrower processing windows, increasing the final product's sensitivity to changes in the properties of intermediate products produced in the spray dryer known as blown powder. Accordingly, an improved control of the properties of the powder will have an impact on some of the reliability issues that occur with higher frequency in the traditional process, such as over-packing, segregation and emissions. From the 52 current recognized outputs from the spray drying process, moisture

content, bulk density and the particle size distribution (PSD) of the blown powder have been identified as the most critical properties to influence the opportunities highlighted.

2.1 Objectives

The objectives of this project are to produce a process control strategy that will:

1. Reduce the transient time during the start up of a batch

2. Improve the control of the chosen output variables during steady state

2.2 Scope of project

P&G has many manufacturing production units around the world, with significant differences between sites. Ideally, the control strategy established will be leveraged globally and developed in small scale production facilities. Therefore, the strategy will need to have a model based approach using theoretical drying models or scale up parameters tested and developed using the pilot plant capability at their Research and Development site in Newcastle.

The pilot plant facilities will be used to increase understanding of:

1. The best current approaches.
2. Input variables and sources of variability for the three main outputs
3. Available measurement techniques for the input and output variables.
4. The impact of changing formulation

A small scale mixed flow spray dryer can be utilized to develop and test the process control strategies produced to meet the objectives of the project.

3 Control of Spray dryers

Control Systems are used throughout industry to improve processes. They are implemented to ensure safe production using alarms and trips, and to optimize the process by ensuring consistent product quality, and reducing costs by increasing yield and maximising product throughput. This creates energy savings and provides a better environmental performance.

In most spray drying processes, numerous simple automatic control strategies are used to enable the manipulation of flow and temperature of the feeds, and mechanical devices such as agitators in mixers. The spray dryer process has a number of feeds, valves and heaters, all of which are controlled using a Programmable Logic Controller (PLC). The PLC provides access to the measurements of all of the input and output variables in the process on one platform. This enables control strategies to be easily implemented into the process.

Although the process is a highly automated system, the control strategy employed during production of the powder is usually carried out manually by an operator. This is because the drying process is, in principle, an inherently self-regulating process; this means that if the operator chooses a set of conditions and there are no fluctuations in the inputs, the outputs should remain the same (Jumah et al. 2014). There has been very little advancement in control methods to replace or aid the operator since the implementation of basic single input, single output feedback and feed-forward control strategies. These strategies include the control of exhaust air temperature or humidity by manipulating the slurry flow or air temperature (Masters 1991). Generally, these strategies have changed little in the last few decades, with recent general publications in drying stating it is one of the least studied areas of process control (Jumah et al. 2014). A number of reasons for lack of progress in control strategies are listed below:

1) Spray drying can be a batch process with frequent product changes

2) Difficulty in measuring and maintaining the properties of the liquid feed

3) Lack of accurate fast sampling methods for moisture content and particle size

4) Properties of the powder are interlinked and difficult to decouple

5) The process is highly complex

6) Processing problems such as blocked nozzles, wearing nozzles affecting atomization, leakage and heat losses from the equipment

7) Lack of standardized design for spray dryers

The control strategy proposed in this project provides solutions to these problems. Advanced empirical process control techniques that fit numerous parameters with extensive training and validation sets have not been taken into account due to the need for a global strategy that can be applied to the various spray dryer processes. With different products being produced in tighter operating windows, it is important to develop an understanding of the process. The use of mechanistic models based on drying theory will enable a sensitivity analysis of the process, and would be adaptable for different dryers. Because of this, this project has concentrated on producing a viable mechanistic model to be used to develop a control strategy.

4   Structure of Thesis

Over the course of this research, multiple projects have been carried out on P&G's small scale mixed flow spray dryer and pilot rig facilities. The structure of this thesis is split into four sections:

- Literature & Materials(Chapters 1-2)

- The influence of the process on the powder properties (Chapters 3-5)

- Development of the process model (Chapters 6-7)

- Conclusions & References(Chapters 8 & 9)

4.1 Literature & Materials

This section contains an overview of the spray drying process followed by a review of the modelling techniques used to describe it. Following this, the materials and methods used during this project have been described, and the limitations of the spray dryer process have been analysed. In some cases the impact of these limitations has been minimized and in others they have helped develop further understanding of the process.

4.2 The influence of the process on the powder properties

Three individual projects were carried out to develop further understanding about the powder's moisture content, PSD and bulk density. The project on moisture content developed a soft sensor to estimate the moisture changes in response to manipulation of process variables. For the powders PSD, efforts were made to understand how the particle develops in the process. This included analysis of the spray entering the process and the development of a control strategy to reach the target specification quicker with less variability. The project on bulk density developed a model that related the drying process to the measurement of the bulk density. The model produced estimated the impact of input variables on the density of the particles, expressing limitations for the methods used.

4.3 Development of the process model

In this section, the findings from each project are combined in order to build a drying model for the process. It describes the method used to compartmentalise the mixed flow spray dryer and estimates its influence on the drying process. Using historical data, drying models were fitted for multiple formulations. The models were then used to simulate the process and assess their viability for use in a model based control strategy.

4.4 Conclusions & References

In this final section, the concluding remarks are made about the projects carried out and the list of references for the thesis are provided.

2. LITERATURE REVIEW

1 Introduction

This chapter presents an overview of studies on detergent production, spray drying and modelling approaches available in the literature. In the review of the literature that focuses on the modelling of the spray dryer process, it is important that the model produced captures enough dynamics to represent the process, but at the same time is not computationally expensive. The suitability of each modelling approach for a global strategy is discussed.

2 Detergent Production

Synthetic Detergents are and have been widely used in the domestic cleaning industry since their advent in the 1930's. Those with coarse powder granules provide an ideal mix of properties as they are free flowing, large enough to be non-dusty and small enough to readily dissolve in water (Masters 1991). These product properties, along with their long shelf life and stability, have led to increased demand and modern day production levels of powder detergents at Procter & Gamble (P&G) are in excess of 5 million tons a year. The company's range of detergent products includes brands such as Ariel, Tide, Daz, Bold, Ace and Bonux. While such detergents provide solutions for a variety of consumer needs, they each have different product characteristics. To address the demand for production, the bulk of these powders are produced in industrial scale spray dryers. Three key characteristics of these "blown powders" (Huntington 2004), which are beneficial to control during the manufacturing process are:

1) Bulk Density

2) Particle Size Distribution

3) Moisture Content

2.1 Bulk Density

Use of a chosen detergent by domestic consumers usually involves the filling a cup of known volume, and pouring this measured dose into a washing machine. Because commercial packaging of detergent in boxes is usually based on volume fill rather than weight fill, powder bulk density, when producing a batch of detergent, is a very important factor. Control of powder density ensures that processing of each batch of product is optimized to produce an ideal amount of the shelved product for sale. The most commonly used method for control of the density of the finished product, is manipulation of the "blown powder" density. This blown powder which is produced by the spray dryer, has a major influence on the final product characteristics, ranging from 40% to 99% of the finished product (Huntington 2004). The bulk density of the blown powder ranges from approximately 300-550 g/l. This density is reliant on the initial density of the slurry mixture supplied to the dryer, and the drying conditions. The density of the slurry depends on the composition of the detergent formulation and ranges from 1300-1700 g/l. The slurry density can be modified by altering the level of aeration in the slurry (Huntington 2004). Depending on the scale of production, this modification can be carried out by dissolving air into the slurry or injecting it into the slurry stream. The drying conditions are responsible for the evolution of the particles and their morphology. They have an impact on the shrinkage behaviour of the atomized droplets and on the development of internal pores in the particles (Koç et al. 2008). Any changes to the volume and structure of the particles leads to variations in the density of the particles which will impact the bulk product density measured. The association of the particle density with internal porosity, is another important reason for the control of bulk density. When porosity is increased, the particles dissolve more easily, so controlling density leads to control over the dissolution rate of a detergent powder.

2.2 Particle Size Distribution

The particle size of a powder affects the look and feel of that product which directly influences the consumer's perception and determines its performance as a detergent. When a product is utilised by a consumer, it is required to meet a desired design performance in terms of dissolution (Huntington 2004), and this factor is critically dependent on particle size. For a given volume, as particle size is reduced the surface area which drives the rate of dissolution rate increases significantly. Also if the particles produced are too coarse, they may look and feel rough to the consumer, and if they are too fine they can create a dusty product. The dustiness can also impacts the sealing process for the cartons or bags in which the powder is stored. During production, the out of specification particles are re-blended into the process to reduce wastage. Ideally the amount of coarse particles, known in production as "overs" ($>1000\mu m$), and the amount of fine particles, known as "fines" ($<50\mu m$), should be minimized to reduce further processing and therefore reduce cost. Producing these out of specification particles leads to extended production times, resulting in over production of the product. This leads to higher production costs for the detergent, as well as additional storage costs for the excess product produced.

2.3 Moisture

A spray dryer's main purpose is to dry the product by removing moisture. A target moisture content is established to achieve a free-flowing product, which hasn't been discoloured by over-drying, and has an acceptable level of insoluble material. The amount of water removed also influences the stability of the product. This is very important in different parts of the world where external conditions differ in their temperature and humidity, as moisture can cause the product to degrade or cake. Control of the moisture content is also used to provide an economical and environmental benefit in production, by reducing the amount of over drying.

By optimizing the air flow and temperature, less of the product will be out of specification, ensuring stability whilst using less energy, saving time and money.

Other powder properties, such as colour and chemical composition could also be taken into account. These have been detailed in the literature (Huntington 2004). However, the measurement and manipulation of these properties can prove to be very difficult. As these properties are often interlinked with the bulk density, particle size distribution and moisture content which is why they were chosen for production control in the scope of this research project.

3   Spray Drying

Spray drying is an integral part of the family of suspended particle processing (SPP) systems, along with fluid-bed dryers and other spray-based processes (Masters 1991). This is because a spray dryer produces droplets from a fluid state, which are dried into individual particles by a hot gas medium, usually heated air. Spray dryers can be combined with other SPP systems to enable customer requirements to be met. An example of this is the mixed flow spray dryer, which combines a co-current spray dryer chamber and a fluid bed. This set up is utilised by P&G for small scale production in their research & development facilities. This equipment was used for the bulk of the research carried out in this thesis.

There are numerous advantages to the use of spray drying in the production of powder products, these have led to its widespread use in the drying industry, and include:

1) Accepts a pumpable fluid as a feed, and discharges a dry particulate
2) Enables the adjustment of particle size and moisture content to a specific range irrespective of dryer capacity and product heat sensitivity
3) Once running under a set of conditions the powder quality remains roughly consistent

4) Operation permits high-tonnage production, which can be continuous and adapted to full automatic control with quick response times

5) As the operating range of temperatures can vary from 150 to 600^{0}C, the efficiency is comparable to other types of direct dryers

The disadvantages associated with spray drying are as follows:

1) Spray drying fails if a high bulk density product is required

2) The feed must be pumpable

3) In general, spray towers are inflexible. A tower designed for fines production may not be able to produce coarse product and vice versa

4) For a given product, larger evaporation rates are generally needed when compared to other types of dryer

5) A high initial investment is required compared to other dryers

6) Product recovery and dust collection increase the cost of drying

3.1 Principles of Spray drying

Spray drying consists of three fundamental processes: liquid atomization, gas-droplet mixing and the drying of liquid droplets (Genskow 2008). A fluid is supplied to an atomization device which produces a spray of droplets. The spray is then mixed with a surrounding hot gas medium, and moisture is removed from the spray of droplets until they are separated from the surrounding medium at the exit of the dryer. These three processes are described below.

3.1.1 Liquid Atomization

Liquid Atomization is a chemical engineering unit operation, which disintegrates a continuous liquid into a dispersed system of drops within a spray (Mulhem et al. 2004). This is the most important operation in the spray drying process, as it determines the size distribution of the droplets and their trajectory and speed, all factors on which the final particle size depends

(Filkova et al. 2014). The characterization of the atomizer equipment is based on the droplet size distribution, droplet size/velocity correlation, local and overall concentration and mass flux distribution. The design of the atomizers, fluid properties and mass flow rates, influence the characteristics of the spray produced. Manipulation of these characteristics is handled by varying the energy input to the atomizer. However, varying the energy input may affect the throughput of the process, depending on the atomization device used. Once the equipment is chosen it cannot be altered during operation, thus highlighting the importance of choosing the correct setup before production. Control of liquid slurries properties is vital to prevent any changes in the spray produced. At P&G, the industrial production scale utilises hollow cone pressure nozzles to meet the high capacity demands. For the small scale production, where low capacity is desired, the alternative two fluid nozzle type is used. Figure 1 depicts the atomization of a liquid from these two types of nozzle.

Figure 1.1: Atomization via Pressure Nozzle   **Figure 1.2:Atomization via two fluid nozzle**
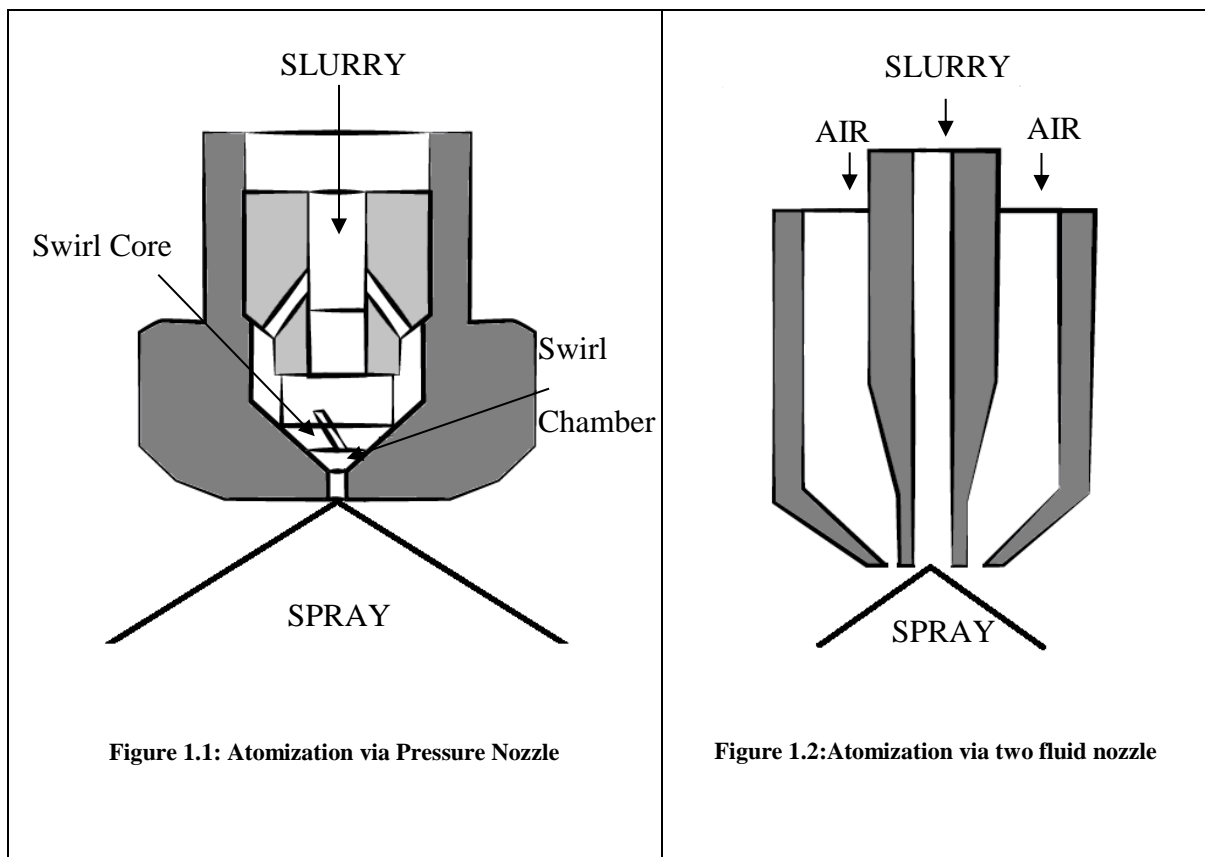
In Figure 1.1, the type of pressure nozzle that is fitted, affects atomization through its generation of a high degree of spin in the swirl chamber, prior to forcing the high pressure liquid through a small orifice to produce the spray (Genskow 2008). This produces a hollow cone spray of droplets leaving the orifice, that in turn produces a range of droplet and particle sizes of 10-800μm (Filkova et al. 2014). Once the nozzle orifice and chamber size are set, the spray characteristics become dependent on the pressure applied. At production scale, maintaining capacity is a priority so it is more effective to change the orifice size to produce the desired spray properties, however, this can't be achieved while the operation is in progress, so it is important to choose the correct set up beforehand. The energy consumption for pressure nozzles is low, especially when compared to that for two fluid nozzles. If large increases in capacity are needed, more than one nozzle is usually used in a ring arrangement inside the spray dryer chamber.

Two fluid nozzles use a compressed air stream to atomize the fluid. This can be done by internally mixing the air in a small chamber before leaving the nozzle, or by externally mixing at the tip of the nozzle. Figure 1.2 depicts an external set up where the slurry nozzle tip is outside of the air chamber. Nozzles of this type typically produce a full cone spray of droplet and particle size ranges between 5-300μm (Filkova et al. 2014). Use of a separate flow for atomization, provides extra flexibility for this type of nozzle, allowing it to produce either small or large droplets. The nozzle tip can be changed to increase capacity and the range of droplets produced.

The formation of the spray produced by a nozzle has become a controversial subject(Masters 1991). A number of theories predominate, each receiving experimental support. This is because of the complexity of the atomization mechanism. The liquid break up can become irregular due to the non ideal liquid distribution in the liquid atomization. Once atomized, there is also interaction with the surrounding air, and between the individual droplets in the spray cloud produced. The theoretical mechanism used to predict the atomization process is based on work carried out on the instability of liquid jets (Strutt & Rayleigh 1878) and built upon to include the effects of air resistance (Weber 1931), and then the ratio of air resistance and viscous effects of the liquid (Ohnesorge 1936). These

Equation 1 provides such a prediction, validated by experimental data using water and sugar solution for the Sauter mean diameter, $D_{3,2}$ (Mulhem et al. 2004).

$$D_{3,2} = 0.21 d_L \cdot Oh^{0.622} \cdot We^{-0.4} \cdot \left(\frac{\dot{m}_L}{\dot{m}_A} \right)^{0.4} \qquad \textbf{Equation 1}$$

where

$$Oh = \frac{\mu_L}{\sqrt{\rho_L \sigma \, d_L}} = \frac{\sqrt{We}}{Re} \qquad \textbf{Equation 2}$$

$$We = \frac{\rho_g d_L V_P^2}{\sigma} \qquad \textbf{Equation 3}$$

where d_L is the nozzle tip diameter, μ_L is liquid viscosity, ρ_L is liquid density, σ is surface tension, ρ_g is gas density, m_L and m_A are the mass flows of liquid and air to the nozzle and V_P is the relative velocity. *Oh* represents the Ohnesorge number to demonstrate the effects of viscosity, and *We* is the Weber number that incorporates the aerodynamic effects on the spray formation.

The predictions produced relate the desired output, which in this case is the Sauter mean diameter, to the possible manipulated variables. The Liquid to air ratio $\left(\frac{\dot{m}_L}{\dot{m}_A} \right)$ differentiates this model to other atomization models used for different nozzle types. It is the ratio of the mass flow rate of liquid to the nozzle, compared to the air flow to the nozzle used for atomization. The recommended method of particle size control from the nozzle supplier involves the manipulation of this variable in order to produce the desired distribution (GEA 2013).

3.1.2 Gas-Droplet Mixing

Gas-droplet mixing in the spray dryer is mainly dependent on the type of spray dryer used. In the detergent industry, the production scale is carried out by counter current spray dryer towers. In these units the air flows in the opposite direction to the product flow, it exits at the top of the tower, whilst the powder is collected at the bottom. To maximise residence time in the tower, the air flow is generated in a swirl-like motion. The slurry can be introduced into the spray dryer at multiple heights in the tower. This increases the throughput of the unit and maximises the tower loading capacity. Changes in the nozzle height impacts the initial conditions the atomized droplets are subject to resulting in a change in powder properties. When running at multiple heights it is important to optimize the conditions in order to reach specification. As mentioned above, P & G use another type of spray dryer to produce smaller amounts of product for research and development purposes. This spray dryer is a mixed flow spray dryer which utilises a co-current air flow in the drying chamber, mixed with the counter current air flow entering from the bottom of the chamber after mixing in a fluid bed. Both of these dryer types are illustrated in Figure 2. In the mixed flow spray dryer (Figure 2.2), the spray produced with compressed air, enters with hot air at the top of the chamber, before meeting air exiting the fluid bed. All of the air exits through the top of the dryer chamber, creating a complex flow pattern inside the chamber. The powder eventually leaves the dryer via the fluid bed at the bottom of the dryer.

Figure 2.1: Counter current Spray Dryer

Figure 2.2: Mixed Flow Spray Dryer
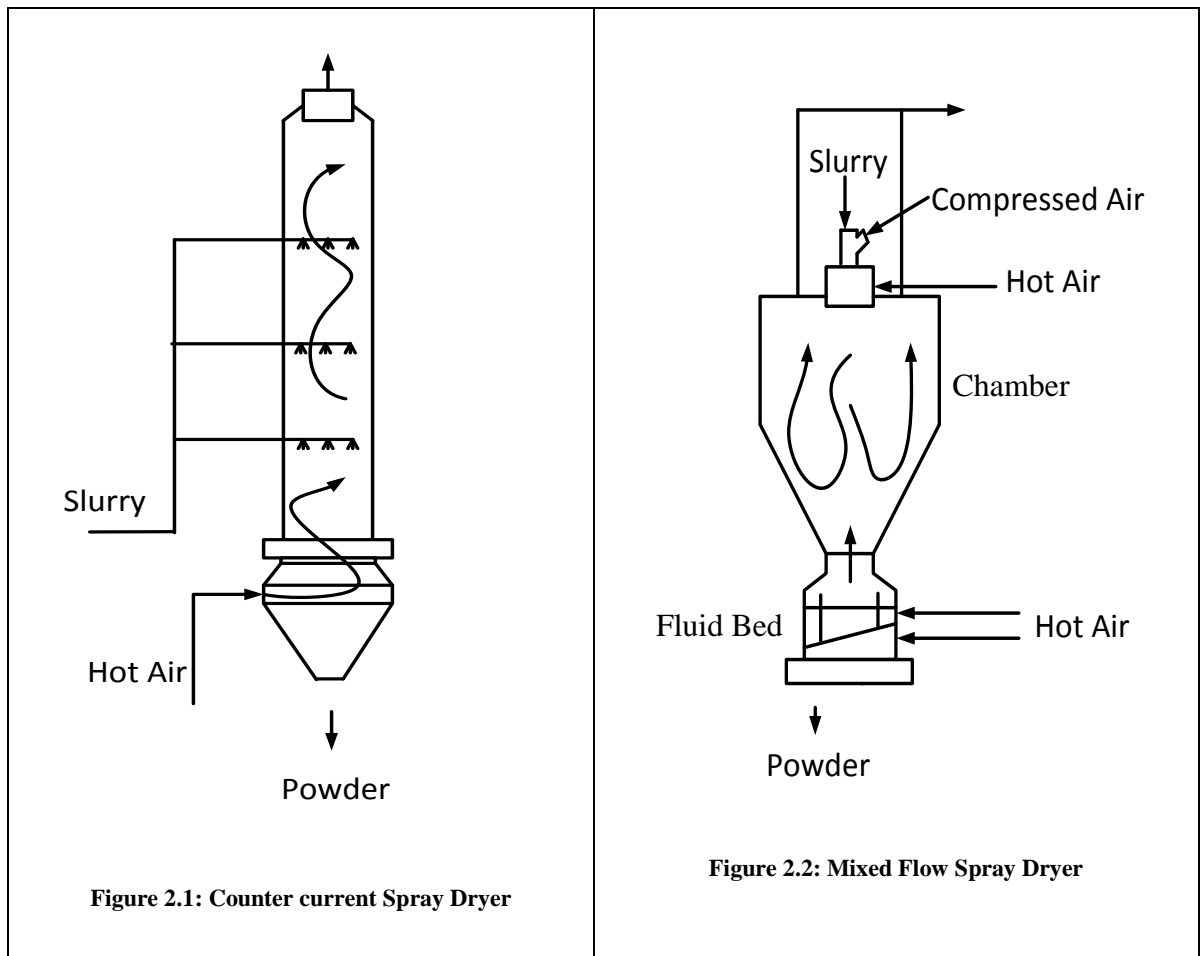
3.1.2.1 Fluidized beds

A fluid bed dryer is utilised in the mixed flow spray dryers, to ensure the target moisture content is achieved by increasing the residence time in the dryer. Fluid beds operate by bubbling gas through a distributor plate in order to circulate particles in a fluid like motion. At low gas velocities, the bed acts as a packed bed as the solids settle on the distributor plate (Chung & Mujumdar 2014). As the velocity is increased, the pressure drop across the bed increases, until the gas is able to support the weight of the whole bed. This point is known as incipient fluidization, where the pressure drop remains constant, and the particles behave as a fluid. This is depicted in Figure 3, where v_g is the gas velocity and Δp_b is the bed pressure drop. At the point of incipient fluidization additional pressure is required to dislodge intermeshed particles

before the pressure settles at a constant value. Eventually the particles are eluted over a weir inside the fluid bed.

Figure 3: Variation of Fluidized bed pressure drop with gas velocity
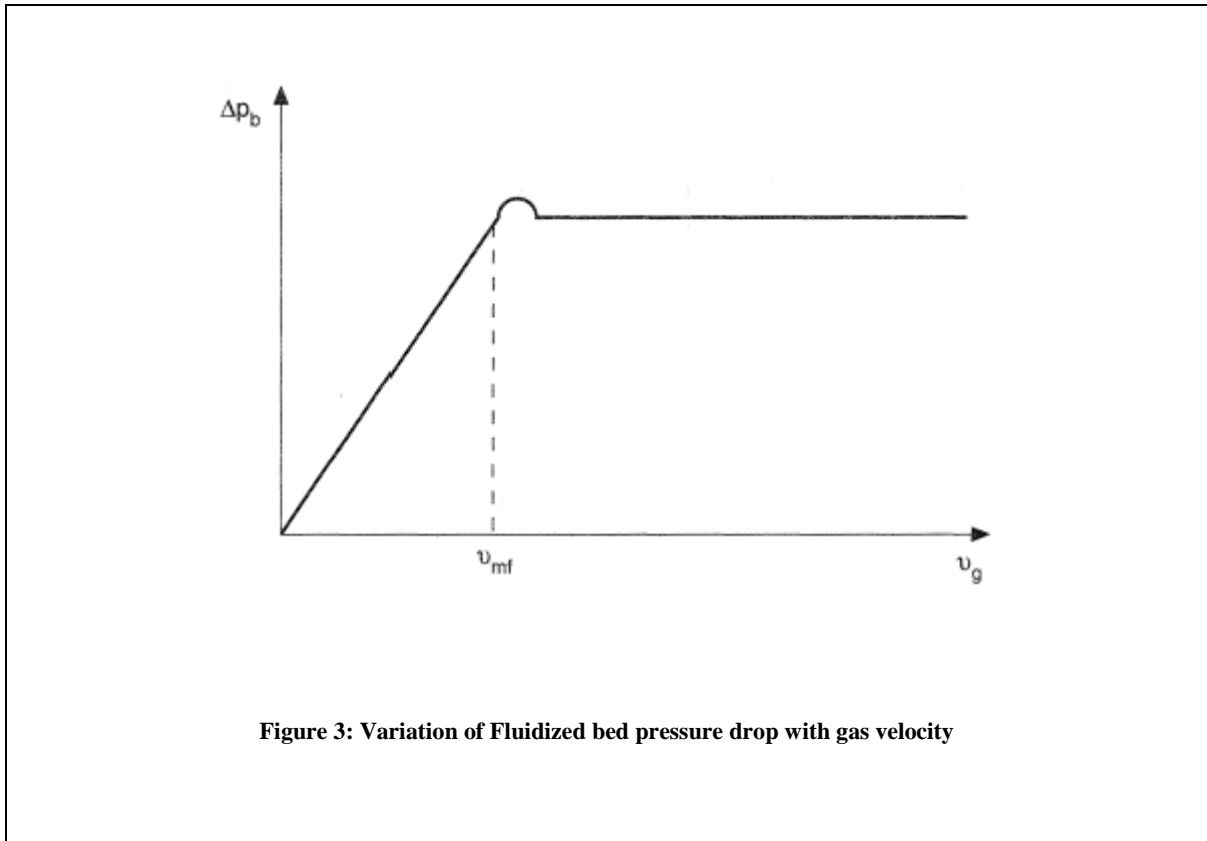
Fluidized bed dryers provide high mass and heat transfer rates, due to the high level of mixing. This high level of mixing also encourages more interaction between the particles which could lead to transformations that effect the particle size distribution such as agglomeration and attrition. Therefore, the drying conditions can differ considerably to those in the counter current tower which may lead to issues in the scalability of any control strategy derived from this unit.

3.1.3 Drying of Liquid Droplets

The drying of droplets is a complex process which involves simultaneous heat and mass transfer (Masters 1991). Contact between the atomized droplets and the heated air, transfers heat convectively to the droplets. This heat is then converted into latent heat during evaporation of the liquid from the droplets. The vapour produced by evaporation is transferred to the air

18

through a boundary layer, surrounding every droplet via diffusion. Along with heat and mass transfer, momentum is transferred between the air and droplets. The droplets are distributed in terms of size, shape and velocity, and mix with air at different velocities and temperatures throughout the spray dryer.

The rate of external heat and mass transfer is reliant on properties of the air and on properties of the droplet. For air, the temperature, humidity and transport properties are important. For the droplet, the rate is dependent on the diameter and relative velocity between the droplet and the air. To explain each property's significance, it is best to look at the rate equations for external heat and mass transfer. A dynamic equilibrium occurs when the rate of heat transfer to the surface via convection becomes equivalent to the rate of mass transfer away from the surface (Genskow et al. 2007). In this case it is assumed that water is freely available at the surface of the droplet. This produces Equation 4 which helps to illustrate the driving forces of drying.

$$k_g \lambda \left(p_s - p \right) = h_c \left(T - T_{WB} \right) \qquad \text{Equation 4}$$

where k_g is the mass transfer coefficient, λ is the latent heat of vaporization, p_s is the vapour pressure at the wet bulb temperature, p is the partial pressure of water vapour in the environment, h_C is the heat transfer coefficient, T is the temperature of the air and T_{WB} is the wet bulb temperature.

The mass and heat transfer coefficients are reliant on the air's transport properties, and the diameter and relative velocity of the droplets. These can be obtained using combinations of the dimensionless groups indicated in Table 1 (Masters 1991).

Table 1: Dimensionless groups

Group	Significance	Derivation
Reynolds (Re)	$\dfrac{\text{inertial force}}{\text{viscous force}}$	$\dfrac{DV_P \rho_g}{\mu_g}$
Prandlt (Pr)	$\dfrac{\text{kinematic diffusivity}}{\text{thermal diffusivity}}$	$\dfrac{C_p \mu_g}{K_D}$
Schmidt (Sc)	$\dfrac{\text{kinetic viscosity}}{\text{molecular diffusivity}}$	$\dfrac{\mu_g}{D_v \rho_g}$
Nusselt (Nu)	$\dfrac{\text{total heat transfer}}{\text{conductive heat transfer}}$	$\dfrac{h_c D}{K_D}$
Sherwood (Sh)	$\dfrac{\text{mass diffusivity}}{\text{molecular diffusivity}}$	$\dfrac{k_g D}{D_v}$

The Reynolds, Prandlt and Schmidt numbers are obtained using properties of the air, and a method to estimate the particle diameter and velocity. The most common method used to obtain the heat and mass transfer coefficients utilises an estimation of the value of the Nusselt and Sherwood numbers. For still air with no movement, the value of the Nusselt and Sherwood numbers is 2 (Masters 1991). For spray drying, where this assumption cannot be made, it is common to use the empirical Ranz-Marshall correlations expressed in Equation 5 and Equation 6. This is the most common method used, and can be found in numerous publications (Chen 2008,Mezhericher et al. 2008; Ranz et al. 1952, Seydel et al. 2006; Wai et al. 2008). This is also commonly used in fluid beds (Papadakis et al. 1993; Kiel et al. 1993), but there have been several extensive studies carried out to obtain numerous different correlations for these numbers, yielding very different results depending on the particle size and bed dimensions (Molerus & Mattmann 1992; Barker 1965; Balakrishnan & Pei 1979). The expected values of the heat transfer coefficients are used to ensure that the most appropriate method is used.

$$Nu = 2 + 0.6 \cdot \mathrm{Re}^{\frac{1}{2}} \cdot \mathrm{Pr}^{\frac{1}{3}}$$

Equation 5

$$Sh = 2 + 0.6 \cdot \mathrm{Re}^{\frac{1}{2}} \cdot Sc^{\frac{1}{3}}$$

Equation 6

As stated above, the heat and mass transfer rate is also reliant on temperature and humidity. The temperature determines the properties of the air. The difference between the bulk air temperature and wet bulb temperature also provides the main driving force for the heat transfer process in this scenario. The wet bulb temperature is the temperature at which the air would normally be saturated without any change in its heat content. It is therefore defined by the bulk temperature and the humidity of the air, as defined in Equation 7.

$$H_A = \frac{M_w}{M_A}\left(\frac{p}{P_T - p}\right)$$

Equation 7

where M_W is the molecular weight of water, M_A is the molecular weight of Air and P_T is the total pressure.

The difference between the humidity at saturation, and the humidity of the air, is the main driving force for mass transfer provided that equilibrium conditions have been established. Equilibrium assumes that the surface of the droplet is fully saturated and the water vapour is transferred from the droplet to the bulk air. This is true for pure water droplets but with detergent, the saturated vapour pressure becomes reduced due to the presence of solids on the surface.

As the drying process continues, the internal transfer rate of moisture to the surface fails to maintain a fully saturated surface of the droplet, so the limiting rate factors change. The process equilibrium can no longer be established, and the heat transfer is used to increase the

temperature of the droplets as water isn't transferred to the surface of the droplet quickly enough. This is best described with the aid of drying curves, as depicted in Figure 4. In each chart in Figure 4, the section AB represents the warming up period of the solids. When drying detergents, this can happen in a matter of milliseconds, as soon as the hot air makes contact with the droplet. In fact, the temperature of the slurry is usually higher than the wet bulb temperature, so the droplets cool down to the wet bulb temperature. Section BC represents the "constant rate period" in which the external heat and mass transfer equations described are most relevant. This is one of two stages historically used to describe drying (Lukasiewicz 1989, Scherer 1990). In this period, the moisture is removed at its maximum rate, whilst the dynamic equilibrium is held. The transport of moisture to the surface of the droplet, matches the rate of removal to the air. Point C is known as the "critical moisture content" (Scherer 1990). At this point, the surface is no longer fully saturated and the drying rate begins to fall. The "constant rate period" now changes to the second stage of drying, known as the "falling rate period" between points C and E. For the drying of detergent, the constant rate period normally only lasts a few seconds due to the slow diffusion rates in the droplets. During the falling rate period, internal moisture movement is the limiting factor that controls the drying rate. As the moisture levels decrease, it becomes harder to remove, and the drying rate drops. The temperature of the droplet during this period begins to increase until it reaches boiling point at point D. At this point, no moisture is available at the surface, and any remaining moisture is removed from inside the particles (Masters 1991). The moisture content of the solid at point E is the equilibrium moisture content. This is the moisture content at which equilibrium is formed with the surrounding air. This is dependent on the solids properties, and the temperature and humidity of the bulk air. To obtain low equilibrium moisture contents, high temperatures and low humidity's are needed in the dryer. This is more common in cocurrent spray towers, as the particles spend significantly more time with the drying air and exit together at the same

temperature. With counter current towers this is not the case, and equilibrium may not be achieved.

As previously mentioned, during the "falling rate period", the driving force of drying becomes reliant on the internal moisture movement, this complicates matters. The impact of internal mechanisms varies with formulation, solid structure and moisture content. The limiting factor is diffusion, which occurs for vapours and liquids inside the droplet. Liquid diffusion occurs as the moisture is transferred to the surface while the temperature of the droplet remains below boiling point. As the temperature increases past the boiling point, vapour diffusion not only occurs at the surface, but also inside the droplet, as the moisture vaporizes from within. The other common mechanism for moisture movement is via capillary action. Free moisture held in interstices of solids or in cell cavities, is transported to the surface due to intermolecular forces. This is heavily reliant on solid structure, as more porous structures may hold water between molecules. When controlled by capillarity, the shape of the falling rate curve may change as the drop off in rate is reduced.

The internal mechanisms are dependent on the solid structure and the location of moisture inside the droplet. Therefore it is important to look at how the droplet evolves during the drying process.
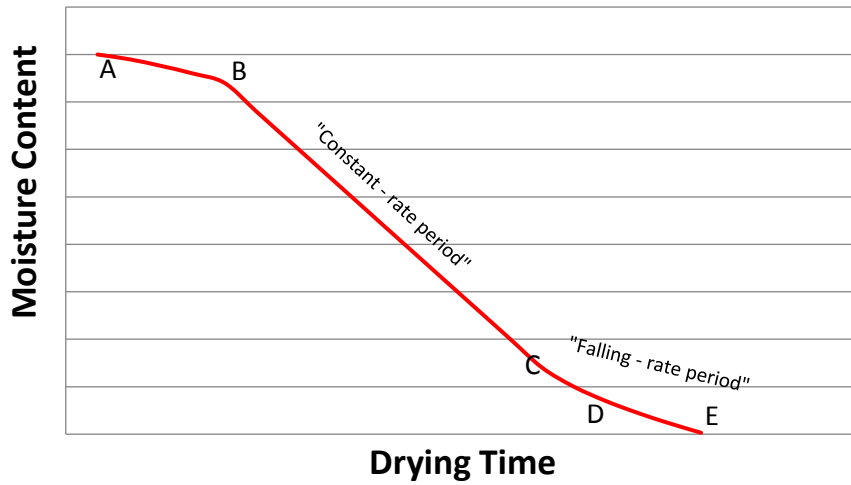
Figure 4.1: Change in moisture content during drying
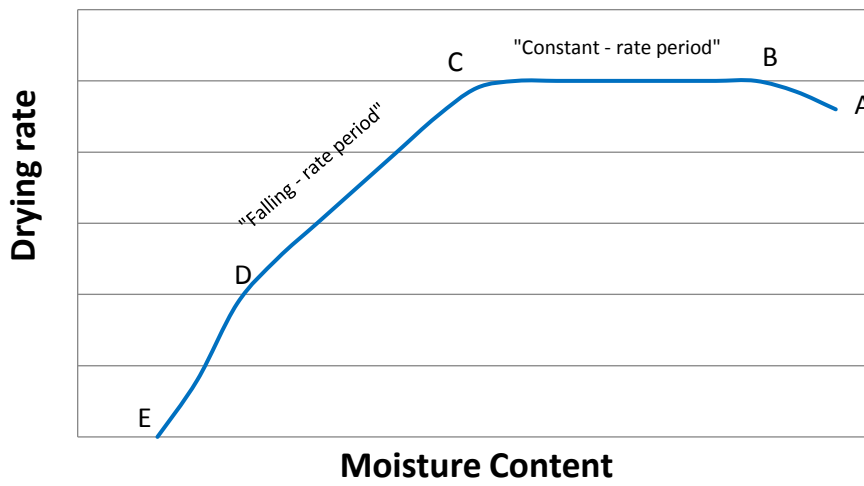
Figure 4.2: Change in drying rate as Moisture decreases
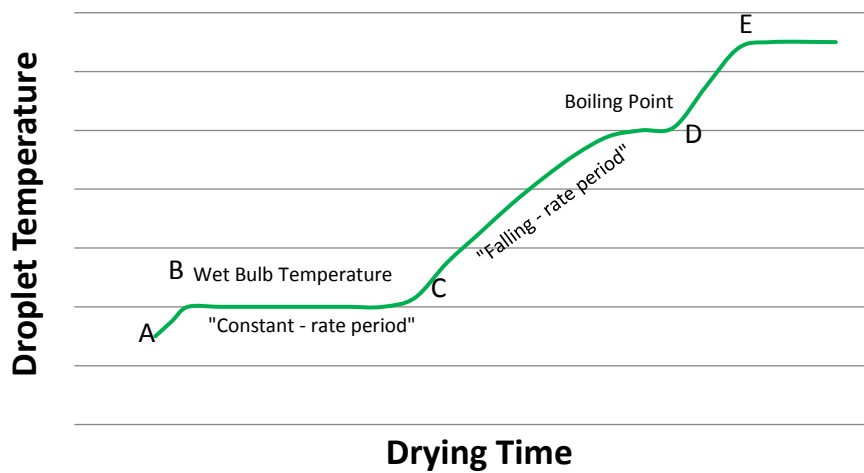
Figure 4.3: Change in droplet temperature during drying

Figure 5 depicts a simplified version of how a droplet develops during the drying process. Shrinkage is expected to occur during the constant rate period, as moisture is removed from the surface. As moisture is removed, the droplet reduces to the size of the final particle, and solid patches begin to appear. The point at which these solid patches appear is the critical moisture content. As moisture continues to be removed, a solid barrier is formed, hindering the moisture transported to the surface of the particle. This formation of a crust causes the temperature at the surface to rise until all free moisture is removed. Handscomb & Kraft (2010), provide a detailed model of the evolution of droplets following the formation of a crust (Charlesworth, 1960). There are a number of different routes this evolution can take, depending on the external conditions. One possibility is the occurrence of puffing. Puffing is caused by vapour expansion inside the particle, effectively enlarging the particle, and is similar to the way popcorn is produced. The effect of puffing has been seen with detergents from single droplet drying experiments (Huntington 2004). This not only changes the shape of the droplet but also change the porosity inside.

Figure 5: Evolution of Droplet to Particle
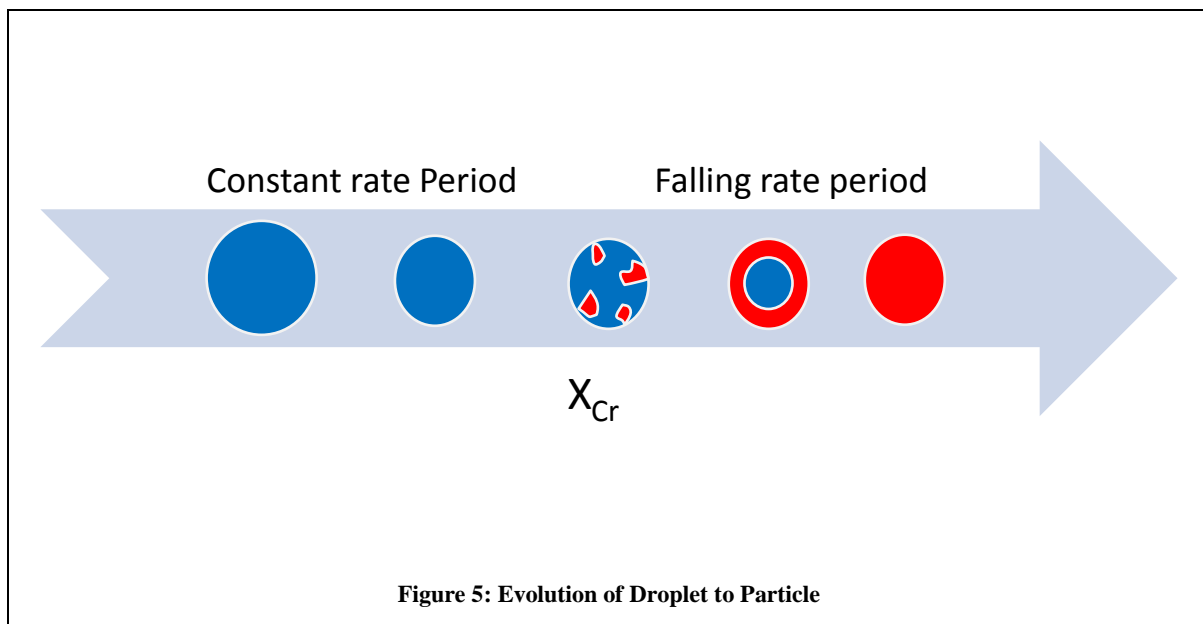
This particle evolution model was derived from analysis of single droplet drying experiments, where, as in reality, the particles are likely to interact with each other, impacting on this evolution. In order to reduce losses of fines in a spray dryer process, it is common practice to reintroduce these particles that exit with the air. This is very common in the food industry where agglomeration is promoted to improve flowability, and modify the particle structure (Gianfrancesco et al. 2008). The fines are reintroduced close to the spray, with the idea that collisions of wet, sticky droplets and the dry fines will promote agglomeration. Collisions may also lead to attrition, the breakup of particles. The possible transformations that can occur, impact on how complex the modelling of the process can be, giving rise to a number of different approaches to this problem.

4 Modelling of drying

Developing a mathematical model of a spray dryer is a difficult and complex task. The process involves a unique combination of particle formation and drying. To represent both the particle formation and the drying in the process, models are needed for the following (Oakley 2004):

- Formation of droplets during atomization

- Particle motion as it interacts with the air in the spray dryer

- Drying rates as the particle moves through the process

- Changes in morphology as the droplets dry and interact with each other

The level of complexity of each model will depend on the requirements of the process model. The models available in the literature for each point have been reviewed separately.

4.1 Formation of droplets

As described in section 3.1.1, the atomization determines the size distribution of the droplets/particles and their initial trajectory and speed (Filkova et al. 2014). This is the most

important stage in the spray dryer process. The complex transient nature of the transformation makes it difficult to model fundamentally and this has led to the application of empirical correlations, validated using experimental rigs (Mulhem, 2004). For two fluid nozzles, the correlations produced in the literature tend to be adaptations of the Nukiyama and Tanasawa equation (Nukiyama & Tanasawa 1939). This equation combines the effects of the Weber (Weber 1931) and Ohnesorge (Ohnesorge 1936) numbers described in section 3.1.1 in order to predict the Sauter mean diameter of the distribution. The equation was further developed from an extensive study into liquid atomization under a variety of physical conditions with subsonic air velocities (Bitron 1955). The liquids atomized included water, and mixtures of water, methanol, ethanol and glycerol. It was found that the equation tended to over predict the particle size produced (Atkinson & Strauss 1978; Canals et al. 1990) leading to numerous modifications that can be found in literature (Canals et al. 1990, Kocamustafaogullari et al. 1994; Semião 1996; Lipp 2000; Mulhem et al. 2004; Thybo et al. 2008). Reasons for the modifications to the original equation, include changes in geometry of the nozzle, changes in the measurement technique used for the particle size distribution, changes in the liquid to be atomized and changes to the operating ranges of the liquid and air feed rates.

When using empirical correlations, it is important to estimate the relative velocity of the air and the liquid being atomized. The average initial velocity of the droplets has been assumed to be the initial velocity of the liquid exiting the nozzle, this was found to be consistent with measurements (Fritsching 2006). Gauvin et al. 1975, found that the initial velocity of the droplets was close to that of the exiting air velocity, however, the particles had rapidly decelerated within a short distance, and the droplet size only ranged up to 44μm. The initial velocity of the air in the spray was taken as the velocity of the air exiting the nozzle. More detailed studies used a distribution function for these velocities when trying to map out the individual trajectories of particles in more detail (Kim et al. 2003).

Another important characteristic of the atomization, is the spray angle. The angle of the spray for two fluid nozzles from the centre of the nozzle can range up to 80^0 depending on the air pressure, liquid feed rate and geometry (Masters 1991). The impact of the geometry of the nozzle on the spray angle was carried out using high speed cameras (Shafaee et al. 2012). It was concluded that the angle is highly dependent on the geometric parameters of the nozzle. This led to the derivation of an empirical correlation, relating the diameters of the holes in which the liquid and air exited the nozzle, the size of the mixing chamber of the nozzle, and angle of the liquid port. The impact of the air and liquid feed rate were concluded to be significant only with low values for the Weber and Reynolds numbers.

Sazhin (2009), has provided a review of recent approaches to modelling sprays with computation fluid dynamics (CFD). In this publication, the break up models implemented struggle, as they assume single size droplets are created after the break up. The transient nature of the atomization also makes the simulation computationally expensive. It is common practice to set an initial velocity, spray angle and size distribution when carrying out CFD analysis. In these cases, the Rosin-Rammler expression is used to fit measurements of the droplet size distribution for different scenarios (Birchal et al. 2006; Wai et al. 2008). The Rosin-Rammler fittings have been used to represent droplet size distributions (Lefebvre 1988), and removes the need to model the formation of the spray.

The control requirements for PSD, are used to maintain the mean particle size of the distribution. The empirical correlations provide a simple relationship between the manipulated air and liquid feeds, and the characteristic diameters of the distribution. For control purposes of the PSD this would suffice, but it is important to ensure the most suitable correlation is used. Due to the variety of correlations available in literature, the PSD measurements from the spray dryer should be used to determine the most appropriate method. In order to use a drying model, it is important to understand the particle journey through the process. The ideal model should

be as simple as possible, so modelling the transient nature of the spray formation using CFD is likely to be an unnecessary complication. Use of Rosin-Rammler fittings provide a simple method to represent the distribution in order to see how changes in the sizes of the droplets impact on their journey.

4.2 Particle motion

Particle motion throughout the dryer is an important factor, as it determines the residence time of the droplet and dictates which conditions the droplet is subject to. This will determine the final moisture content of the particle, its properties and the morphology (Oakley 2004). Three levels of complexity are usually applied to drying processes. These are the assumption of well mixed dryers with uniform air properties and flow, simplified analytical solutions to particle motion and simulation of the motion via CFD. Langrish (2009) has provided a detailed summary of the three different approaches, with examples of the modelling equations used. The first approach assumes that the dryer process can be treated like a chemical reaction in a reactor. This enables the use of ideal reactor models such as the plug flow reactor (PFR) and continuously stirred tank reactor (CSTR), to represent the process. This is a common approach for fluid bed dryers which are assumed to behave like a CSTR (Setty & Murthy 2003; Burgschweiger & Tsotsas 2002). By using a CSTR with the well mixed assumption, the properties of the powder throughout the dryer are equivalent to the properties at the exit. Experimental measurements of the residence time, enable the fitting of the most ideal reactor model to the dryer. The residence time of the dryer is normally estimated using a tracer approach. An example of this is dyeing the liquid at a certain point in a batch, and then measuring the change in colour at the exit of the dryer. This change in colour is a function of the concentration which can be used to fit a residence time function for the dryer (Richardson & Peacock 1994). The fitting of this function to various ideal reactor models is expressed in detail in the literature for various outlet responses (Fogler 2006). However, if one tracer

experiment is used, the fitting is only to one set of operating conditions and the residence time is likely to change if the air and liquid flows in the process are manipulated. Therefore, it is important to understand the sensitivity of the function to the operating conditions that may be manipulated.

In the second approach, simplified analytical solutions assume that the air flows in parallel to the particles. The velocities are represented by values for the tangential, axial and radial directions throughout the dryer. There are numerous examples of the application of these models (Keey 1991; Dlouhy & Gauvin 1960; Gauvin et al. 1975; Zbicinski et al. 2005). The flaws in these models are the parallel flow assumptions, their reliance on specific geometries of the spray dryer and on set inlet conditions. By using vectors to represent the air flows it does provide a lot more insight into possible variations inside the dryer than using the CSTR assumption.

The final approach using CFD has become used increasingly in industry due to its lower cost and because of the increased capability of computers over time. Because of these factors, CFD in the chemical industry has become a strong, necessary step in the optimal design of industrial processes (Gosman 1998). There are numerous examples of the use of CFD for modelling spray dryers (Wai et al. 2008; Chen 2008; Birchal et al. 2006; Woo et al. 2008; Zbicinski et al. 2005; Langrish & Kockel 2006). These approaches provide much more information about a given set of conditions, but their credibility is highly dependent on the user's experience, the choice of models and the measurements available to validate the findings from the spray dryer. Analysis of the simulations has led to a reapplication of the first approach, but with significantly more detail available. The simulated conditions in the dryer are used to split the dryer into subsections or control volumes which are individually modelled by CSTR or plug flow reactors (PFR) in series (Birchal et al. 2006; Ali et al. 2014). Use of these models reduces the complexity of the CFD model and its computation time considerably. This is a useful approach when trying

to fit a simplified model to a process where the geometry and air flow patterns are complex, such as that in the spray dryers used at P & G.

4.3   Drying

As the level of details known about the particle motion in the process is increased, more sophisticated drying models can be devised and implemented. There are three levels of complexity (Oakley 2004):

Level 0:   Heat & Mass Balances

Level 1:   Heat & Mass balances with Equilibrium models

Level 2:   Rate based models

4.3.1   Level 0: Heat and Mass Balances

The first step taken when modelling a spray drying process, is to carry out overall mass and heat balances. These balances are used in some form for all mechanistic spray dryer models. Assuming steady state operation, the balances can be used to estimate the total drying rates in the process, and the efficiency. In general, spray dryer systems have two inlets and two outlets. These include the slurry inlet, gas inlet, powder exit and exhaust outlet for the gas. Assuming the flows can be split into components of solids, moisture and gas, then the following mass balances can be obtained:

$$\dot{m}_{solids,slurry} + \dot{m}_{solids,air} = \dot{m}_{solids,Powder} + \dot{m}_{solids,Exhaust}$$

Equation 8

$$\dot{m}_{water,slurry} + \dot{m}_{water,air} = \dot{m}_{water,Powder} + \dot{m}_{water,Exhaust}$$

Equation 9

$$\dot{m}_{dryair,slurry} + \dot{m}_{dryair,air} = \dot{m}_{dryair,Powder} + \dot{m}_{dryair,Exhaust}$$

Equation 10

In these equations, m stands for mass flow. In general, the values of $m_{Solids,air}$, $m_{Solids,Exhaust}$, $m_{dryair,solids}$ and $m_{dryair,Powder}$ are assumed negligible, and set to zero.

The overall heat balance for the spray dryer is:

$$H_{slurry} + H_{Air} = H_{Powder} + H_{Exhaust} + Q_{Heatloss}$$

Equation 11

where $Q_{Heatloss}$ is the heat loss from the process. The flux of energy associated to each mass flow, H_i is represented by Equation 12.

$$H_i = m_i Cp_i \int T_i dt$$

Equation 12

The temperature of the stream is compared to a reference value to obtain the derivative. Each flux of energy is the combination of the heat provided by all three phases. Water is present in both the liquid and gaseous phases. For water vapour contents in the gas phase, an addition of the latent heat of vaporization (λ) is needed to account for the conversion of liquid water to vapour. According to Hess's law, the end result is always the same, irrespective of the path taken, therefore the vaporization for the water already located in the air inlets, was assumed to occur at a reference temperature for all cases. For water vapour in the air, Equation 12 becomes:

$$H_{i,Vapour} = m_i (\lambda_{ref} + Cp_i \int T_i dt)$$

Equation 13

With the use of the listed assumptions and steady state operation, the measurements from the drying process can be used in the mass and heat balances to estimate the flow of water in and

32

out of the dryer. For mass balances, it is ideal to measure the humidity of the air in the exhaust. With the steady state assumption, this can be used with the inlet flows to calculate the moisture of the powder. To use the heat balance, the temperature of the powder, and the heat losses from the process need to be estimated. The method used to ascertain the temperature of the powder depends on the type of spray dryer. For co current dryers, it is routinely assumed that the powder and air are in equilibrium, and therefore leave at the same temperature. With counter current dryers, the temperature of powder needs to be measured or assumed to be equivalent or offset of an air temperature measurement at the powders exit (Langrish 2009). To estimate the heat losses, the assumption of steady state means that the heat losses in the process are constant. Therefore, if a manual measurement of moisture was used to estimate the heat losses, the heat balance could be used to estimate any changes in the moisture content from that point onwards.

4.3.2   Level 1: Heat and Mass Balances with Equilibrium Models

These models incorporate equilibrium relationships such as the desorption isotherm, for a given material as depicted below in Figure 6, to predict the moisture content. These isotherms can be fitted to correlations such as the recommended fitting in Equation 14 (Papadakis et al. 1993).

$$X_{eq} = A \exp\left(-BT_{air} \ln(1/\psi_{air})\right)$$

Equation 14

where X_{eq} is the equilibrium moisture content, A and B are empirical constants and ψ_{air} is the relative humidity of the surrounding air.

Figure 6: Typical Desorption Isotherm
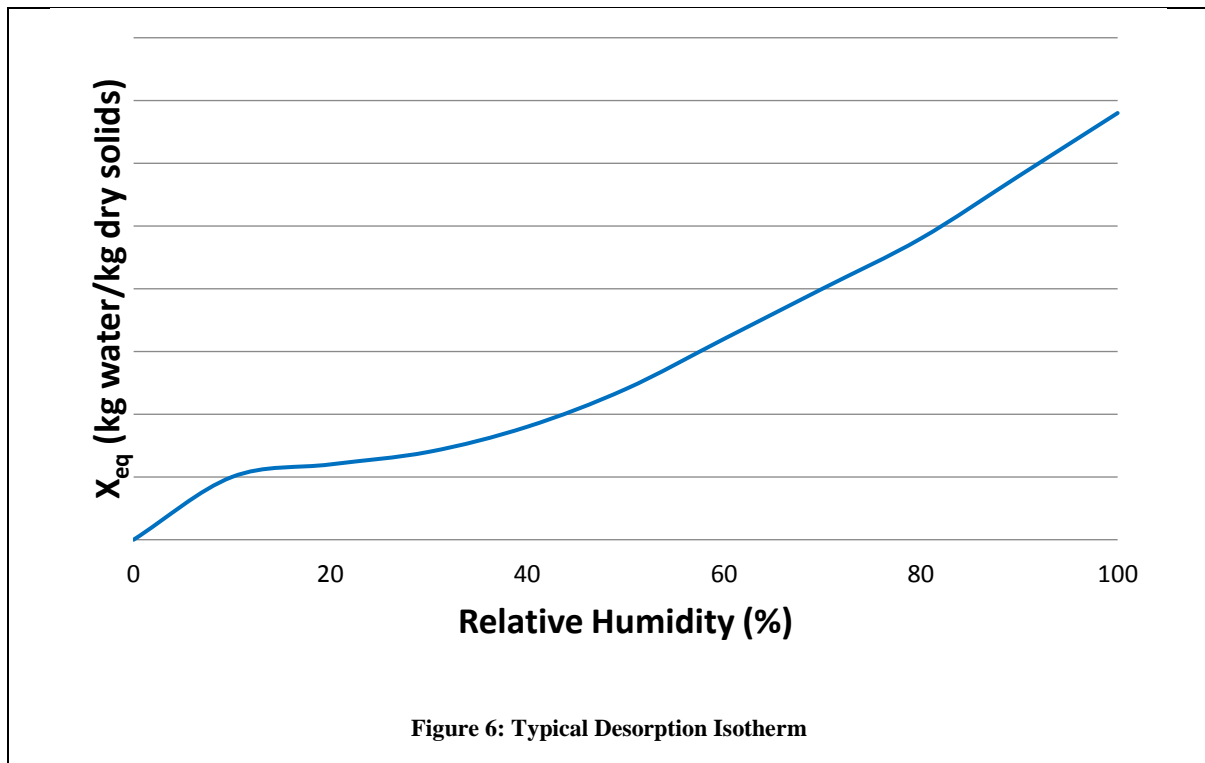
The desorption isotherms are dependent on the temperature, humidity of the air and the material's properties. They are derived experimentally, and require the powder to reach equilibrium with the surrounding air. The amount of time needed to reach equilibrium varies considerably with particle size (Oakley 2004). As counter current dryers rarely reach equilibrium and the relative humidity is normally only measured in the exhaust, these models would not be valid for representing the moisture content. However, they do provide limits for the moisture content, given the outlet conditions of the dryer.

4.3.3 Level 2: Rate-Based Models

The rate based models aim to predict the drying rate of a single droplet in order to estimate the final moisture content. These models are implemented along with the simplified analytical solutions and a method to represent particle motion through the dryer. In recent publications where CFD has been used to simulate the particle motion (Wai et al. 2008; Chen 2008; Birchal et al. 2006; Woo et al. 2008; Zbicinski et al. 2005; Langrish & Kockel 2006), the characteristic

34

drying rate curve (CDRC) and the reactor engineering approach (REA) are the most common lumped parameter models utilised. This is mainly due to their simplicity, as they provide a function for the reduction in the drying rate, related to the moisture content of the particle. Other models implemented include distributed parameter models based on the diffusion rates in and out of the droplets (Birchal et al. 2006; Mezhericher et al. 2008; Handscomb & Kraft 2010). Descriptions of each have been provided to highlight the differences between them.

4.3.3.1 CDRC Approach

The CDRC approach was first suggested in 1958 (Meel 1958). Its main purpose is to simplify the mathematics of drying kinetics, by producing a single characteristic drying curve for a given material. There are numerous examples of its implementation published in literature (Wai et al. 2008; Chen 2008; Birchal et al. 2006; Woo et al. 2008; Zbicinski et al. 2005; Langrish & Kockel 2006).

The theory behind this approach is based on the assumption of the two distinct periods of drying described (Wai et al. 2008). It concentrates on the heat or mass transfer to the droplet during the "constant rate period". For example, the heat transfer for a droplet is expressed in Equation 15 as:

$$m_{Droplet} Cp_{Droplet} \frac{dT_{Droplet}}{dt} = h_c A_{Droplet} \left(T_{air} - T_{Droplet} \right) + \lambda \frac{dm_{Droplet}}{dt} \qquad \textbf{Equation 15}$$

where $A_{Droplet}$ is the surface area of the droplet

During the "constant rate period" the temperature of the droplet remains at the wet bulb temperature, as there is no accumulation of energy, i.e. the left hand side of the equation equals zero. Rearranging Equation 15 provides an estimation for the maximum drying rate as follows:

$$\hat{N} = -\frac{dm_{Droplet}}{dt} = \frac{h_c A_{Droplet}}{\lambda}\left(T_{air} - T_{WB}\right)$$

<div align="right">**Equation 16**</div>

As the droplet enters the second stage of drying, the drying rate decreases from the unhindered

drying rate, $\hat{N}$. The CDRC approach models the drying rate using a relative drying rate fraction

, f of the unhindered drying rate in Equation 17 where f lies between the value of 0 and 1.

$$N = f \cdot \hat{N}$$

<div align="right">**Equation 17**</div>

This approach assumes that a given material has a unique relative drying rate which is related

to the characteristic moisture content, ϕ defined in Equation 18:

$$\phi = \frac{(\overline{X} - X_{eq})}{(X_{Cr} - X_{eq})}$$

<div align="right">**Equation 18**</div>

where $\overline{X}$ is the average moisture content and X_{Cr} is the critical moisture content at which the

second stage of drying begins.

The relative drying rate is assumed to be related to the characteristic moisture content according

to Equation 19. The initial relationship had been assumed to be linear, but further work showed

that the addition of the parameter n allowed the model to cover more materials due to the

relative difficulty of removing moisture from a material (Keey 1991).

$$f = \phi^n = \left(\frac{\overline{X} - X_{eq}}{X_{Cr} - X_{eq}}\right)^n$$

<div align="right">**Equation 19**</div>

For the constant rate period, f takes the value of 1. Once a droplet is dried to the critical moisture

content, the value of f follows the stated relationship until it reaches a value of zero at the

equilibrium moisture content, X_{eq}. The critical moisture content is assumed to be constant and

independent of the drying conditions. Taking this into account, the drying rate equation now takes the form of Equation 20.

$$N = f \frac{h_c A_{Droplet}}{\lambda} \left(T_{air} - T_{WB} \right)$$

<div align="right">**Equation 20**</div>

The CDRC approach has been utilised because of its simplicity and flexibility. It is commonly used in the simulation of drying processes. Another advantage of its simplicity is that additional models can be used to describe properties of the droplets that have not been included, such as the moisture content on the surface (Wai et al. 2008).

4.3.3.2 REA Approach

The REA approach was suggested as an alternative approach to the CDRC in 1997 (Chen & Xie 1997). As the method is relatively new, it is generally used for comparison to the CDRC approach to decide on which is the best method to describe the drying rate (Wai et al. 2008; Chen 2008; Chen & Xie 1997; Woo et al. 2008). In general, the performance of both of these approaches is very similar, with each method outperforming the other in different scenarios. The models may struggle if external conditions cause complications in the particle evolution, as both need an additional model or assumption for the surface area of the droplet.

The REA method follows a similar approach to the CDRC, but concentrates on the mass transfer during the drying process. The main difference between this method and the CDRC approach is the fact that there is only one drying period. The mass transfer during the drying process is described using the evaporation rate expressed in Equation 21:

$$\frac{dm_{Droplet}}{dt} = -k_g A_{Droplet}\left(\rho_{v,s} - \rho_{v,\infty}\right)$$

where $\rho_{v,s}$ and $\rho_{v,\infty}$ are the vapour concentrations at the surface of the droplet and the bulk drying air (Chen & Xie 1997).

The value of the vapour concentration at the surface changes during the drying process. During the "constant rate period" this can be assumed to be equivalent to the concentration at saturation assuming it evaporates at the same rate as a pure water droplet. To express how the vapour concentration falls from this value, the relative fraction, ϕ is used in Equation 22:

$$\rho_{v,s} = \phi \cdot \rho_{v,sat}(T_{Droplet})$$

where $\rho_{v,sat}$ is the vapour concentration at saturation.

The relative fraction has a maximum value of one, and reduces as the drying process continues. The model reaches an equilibrium state when the vapour concentration at the surface is equivalent to the vapour concentration of the bulk air. This will occur when the relative fraction equals the equilibrium relative humidity, and the temperature of the droplet is equivalent to the bulk temperature of the air. Following the equilibrium models, it can be deduced that the relative fraction is equivalent to the relative humidity at the surface of the droplet.

To estimate the relative humidity, it is assumed that evaporation is an activation process, hence the approximation can be made using Equation 23:

$$\phi = \exp\left(\frac{\Delta E_v}{RT_{Droplet}}\right)$$

where ΔE_v is a correction factor in the apparent activation energy for drying, and R is the universal gas constant.

The correction factor, ΔE_v is dependent on the average moisture content. When fully saturated, ΔE_v approaches zero causing the relative humidity to approach one. As drying becomes more difficult, and moisture content falls, the correction factor increases, forcing the value of the relative humidity at the surface towards zero.

Following the use of an activation process for evaporation, the saturation vapour concentration, $\rho_{v,sat}$, can be expressed in Equation 24:

$$\rho_{v,sat} = K_v \exp\left(- \frac{E_v}{RT_{Droplet}} \right) \qquad \text{Equation 24}$$

where K_V is the apparent reaction frequency and E_V is the activation energy for pure water evaporation.

The value of K_V at 1 atm was estimated as 2.62236×10^5 kg m^{-3} and E_V was found to be close to the latent heat with a value of 40.207×10^3 J mol^{-1} (Keey 1991).

Following on from this, a method to relate the correction factor to the average moisture content is needed. Scaling the correction factor against its maximum value is a proposed method for doing so in Equation 25 (Chen 2008).

$$\frac{\Delta E_v}{\Delta E_{v,\infty}} = f\left(\overline{X} - X_\infty \right) \qquad \text{Equation 25}$$

where

$$\Delta E_{v,\infty} = RT_\infty \ln(\psi_\infty)$$

<div align="right">**Equation 26**</div>

The subscript ∞ represents the bulk value, which in this case is the air inside the dryer. These values represent the limits for temperature and humidity at the surface of the droplets. When the surface properties match the bulk values, equilibrium has reached and no further transfer will occur.

The function of average moisture content recommended is expressed in Equation 27 following on from experimental results gained from drying skim milk droplets (Chen 2008).

$$\frac{\Delta E_v}{\Delta E_{v,\infty}} = A \exp\left(-B(\bar{X} - X_\infty)^C\right)$$

<div align="right">**Equation 27**</div>

The REA approach is heavily reliant on the correct estimation or measurement of the relative humidity and the temperature of the air in the dryer. From this, the vapour concentrations are estimated, and steps can be taken to estimate the function expressed in Equation 27 in order to calculate the relative humidity at the surface, φ. The relative humidity controls the value of the vapour concentration at the surface, $\rho_{v,s}$, which controls the drying rate expressed in Equation 21. Taking this into account, the level of computation used in this method and for the CDRC approach is very similar and both require a fitting from experimental results.

4.3.3.3   Diffusion model

Models based on the diffusion during the drying process tend to be computationally expensive, with numerous partial differential equations to be solved. The "constant rate period" is again described using the external conditions around the droplet, as the equilibrium stands between the heat transfer and mass transfer to the surface. During the "falling rate period" it is assumed

that mass transfer can be expressed by the rate of liquid diffusion. For a droplet, assuming it remains spherical, Equation 28 describes the main mechanism for liquid diffusion (Pakowski & Mujumdar 2014):

$$\frac{\delta X}{\delta \tau} = \frac{1}{r^2} \frac{\delta}{\delta r} \left[r^2 D_{eff} (T_{Droplet}, X) \frac{\delta X}{\delta r} \right]$$

Equation 28

where τ is the drying time, r is the radius of the particle, D_{eff} is the effective diffusion coefficient.

As moisture is removed, the diffusion coefficient reduces, thus reducing the rate of mass transfer, as seen in the falling rate period. This equation, or similar forms, have been used in the modelling of dryers (Birchal et al. 2006; Mezhericher et al. 2008; Handscomb & Kraft 2010). However, along with this equation, there must be methods to estimate the moisture and temperature distribution in the droplet, the shrinkage of the droplet and change in the diffusion coefficient in respect to the temperature and moisture content. These additional equations increase the complexity of the model and require numerical methods to find a solution. However, the models do provide much more information that could be used to more fully understand the drying process. This extra level of detail is used to help describe transformations such as agglomeration and attrition, but it does require extra computational effort. This modelling technique has not been applied to the process. As the goal is to provide a model for control the level of detail would make the computational effort too much to provide solutions in a timely manner.

4.4 Morphology

The final area to be modelled is the change in the droplets morphology as it becomes a particle. In some cases the change in droplet size is assumed to be negligible (Cheong et al. 1986;

Mezhericher et al. 2008). In general, the transformations that can occur include puffing, shrinkage, agglomeration and attrition.

4.4.1 Shrinkage

The main transformation of a single droplet in the droplet evolution model is shrinkage. In the model, shrinkage only occurs in the constant rate period. If the initial moisture content is found to be below the critical moisture content, then this assumption of no change could hold true. Shrinkage does not occur in the falling rate period due to the crust formation as the water recedes in the particle. When applying the REA drying model, there is no transition between the two periods which would make it difficult to apply this assumption. There are a few equations to represent shrinkage such as a trial and error based fitting in Equation 29 (Wai et al. 2008):

$$\frac{D}{D_i} = b + (1-b)\frac{X}{X_i}$$

Equation 29

Where the subscript i represents the initial value, and b is a fitted value which is usually quite high (>0.9) for REA and close to unity for the CDRC approach. Fitting with high values of parameter $b,$ suggests that there is little shrinkage in the dryer, especially for short "constant rate periods", but will depend on the slurry properties.

A study into the shrinkage behaviour of skim milk droplets (Fu et al. 2013) showed that the amount of shrinkage was clearly dependent on the surrounding air temperature. A more detailed solution is to replace the area of the particle (A_P) and the mass of the particle with a differential function of radius in the mass and heat transfer equations. The mass is simply the product of the density of the droplet and the volume, which is dependent on the droplet radius. However, the mass and heat transfer coefficients are calculated using the droplet diameter, so the Ranz-Marshall equations must also be included. For heat transfer, Equation 16 can be rearranged to form Equation 30 (Farid 2003) to show how shrinkage occurs over time:

$$\frac{dR}{dt} = -\frac{h_c}{\lambda \rho_P}\left(T_{air} - T_{WB}\right)$$

<div align="right">**Equation 30**</div>

The impact of shrinkage should be taken into account when estimating any change in the density of the powder. The shrinkage directly impacts on the volume of the particles and may play a significant role. Single droplet experiments have suggested that the shrinkage would have less impact on the surface area of the droplets as it also effects the sphericity of the particle which would lead to an increase in surface area (Walton 2004).

4.4.2 Agglomeration and Attrition

Agglomeration and attrition are highly dependent on the material properties and individual trajectories of the particles. A summary of where the agglomeration takes place in the spray dryer can be found in the literature (Huntington 2004). The trajectory of the particles dictates where particles will collide, either with each other or with the walls of the spray dryer. The contacts with the walls are dependent on the geometry of the dryer and the air flow patterns (Keshani et al. 2015). CFD has recently been used heavily to study the wall deposition process to aid the design of new dryers (Langrish 2009). When using CFD to simulate the spray dryer process, it is normally assumed that the particles simply rebound off the walls. However, a recent study (Francia et al. 2015) suggests that wall deposition plays a critical role in the production process in swirl spray dryers. In this study, the wall generated >20% of the product, and had a considerable effect on the residence time of the particles in the spray dryers.

To see the impact of the transformations on the size distribution, the initial droplet size distribution can be compared to the final PSD. Whether or not a model for agglomeration in the process is necessary, depends on the extent of its impact on the final particle size, for a specific dryer. To model the fundamentals of the transformations, distributed parameter models would be needed to estimate the material properties at the surface of the droplets/particles.

Using these models would consequently increase the complexity of the process model. For the purpose of building a model for control, it would be ideal to produce a simple empirical model. This model would be dryer specific and would interact with the models for particle motion and for drying in the spray dryer.

5   Conclusions

From the literature reviewed, it has become apparent that the future of spray dryer control is dependent on advancements being made in the application of model based techniques to spray dryer processes. This could also be aided by new methods of measurement which have been difficult to find. They will need to provide quicker, more accurate estimations for the properties. As products change regularly, it is likely that the control strategies used will have to be adaptive and/or use inputted data about the dynamics of the drying of the product being produced. The increased use and application of models of the spray dryer process will lead to further advancements in modelling and an increased understanding of the process. They will also have the same requirements of measurement techniques in order to succeed. As understanding is increased, it is hoped that a universal approach will be achieved that can be applied to any formulation and any spray dryer.

For process control purposes, it has been important to obtain an accurate representation of the outputs, and the effect of the inputs on them, not on the process itself. The level of detail in the model of the process needed is unknown, but fast response times are essential. By utilising the extra capability of the small scale spray dryer process, the level of detail needed to control the output properties could be determined, and it is hoped that the approach taken to modelling can be reapplied on the larger scales in the future.

3. MATERIALS & METHODS

1 Introduction

Procter and Gamble (P&G) use 3 different scales of spray dryer to produce detergent. The first scale (>*50Tonne/hr*), used for consumer production, is a counter current tower. The remaining 2 scales, a counter current tower (1-2 *Tonne/hr*), and a small scale mixed flow spray dryer (*50kg/hr*),, are utilised by Research and Development (R&D). The use of multiple scales enables test runs to be completed at much lower capacity and cost whilst also achieving a greater understanding of the drying process. This can lead to innovative solutions for processing issues on the manufacturing scale, and allows for the testing of new capabilities. In R&D both spray dryer scales aim to mimic the drying external conditions and residence times of the large production scale, in order to make the transfer of knowledge between the scales easier. The counter current tower is of approximately equal height to the production scale but has a much smaller diameter with 50 times lower capacity. The smaller mixed flow spray dryer has a capacity 500 times lower than production scale. When testing new methods or formulations, it is cost effective to use the smaller scales for testing and justification before mass production for consumers. This also avoids disrupting the production line unless completely necessary.

This research in this thesis concentrates on results achieved with the smaller scale mixed flow spray dryer, with help and guidance from the multi scale understanding centre at P&G. Inherently, the use of small scale provides much more measurement capability at much lower cost than using the larger scales. There is also more flexibility, enabling the implementation of new techniques and methods in shorter time scales. Using smaller capacity also enables processing issues, such as blockages, to be handled more quickly with fewer consequences allowing the process to be pushed to greater limits. However, there are a few disadvantages to this as well. The smaller scale provides different flow patterns and different atomization techniques that may provide a vastly different environment to that of the counter current towers.

The small scale mixed flow spray dryer, and the associated experimental rigs that have been utilised, are described in this chapter. The mixed flow spray dryer process is described in section 2. The measurements that can be taken on the unit for all process streams are summarised in section 3. Section 4 introduces an additional rig that was used to analyse the spray produced from different types of nozzles. To use the two fluid nozzles, I made modifications with the internal engineering team to enable the use of the nozzle on the rig. This is described along with how the rig is operated and how measurements are taken. In section 5, the tests, findings and solutions to processing issues relevant to detergent processing in the spray dryer are detailed. These findings are used to challenge assumptions made when applying models to the spray dryer and to highlight possible bottlenecks.

2 Small Scale Mixed Flow Spray dryer

The mixed flow spray drying process is illustrated in the five step process flow diagram depicted in Figure 7. Firstly the slurry is mixed and then transported towards the dryer. On the way to the dryer there is the option to inject air into the slurry line before it reaches the atomization device. As it enters the dryer, the slurry is atomized into the drying chamber. The entry point for the atomization device is the centre of the air inlet and the fines recycle loop re-enters by the nozzle directed at the main air flow. At the top of the drying chamber there are two outlets for exhaust air and fines to leave the process. At the bottom of the chamber, powder continues into the fluid bed. Eventually the powder is eluted from the fluid bed via an outlet on the outer compartment and samples are taken to measure the powder properties. Hot air also enters the fluid beds to dry the slurry and exits via the drying chamber.
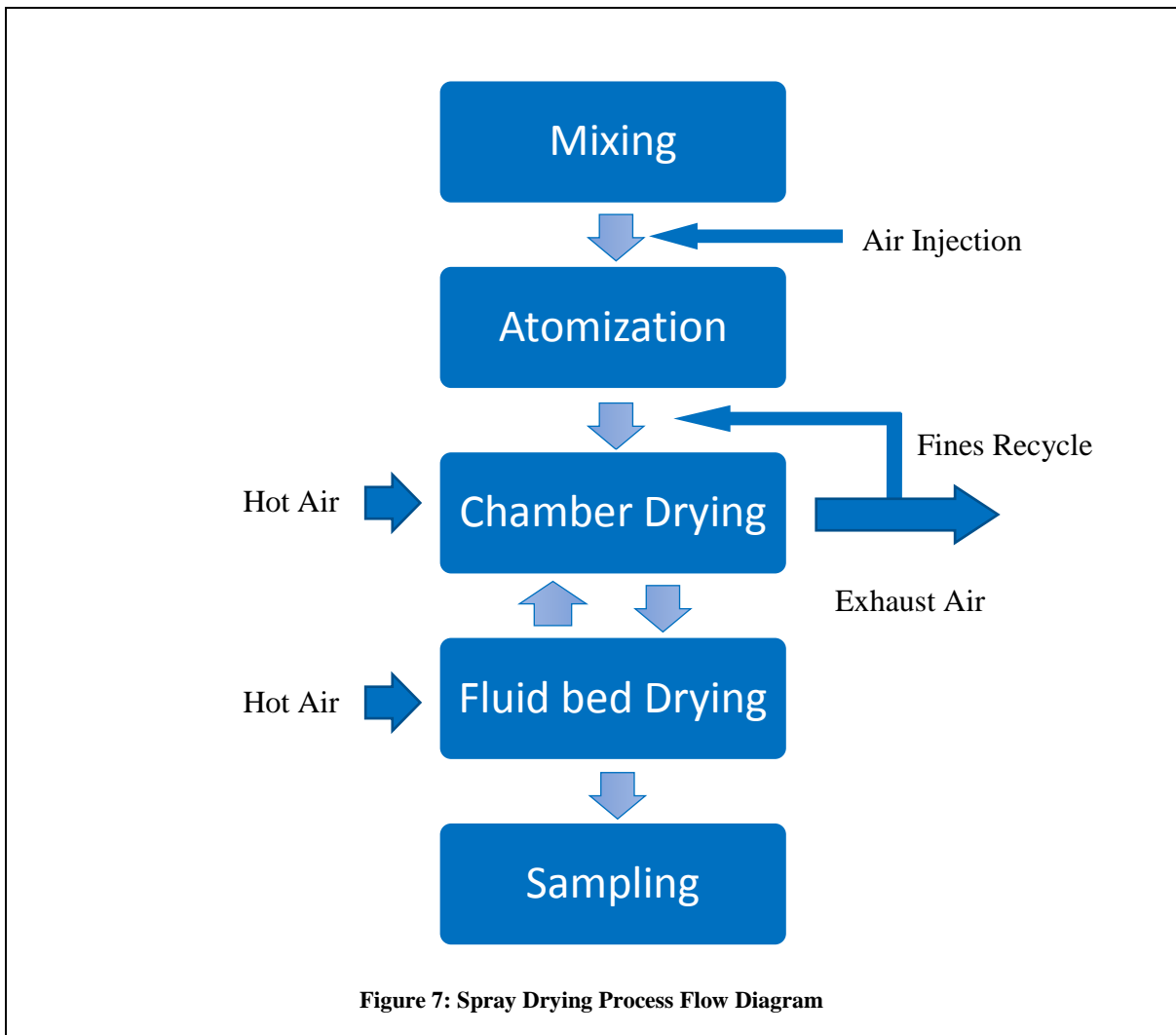
Figure 7: Spray Drying Process Flow Diagram

2.1 Spray Dryer Chamber

The spray dryer chamber is illustrated in Figure 8. The inlet for the air and the nozzle is situated in the centre of the roof of the chamber. As illustrated, the inlet air flow enters at the same point as the nozzle surrounding it in a cylinder. The exhaust outlets are found either side of the inlet, and the powder exits at the bottom. The total height inside the dryer is approximately 2.1m, in comparison; the counter current spray dryer towers can be more than 25m. The cone section of the chamber gradually reduces in diameter towards the outlet and the diameter of the cylindrical fluid bed.
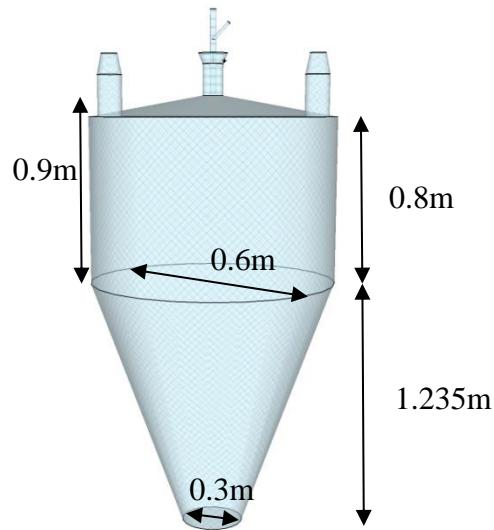
Figure 8: Chamber Dimensions

2.2 Fluid Bed

The fluid bed is split into two sections: the inner fluid bed (IFB) and the outer fluid bed (OFB). Powder is guided from the chamber exit into the IFB. The powder is quickly fluidized by high velocity air flows produced by a perforated plate at the bottom of the bed. As depicted in Figure 9, when the level of the fluidised bed is higher than $0.1m$, the powder can be eluted out of the inner section over a weir. The weir height can be modified by adding $2.5cm$ metal inserts up to an additional height of $0.175m$. Once in the outer section, the opening of a valve enables the powder to flow out of the fluid bed and out of the dryer. The timing of the valve opening can be adjusted by the operator; the valve can also be opened manually to allow removal of powder from the fluid bed. The fluid bed is slightly wider than the outlet to the chamber which are connected by a mechanical system which enables the operator to change fluid beds. The connection is roughly *0.1m* and the internal diameter increases to match the fluid bed.

Figure 9: Fluid Bed Dimensions
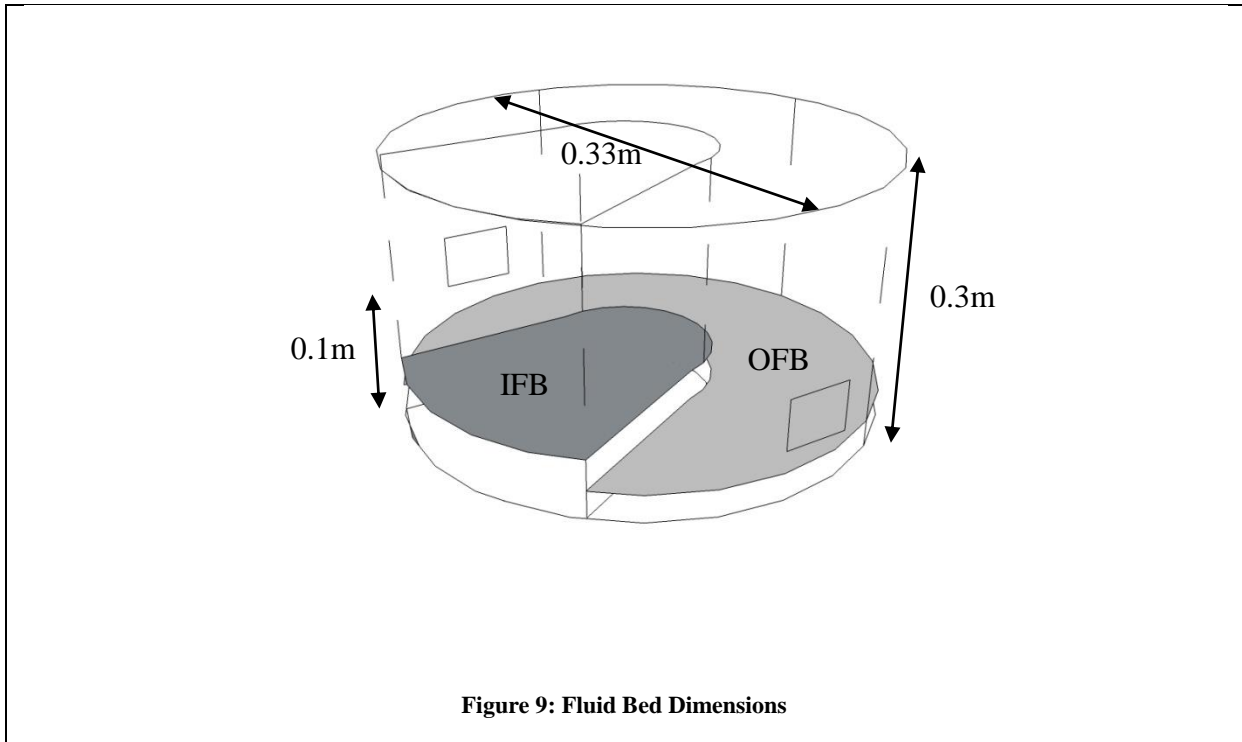
3 Measurements and Estimations

The process and the measurements available are illustrated in greater detail in Figure 10. In this figure shows two mixers which are designed to replicate each other. During the process run, these mixers operate alternately allowing the next batch to be prepared as the current batch is running, enabling short changeover times. Two methods are used to measure the slurry flow towards the tower in each mixer. This can be estimated from the change in weight of the mixer, measured by the load cells installed, or, by a correlation with the pump speed used. The air injection option is then available as the slurry is transported to the dryer. The final measurements noted on the slurry during operation, are the temperature and pressure of the slurry just before it reaches the nozzle. For all the air flows into the process, there are three measurements made: temperature, pressure difference and humidity. The compressed air line feeding the nozzle is from the same source of the fines compressed air so the humidity is assumed to be the same. Using the temperature and pressure differential, the flow rate of the

air is calculated. Additional temperatures are measured where heaters are used to ensure the air is heated to the correct temperature before entering the dryer. The third measurement, humidity, is measured for the main inlet, the compressed air line and also the exhaust of the dryer. The fluid bed inlet humidity is assumed to be the same as the main inlet. Humidity probes measure relative humidity and temperature, and use built in psychometric equations to calculate the mixing ratio which states the ratio of water to air. Additional measurements made in the process include: temperature measurement inside the fluid bed compartments and the pressure in the drying chamber. In addition to this, powder measurements are made after the powder exits the process. During operation, the pressure in the chamber is maintained at -1mbar by the exhaust fan, to ensure the air exits at the exhaust. Powder measurements made at the sampler are inputted manually or automatically into the process control system. To reach the sampling point, the powder exits the fluid bed onto a conveyor belt at the bottom of the dryer. It is then lifted above the measuring equipment and fed to the measurement devices available. These devices provide automatic measurements for density and particle size distribution and manual measurements for various powder properties such as moisture content.

To explain how the measurements are made in more detail they have been split into the following categories:

1) Slurry Measurements/Estimations

2) Air measurements

3) Powder measurements

3.1 Slurry Measurements/Estimations

Slurry measurements are vital for control of the process. Put simply, the flow rate is directly related to the throughput, and this determines the amount of energy needed for drying. The slurry properties can be used to determine the efficiency of the drying in comparison to other

formulations. The slurry properties and the flow play a key role in the atomization of the slurry, impacting on the initial particle velocities, residence time and the evolution of the droplets which determine the final powder's properties.

In current operation, the initial moisture content is estimated from the water content of the ingredients in the formulation. The amount of water in each in ingredient is summed up and divided by the total mass. Assuming perfect mixing, the moisture content is expressed on a wet basis in Equation 31.

$$SMM = 100\left(\frac{m_w}{m_w + m_d}\right)$$

Equation 31

where *SMM* is the slurry mixed moisture content, m_w is the mass of water in the slurry and m_d is the mass of dry material.
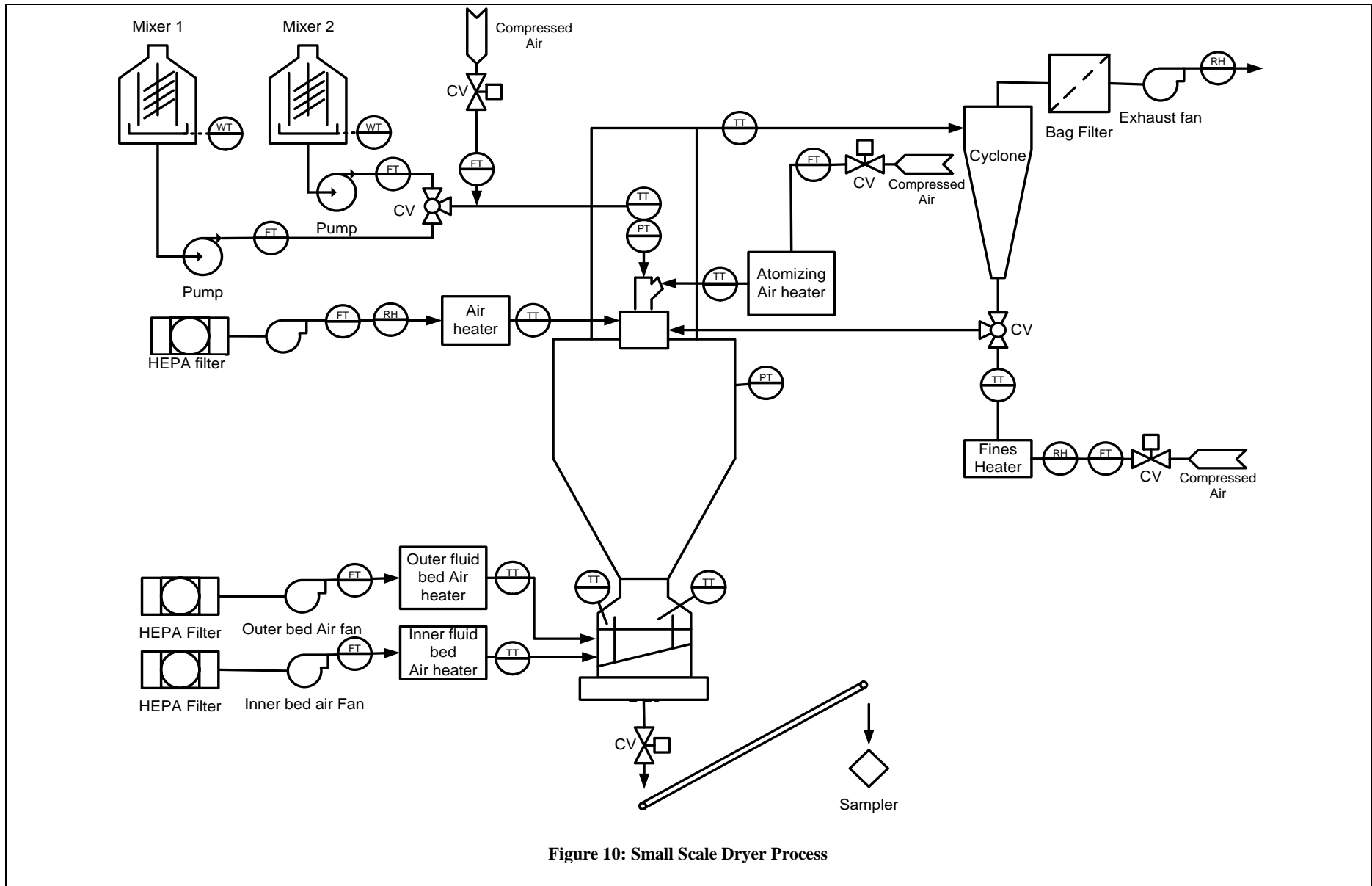
Figure 10: Small Scale Dryer Process

The density of the slurry is manually measured by filling a 500*ml* cup with slurry and measuring the mass. Online methods, based on the Coriolis effect, were attempted. As density increases so does the vibration of mass which in turn affects the resonant frequency. This density measurement is designed for liquids. However, because of the presence of air entrained in the slurry, the measurement is often caused to fail. The lack of robustness over the formulation portfolio has led to little use of this measurement.

As mentioned in the process description, slurry flow is measured using two different techniques. The main method utilised by the operators is the pump correlation. However, they first use the load cell to check the pump correlation is representable of the flow. According to pump affinity laws, for a positive displacement slurry pump the volumetric flow rate is directly proportional to pump speed (Vaillencourt, 2014). The law is represented by Equation 32.

$$\frac{Q_1}{Q_2} = \frac{N_{P,1}}{N_{P,2}}$$

Equation 32

where *Q* represents the volumetric flow rate and N_P is the pump speed in revolutions per minute.

The pumps have stationary parts known as stators which wear away over time. As the stators near the end of their life and reach the 'cliff', performance of the pump drops significantly and becomes unstable and they need to be replaced. It is important to re-fit the model every time the stators are replaced. The model used is stated in Equation 33.

$$\dot{m}_F = \rho \cdot Q = \rho \cdot \left(A \cdot N_P\right)$$

Equation 33

where m_F is the mass flow rate and *A* is a fitted constant

To obtain *A*, a simple experiment with the load cell measurements and water is carried out. Knowing the density of water to be 1000 *kg/m³* and measuring the flow rate with the load cell, two different pump speeds will provide the value of *A* using Equation 32 and Equation 33. To validate both the load cell and pump correlation, the water can simply be collected at the exit of the nozzle over a period of time to calculate the flow rate.

When pumping slurry, the manual measurements of slurry density are inputted into the equation to provide the mass flow rate (assuming the density does not change). If the load cell and the pump correlation are not equivalent, modifications are made to the density in the equation.

The load cell estimates flow rate by simply dividing the difference between two weight measurements and the time taken between them as in Equation 34.

$$\dot{m}_F = \frac{\dot{m}_{mixer}(t) - \dot{m}_{mixer}(t-1)}{Time(t) - Time(t-1)}$$

Equation 34

where m_{mixer} is the mass of the mixer and *t* is the sample time point.

The other measurements taken are the temperature and pressure in the slurry pipe just before reaching the nozzle. Changes in the temperature or pressure of the slurry during a constant flow rate are clear indicators that the slurry properties are changing, so it is ideal to keep them constant as these properties are unmeasured and assumed constant. Any significant change in the pressure is also a clear indicator of a blockage or inefficient atomization at the nozzle, leading to operator intervention by manually stopping the batch to clean out the system and replacing the nozzle tips.

3.2 Air Measurements

As mentioned, the air measurements made are temperature, pressure difference and humidity. The pressure difference and temperature are used together to calculate the air flow rate into the process:

$$\dot{m}_{Air} = A + B\theta + C\theta^2 + D\theta^3$$

Equation 35

where *A,B,C* and *D* are constants to be fitted and

$$\theta = \left(\Delta P \frac{293.15}{273.15 + T_{air}} \right)$$

Equation 36

where *ΔP* is the pressure differential and T_{air} is the temperature measurement in ^oC

These equations and there fitting were carried out by the engineering team as part of the user requirement specification for the spray dryer control system.

The mass flow rate of air in a pipe is dependent on any changes in velocity and density. The velocity of the air is also proportional to the pressure differential according to Bernoulli's equation, and density is dependent on pressure over temperature according to the ideal gas law. Knowing this, the empirical correlation stated in Equation 35 was fitted to estimate the mass flow rate when the fans were installed.

The pressure differential is measured by pitot tubes. The pitot tubes convert air velocity into pressure differentials as the velocity of the air inside the tubes is proportional to the pressure difference. Temperature measurements are made using Platinum Resistance Thermometers. The probes are inserted into the designated pipeline and the change in resistance is measured. The resistance of the platinum changes with temperature and the probes have an automatic linearization of the resistance to provide a temperature reading.
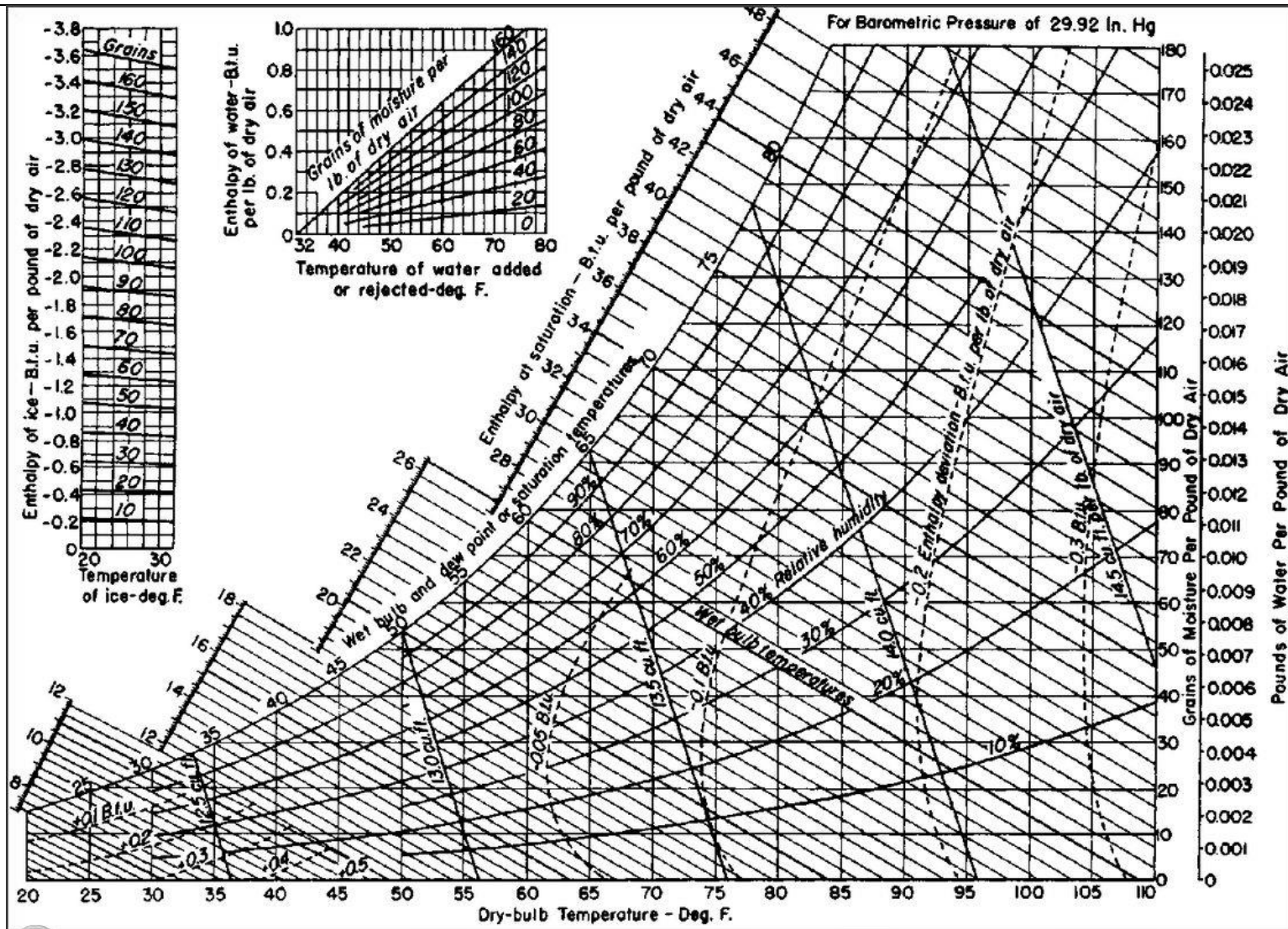
Figure 11: Psychrometric chart

Humidity is measured using Rotronic humidity probes. These probes measure the relative humidity and temperature of the air and output the mixing ratio of kilos of water per kilo of air. Figure 11 illustrates the psychrometric chart for air-water systems that form the basis for converting the measurements into a mixing ratio. Using the dry bulb temperature and the relative humidity value, the mixing or humidity ratio can be obtained.
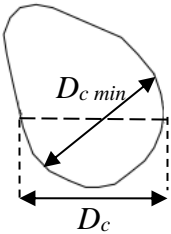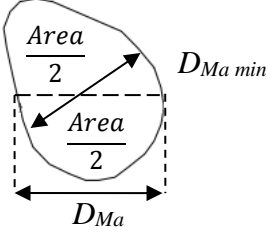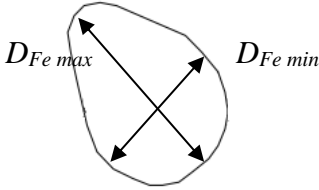
3.3 Powder Measurements

Powder from the dryer is transported via a conveyor belt to a system of feeders which separate samples for particle size analysis and an automatic density cup measurement before falling into a box to store the powder produced. The product collected at the exit of this instrumentation can also be used for manual measurements of powder properties. The particle distribution parameters are measured using a Retsch Technology CAMSIZER which uses image analysis to determine the distribution. A small sample of approximately 1% of the powder is fed to the image analyser, which fits a distribution from a designated sample size. The measurements take on average one minute with a cleaning step between each measurement. The CAMSIZER provides numerous methods to characterise the powder. The diameter measurements available are listed in Table 2. On the large scale, sieve analysis is used to measure the particle size distribution. A calibration procedure was fitted to convert the distribution measured using the minimum chord length, $D_{c,min}$ into the values expected from sieve analysis. $D_{c,min}$ was found to have the most correlation with sieve measurements in an internal report. To carry out the calibration, the characteristic diameters of the distribution and the span were used. The 50th percentile volume diameter is recorded with a target set point of $375 \mu m$. Ideally, the span calculated using Equation 37 is as small as possible, the target is to get a value under 2.

$$SPAN = \frac{D_{V,90} - D_{V,10}}{D_{V,50}}$$

Equation 37

Table 2: Particle Diameter Measurements

Measurement	Description
D_{Area}	Particle diameter calculated by the area of particle projection $$D_{Area} = \sqrt{\frac{4 Area}{\pi}}$$ Diameter of the area equivalent circle with a volume of a sphere with the diameter of D_{Area}
$D_{c\ min}$	Particle diameter which is the shortest chord of the measured set of maximum chords of a projected particles width and breadth
$D_{Ma\ min}$	Particle diameter which is the shortest Martin diameter, which is dividing the area of the particle projection into two halves
$D_{Fe\ min/max}$	Particle diameter which is the shortest or longest Feret diameter of the measured set of Feret diameters of a particle projection. Feret diameter is the distance between two parallel planes placed perpendicular to the measurement direction.
D_{Length}	Particle size which is calculated from the longest Feret diameter and the smallest Chord or Martin diameter of each particle projection $$D_{Length} = \sqrt{D_{Fe\ max}^2 - D_{c\ min/Ma\ min}^2}$$

Bulk density is measured online and offline using essentially the same method. Online measurement involves placing a cup automatically in the outlet stream until it is filled with powder and then measuring the weight and emptying the cup. The manual technique follows the same principle with the operator manually filling and cleaning the cups.

Moisture content is measured using a Mettler Toledo moisture analyser. The analyser uses a direct method of heating a $2g$ sample up to $160^{o}C$ on a scale for 5 minutes and measuring the weight loss to provide moisture content on a wet basis, assuming all the remaining moisture has been removed. The 5 minute time scale was defined based on Karl Fisher moisture measurements. Sampling for manual measurements typically takes around two minutes to ensure enough powder is collected for the density measurement. Adding time for transition and preparing the sampling, a manual measurement for moisture and density is usually inputted into the data logging system after 8 minutes. To assess the repeatability of the measurements, 10 samples were taken using the same $2kg$ sample from the spray dryer. Assuming the moisture content in the $2kg$ sample is constant. The standard deviation of the resulting measurements was 0.13% moisture content.

4   Atomization Rig

Once inside the dryer, no measurements of the droplets and particles were made until they exited the spray dryer. As the atomization is known to be the most important step in the spray drying process, an experimental rig was set up to analyse the sprays produced from pressure nozzles. As the small scale uses two fluid nozzles, I made modifications to the process so a custom nozzle could be fitted on the rig. The process is illustrated in
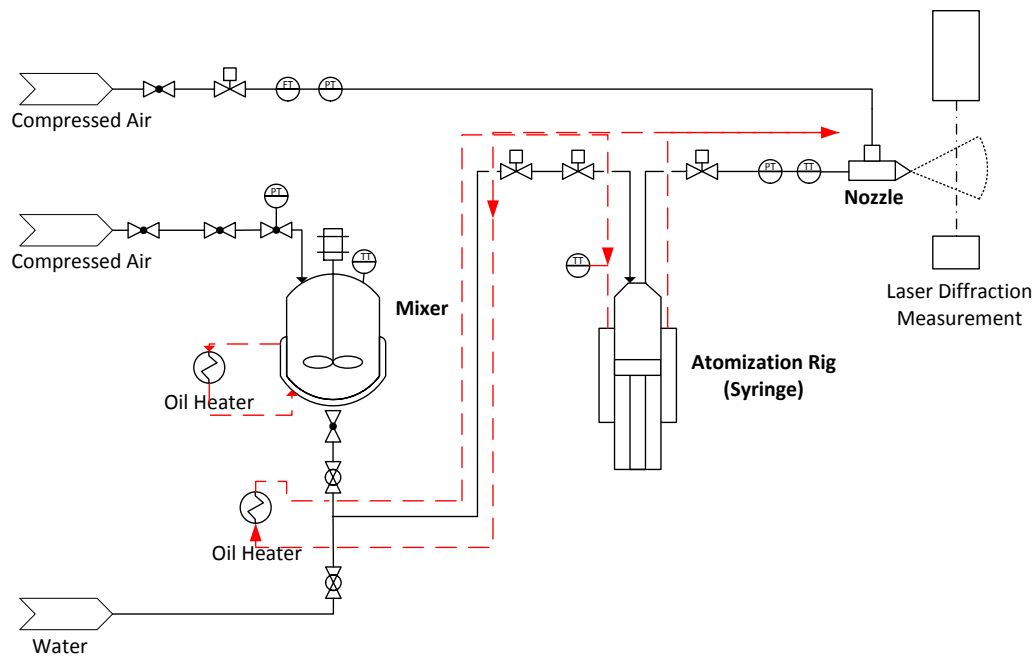
Figure 12. The slurry is mixed and heated up to process conditions and sprayed into a container where the droplet characteristics can be measured. To heat up the slurry, the pipe line and the mixer is jacketed with a hot oil stream. Compressed air is also used to ensure the mixer is pressurized to transport the slurry from the mixing vessel to the syringe. The volume of slurry in the syringe is sprayed at a specified rate into a spray chamber according to the piston speed. Once sprayed the characteristics of the spray are measured. To produce the spray with the two fluid nozzle, compressed air is supplied separately and can be manipulated using a control valve. There are a few differences between this set up and that of the spray dryer. Firstly, the slurry is not supplied continuously to the nozzle. The flows must reach an equilibrium before the measurements are analysed. Secondly, the nozzle is set up horizontally. This will have an impact as gravity acts in a tangential direction. It has to be assumed that in the short distance travelled the impact of this is negligible.

Figure 12: Atomization rig
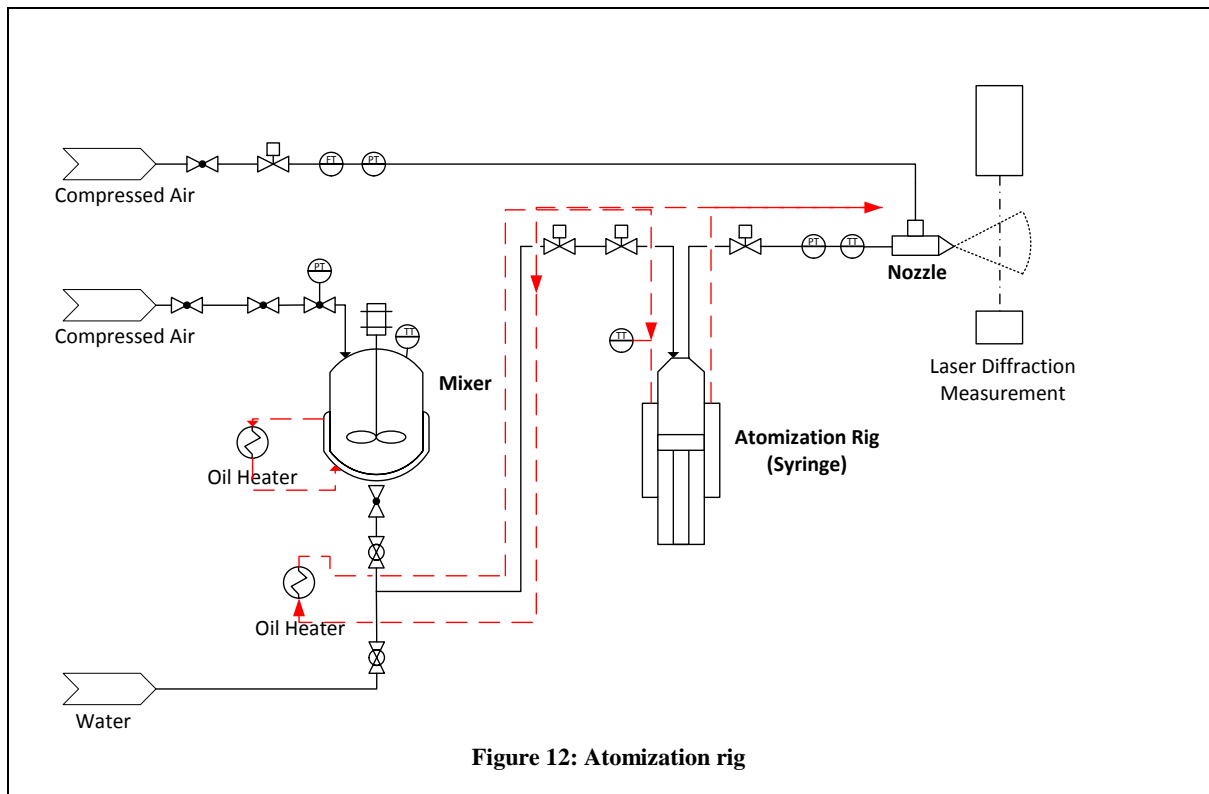
4.1 Nozzle Modifications

The atomization rig was designed so that small nozzle fittings could be alternated at the entrance to the chamber. The two fluid nozzles used on the small scale mixed flow spray dryer are illustrated in Figure 13 and included a large lance. The droplet measurement device is located $0.3m$ into the spray chamber, so significant changes to the nozzle would be needed in order to fit it and produce a stable spray before the measurement device.

Figure 13: Two Fluid Nozzle Dimensions
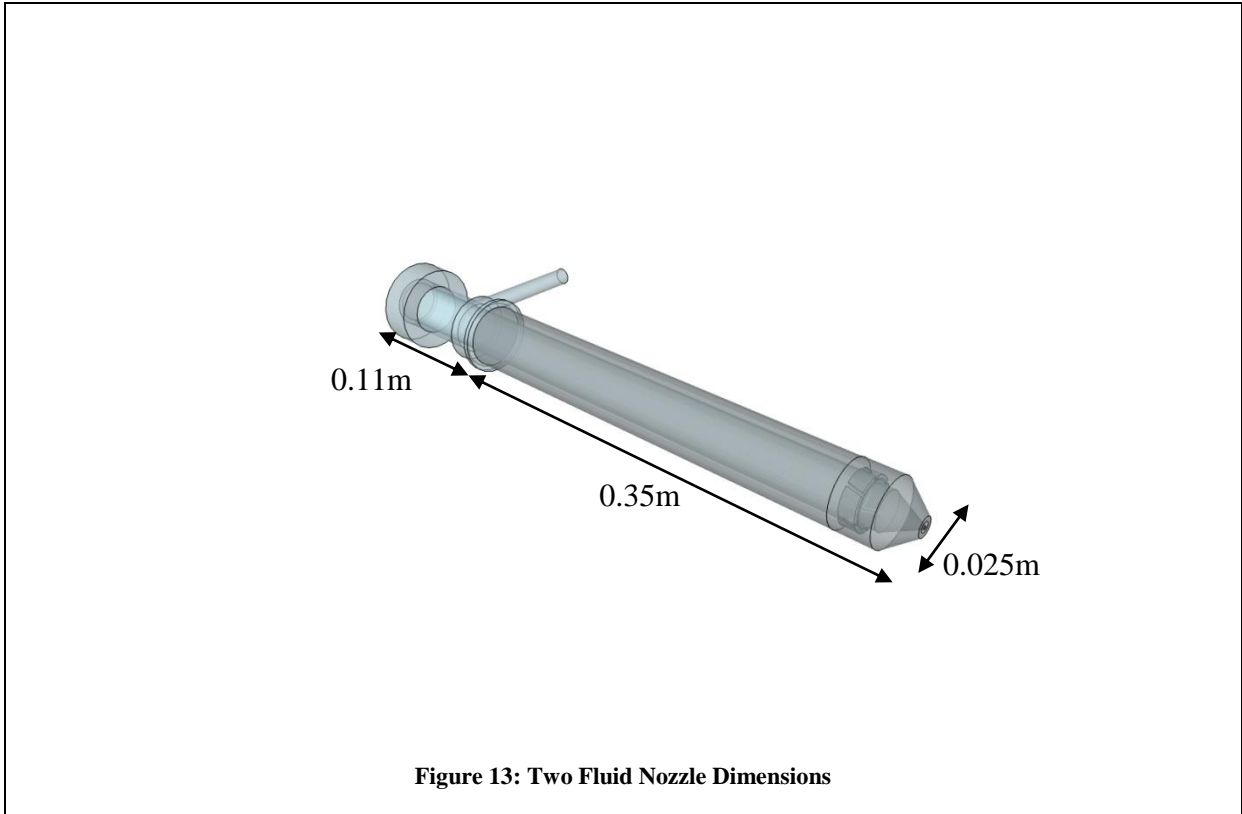
The length of the nozzle was shortened to $0.075m$ as seen in Figure 14. Before making the alteration, the manufacturer, NIRO was consulted to discuss whether this would affect the nozzle's performance. It was concluded that the nozzle's performance was not reliant on the length of the lance, and its length could be altered for use. However with no way of comparing the nozzle performances, their effect on the stability of the spray produced is unknown.

Figure 14: Nozzle Modification
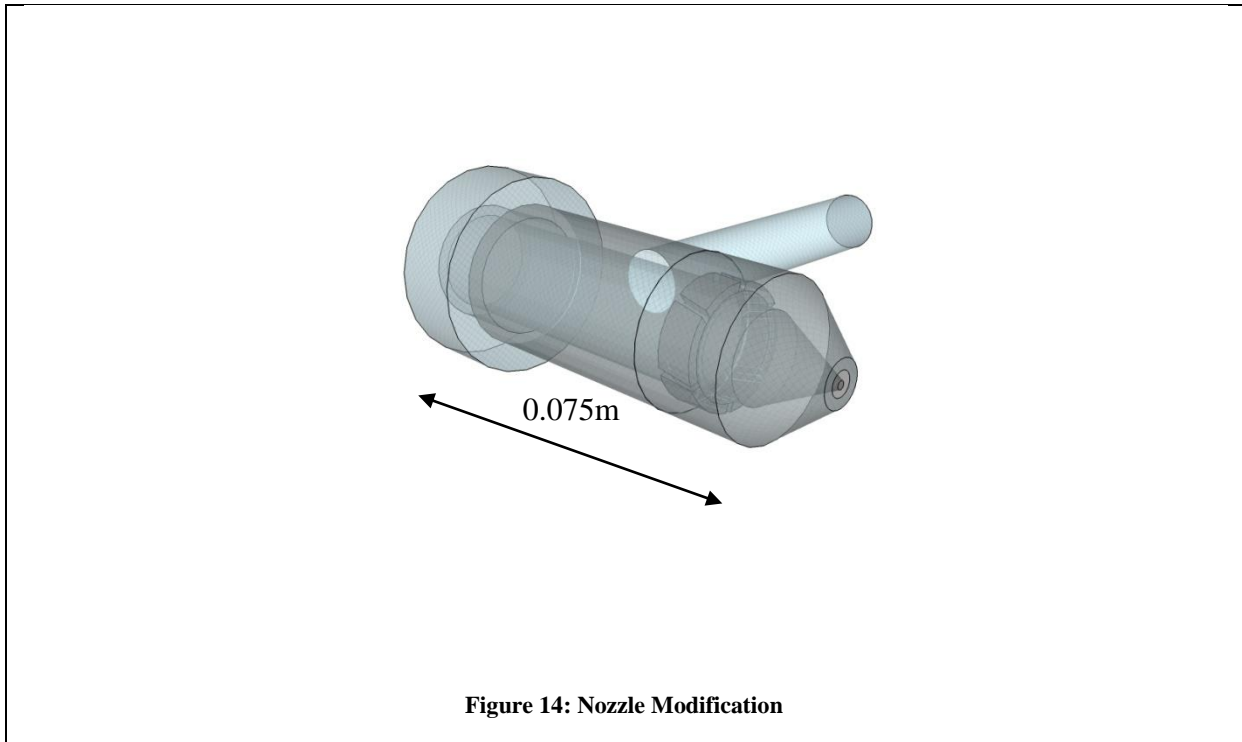
4.2   Slurry flow measurements

The slurry rate is estimated in a similar fashion to the pump correlation on the small scale dryer. Using affinity laws, the mass flow rate is assumed to have a linear relationship with the speed of the piston that empties the syringe. The syringe is filled and emptied according to volume, so, in order to calculate the mass flow rate, an input of the density of the slurry is needed. Measurements of temperature and pressure are also carried out after the syringe, providing data to the operator. If the pressure deviates it is due to nozzle blockages or lack of slurry in the syringe. If this is noticed then the experiment has to be terminated and rerun.

4.3   Air flow measurements

An additional air line was needed to provide compressed air to the nozzle. The air flow needs to be stable during atomization at different mass flow rates in order to understand what effect a change to the atomizing air flow has on the atomization. To do this a Bronkhorst air flow controller was installed with a valve that could be electronically manipulated via the free visualisation software, Flowplot. The setup used compressed air from a reservoir that was

available for 30 second time periods. In this time period a PID controller in the software had to stabilise the air flow at a desired set point and the droplet size distribution produced was measured. The air was supplied at room temperature, so a batch was carried out on the small scale dryer with cold air to ensure the findings would be comparable.

4.4 Droplet Distribution Measurements

The droplet size distribution was measured using Malvern Insitec laser diffraction analysis equipment and reviewed using RT Sizer Spraytec software. A laser is passed through the spray produced by the nozzle. As the laser passes droplets it is scattered according to their size. The Mie theory dictates the relationship between the scattered light and the droplet size, with large droplets scattering the light intensely at a narrow angle and small droplets causing wider scatters at low intensities. The Mie theory was used to estimate the size distribution from the scattered light pattern for the spray. The refractive index was set to 1.5+0.5i for slurry droplets and 1.33 for water.

5 Processing Issues & Solutions

In all processes there are issues that need to be understood, dealt with and/or taken into account before introducing control strategies. Each process is different, and as the scale of production changes, the main causes of variability differ. A simple example is measurement of temperature. The temperature measurement in a small vessel can be assumed to be uniform throughout, but as the vessel becomes larger, the temperature gradients become more significant and a single measurement of temperature will no longer suffice. This is very important when working on multiple scales of spray dryer. Many issues with the small scale will simply be irrelevant for the larger scales and vice versa. For a strategy to be recommended for different scales, its reliance on different aspects of the process needs to be fully understood. This chapter details tests carried out to check the reliability of important measurements and

assumptions made about the small scale spray dryer process which are used as a basis for process modelling.

5.1   Mixed Flow Spray dryer

5.1.1   Slurry flow

In the manufacturing scale, the formulations produced are well known and the process is optimized for a product. However, there are numerous sites around the world producing different products using different ingredients. In the R&D environment, the small scale dryer is used to produce a range of products as well as new formulations. Choosing the most optimal settings becomes a more complex task. If the correct settings are not applied, changes in slurry properties can occur as a result of inadequate mixing. This leads to composition gradients changing the slurry viscosity and density. Direct measurements are not available, so changes in the slurry temperature and pressure at a constant slurry rate are used to indicate that the slurry is not uniform. The operators have numerous parameters to monitor, and mainly concentrate on the powder properties, so these changes are rarely noticed before they impact the product quality. The change in density can also be seen as it alters the slurry rate into the process. The pump correlation maintains a constant volumetric flow of slurry and will only change the slurry rate if the manual input of density into Equation 33 is altered. The load cell measures the change in weight, and so clearly highlights that the rate is changing. However, the load cell measurement is very noisy, so an actual drop off in flow can be difficult to determine. The change in rate and slurry properties impacts the atomization, causing the change in product quality. The operators compensate for this by continuously correcting the atomization and energy input into the process. Multiple batches may be needed to find the most optimal mixing settings depending on the importance of the product. An example of this issue is depicted in Figure 15.
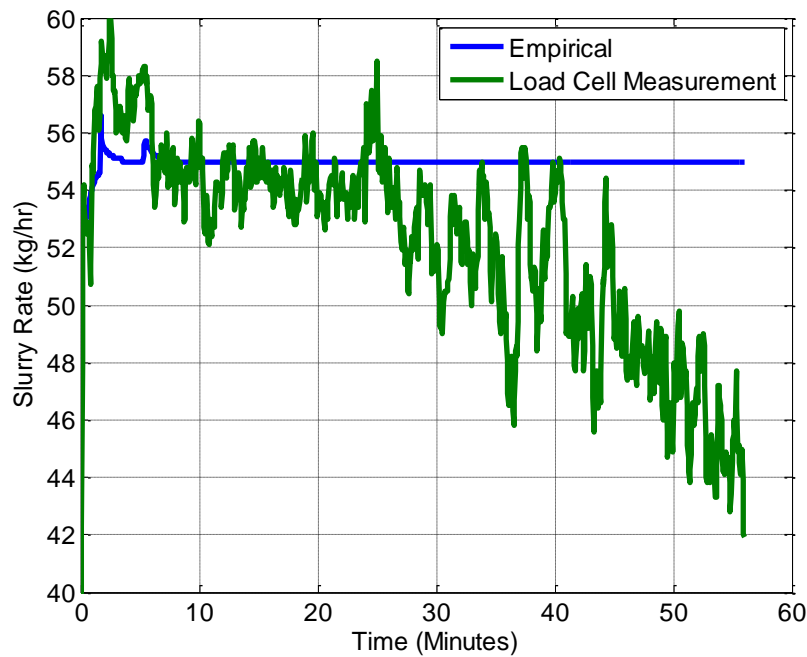
Figure 15: Drop in Slurry rate due to change in slurry properties

Figure 15 highlights 3 issues. In the first 10 minutes it can be seen that the operator has changed the density input in Equation 33 to match the pump correlation to the load cell. The problem is that the level of noise makes it difficult to match the two estimates of slurry rate, and the pump correlation is likely to be a couple of kilos per hour off. From 10 to 25 minutes into the batch run, it can be seen that the empirical correlation is approximately 1 *kg/hr* higher than the load cell measurement. The second issue is the obvious change in density during the trial, as the rate has dropped off by up to 10 *kg/hr* at the end of the batch. This was also highlighted separately by an increase by 3 degrees in the temperature. In fact, in this scenario, the correct settings were not chosen, as the temperature of the slurry was supposed to be 10 degrees higher before starting the batch, which was overlooked. The third issue is the noise and sudden peaks and troughs in the load cell measurement. The main cause of this is related to vibrations around the load cell which are caused by operator movement around the area, misplaced tools, manual inspection of the slurry inside the mixer and debris or leakage on to the load cell. The impact

67

of movement around the area is clear as a disturbance also occurred in the mixer load cell that wasn't being used for the batch. After highlighting this to operators, cleaning the area, reducing movement around the mixers and altering the sensitivity of the load cell, the noise was reduced as seen in Figure 16. The variance in the slurry rate was reduced from approximately ±2 *kg/hr* to ±0.5 *kg/hr* providing a significant improvement in the load cell accuracy.
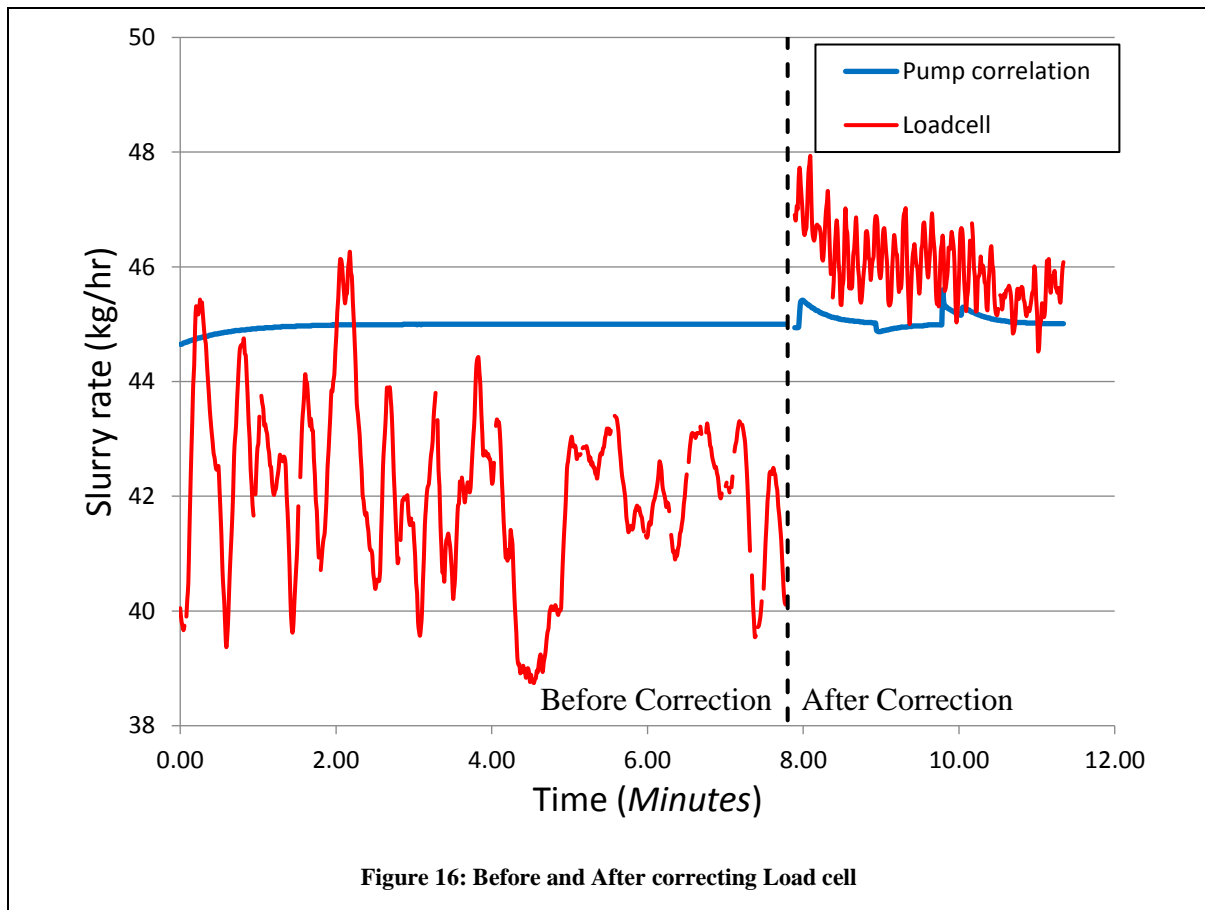
Figure 16: Before and After correcting Load cell

When manual additions are required for a batch, it is not possible to prevent movement around the load cells. In this situation, a sample and hold technique is recommended to prevent any change if there is a disturbance in the unused load cell measurements. The sample and hold technique will maintain a value whilst a check is out of range. Usually this is the gradient of change in the measurement. If there is a sudden change over a specified value it will hold the signals measurement until the gradient of change settles below the specified value. This is important if the load cell measurement is utilised in a control strategy to prevent unnecessary control action.

The change in density provides a more challenging task. It is clear that the pump empirical correlation needs an update to the manual density input, in order to change the volumetric flow rate and maintain a steady mass flow rate into the process. The density measurement based on the Coriolis effect can be used to update the density that is usually inputted manually. Figure 17 shows the density measurement and how it manipulates the pump speed in order to control the mass flow rate (illustrated in Figure 18). The load cell clearly shows a constant flow rate into the process despite the manipulation of the volumetric flow via the pump speed. However, the change in density was not significant in this trial leading to a maximum change of 0.2rpm equivalent to 0.5 *kg/hr*. The density measurement, as mentioned, is designed for liquids and can fail due to the presence of entrained air. When it fails, the value drops to a default minimum value of 0.5g/cl. The model would then change the pump speed to compensate, causing significant issues, so this approach is not adopted. The main solution to this issue has been to highlight the importance of the slurry rate deviations and put emphasis on the importance of choosing the correct settings for the mixer.

5.1.2   Powder flow

In general, the flow of powder from spray dryers is not measured. However, one of the key assumptions to numerous process models is that a steady state has been reached and the flow out is equivalent to the flow in. Taking into account that water is dried from slurry, Equation 38 can be used to estimate the flow out following this assumption.

$$m_{Powder} = m_{slurry}\left(\frac{1-SMM}{1-X}\right) \qquad \textbf{Equation 38}$$

To test the validity of this assumption, a scale was used on the outlet to measure the mass change every 10 seconds. This measurement was then mean averaged over the batch to create a smoothed estimation of flow from the scale.
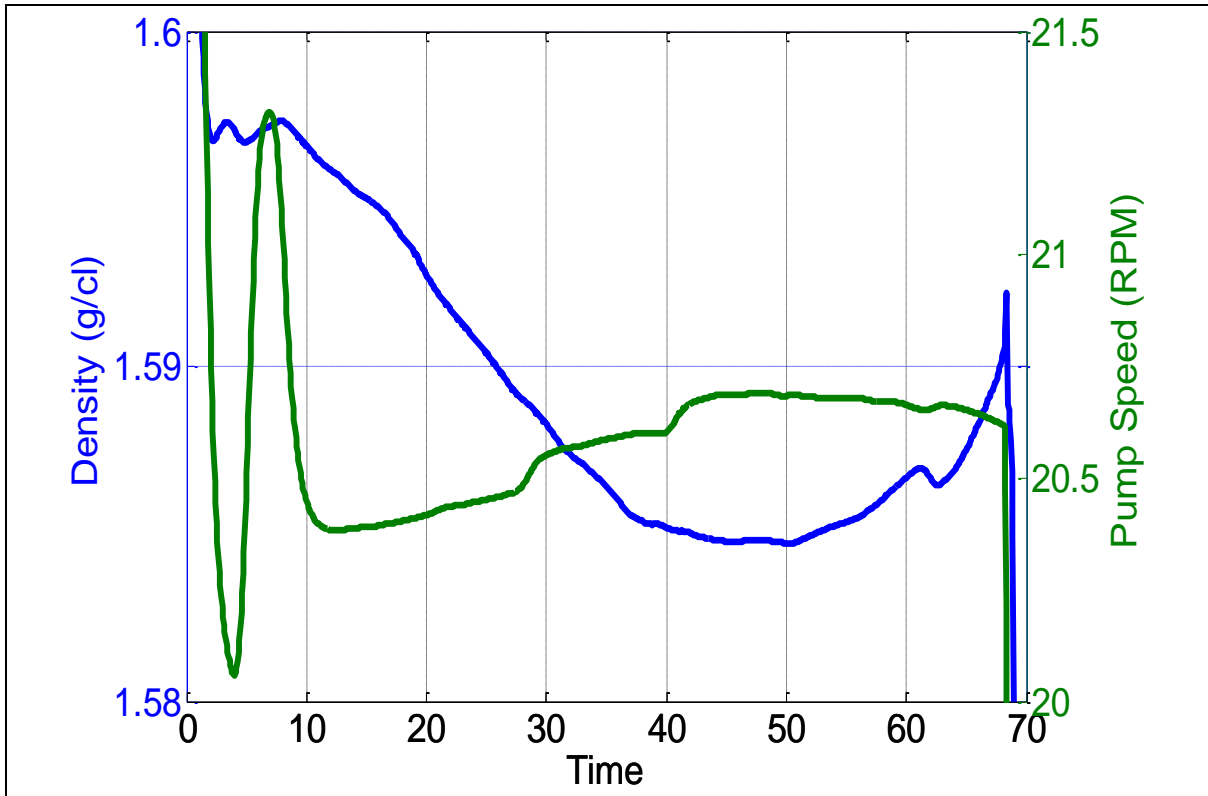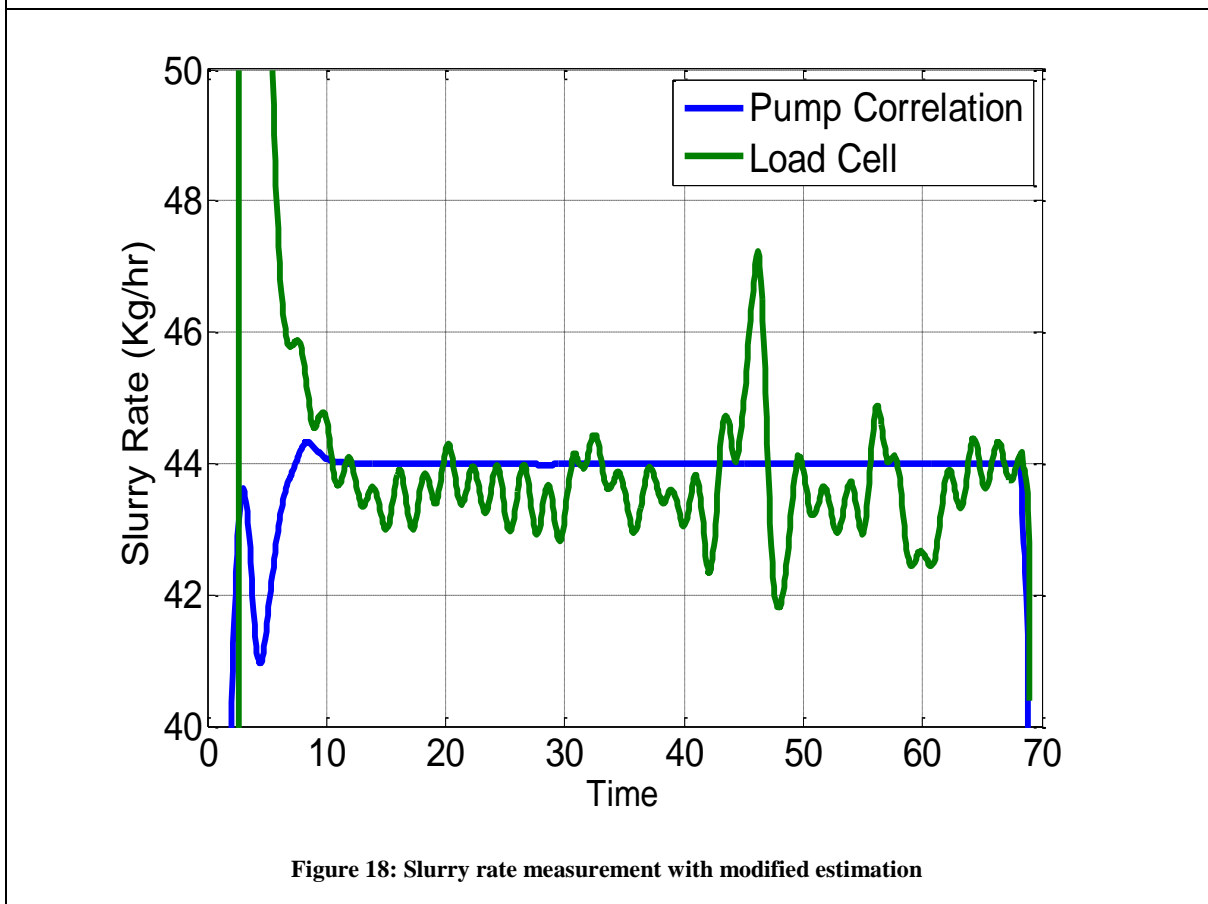
Figure 17: Pump Speed manipulation with density change

Figure 18: Slurry rate measurement with modified estimation

Figure 19 shows one of the batches when the scale measurement was taken. The steady state estimate from Equation 38 and the scale measurement are shown. To use Equation 38, the average value of the moisture content measured during the batch was inputted, this was approximately 2%, and the slurry rate was represented by the pump correlation. The process reaches a steady condition about 20 minutes into the batch, and both the estimate and the scale show approximately constant values. This is significant as it is assumed that the process will be steady when the pump correlation is constant after 10 minutes. There is about 2 *kg/hr* (4% total product flow) missing during this period, this is likely to have been lost in the makeup of the tower or in building up the fines recycle in the process. During the batch, the air flow to the nozzle was altered to change particle size. A decrease in compressed air flow to the nozzle was made 49 minutes into the batch, and the impact on powder mean particle size can be seen in Figure 20. Once this has happened, the mass flow measured by the scale increased by 2 *kg/hr* to a new steady state closer to the estimated value. The change in atomization must have either reduced the flow of fines in the process, or reduced build-up of make up on the dryer walls. This highlights the importance of particle size control to ensure the state of the process doesn't change. It would be ideal for control purposes and process knowledge to have this measurement online for all batches, and to measure the powder flow in the fines, but the resources were not available to implement this. This could have a serious impact on the accuracy of the models to be implemented, especially if the steady state changes as seem in the 49th minute. In Figure 20 the changes in mean particle size can be quite sharp. However, they tend to reduce in oscillations over a consistent value suggesting that by reducing sampling frequency the change would be smoother.
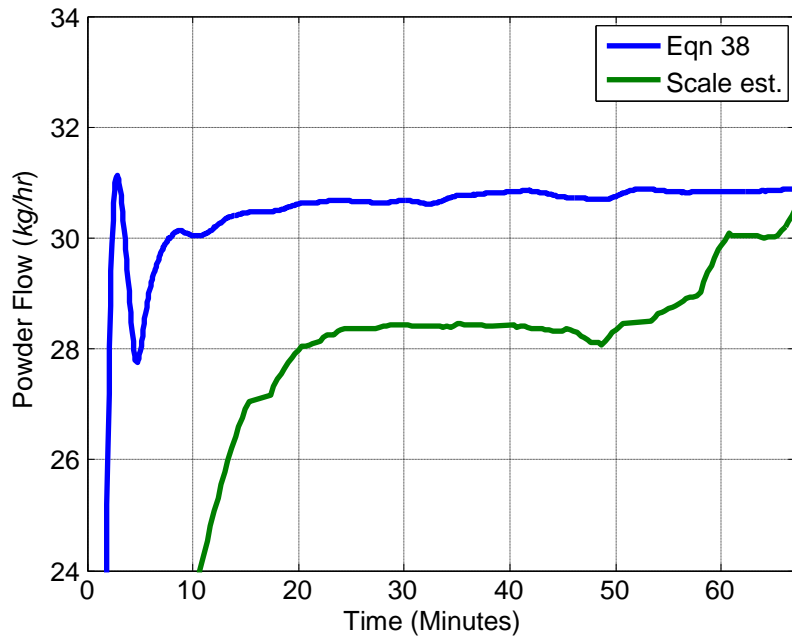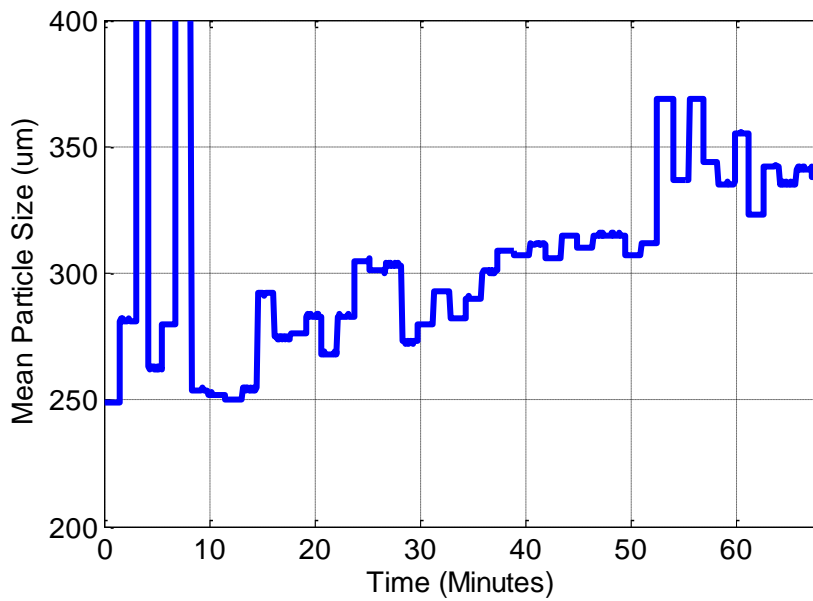
Figure 19: Powder flow measurement

Figure 20: Mean Particle Size change during batch

5.1.3 Air measurements

Measurement of humidity in the air provides information needed to calculate the amount of

water dried from the product. This factor is extremely important when used in mechanistic

models of the process. The Rotronic humidity probes installed in the spray dryer, output the mixing ratio of kilograms of water per kilogram of air into the PLC. These probes measure the relative humidity and temperature but lack the interface to see what values are being recorded. Using the closest temperature measurement to the probe, and a psychrometric chart, it was clear that the relative humidity measurement was fixed at 100% and the probes needed recalibration. It is also clear that the calculation assumes that the pressure is atmospheric, so the humidity measured in the compressed line is also incorrect. After recalibrating, the calibration certificate stated the probes accuracy was ±1% relative humidity. Using the temperatures found in the exhaust line, this leads to an error in the mixing ratio of up to 10%. This is quite significant, and will lead to errors in the mass balance on the process. The accuracy needs to be taken into account and factored out using a calibration method during a batch. To test this hypothesis, the spray dryer was run using water fed directly to the nozzle. To ensure the water evaporated, a control loop was set up to maintain the exhaust temperature at $100^{0}C$ by changing the water flow to the process. The air flow and temperature were then manipulated to modify the amount of water needed to maintain the temperature at $100^{0}C$. The controller was tuned during the experiment to provide a more stable water flow to the process. Figure 21 shows the water flow into the process and the estimated water flow out, using a mass balance. As the process air flows are changed, so is the accuracy of the mass balance. However, at a constant air flow the error remains constant. Changes before 100 minutes relate to the chamber air flow, at 100 minutes are in the inner fluid bed and at 130 minutes are in the outer fluid bed air flow. Carrying out this experiment on a second occasion led to different errors, but they remained constant if air flow wasn't changed. As the error is constant it indicates that it is accuracy related and not precision, so an offset could be used to correct the water content. However, if the air flow is changed during a batch then the offset would need to be corrected.
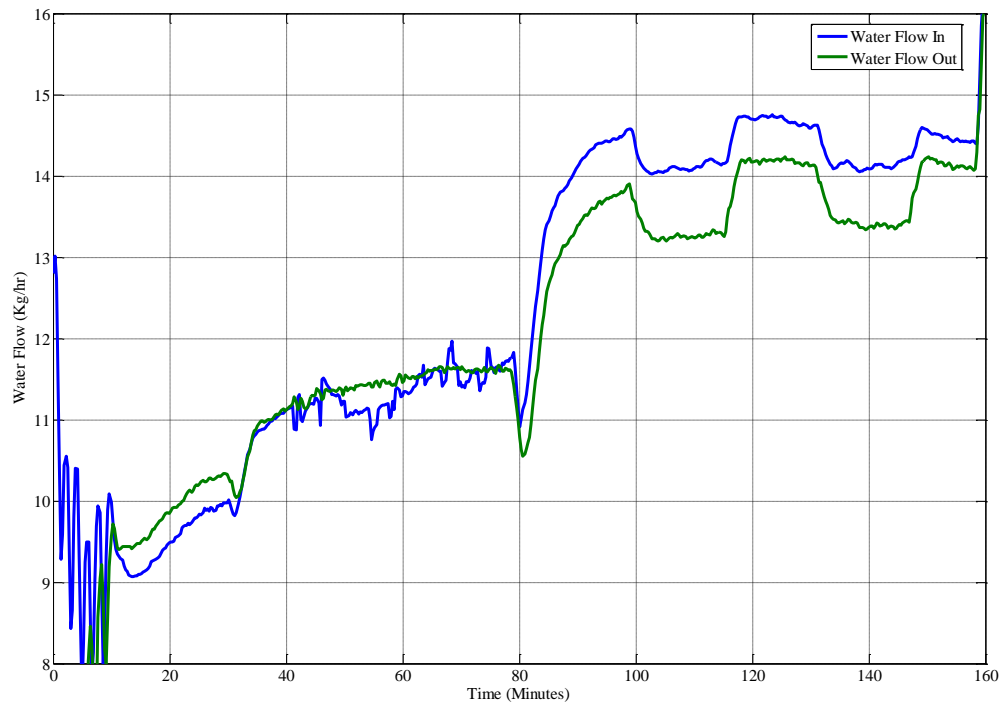
Figure 21: Water Flow estimate during Air flow changes

The final issue with air flow, is the measurements made in the fluid bed. Whilst running the process with water it was noticed that the temperature measurement made inside the fluid bed in some instances was greater than the inlet temperature measured for the air flow to the fluid bed. This is shown in Figure 22. The inlet temperature of the Inner Fluid Bed (IFB) and the Outer Fluid Bed (OFB) are shown as well as the temperature measured inside each section of the fluid bed. In reality this is not possible as heat is not supplied to increase the temperature, and heat losses should lead to a lower temperature inside the fluid beds than the temperature of the air supplied to the process. It is also likely that no water reaches the fluid bed, as it evaporates in the chamber, meaning only air is present in the fluid bed. This means the initial temperature of the air entering the fluid bed must be incorrect.

Figure 22: Fluid bed Temperatures
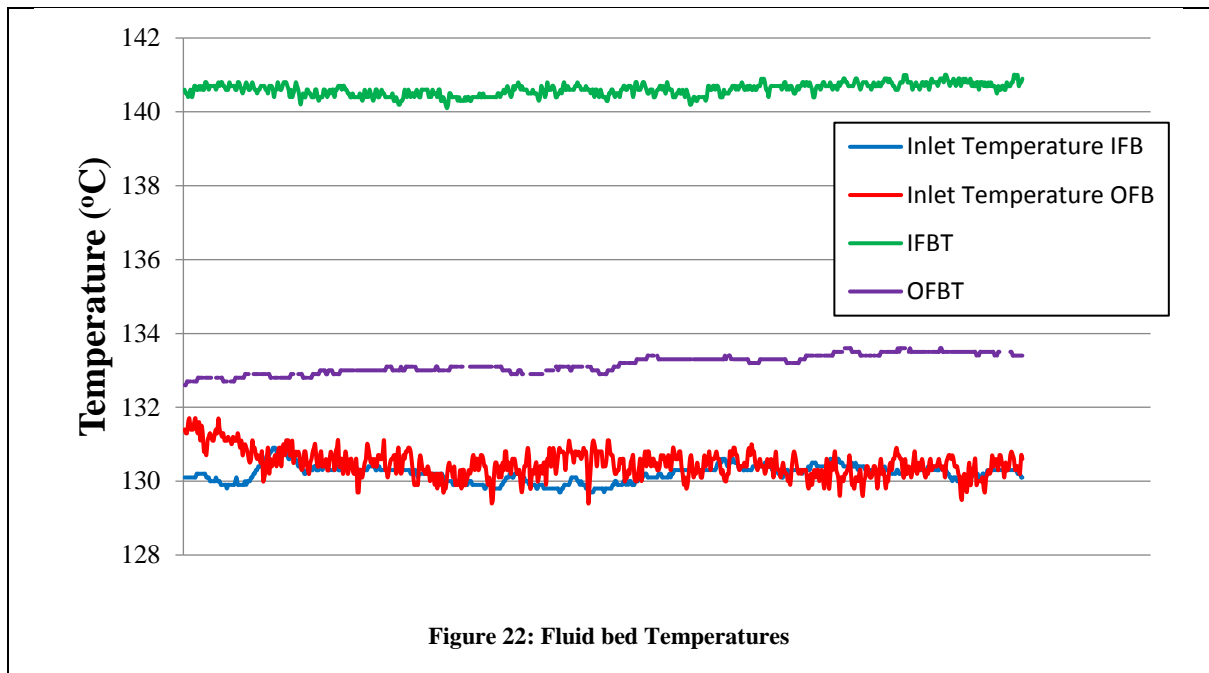
The temperature is measured using platinum resistance thermometers. To test the probes worked correctly, a hot oil bath of known temperature was heated to different temperatures and the probes were submerged. It was noted that the entire probe had to be submerged to achieve the same temperature measurement as the temperature measurement in the hot oil bath using a thermocouple. This showed that the temperature measurement is an average of the temperature over the length of the probe. The probes are inserted so they reach the centre of the pipe. For the average temperature over this length to be an accurate representation, the air flow would have to be uniform in the fluid bed inlet pipes. By inserting a thermocouple at different distances along the probe, the temperature profile in the $0.1m$ pipeline was measured at four locations across the radius. These were 0.04, 0.02, 0.01 and $0m$ away from the centre of the pipe. Figure 23 illustrates that the temperature profile approximately fits the linear drop in temperature expected in order for the temperature probe to measure a temperature of 130^0C. This was unexpected, as there is a considerable drop of temperature from the centre to the wall with temperatures of 172^0C measured in the centre. As the Reynolds number in the pipe is >15000, the flow is turbulent and should be well mixed, this would not explain the temperature

gradient. As the temperatures in the fluid beds were higher, the flow is clearly not uniform and more air must be situated towards the centre or other side of the pipe in which the temperature was not measured. This was also measured for the main air flow, but the air temperature only changed a few degrees across the diameter of the pipe, which was what was expected of the fluid bed inlets. The likely reason for the large temperature difference is radiation to the cold surroundings as this section of pipe has no lagging at the exit of the heater. The air only travels a short distance before it enters lagged pipelines until it reaches the fluid bed. Despite this, a higher temperature would be needed to represent the air in order to estimate the heat losses of the process correctly.

Figure 23: Temperature profile in fluid bed pipeline
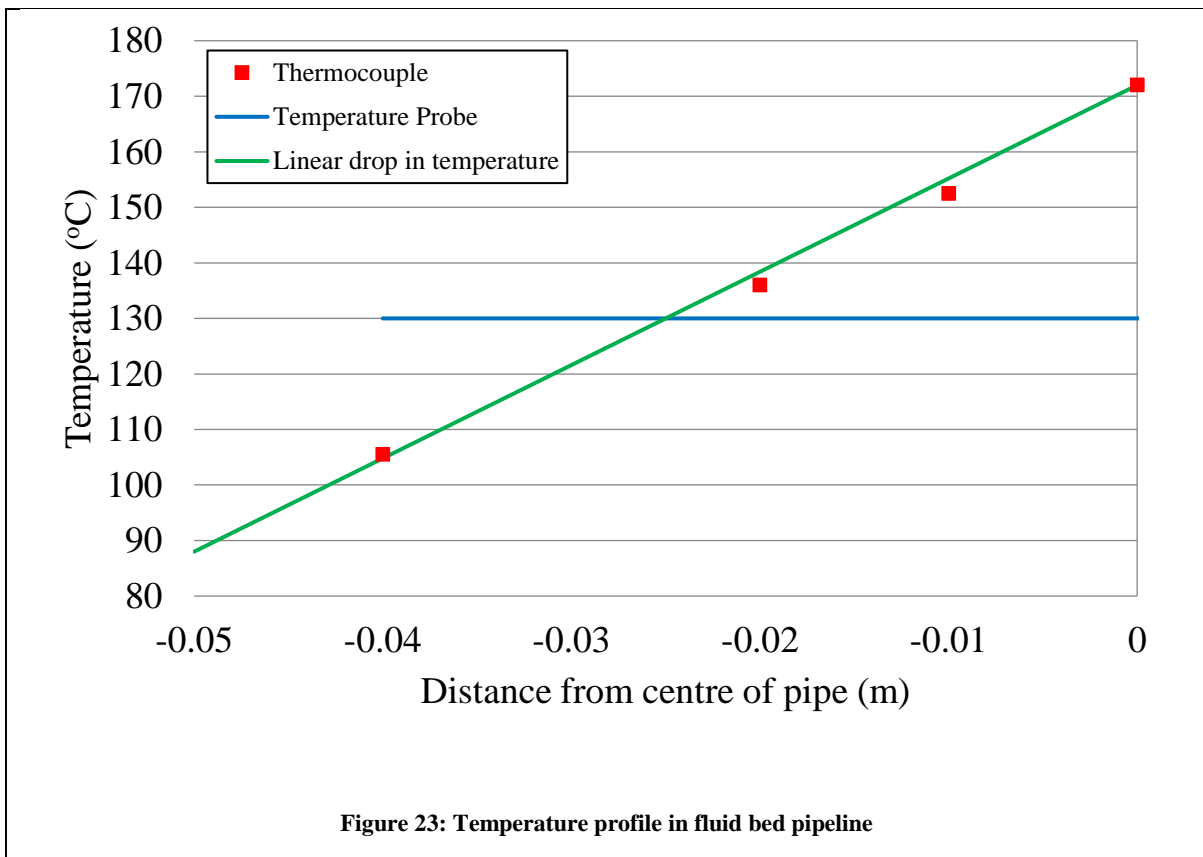
The temperature differential between the inlet to the fluid bed and the measured value from inside can also be altered by changing the dispersion plate. There are two plates available, one with a directional change in the IFB and one without, as illustrated in Figure 24 which shows

the direction of the holes in the plates. The use of directional change forces the air flow towards the weir and this helps the air between the two fluid beds to mix, leading to a more even temperature distribution in the fluid beds as the temperatures settle at $138^{o}C$ and $136^{o}C$ instead of $141^{o}C$ and $133^{o}C$. The overall heat losses remain the same if you assume the air leaves the fluid bed at the temperature measured. This may reduce drying in the fluid beds as it reduces the energy available in the IFB in which the slurry spends more time.

Figure 24: Fluid bed Distributer plates, 1) Directional Change, 2) Straight
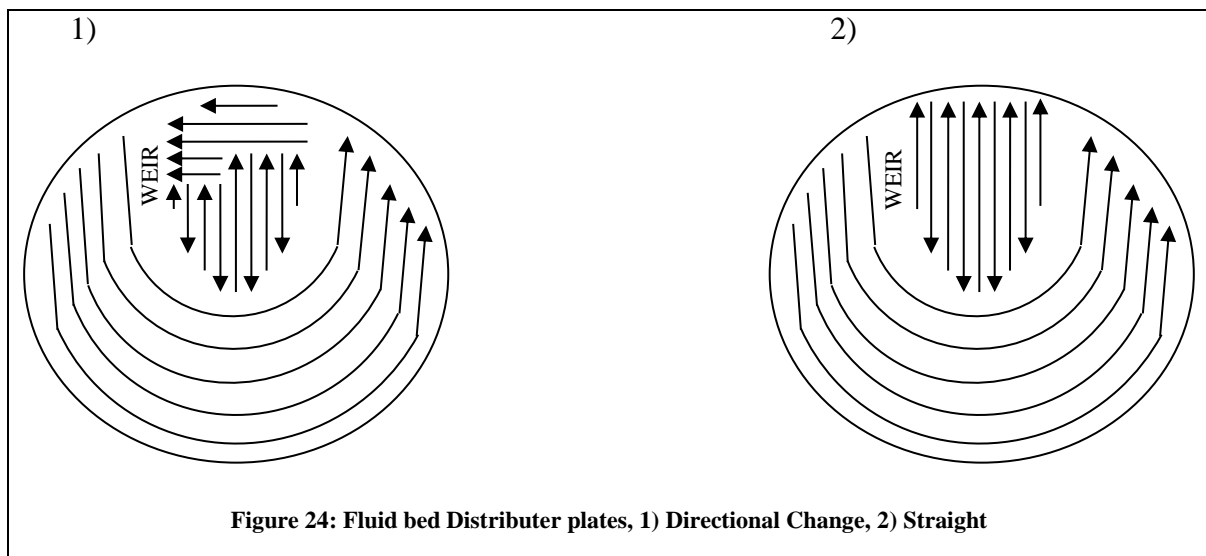
5.1.4 Particle size measurement

Measurement of particle size is done on small samples diverted from the main powder stream. These particles are diverted every periodically every 5 seconds from the main stream through an opening valve on a product shoot. The measurements take on average one minute with variance caused by the cleaning step in between each measurement. Certain powders may stick to the feed tray preventing measurement as the cleaning step cannot finish, necessitating operator intervention. This may lead to long periods where the particle size isn't measured or powder clumping together on the feed tray causes high measurements of particle sizes that are not representative of the powder. This is a result of the powder formulation and its moisture content, and generally occurs when out of specification at the beginning of the trial. If an automatic strategy was implemented, it could be detrimental, leading to unnecessary control

action. Manual control leads to regular monitoring of the particle size, so the lack of measurement would be noticed and the clumps removed with no change in operating conditions. To overcome this issue, the operators must be trained to check regularly during operation, especially at the beginning of the trial where atomization is manipulated most often.

5.2 Atomization Rig

5.2.1 Air flow manipulation

The compressed air supply to the atomization rig was one of the modifications made to the rig. This limited the supply which was only available for 30 seconds stints, leaving a short amount of time to stabilise the air flow and provide a measurement of the spray's characteristics. The atomization at the nozzle is dependent on the air and the processed fluid. As the fluid to be atomized is changed, the dynamics at the nozzle tip change, as the fluid is more or less difficult to atomize. This change in dynamics impacts on the performance of the PID controller used to control the air flow to the nozzle. This was apparent when changing the process fluid from water to slurry, and the tuned controller failed to stabilise. Figure 25 illustrates a typical manipulation of the valve and the response of the controlled output mass flow rate of air. It was found that the introduction of an overshoot of air flow rate led to more stable air flow around the desired set point for approximately 10 seconds. In other cases, where the valve was slowly opened, the flow rate showed a sudden dip and stabilised at a lower flow rate. On some occasions this occurred using this method, as seen in Figure 26, and opening the valve more seemed to have no effect. No measurements available indicated when this would occur, but with this tuning strategy it was a lot less frequent. It is likely that this is linked to the stability of the atomization, but no firm solution could be found to predict whether it would happen or not. The measurement of the droplet distribution takes 0.05 seconds so a window of 10 seconds of constant air flow provided more than enough time to make a reliable measurement.
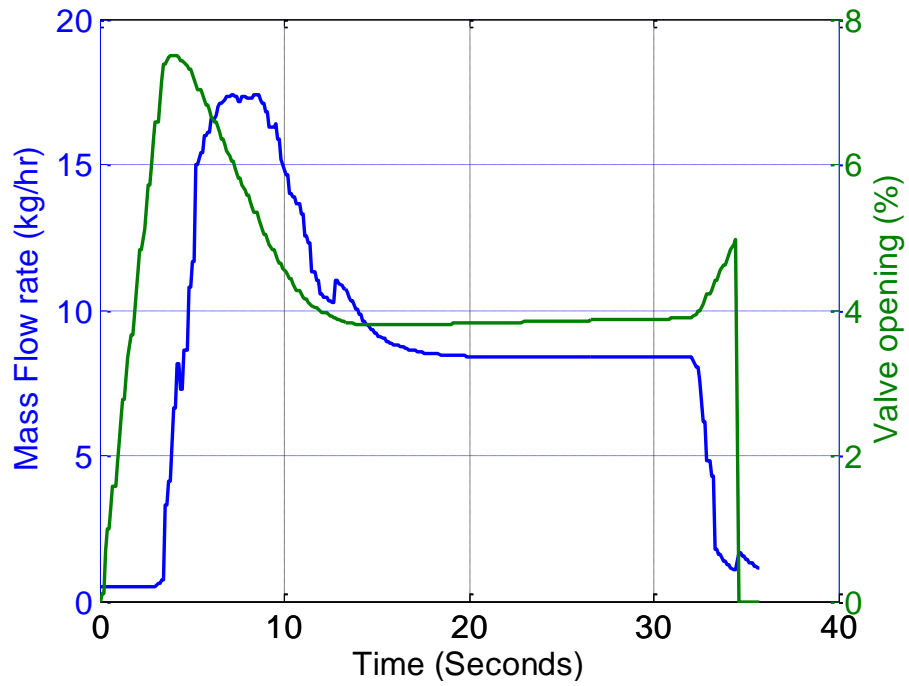
Figure 25: Typical performance of Air flow Controller
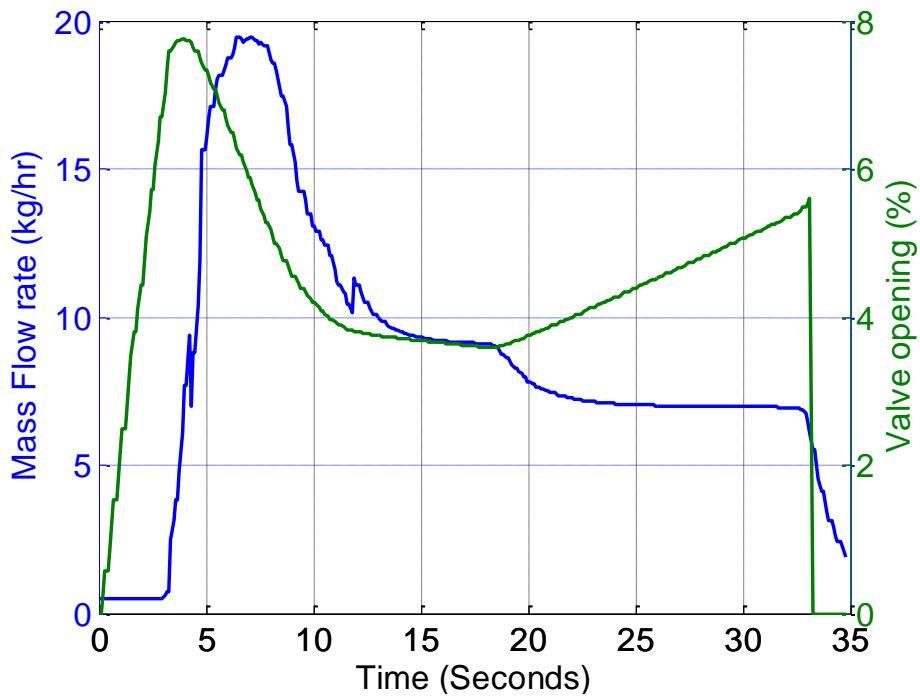
Figure 26: Sudden drop in Mass flow rate

5.2.2 Nozzle set up

The two fluid nozzles have two components, the nozzle tip and the nozzle chamber. The nozzle tip is screwed into the liquid feed line, and the chamber is tightened around the nozzle. The aim of this setup is to have the nozzle and chamber outlets directly in line and symmetrical as seen in Figure 27. This results in the air being evenly spread around the nozzle tip, producing a uniform spray.
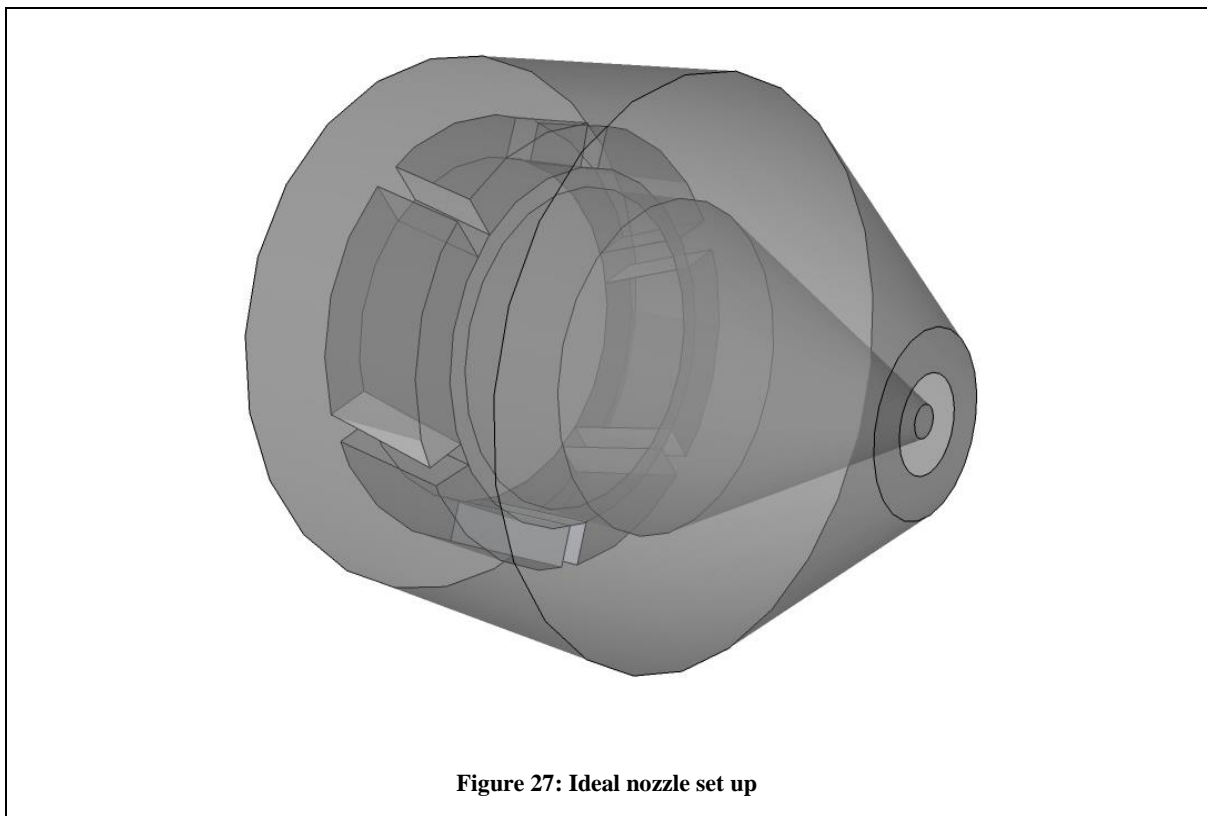
Figure 27: Ideal nozzle set up

As the nozzle tips wear away, they are replaced roughly every 6 months to a year. They are tightened onto the liquid feed line using the same set up. This is a common procedure carried out by multiple personnel, but reports of issues with the atomization have been made by operators. Because of these issues, a sensitivity analysis was carried out using the atomization rig to understand the impact of the nozzle and chamber exits not being in line.

Figure 28 shows how the sauter mean diameter of the distribution produced is dependent on how inline the nozzle tip is to the nozzle chamber. Sauter mean diameter is used as it represents the area in ratio to the volume. This is the most important characteristic when working with heat and mass transfer of distributions. In the figure, an inline nozzle is represented by 0*mm*. Positive distances such as 0.5*mm* are equivalent to the nozzle tip being external to the chamber, and negative are internal. The fully internal -1mm set up showed a clear pattern, increasing the particle size exponentially as the air flow was reduced. This was fully internal as the nozzle and chamber were fully tightened, following the usual practise from the fitters, this is the most likely set up of the small scale, despite recommendations for the nozzles being inline from the supplier. Having the nozzle inline also showed a similar relationship, but with a more gradual increase, however a measurement could not be established at air flows below 4 *kg/hr*. This was due to the air flow not stabilising at this low flow rate in this particular set up. Interestingly, the other internal set up at -0.5mm did not provide the expected results which should lie between the inline and the fully internal set up. The external set up had a similar response but, as expected, produced larger droplets as atomization would be less efficient. There could be multiple reasons for this variability. Firstly, as the nozzle is tightened, it may not necessarily stay in the centre of the chamber causing issues with symmetry. Secondly, if the nozzle hasn't been fully tightened it may not remain stable during atomization. Another issue is related to the production of the nozzle for this rig by shortening the lance. The main impact of this is a reduction in the distance between the air supply and the nozzle. The shortened distance may have led to a less uniform air flow as it reached the nozzle, leading to a non-uniform supply of air in the chamber.

This test highlighted that the change of a nozzle tip can have a significant effect on the atomization if the correct set up isn't ensured. To ensure this is not an issue, standardised

washers should be used, and further checks on the alignment of the nozzle tip should be made during replacement.
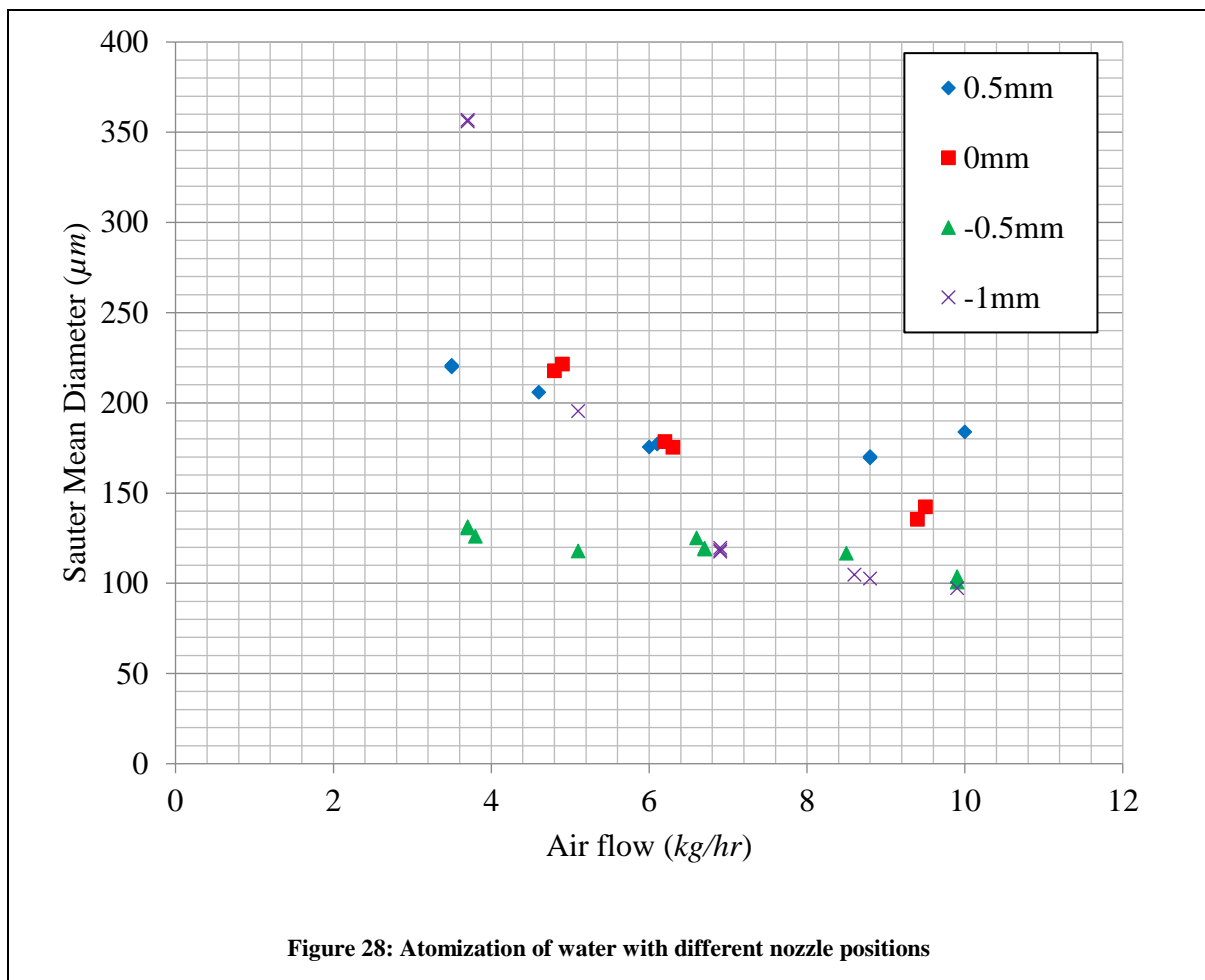

Figure 28: Atomization of water with different nozzle positions

4. MOISTURE CONTENT

1 Introduction

The efficiency and performance of a spray dryer is assessed through measurement of the amount of energy used to remove moisture from a product. The moisture removed from a powder is the main output of the spray dryer process, and is reliant on every input into the process. Direct measurements of the moisture removed from a product being dried in the small scale dryers and on the other scales, are made at line, and are inputted into the computer system. The measurement itself takes 5 minutes, after separating a sample of $2g$ from the powder stream. According to control experts and controller tuning guides, to represent the dynamics of the output accurately, it is best practise to have a sample time ten times smaller than the time constant of the response. To estimate the time constant, it is assumed that the moisture levels are directly linked to the temperature of the product exiting the process. This assumption is made due to the high sampling frequency of temperature measurements made during the process. As the outer fluid bed temperature is the last temperature measured, it is assumed that this is representative of the product temperature. The impact of a change in an input, such as the air flow to the nozzle, on this measurement, affects the dynamics of the process, as illustrated in Figure 29. The change in atomization was chosen for measurement as the amount of product being dried, and the initial drying conditions remain unaffected. As such, any change in the temperature of the outer fluid bed is related to a change in product temperature, and therefore, the moisture content of the product. In Figure 29, the change in air flow is represented by a step change at approximately 39 and a half minutes. The time constant is estimated to be the time taken to reach 63.2% of the change in the output. By approximating the change with a linear fitting, the final temperature after the change is 122.25^0C so 63.2% of the 3.5 degree change from 125.75^0C occurs at roughly 123.5^0C. The time to reach this value is around 90 seconds which is taken as the time constant. This means ideally a sampling time of 9 seconds should be applied to capture the dynamics.

Figure 29: Effect of changing air flow to the nozzle on the product temperature
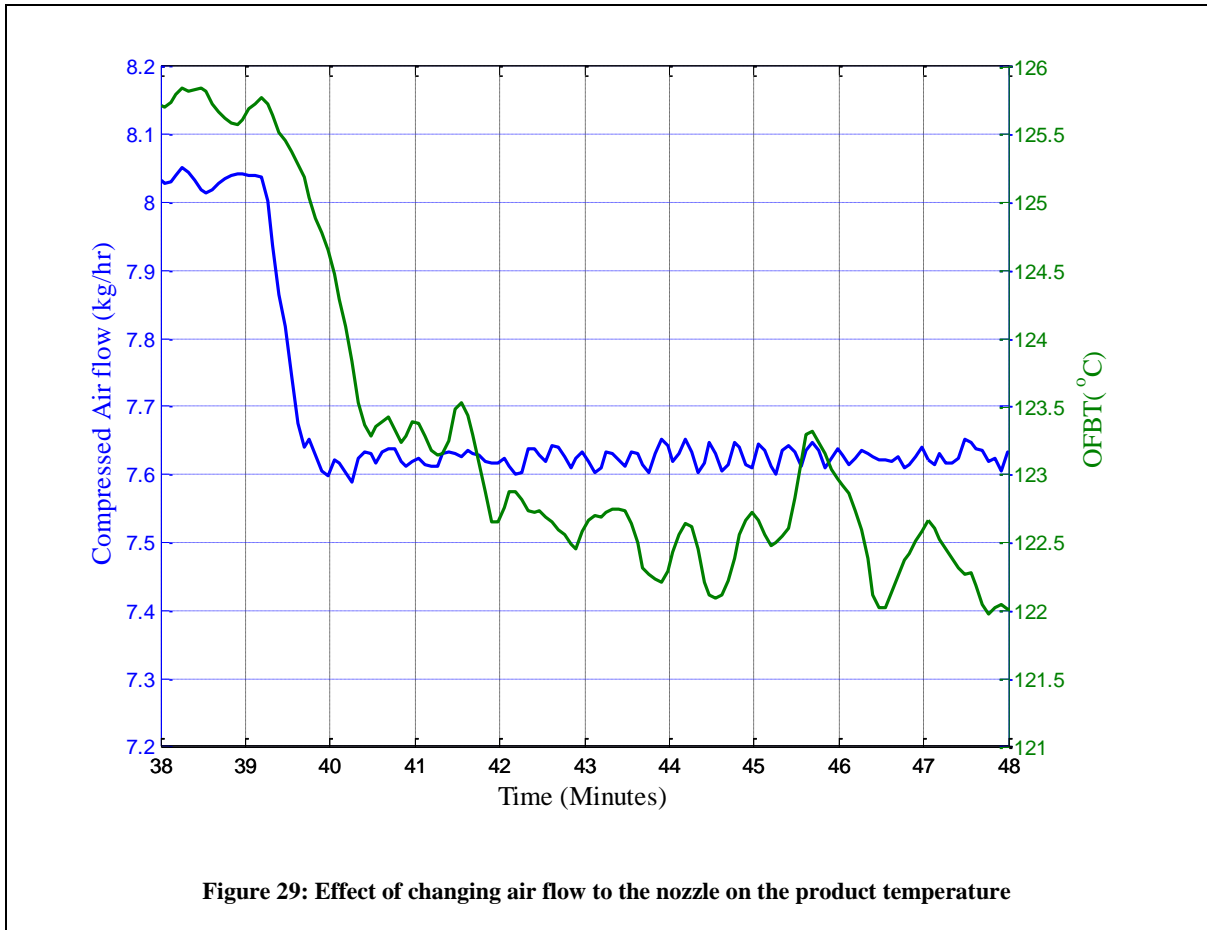
However, for the ideal sampling time of 9 seconds, the direct at-line measurements are insufficient to control the moisture content. This has led to the necessity of obtaining online measurements of the moisture, using process models to estimate the moisture content of the powder. A number of available process models are described in section 3 of the Literature Review.

In this chapter, the simplest approaches, such as the empirical approach, and overall mass and heat balances are analyzed. A general method used by operators, where no models are implemented computationally, involves the empirical approach using the assumptions mentioned. In this method, a manual measurement of moisture content is made and the temperature of the outer fluid bed is noted. This temperature is maintained by the operator when the moisture reading is close to its target value. If the target value is not reached, then the

operator manipulates the inlet air temperatures to change the outer fluid bed temperature. This is a type of inferential control of the moisture content, where the operator assumes the empirical relationship between the temperature and moisture from their experience, before making a change. This method is much easier for operators on production scale, as products rarely change and the impact of a change remains the same. In smaller scales, where process conditions continually vary and formulations change, this approach can be difficult.

For the analysis of the performance of each model in the estimation of moisture, 3 formulations were used over 23 batches. Each batch was supervised by the author, and used for different purposes during the four year duration of this project. Post processing has been used to fit the models, and to assess whether they can be used to predict the measurement of changes in moisture content for the duration of the batch.

2 Empirical approach

In the spray drying process, all inputs affect the efficiency of the dryer, and may therefore affect the moisture content exiting the process. For simplicity, an empirical approach which concentrates on changes to the slurry flow and temperature from a given point, has been applied. This approach is based on the current method used by the operators to maintain the moisture content of a product. This method compares the value of the process conditions at a manual measurement of the moisture content, with the current conditions, to estimate how the moisture content has changed from the measurement point. To estimate the new moisture content, the change in the slurry flow, inlet temperature and the outer fluid bed temperature are used in Equation 39.

$$X_{emp} = X_{manual} + A \cdot Slurryrate_{dev} + B \cdot SlurryT_{dev} + C \cdot OFBT_{dev}$$

<div align="right">**Equation 39**</div>

where *A*, *B* and *C* are constants to be fitted, and each derivative variable is represented by:

$$Y_{dev} = Y - Y_{manual}$$

To fit the constants, each manual measurement made during the 23 batches was used. The error in the prediction for all manual measurements was minimized by changing the constant values in an optimization function in MATLAB. As there are two representations of the slurry rate available, both were used to fit the model. Although there was little difference between them, with the pump correlation performed marginally better due to the lack of noise.

2.1 Model Performance

A typical performance, using an empirical approach to estimate moisture content during a batch, is shown below in Figure 30. This batch was chosen as it provides numerous measurements of moisture content over the general range that the spray dryer is operated in. Figure 30 shows an example of what an operator would see during a batch, a time delay has been introduced to allow for the time factor involved with the taking and recording of manual measurements. The manual measurements of the powders moisture content are plotted in red for the time point at which they were taken. Error bars have been included on the manual measurements to represent their variability. As each measurement is a bulk representation, and only two grams samples were used, inaccuracies in measurements are likely. To test the repeatability of a measurement, it was carried out 10 times on the same sample to get a distribution. Two standard deviations have been used either side of the measurements and an additional error bar has been added horizontally in the time domain. The horizontal error bar represents the error associated with taking the sample from the dryer at the time point

represented. This time point can vary if the sample is left for too long or taken too early by the operator.

The empirical approach shown in blue cannot use these values until the readings are made available in the computer system. The length of time taken is assumed to be approximately 8 minutes, to include the time needed for sampling and measurement of the moisture content. The empirical approach is then able to calculate its next value according to the derivatives of the inputs described.

Figure 30: Typical Performance of Empirical Approach
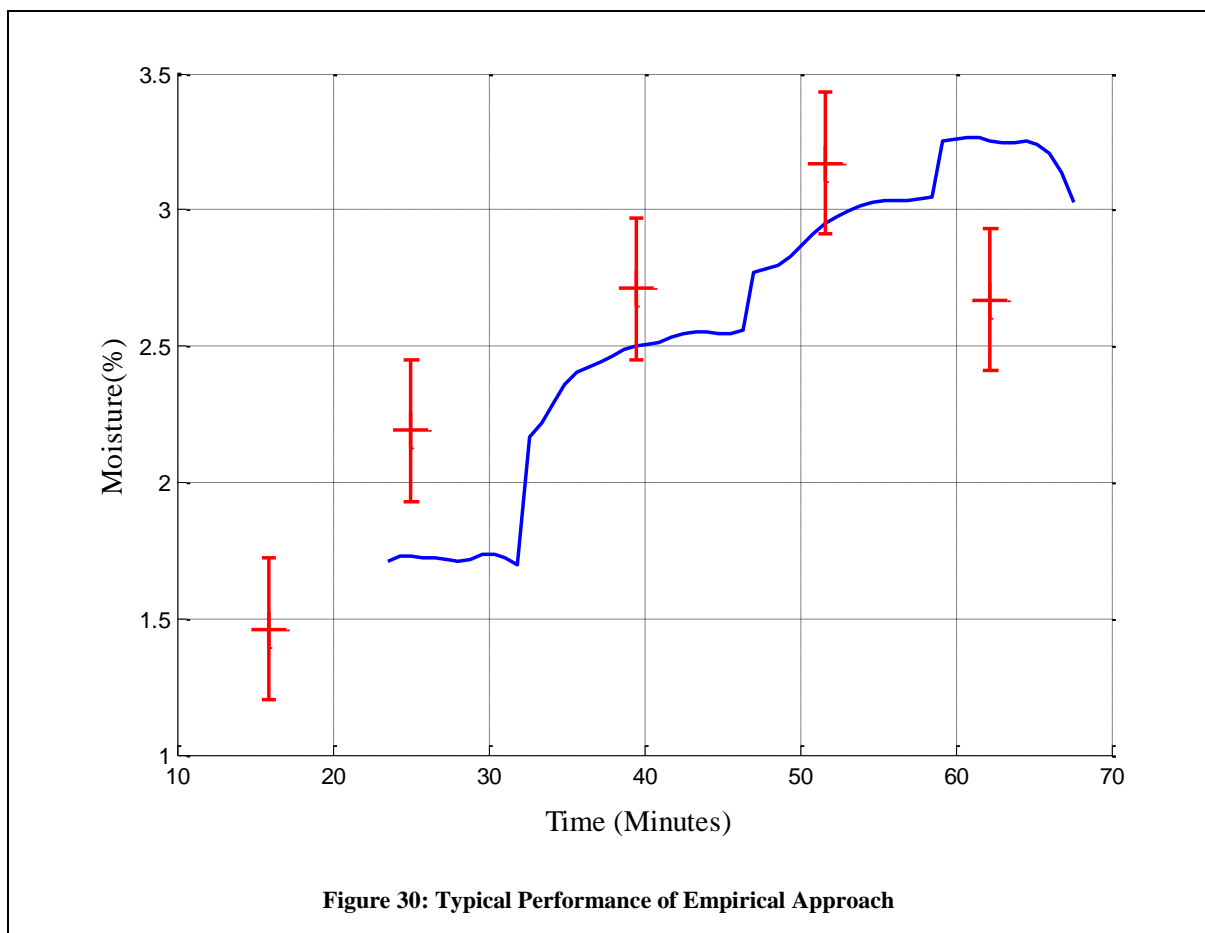
Each of the five manual measurements of moisture is used to correct the model, and those corrections can be seen in Figure 30 when the manual measurement is inputted, 8 minutes after the sampling point. As can be seen, the method often under-predicted the changes in moisture in this particular case. The model constants are a best fit solution for all of the batches

undertaken in the process. There was no clear benefit seen when using separate fittings for the three formulations, indicating that noise from other sources has more impact on the predictability of the moisture content.

The overall performance of this model has an average error of 0.35% moisture with a RMSE of 0.48% over all 23 batches. To calculate the error the model is used as a live tool. Therefore the error is the difference between the models estimation and the manual measurement at the point of time of the measurement. Figure 31 illustrates how accurately the model predicted the moisture content. Given that the manual measurements have a standard deviation of 0.13% moisture, this model performs very well. When large changes in moisture are made, the model does struggle, but in everyday operation this is unlikely, unless a very sensitive formulation is being used. At the production scale the 8 mins quoted is applicable. Less measurements are made as there is more trust in the process that the moisture will not vary. Having this as an indicator would be a useful to let the operator know another measurement should be made.

Figure 31: Empirical model performance
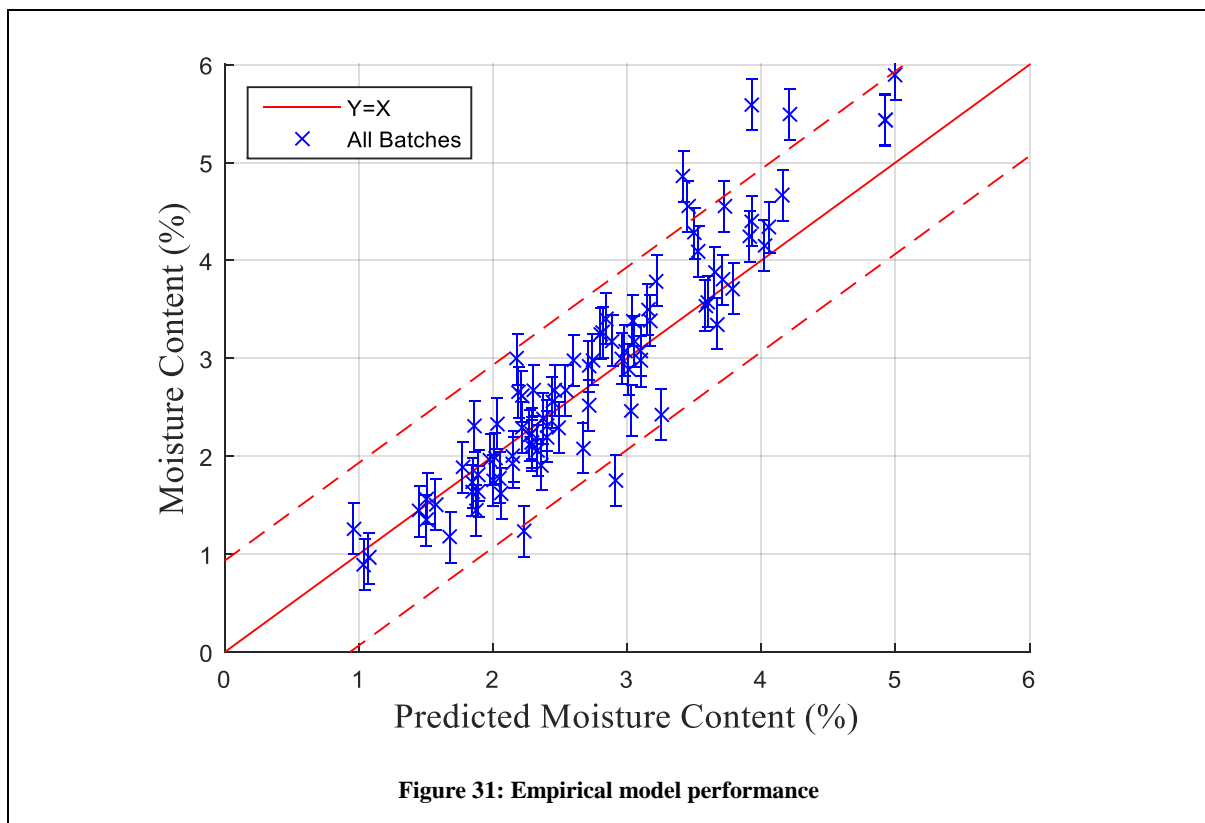
3 Mass Balance

3.1 Modelling Approach

To carry out a mass balance, all of the flows in and out of the process must be established.

Figure 32 illustrates the mass flows of air in and out of the process, and the mass flows of the slurry and powder. The air flows are depicted in red, and the slurry and powder flows are shown in green. All of the flows can be separated into three components; solids, water and dry air. For simplicity, it is assumed that solids do not leave with the air in the exhaust, and the air does not leave with the solids in the powder. In reality, small fines may exit with the air, and air can be entrained in the solids, however, as the amounts are negligible compared to the total mass flows, these have been assumed to be zero.

Figure 32: Mass Flows in and out of Spray dryer process, -- Air flow, -- Slurry flow
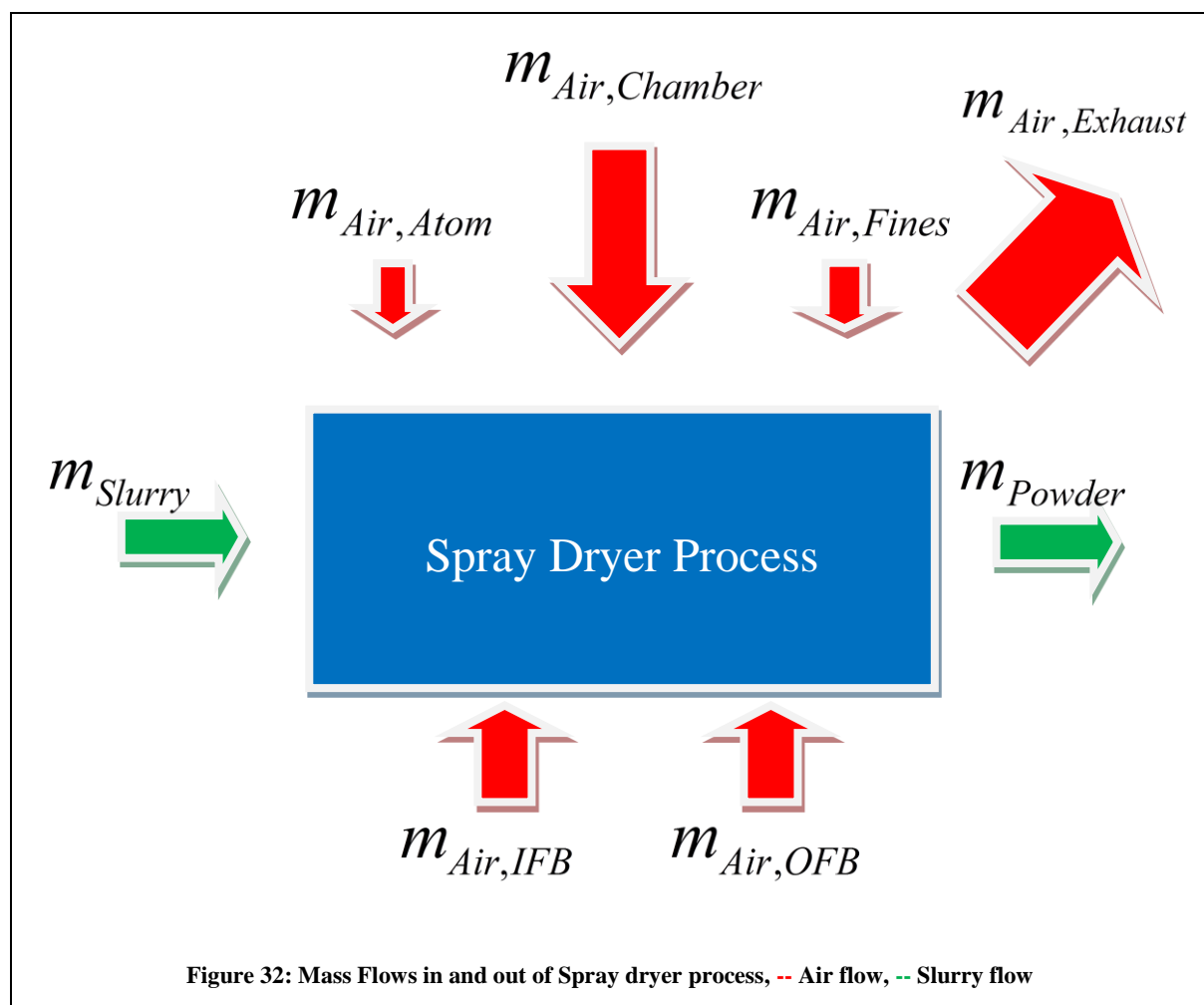
In order to split the flow streams into the different phases, humidity probes are used to measure the water content of the air. Moisture is estimated in the slurry and also measured manually for the powder. As the solid content in the air is assumed to be negligible, the air flow measured is represented by the two phases shown in Equation 40.

$$m_{Air} = m_{dryair} + m_{water}$$

<div align="right">**Equation 40**</div>

Humidity probes are used to measure relative humidity and temperature in order to estimate a mixing ratio (*MR*) which is then used to produce a ratio of kilograms of water per kilograms of air. Therefore, as in Equation 41, the water content can be expressed as:

$$m_{water} = m_{dryair} \cdot MR$$

<div align="right">**Equation 41**</div>

By substituting Equation 41 into Equation 40 and rearranging, Equation 42 and Equation 43 are generated to represent the phase flows in terms of the air flow measurement and the mixing ratio measurement.

$$m_{dryair} = \frac{m_{Air}}{(1 + MR)}$$

<div align="right">**Equation 42**</div>

$$m_{water} = m_{Air}\left(\frac{MR}{1 + MR}\right)$$

<div align="right">**Equation 43**</div>

The humidity probes are located on the chamber air flow inlet, the compressed air feed line and on the exhaust flow outlet of the dryer process. Assuming that the inlet conditions for the chamber and fluid bed air flows are the same, the humidity probe in the chamber inlet can be used to represent the fluid bed inlets. The humidity probe on the compressed air line is used to express the water content of the air flow used in the fines recycle line and air used for

atomization. For simplicity, the air flows into the process can now be reduced to two streams rather than five, as shown in Equation 44 and Equation 45.

$$m_{Air,1} = m_{Air,Chamber} + m_{Air,IFB} + m_{Air,OFB}$$

Equation 44

$$m_{Air,2} = m_{Air,Atom} + m_{Air,Fines}$$

Equation 45

The exhaust air flow is not measured in this process, so, by assuming there is no leakage in the process, the dry air flows in the exhaust is equivalent to the summation of the dry air flows in. The air phase mass balance is equivalent to that shown in Equation 46.

$$m_{dryair,1} + m_{dryair,2} = m_{dryair,Exhaust}$$

Equation 46

However, for the water phase, the water flows out of the process in two different streams. Water also flows in both the air flow and the slurry, so the water phase mass balance is as expressed in Equation 47.

$$m_{water,Exhaust} + m_{water,Powder} = m_{water,1} + m_{water,2} + m_{water,Slurry}$$

Equation 47

The water dried from the powder can be expressed in two ways; the amount of water removed from the slurry, and the amount of water gained by the air. The first way is expressed in Equation 48.

$$m_{water,dried} = m_{water,slurry} - m_{water,powder}$$

For the second method, by substituting Equation 46 into Equation 41 and using Equation 47, Equation 40 can then be used to obtain an expression for the water gained by the air in the process.

$$m_{water,dried} = m_{dryair,Exhaust} \cdot MR - m_{water,1} - m_{water,2}$$

This can now be related to the slurry and powder flows, to find an expression for the moisture content of the powder. As the solids content in the air is assumed to be negligible, and steady state production states that the accumulation term in the process is zero, the flow out in terms of solids must equal the flow in. The final mass balance in the solids phase is as expressed in Equation 50.

$$m_{slurry,Solids} = m_{Powder,Solids}$$

The total powder flow is not measured in the process, and is a function of the water content. Water content on a wet basis is expressed as a fraction of the total flow. The solids content is therefore the remainder of the flow, leading to the expression of the total powder flow in Equation 38.

$$m_{Powder} = m_{slurry} \left(\frac{1 - SMM}{1 - X} \right)$$

Using this representation of the powder flow to estimate the water content in the powder, Equation 48 can be rearranged to have an expression for moisture content in the powder

$$X = \frac{m_{slurry} \cdot SMM - m_{water,dried}}{m_{slurry} - m_{water,dried}}$$

<div align="right">**Equation 52**</div>

In Equation 52, the amount of water dried is calculated using Equation 49 during a batch.

3.2 Model Performance

The use of mass balances alone, without any input from the manual measurements, led to significant overestimates of the moisture content. This issue is discussed in section 5 of the Material and Methods chapter, in which a test on the spray dryer with water was carried out. It was found that an offset occurred when estimating the water content of the air. This offset changed with air flow and temperature, and also varied on a day to day basis. In this test, where only water was sprayed, the offset is likely to be the result of the accuracy of the water content measurement of the air. The humidity probe calibration certificates stated that the accuracy of the relative humidity measurement was ±1%RH. This measurement is used with temperature to estimate the water content in the air, using an internal calculation in the probe. The calculation mimics the use of psychometric charts to link the mixing ratio and relative humidity. As the temperature increases, so does the impact of the inaccuracy of the RH probes. In the temperature ranges seen in the process, the accuracy of the relative humidity relates to an error of 10% in the mixing ratio estimate. For a given batch, the total dry air flow would be approximately 430 *kg/hr*. Given that the target moisture content of the powder is 2.5%, then at a slurry rate of 45*kg/hr* the total water removed with an *SMM* of 30% would have to be 12.7 *kg/hr*. The mixing ratio estimated would be approximately 0.03*kg/kg,* and an error of 10% leads to ±1.3*kg/hr* of water. This equates to ±4% in the moisture content estimate, at a slurry rate of 45kg/hr. This is a significant issue that requires the introduction of an offset for the measurement. It may also impact on the precision of the models reliant on this estimate, as

changes are made to the process. At industrial scale the difference between air flow and slurry flow is similar with a 10:1 ratio. Therefore the errors are likely to have the same impact.

Other reasons for this offset include over estimating the water content in the slurry and the measurement of the slurry rate. Also, test results on the powder flow in the Material and Methods chapter, showed that the flow could change depending on how the spray dryer was operated. This highlighted that different steady states could be achieved in relation to the flow of slurry/powder through the process. However, on reaching the target particle size of $375\mu m$, the powder flow was consistent with the estimates from the mass balance, so if operated correctly the state should not change.

The slurry mixture moisture content (*SMM*) is estimated to be ±1% moisture content. At 45 *kg/hr* this equates to ±0.45 *kg/hr* of water, and, as the assumption of perfect mixing is used, the *SMM* is constant for the entirety of the trial. This provides an additional error of ±1.4% moisture in the powder at this slurry rate, helping to further explain the differences in accuracy between batches.

 It is clear that when the water content measurement of the air alone is used, an offset needs to be estimated. Over the 23 trials undertaken, the average offset was 3.6 *kg/hr* ranging from 1 to 6 *kg/hr* with a standard deviation of 1.1 *kg/hr*.

The mass balance can be calculated using two methods to describe the slurry rate in the process. Each method is shown in Figure 33 which illustrates how they compare to each other. A clear disadvantage of using the load cell mass balance was apparent during the trial, as noise around the load cell caused an over exaggeration in the moisture prediction between 41 minutes and 50 minutes. In general, using the pump correlation is the more advantageous, but the load cell becomes useful if poor mixing leads to significant changes in the slurry rate.

Figure 33: Typical Performance of Mass Balance
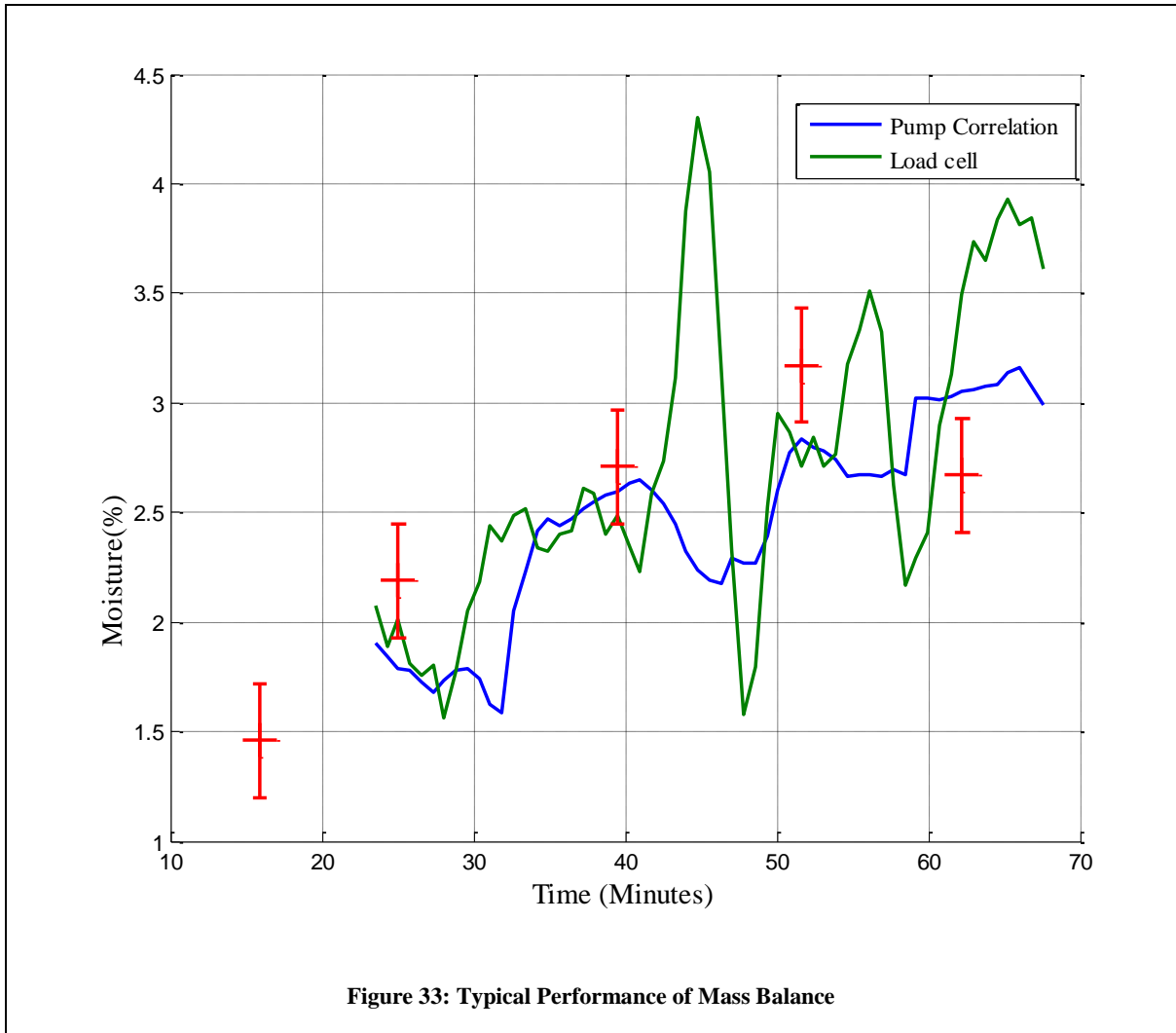
The prediction of moisture for the first batch of the day was significantly worse than that for the other batches. This is likely to be the result of the additional time needed to reach a steady state. The spray dryer needs to heat up sufficiently and flows need to stabilise which may take a significant time when the spray dryer has been idle for a significant amount of time. Because of this, the performance was assessed for all batches, without that of the first batch. The model uses an update for the offset of every measurement to enable the prediction of the next measurement. For the pump correlation, there is an average error of 0.65% moisture with a RMSE of 0.91% for all batches. By removing the first batch this was reduced to an average of 0.51% and RMSE of 0.66%. For the load cell, the average error more than doubled to 1.8%,

due to the noise in the measurement. Figure 34 depicts how mass balance performed using the pump correlation.

Figure 34: Mass Balance Performance
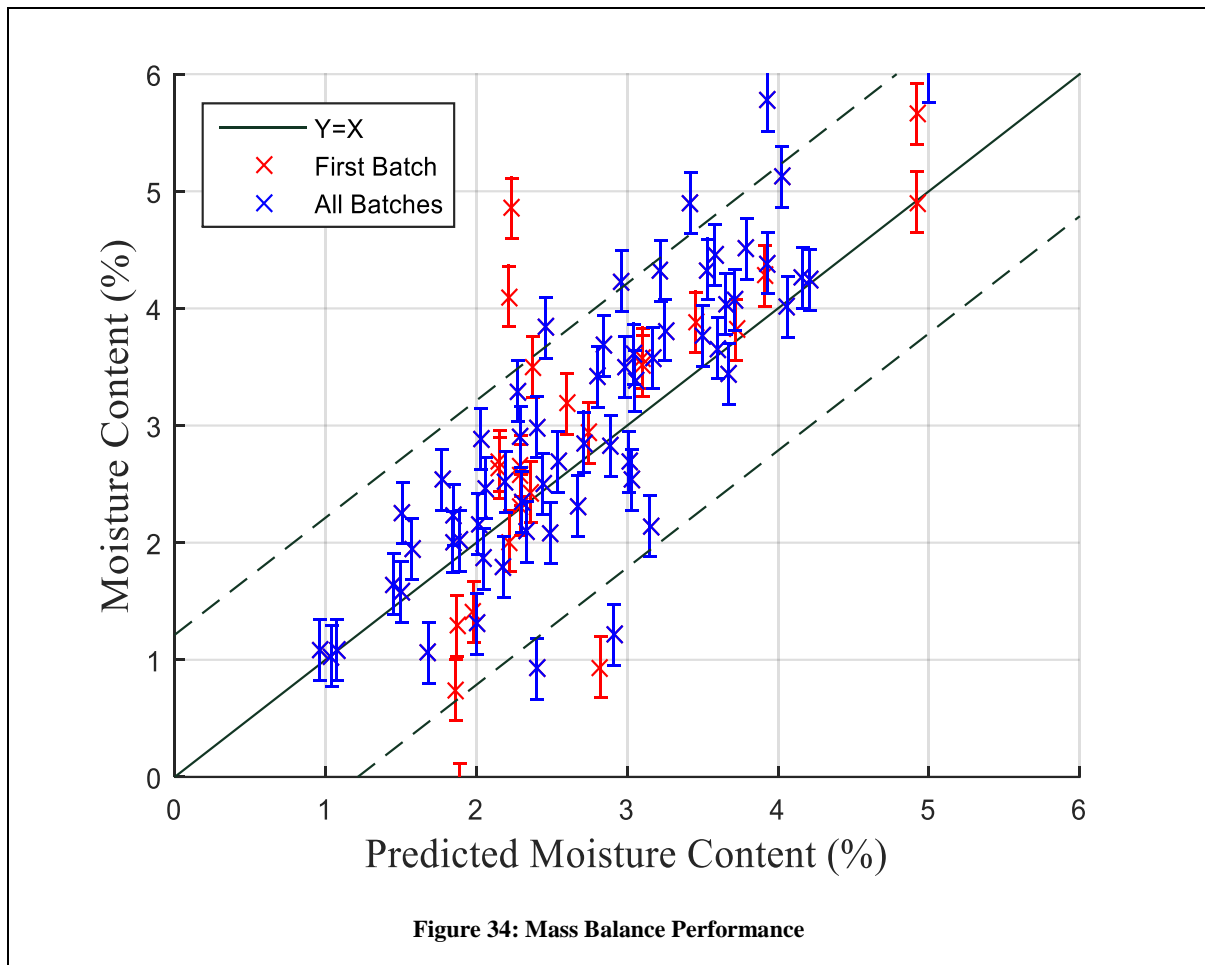
4 Heat balance

4.1 Modelling Approach

The approach for the heat balance is similar to that for the mass balance, with an additional term for heat loss. This is depicted in Figure 35.

Figure 35: Energy Flows in and out of Spray dryer process, , -- Air flow, -- Slurry flow, -- heat loss
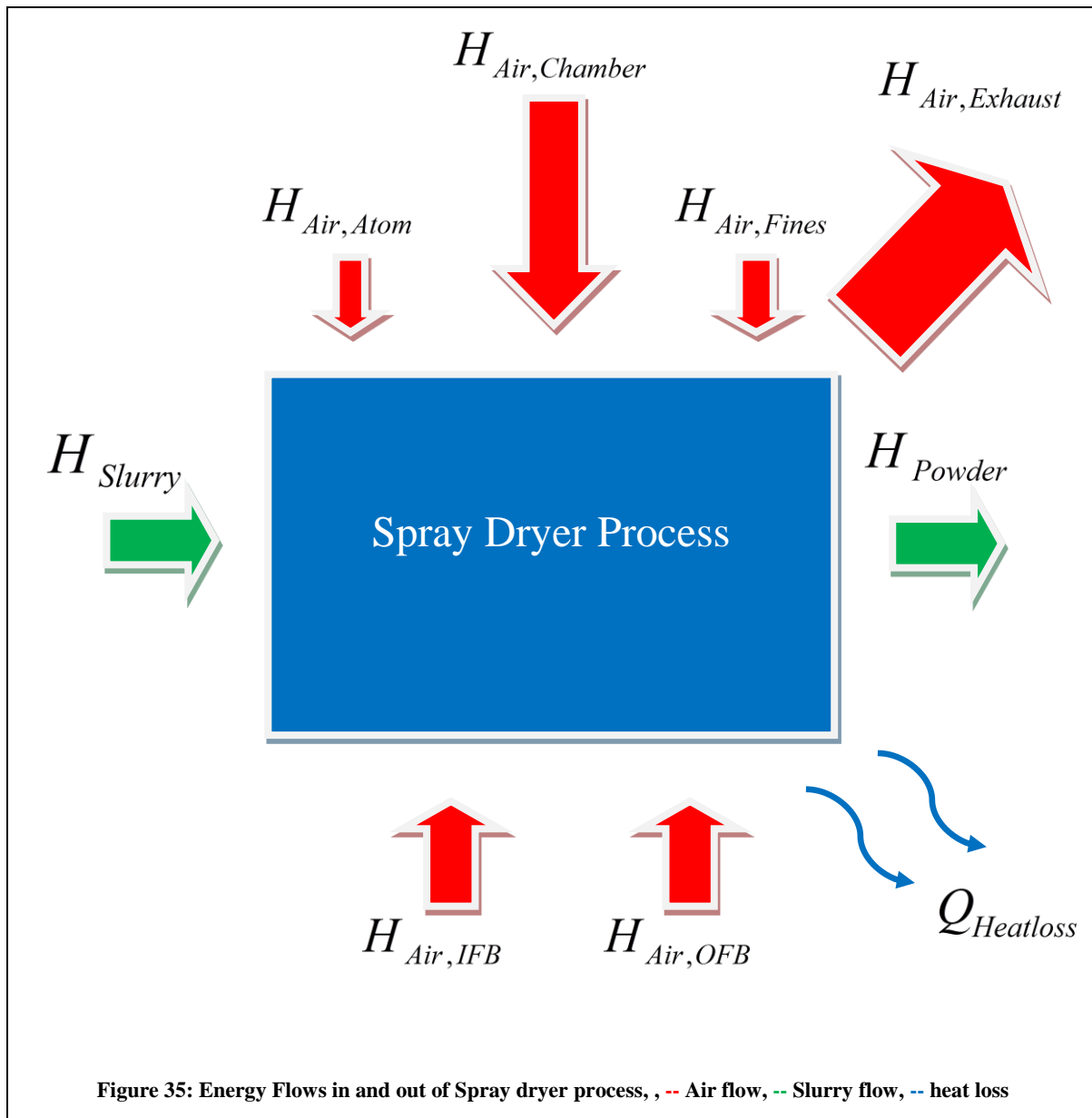
To carry out a heat balance, all of the mass flows from the mass balance are utilised to calculate the heat flows in the steady state overall heat balance, as expressed in Equation 53.

$$H_{slurry} + H_{Air} = H_{Powder} + H_{Exhaust} + Q_{Heatloss}$$

Equation 53

where $Q_{Heatloss}$ is the heat loss from the process

Again, each flow needs to be split into the three phases of solids, water and air. For the solids, liquid water and the dry air, the heat flow can be represented by the enthalpy in Equation 54.

$$H_{Solids/Water/DryAir,i} = m_i Cp_i \Delta T_i$$

Equation 54

The temperature of the stream is compared to a reference value to obtain the derivative. The slurry specific heat capacity Cp_{Slurry}, is assumed to be 1150 *J/kgK* following previous work to quantify it at *P & G*. For dry air and liquid water vapour, empirical correlations were fitted to tabulated data (The Engineering toolbox 2010) where the temperature is in degrees Celsius (^oC) for air and Kelvin for water.

$$Cp_{Air} = 1002.64 + 0.07114 \cdot T + 0.000214 \cdot T^2$$

Equation 55

$$Cp_{Water} = 2823.3 + 11.828 \cdot T + 3.5043e - 2 \cdot T^2 + 3.601e - 5 \cdot T^3$$

Equation 56

For water vapour contents, an addition of the latent heat of vaporization (λ) is needed to account for the conversion of liquid water to vapour. According to Hess's law, the end result is always the same, independent on the path taken, therefore the vaporization for the water already located in the air inlets, is assumed to occur at a reference temperature for all cases. Equation 57 is used to represent heat flows for the water vapours in the process.

$$H_{Vapour,i} = m_i(\lambda_{ref} + Cp_i \Delta T_i)$$

<div align="right">**Equation 57**</div>

The specific heat capacity is calculated using the empirical correlation stated in Equation 58 using °C .

$$Cp_{Vapour} = 1854.62 + 0.31707 \cdot T + 0.000509 \cdot T^2$$

<div align="right">**Equation 58**</div>

The latent heat of vaporisation at the reference temperature is calculated using another empirical equation expressed in Equation 59 which is a polynomial fitting for water vaporization between -25 and 40 °C (Rogers 1989).

$$\lambda_{ref} = 2500800 - 2360 \cdot T_{ref} + 1.6 \cdot T_{ref}^2 - 0.06 \cdot T_{ref}^3$$

<div align="right">**Equation 59**</div>

Each heat flow in Equation 53 can be represented by a combination of the equations for solids, water and air. However, the heat loss, $Q_{Heatloss}$ is unknown, and an additional measurement is needed to estimate it. The heat balance could use the estimate of water content in the air from the mass balance, in order to estimate the heat losses, but in steady state, heat losses are assumed constant. Therefore, a single measurement of the moisture content, during steady state in a batch, can be used to estimate the heat losses, and a new estimation for moisture content can be established without using the humidity probes. Steady state can be determined by assessing the process signals. If there is little variability in the temperatures and particle size produced and the inlet conditions haven't been changed it can be assumed a steady state has been reached.

Each manual measurement provides an estimate for the heat losses. Using this, the unknown variable, water removed in the exhaust, $m_{water,evap}$ is extracted and relates to the moisture content of the powder in Equation 60.

$$X = \frac{m_{slurry} \cdot SMM - m_{water,evap}}{m_{slurry} - m_{water,evap}}$$

Equation 60

4.2 Model Performance

For the heat balance to be used, the heat losses from the process must be estimated. To do this, manual measurements can be used, and assuming steady state, the heat losses should not change. Using the results from the 23 batches for analysis, the heat losses for the spray dryer process had an average value of 0.88W, this is on average 12% of the total heat added to the process. This value varied during and between batches with a standard deviation of 0.22W. As with the mass balance, the heat balance can be calculated using the load cell or the pump correlation to represent the slurry rate. The performance of the heat balance is illustrated in Figure 36. Out of all of the models, the heat balance tends to over exaggerate the effect of changing process conditions. The estimated moisture changes between measurements tend to be significantly higher than the changes estimated by the mass balance and the empirical models. This seems to be a result of incorporating more process measurements into the model. By adding these measurements, there are more sources of variability in the model. Any inaccuracies in the temperatures and the flows in the model are amplified leading to a more sensitive estimation.

The difference in the performance of the heat balance with the pump correlation estimate, and with the load cell was reduced using the heat balance. For the pump correlation, the average error in the estimation is 1.4% moisture with a RMSE of 2% for all batches. The load cell had an average error of 1.8% moisture and standard deviation of 2.5% moisture. Again if the first

batch is not taken into account, the error drops significantly to an average of 1% and RMSE of 1.5%, using the pump correlation. The performance is indicated in Figure 37 where there are significant outliers shown in the predictions.

The poor performance of the heat balance can also be related to the assumption that a single steady state has been reached for the process. The steady state assumption implies that the heat losses would remain constant for the entirety of the batch. During the first trial of the day, the heat balance performs very poorly. Not taking this batch into account improves the performance to an average error of 1.1% and decreases the standard deviation to 1%. This is due to the unit taking longer to heat up than expected in the first batch, so the heat losses vary significantly. The performance improves as the heat losses become more stable towards the end of the first batch, and in subsequent batches during the day. This improvement continues alongside the continual increase in the exhaust temperature throughout the batch. To further improve the performance, correlations would be needed to relate the changes in temperatures of the process to the heat losses in the process.
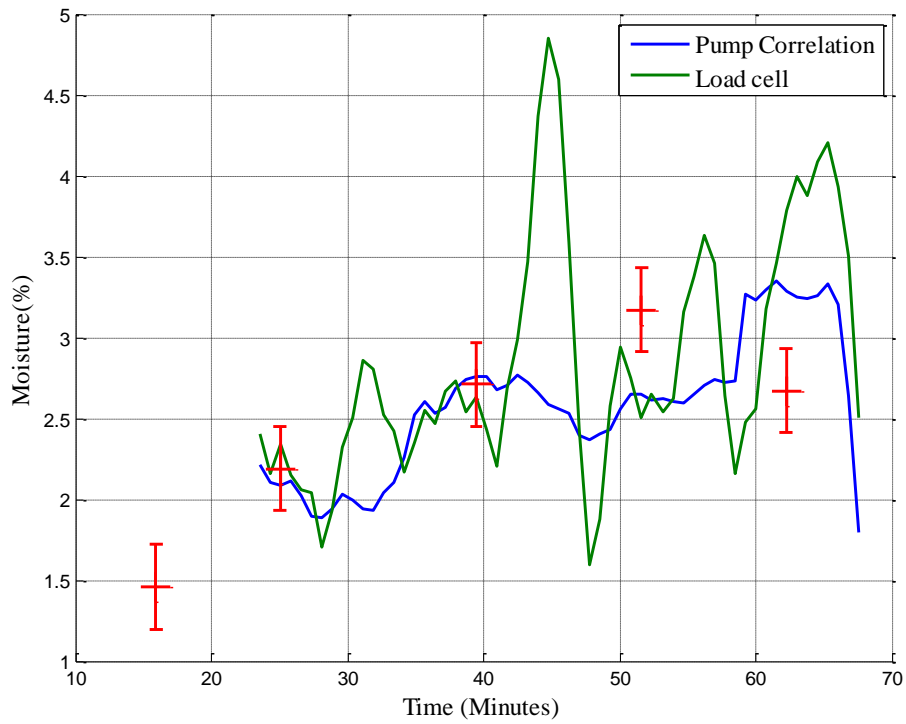
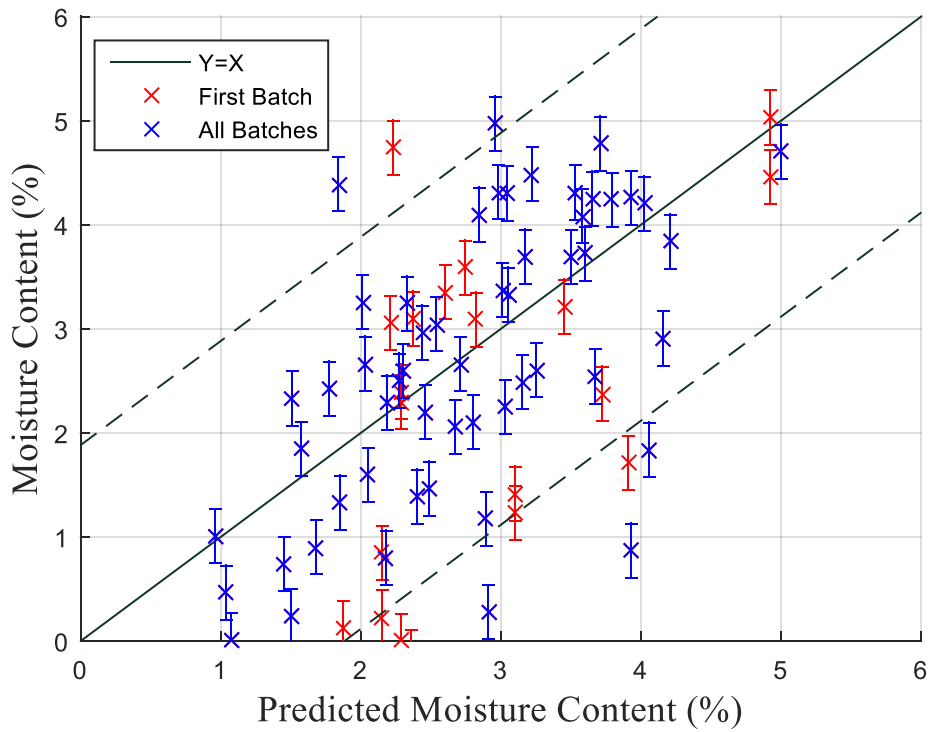**Figure 36: Typical Performance of Heat Balance**

Figure 37: Heat Balance Performance

103

5   Conclusions

For the three models tested, the empirical approach performs best over the 23 batches tested, with an average error of 0.35% moisture content. None of the models can be used without the use of measurements of the outlet conditions of the batches, so any studies into their performance cannot be carried out without implementation on the spray dryer process. The poorer performance of the mechanistic models can be related to two key issues. Firstly, the accuracy of the measurements and estimations used in the models provides significant sources of error. For the mass balance, these errors are addressed by incorporating an estimate of an offset for the water content leaving in the exhaust. For the heat balance, all sources of error impact on the estimation of the heat losses used to predict further changes to the moisture content. The second issue is the assumption of constant steady state conditions. When measuring powder flow rate, it was noticed that the state may change as a result of a change in atomization. This is more significant in the first batch as the unit fills with powder. The unit also takes more time to warm up for the first batch, so using a constant value for heat losses does not suffice. For the majority of batches, it can be seen that steady states are achieved, but by the time a manual measurement of moisture is made during this period, a significant proportion of the product would be lost. Understanding the impact of changing process conditions on the state of the process is necessary to improve on these models. With better understanding, the steady states could be achieved quicker, and maintained for longer, to ensure the quality of the product.

5. PARTICLE SIZE DISTRIBUTION

1 Introduction

Particle Size Distribution (PSD) plays a critical role in all aspects of the drying process and generally dictates how the dryer will perform. The size distribution provides the contact surface area in the dryer and determines the heat and mass transfer rates and their relative velocity to the air provide will help estimate the overall residence time. This means that, for a set air flow and temperature in the process, the amount of drying can vary significantly, impacting on other powder attributes. The initial droplet size distribution from the nozzle evolves throughout the drying process, eventually leaving as dried particles. The evolution of the droplets depends on transformations that can take place in the dryer, such as agglomeration, attrition and shrinkage. The influence of each transformation is dependent on the atomization and the process conditions, which can favour one transformation over another. The use of nozzles enables the manipulation of the initial droplet size distribution in order to control the PSD. The two fluid nozzles provide the flexibility to manipulate this, by altering the air flow fed to the nozzle. However, the result of the change in atomization on this process can only be measured in the distribution of the powder leaving the dryer. By studying atomization, the relevance of the other transformations can also be understood and the correct approach can be determined to minimize or utilise their role.

With more insight into how the PSD develops in the spray dryer process, the most appropriate strategy for particle size control can be recommended and reasons for deviations can be better understood.

2 Atomization Study

To analyse the initial droplet size distribution, a purpose built atomization rig was utilised to mimic the atomization from the process, and provide a measurement using laser diffraction.

Details of the rig and modifications made are discussed in the materials and methods chapter. In summary, the slurry is stored in the pressurized, jacketed mixer that aims to provide the same conditions of the mixers used in the spray dryer process. It is then fed to a syringe in which the total volume of slurry to be sprayed is stored. The set volume of slurry for the experiment is then sent to the nozzle, at a set flow rate or pressure, and the spray is measured at a fixed distance away from the nozzle exit using laser diffraction. A modification was made in order to use the twin fluid nozzle. As the spray was measured at a fixed distance, the length of the nozzle was limited. The original nozzle is depicted in Figure 38 and the laser diffraction was measured $0.3m$ away from the nozzle fitting. After consulting the manufacturer, it was assumed that shortening the length would not impact the spray produced, and the length was reduced to $0.075m$ as seen in Figure 39. A slight concern is that the shortened distance to the laser diffraction measurement may have an impact. It is possible that the slurry may still be in transition from the bulk liquid to atomized droplets.

The laser diffraction measurement of the spray produced, enabled estimation of numerous characteristics about the distribution of droplets. The cumulative particle size values, such as the mean particle size ($D_{v,50}$), are all estimated along with a number of other important characteristics. The sauter mean diameter ($D_{3,2}$) is a significant characteristic of the spray used in drying, this is measured and used to calculate the contact surface area. Because of its importance in heat and mass transfer, correlations have been produced in literature (Mulhem et al. 2004a; Lipp 2000) to predict the value of the average size as a function of the air to liquid mass ratio, fed to the nozzle.
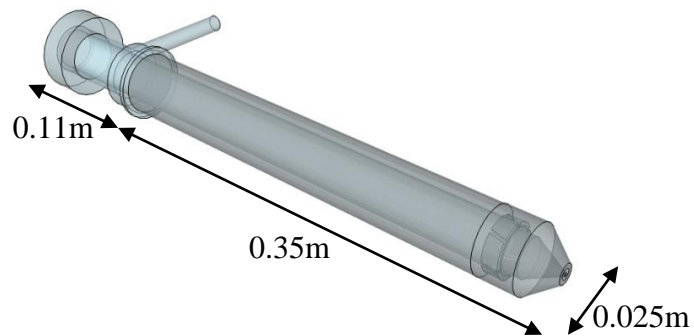
Figure 38: Two Fluid Nozzle Dimensions
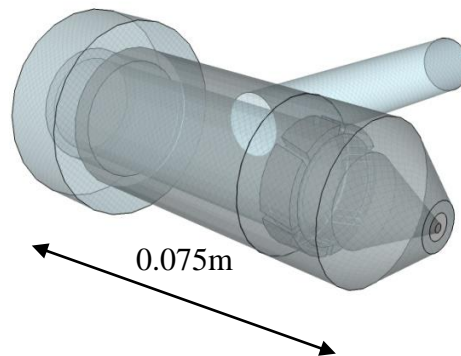
Figure 39: Nozzle Modification

It was found that the estimate of $D_{3,2}$ from the laser diffraction was much more consistent compared to the, $D_{v,50}$ which can vary significantly under the same conditions. This is due to the dependency of $D_{v,50}$ on the larger droplet sizes, which are measured significantly less frequently than smaller sizes droplets. $D_{3,2}$ is much more dependent on the sampling frequency,

and so the impact of larger particles is diluted by the frequency of the smaller particles. Further reasons for variability in the measurements are described in section 4 of the Material and Methods chapter.

For each spray, an average value of the $D_{3,2}$ was taken over the time period in which the air flow fed to the nozzle was constant. For each experiment, the air flow to the nozzle was available for 30 seconds, in which the target air flow was usually reached after 15 seconds. A fixed volume of slurry was also used for each experiment. This meant that the window to average the $D_{3,2}$ of the spray reduced as the slurry rate was increased. For 30 and 40 *kg/hr* slurry rates, this region lasted for up to 7.5 seconds, but for 50 *kg/hr* this was 2.5 seconds. The measurements of the spray occurred every 0.05 seconds, and all results were stored in data files in the INSITEC RTSizer software package. After each experiment, the data was displayed as seen in Figure 40. This tool also enabled the user to select a region in order to produce an averaged distribution, as seen in Figure 41, or export all of the data recorded via text files. The air flow, nozzle pressure and piston speed, were all measured separately and stored in text files.
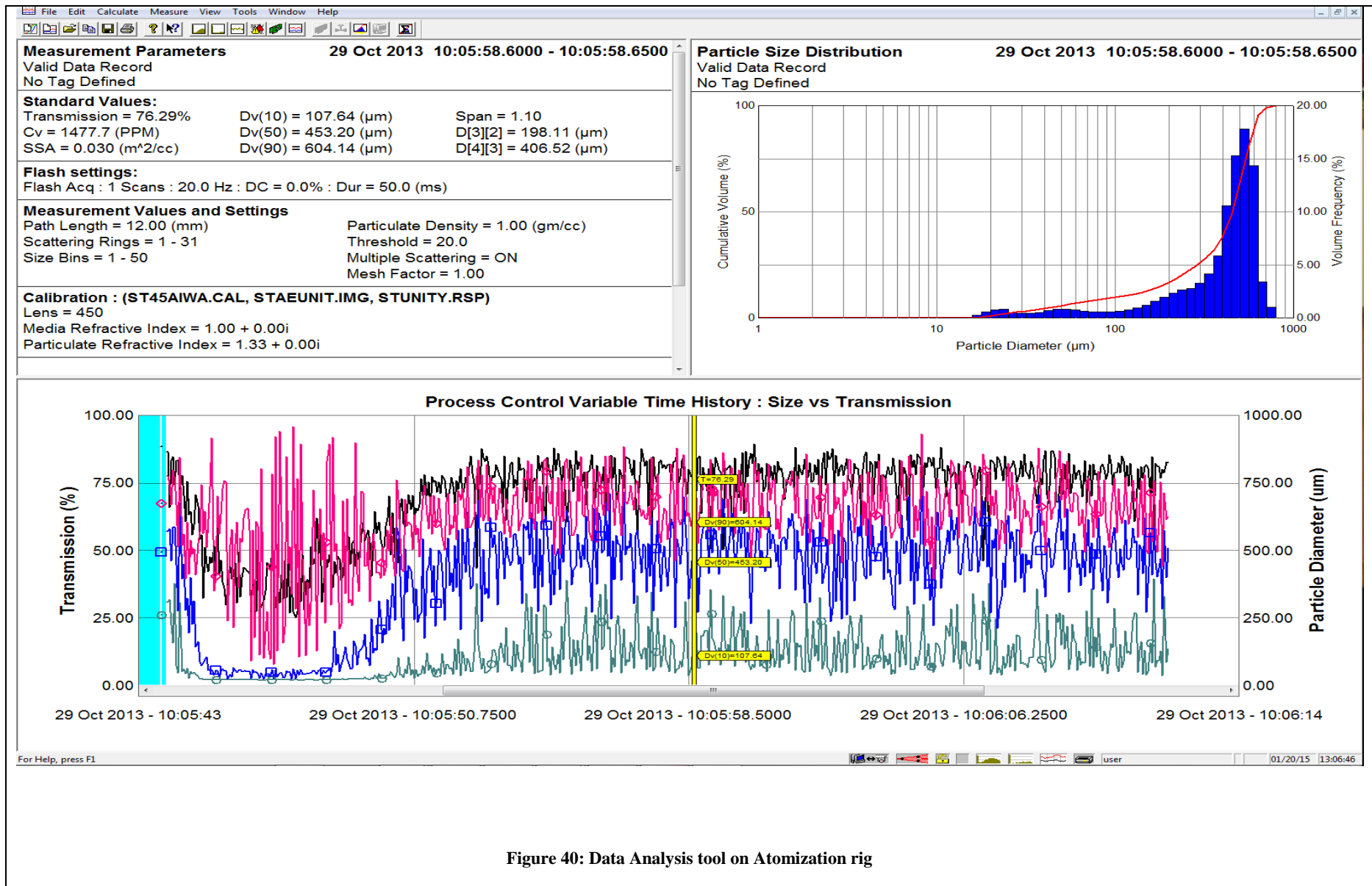
Figure 40: Data Analysis tool on Atomization rig

110
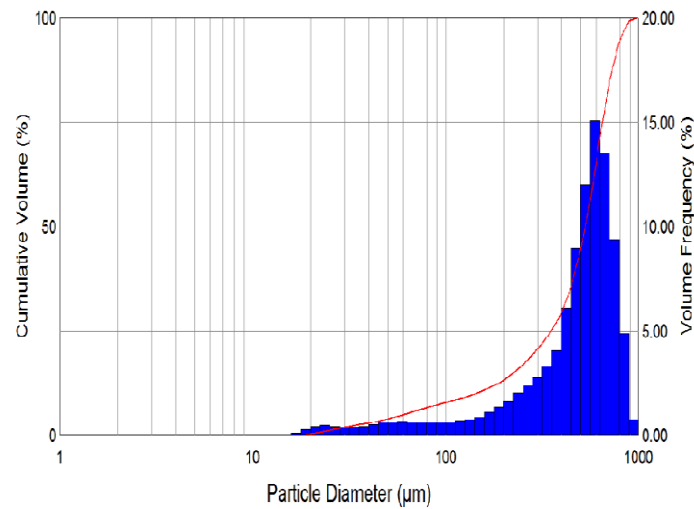
Figure 41: Averaged Distribution under stable conditions

To enable quicker analysis, MATLAB was used to sort all of the data into structured variables containing all the necessary information. With all the data available, the correct region and its corresponding values could be extracted to ensure that the correct results are used to represent the set conditions. With the region chosen, analysis was also made to ensure that the slurry flow was constant during the spray. Common processing issues including blockages, sedimentation, gelling and lack of slurry in the mixer which could be checked by analysing the piston speed and nozzle pressure. Figure 42 illustrates how, through a combination of data, one can see how the changes in air flow relate to the measurement of $D_{3,2}$. In this case, water was sprayed at a flow rate was 40 kg/hr, the air flow of 4.8kg/hr and the $D_{3,2}$ was averaged to 231μm. Figure 43 depicts the operating conditions; each has been averaged over a second to reduce the noise in the measurement, and they indicate that nothing occurred during the run that would have had a significant impact on the measurement. The run is at a very low pressure as water was being sprayed, however, small changes in the piston speed, especially during the last 7 seconds when air flow is constant, were the cause of the variance in the measurement of the MPS.

111
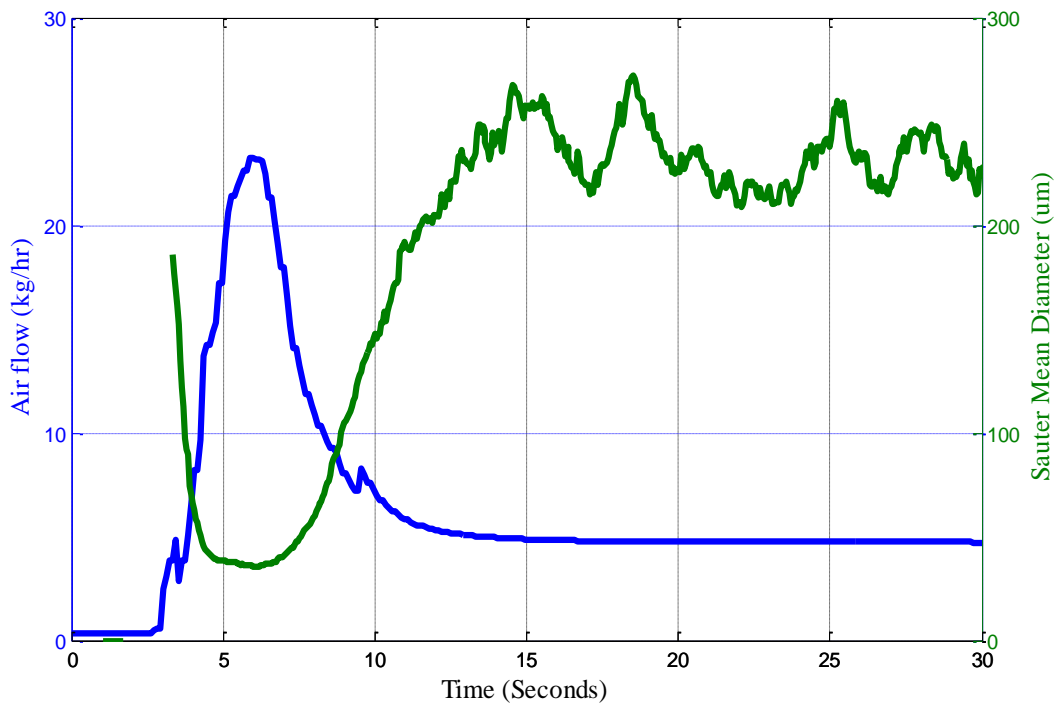
Figure 42: Illustration of how D$_{3,2}$ changed with Air flow
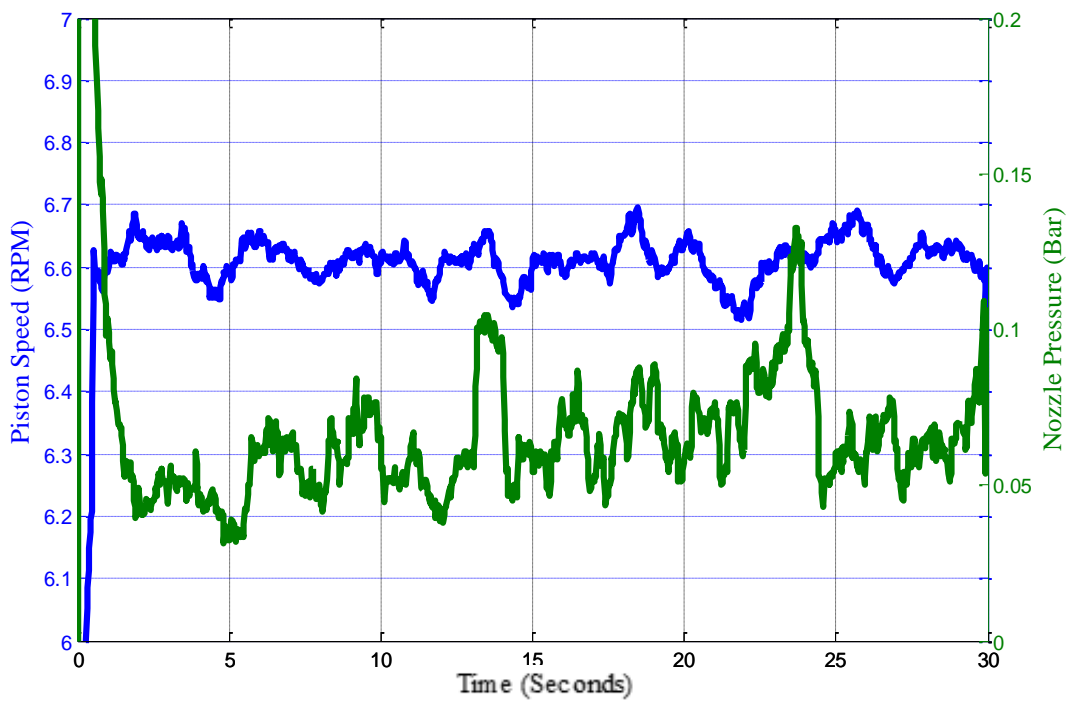
Figure 43: Check of operating conditions during run

2.1 Atomization Results

2.1.1 Spraying Water

Numerous runs were carried out on the atomization rig to assess the relationship between the air flow, fluid flow and the characteristic particle sizes. The recommended method for changing the particle size distribution using this nozzle, is to manipulate the mass ratio of the gas and liquid feed. To begin with, the nozzle was tested using water as the fluid to be atomized. Water is advantageous because it has been used for validation in the models recommended in literature (Mulhem et al. 2004b). The models and there definition are discussed in the literature review. An example of a model for twin fluid nozzles in literature is shown in Equation 61 (Mulhem et al. 2004a):

$$\overline{D_{3,2}} = 0.21 d_L \cdot (Oh)^{0.622} \cdot (\text{Liquid to Air Ratio} / We)^{0.4} \qquad \textbf{Equation 61}$$

In this model, the Ohnesorge number is constant for a given liquid under set conditions. The use of the constant 0.21 in the model is based on fitted correlations that depend on solid concentrations and particle shape. This may not apply for complex slurries so a simplified approach has been taken in Equation 62. The constant *A* now represents the combined influence of the viscous forces and the nozzle characteristics.

$$\overline{D_{3,2}} = A \cdot (\text{Liquid to Air Ratio} / We)^{0.4} \qquad \textbf{Equation 62}$$

To calculate the Weber number, the initial velocities of the air and water are needed to calculate the relative velocity. To estimate this, the diameter of the nozzle tip (2mm) and the outer chamber (5mm) are used to calculate the area at the exit of the nozzle, and the volumetric flow is derived using the density of the liquid and air. Figure 44 shows how the estimated Sauter mean diameter, $D_{3,2}$ relates to the proposed function from literature. Three different

water flowrates were supplied to the nozzle and the air flow was manipulated for each. The error bars depict one standard deviation of the measurements that were averaged for a single run. The variance is quite large, but repeated runs showed that only small changes to the average occurred. The model fitting provided an RMSE of 22.3 μm and R^2 value of 0.94. The fitting accuracy appears to be impacted by changes in the liquid flow rate, especially at lower sizes (high air flow). This could be a direct result of the variance in the measurements, which was noted to be related to the piston speed. As the liquid rate is decreased and the variability in the piston speed remains the same, the impact will become larger, leading to more variability at lower liquid flow rates. The piston is designed for much larger flow rates so its accuracy may not be sufficient at these flow rates. In general, the trend remains the same when the liquid flow rate is changed. This means the impact of changing the air flow on the ratio will remain the same. However, it shouldn't be assumed that $D_{3,2}$ will remain constant if the value of this function is maintained during changes to the liquid rate.

Figure 44: Droplet size changes as a result of manipulation of the liquid to air mass ratio at different water flow rates
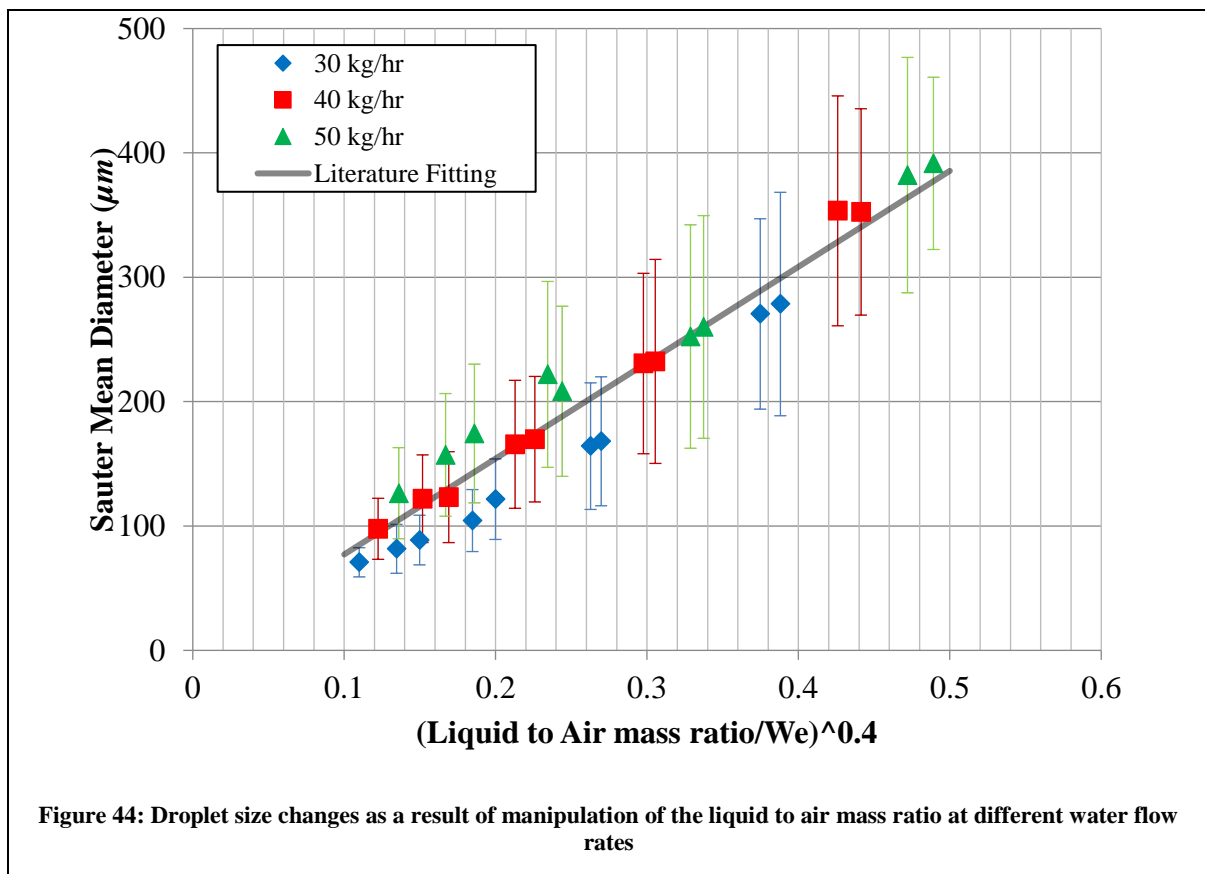
Calculation of the Weber number relies on an estimate for the surface tension of the liquid, which can be difficult to estimate for slurry. The use of this model may be an unnecessary complication for use in control if the effect of changes in air flow rate alone can be modelled by a simple equation. Figure 45 illustrates how particle size changes as the air flow rate is manipulated. In each case the water flow rate was set and the control loop on the air flow reached the target air flow for the experiment. It can be seen that the different water flow rates provide three different trends. The difference between each trend remains roughly constant throughout, with the increase in liquid flow rate shifting the trend upwards. The rate of change in particle size increases as the air flow rate is reduced. During operation of the spray dryer, the powders sauter mean diameter ranges from 200 μm to 400 μm. The same range has been used for the droplets assuming the size of droplets doesn't change significantly after atomization. Using the closest manual measurements to this range, the linear gradient for each water flow rate as they increase are -9,-10.1 and -10.9 per reduction of 0.1 kg/hr in air flow rate. This lack of difference in the gradient over the range could mean that a simple linear relationship with air flow rate may suffice for modelling changes in the particle size. In general operation it is preferred to maintain the liquid flow rate and therefore the capacity of the dryer. Changing the liquid flow rate will also have a greater impact on the amount of drying required.

Figure 45: Changes in droplet size with air flow rate
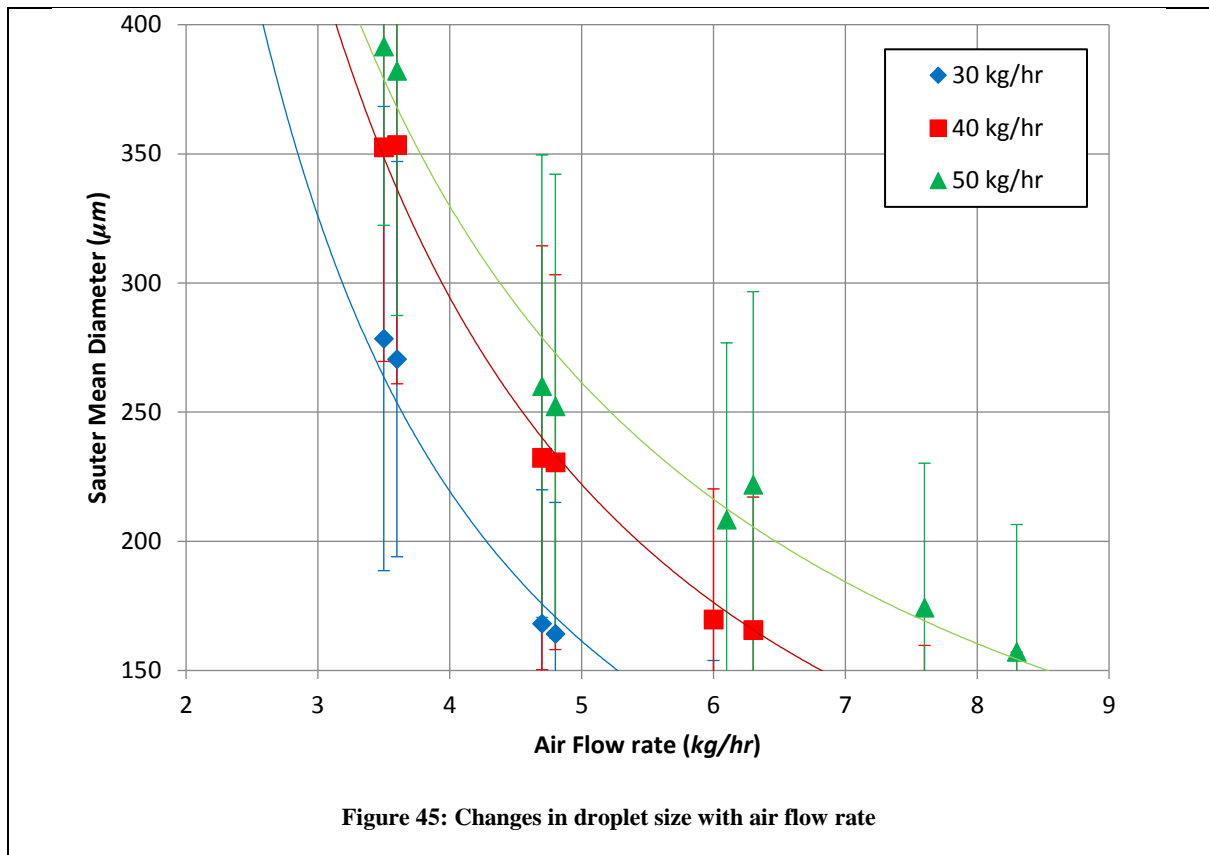
2.1.2 Spraying Slurry

According to the model in Equation 61, the difference between spraying water and slurry should be the increased impact of the viscous forces and lower surface tension on the spray produced. It should also be noted that the water should be more homogenous with less complex properties. This should increase the value of constant *A* and the influence of the Weber number. Figure 46 illustrates the effect of ratio changes on the droplet size at different slurry flow rates. The model fitting provided an RMSE of 36 μm and R^2 value of 0.82. It is clear that the variability increased as more complex liquids were atomized. In general, the variance in the measurements increases as higher slurry rates are used. This is clear with 40 *kg/hr*, where measurements at *(slurry to air ratio/We)^0.4* values around 0.1 provided a range of $D_{3,2}$ from 150 to 250 μm. It also seems that the values of $D_{3,2}$ plateau at a value around 370 μm after 0.15 on the x axis. This could be a limit for the atomizer, as no further measurements could be

116

recorded at lower air flow rates. When comparing this to water the larger sizes are reached at much lower values on the x axis, this is because the value of the constant *A* is three times larger

Figure 46: Droplet size changes as a result of manipulation of the slurry to air mass ratio
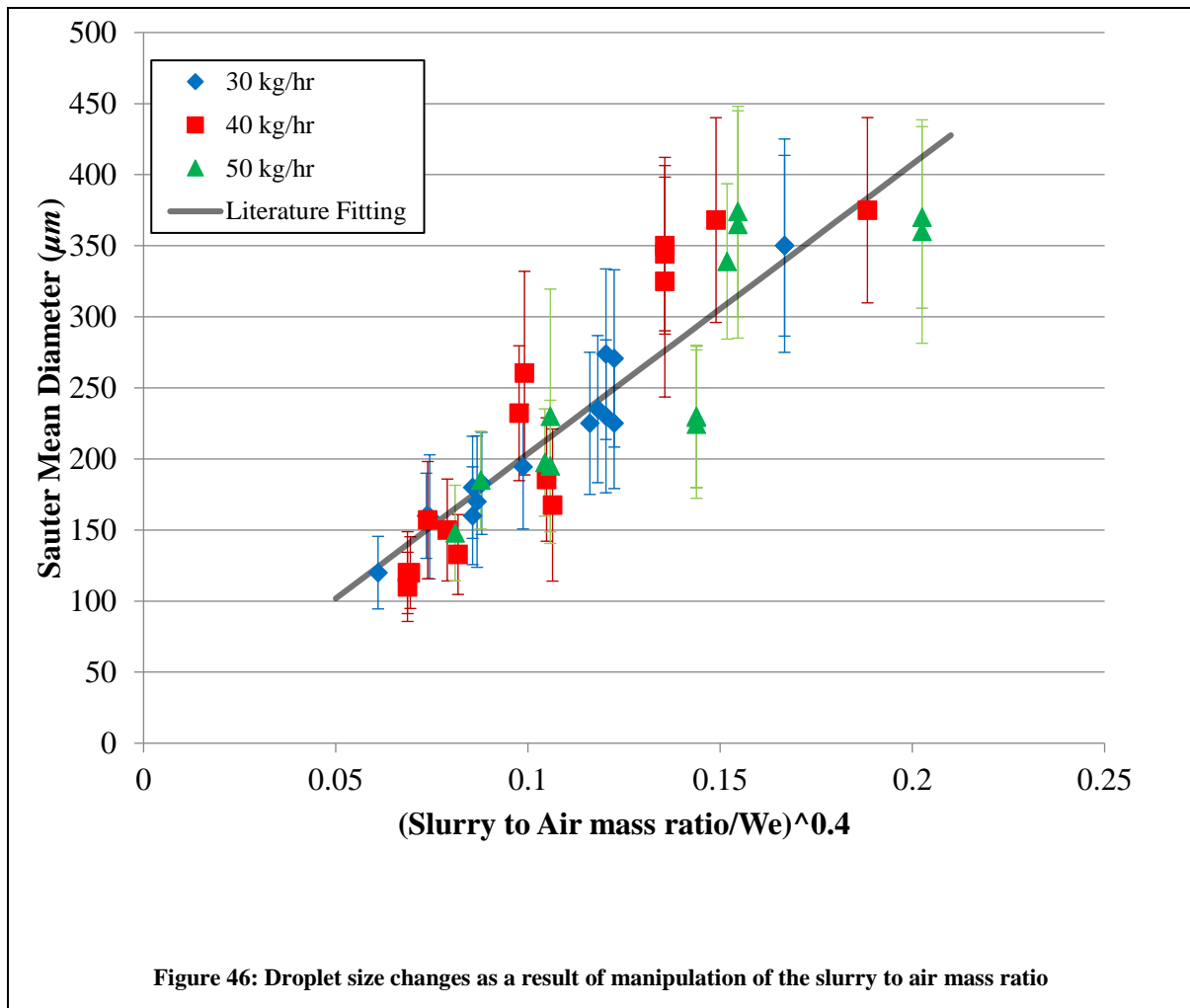
Figure 47 shows the change in the $D_{3,2}$ in relation to the air flow rate. It becomes difficult to distinguish between different slurry rates as the measurements overlap, this is not the case with water. However, the general trend remains the same as with water when the air flow is manipulated. The overlapping is due to an increase in variability as the slurry plays a more critical role in the atomization. This could be as a result of numerous sources of variability such as the slurry handling. A large source of variability is attributable to the supply of the slurry to the experimental rig. The slurry was transported from the main batch mixer to the rig via 3 *kg* containers and then stored in an oven. During transport, there was no control over the

environment surrounding the slurry and no agitation to suspend the slurry took place. The slurry was also poured into the mixer before closing the system. A possible issue is sedimentation over time, which would lead to variation between runs and a change in aeration of the slurry. The mixer agitator would remix the slurry to make it more consistent but product could have been lost in the containers and it cannot be guaranteed that once separated the slurry will become homogenous again. Ideally the slurry would have remained in the mixer until needed for the runs which take a maximum of 10 minutes per 3kg container. Another potential source of variability is blockages in the rig pipelines. Whilst spraying, the nozzle can block regularly due to slurry build up. Such a build up would impact on the flow of slurry in the process. To clear a blockage, water is pumped through the process until the operator has decided that the pipeline is clear. This changes the conditions inside the pipes, which could impact on the exiting slurry rate and therefore the atomization.

Figure 47: Changes in particle size of slurry with Air flow rate
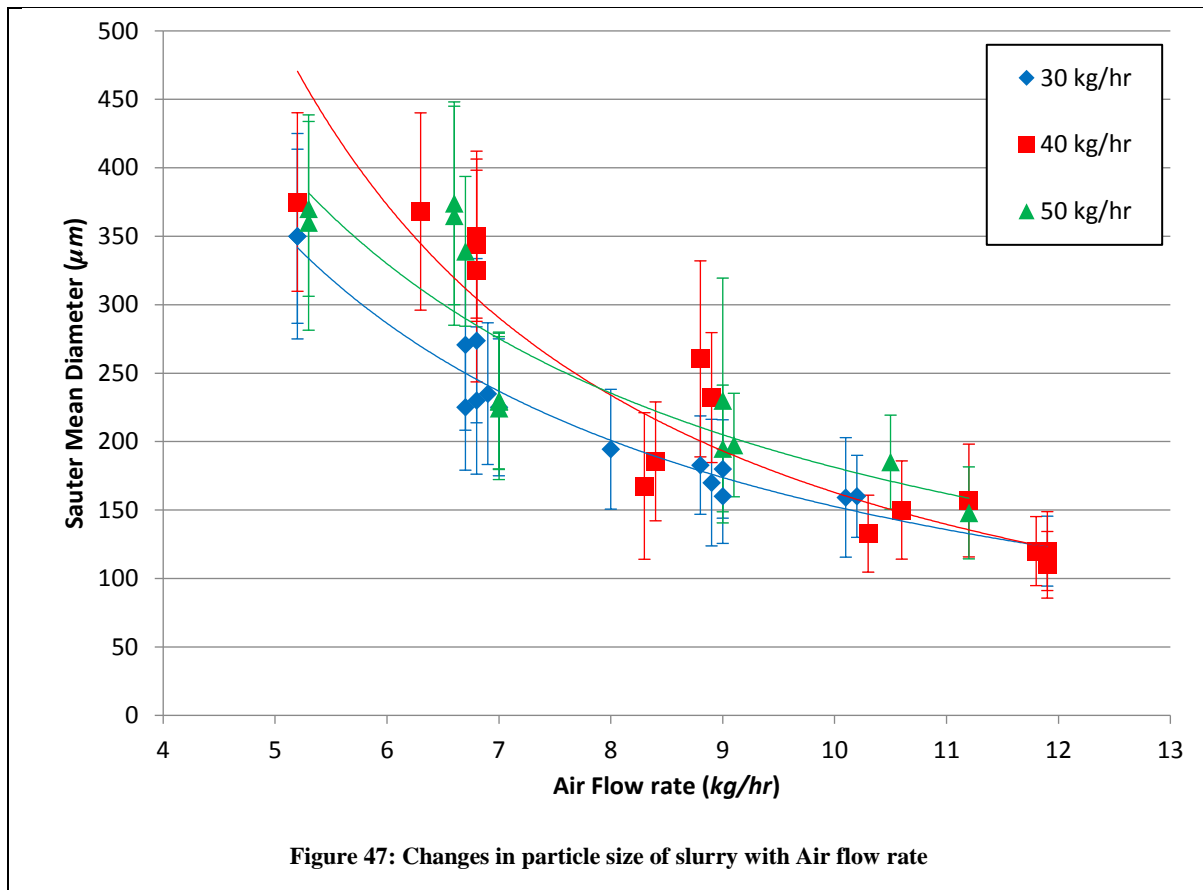
2.1.3   Spray vs Powder

The slurry used in the experiments was produced on the small scale dryer at slurry rates of 40 *kg/hr* and 50 *kg/hr*. Figure 48 and Figure 49 compare the droplet and powder sauter mean diameters produced, using the same initial conditions and slurry rates. The average value of $D_{3,2}$ for the powder was calculated from the image analysis technique used on the dryer at constant air flow rates. It is important to note that this analysis compares two different methods to measure the particle size distribution, so the final values may not necessarily be the same. However, you would expect them to follow a similar trend. At both slurry flow rates, the trends agree, following a linear increase in $D_{3,2}$ in respect of the proposed function. The gradient of change reduces at higher slurry rates when it should be equivalent. This finding suggests that matching this function value would not create the same distribution, as the results indicate that it becomes more difficult to atomize the spray at higher slurry rates.

Figure 50 and Figure 51 compare the atomization trends of the powder at different slurry flow rates. In both cases, the rate of change in $D_{3,2}$ is the same for the powder and the droplets at the flow rates measured. This indicates that the influences of other transformations whilst changing air flow to the nozzle do not change. As the powder size is larger than the droplet size at 50 *kg/hr*, this could indicate that more build up occurs, however, due to comparison of two different techniques, this would be difficult to quantify.

2.2   Conclusions

The proposed model from the literature provides a method to estimate the change in $D_{3,2}$ for water and slurry but simpler models would suffice. There are numerous additional sources of variability which are assumed to be the cause of the reduction in performance of the model when estimating the spray characteristics for slurry. These are mainly related to slurry handling. The results indicate that the change in liquid flow rate may have a larger impact, meaning that if the aerodynamic conditions are matched, the same size droplets are not necessarily produced. This has also been hypothesized in the literature (Thybo et al. 2008). However, for the experiments carried out, this could simply be as a result of the variability in the measurements made. The powder measurements carried out under the same conditions, followed the same trends at different slurry rates. This indicates that the impact of other transformations is constant whilst making changes to the atomization.

The experimental data suggests that the ratio model should be applicable for use in controlling the particle size distribution. However, it is also plausible to use air flow alone, as the gradient of change in the range of distributions produced on the unit does not differ drastically.
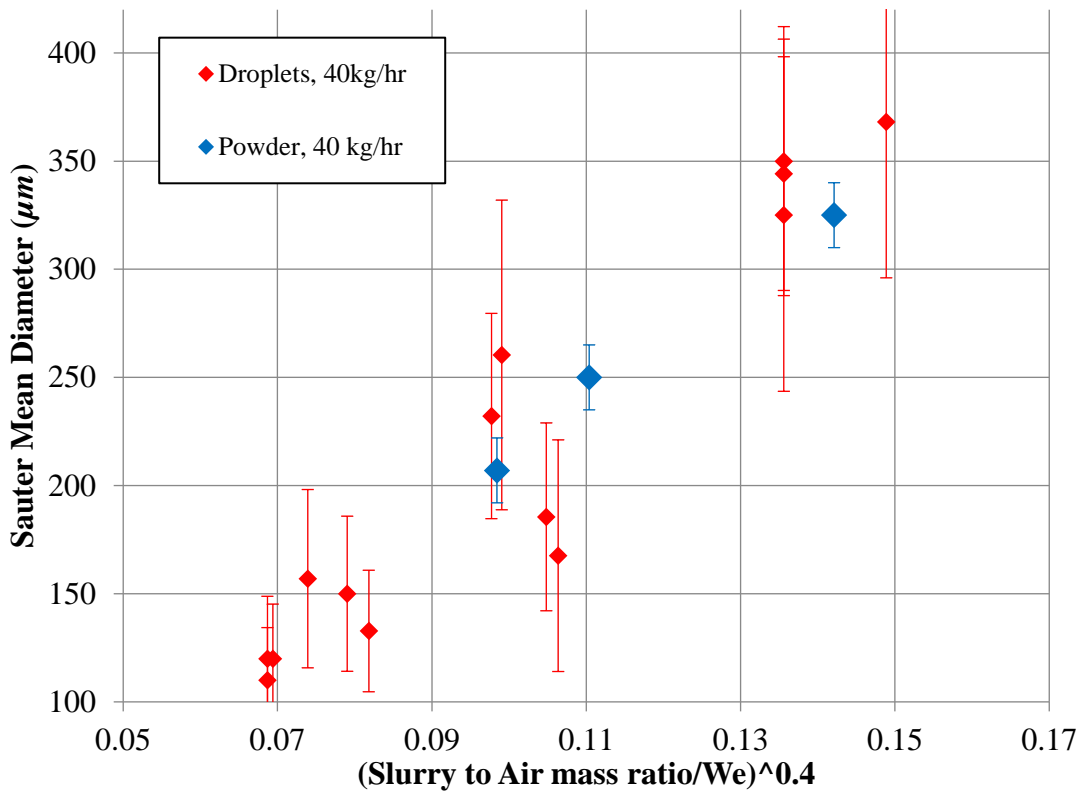
Figure 48: Comparison of droplet and powder measurements for recommended literature fitting at 40 *kg/hr*
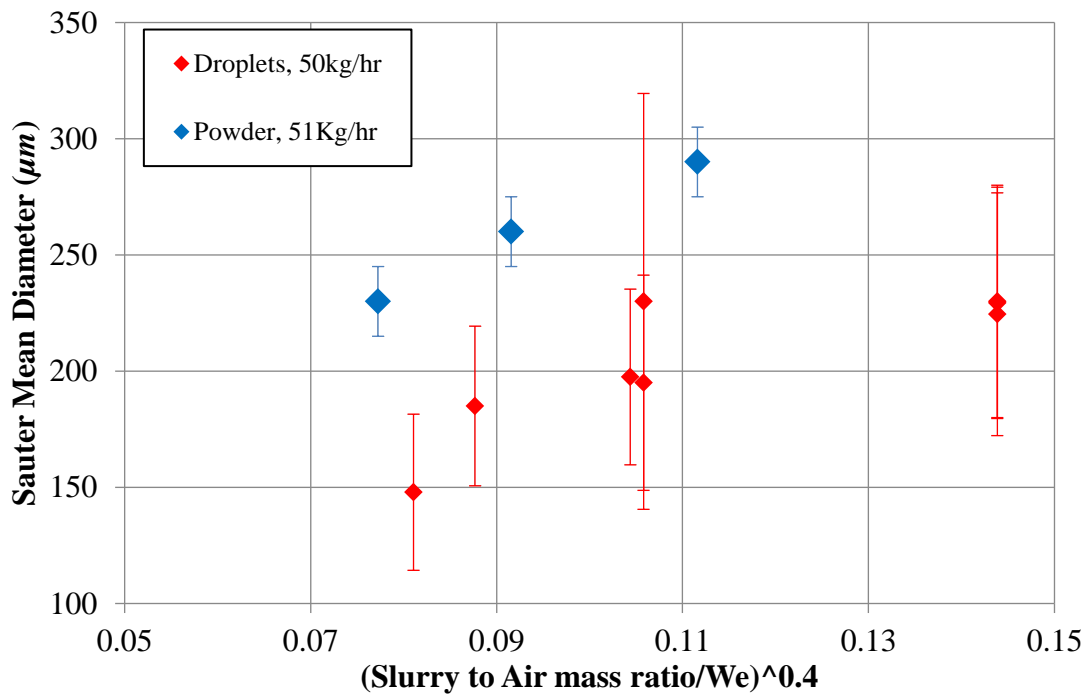
Figure 49: Comparison of droplet and powder measurements for recommended literature fitting at 50 *kg/hr*
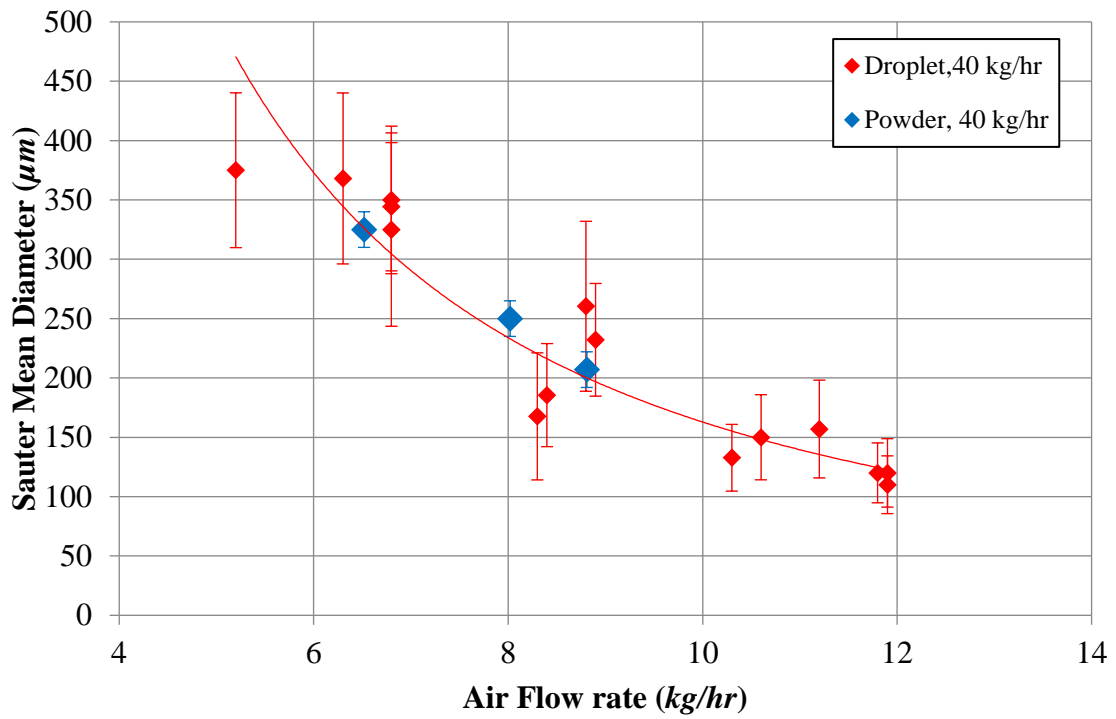
Figure 50: Comparison between Droplet & Powder measurements at a slurry rate of 40*kg/hr*
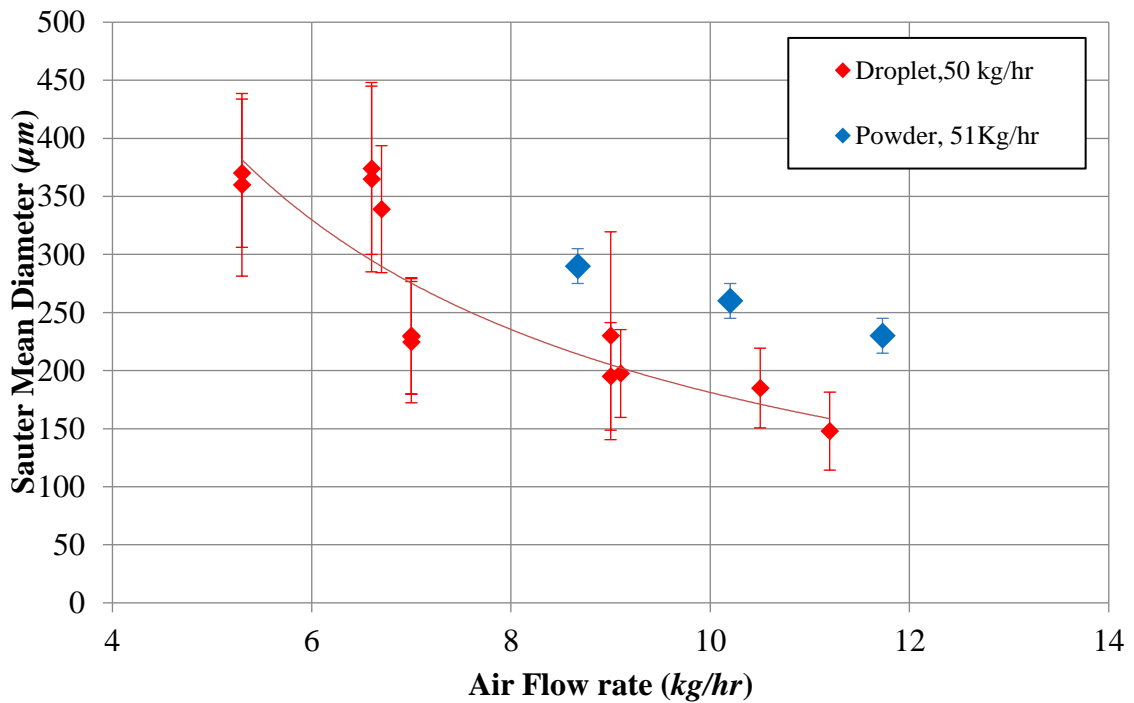
Figure 51: Comparison between Droplet & Powder measurements at a slurry rate of 50*kg/hr*

3 Control of the Powder Particle Size distribution

Ratio control has already been implemented on the spray dryer unit, as it was recommended by the supplier of the nozzle (GEA 2013). Manipulation of the ratio is carried out manually by the operator, as it is assumed that if the ratio is maintained, then the atomization will remain the same. In order to implement cascade control, additional simulations were carried out to tune the control loop.

3.1 Cascade Control

Cascade control has been utilised in the past to control characteristics of the droplet size distribution (Allen & Bakker 1994). The cascade loop is a combination of two feedback loops, where one "slave" loop is controlled by a "master" loop that sets the desired value of the output. The "slave" loop refers to the feedback loop which is used to change air flow to the nozzle by opening and closing a valve on the air inlet stream. The master loop is the feedback of the error in the MPS from measurements made at the exit of the spray dryer, which is manipulated to provide the set point for the air flow that runs the slave loop. The performance of the cascade loop depends on the slave loop having faster dynamics than the master loop, which in this case is true, as the changes in air flow are much quicker than the spray dryer process. The basic flow diagram for the cascade loop is illustrated in Figure 52, where there are two processes, $G_A(s)$ for the actuator or air flow valve, and $G_p(s)$ for the spray dryer process. There are two manipulated variables, the air flow rate, $F_{Air}(s)$ and the valve position, $V(s)$, two methods to measure the outputs which are a flow meter, $F_m(s)$ and the Camsizer, $C_m(s)$ and two controllers, $G_{C,1}(s)$ and $G_{C,2}(s)$.

Figure 52: Cascade Loop flow diagram
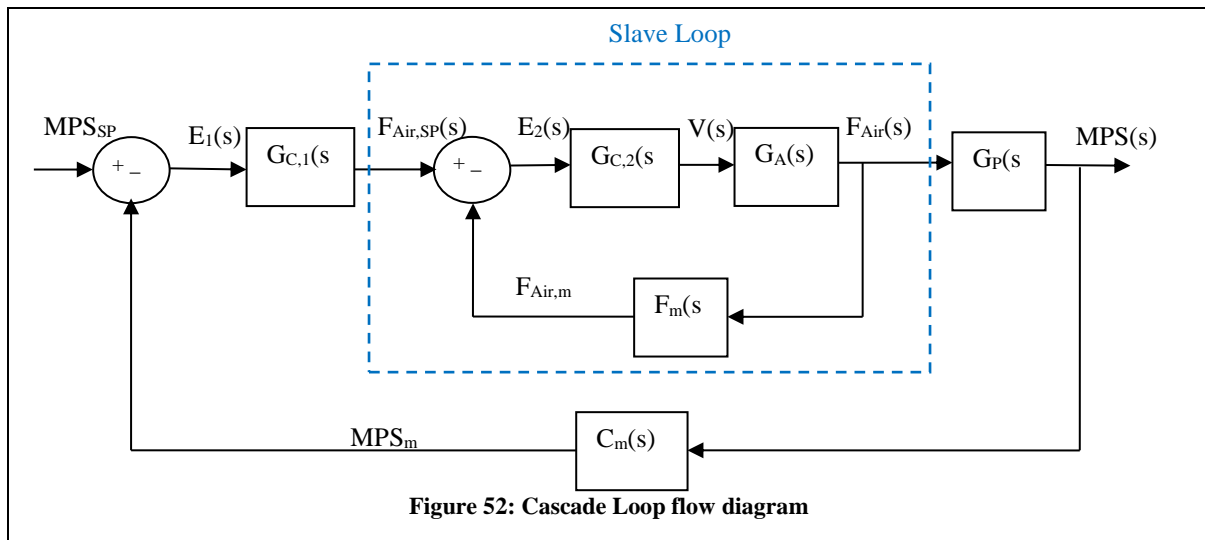
The two controllers need to be tuned to maximise the performance of the cascade loop. In practise, the slave loop should be tuned first, followed by the master loop. In this situation, the slave loop process is an actuator, which was already tuned for use in the ratio control scheme, so no more tuning is required. Tuning of the master loop involves consideration of the effect of the entire dryer process on the MPS, and has more complicated dynamics. These dynamics may include numerous transformations occurring inside the dryer that can affect the MPS, such as atomization, agglomeration and attrition. It is also common that out of specification particle size causes the fluid bed to block, leading to the shutdown of the spray dryer. This prevents the use of tuning methods such as Ziegler-Nichols, as the process would shut down before oscillations in the output would occur. Using a fully automatic approach also presents additional problems, such as a blockage to the Camsizer feed. Therefore, before implementing the cascade loop on the process, it is best to complete a sensitivity study using the simulation model. Simulations allow the wrong setting to be applied, avoiding repercussions and the costs of running the spray dryer. By including as much information as possible, simulations can also enable the user to identify the best way to set up a control network to maximise performance, leading to the best solution in a much shorter time.

3.1.1   Simulation

The process was simulated using SIMULINK® to determine the control parameters in the Mean Particle Size (MPS) cascade control loop. A model structure for the process is depicted in the block diagram given in Figure 53. In this model, the desired MPS is set, and the residual MPS, i.e. the difference with the current measured value of the MPS, is manipulated by the PI controller. The PI controller converts the residual error into a set point, for the air flow fed to the nozzle. The effects of the air flow rate changes and any alterations to the slurry rate on the PSD are summed to represent the dryer process. Additional delays caused by the transport of the powder and sampling, are then taken into account, including the effect of a blockage before the MPS is measured. A PI controller has been chosen on the assumption that there is a significant amount of noise in the process that would affect the derivative action.

Figure 53: Model of Spray Dryer
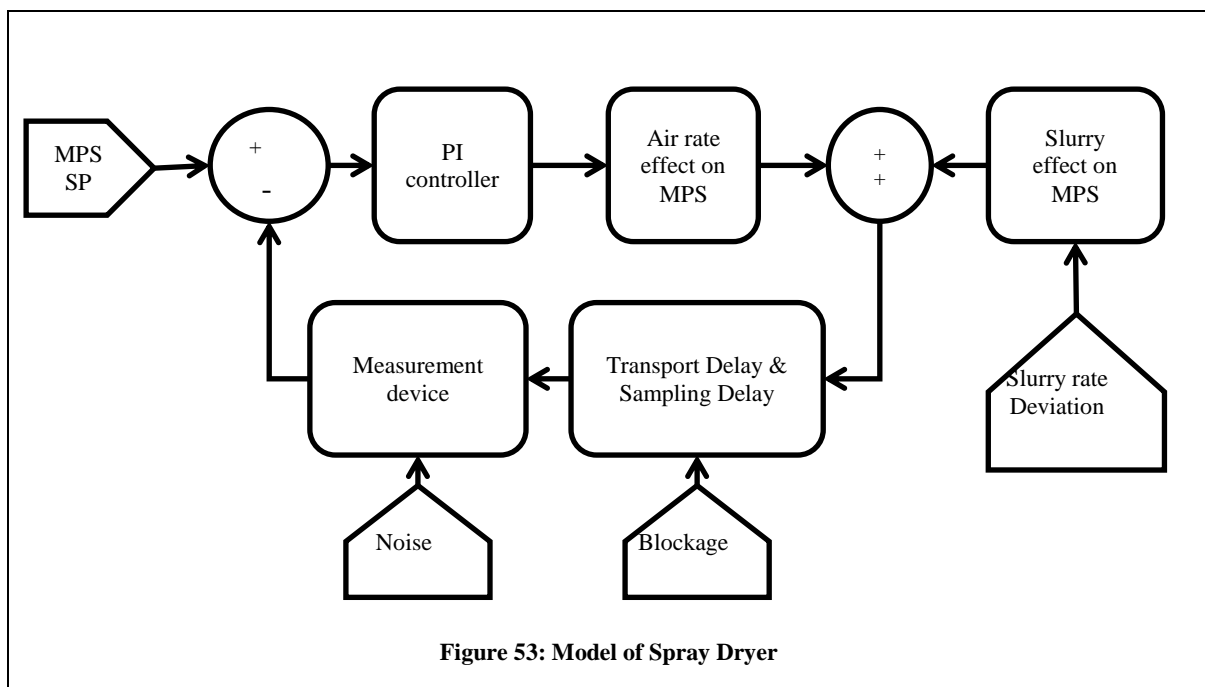
Implementation of the model depicted in Figure 53 necessitates that each process block is estimated using historical data. This data was generated from 4 batches of 3 different formulations that were considered representative of the portfolio of products produced in the

spray dryer. Each formulation had significantly different compositions, and required different operating conditions to ensure acceptable product quality. From the historical data, it was determined that the average effect of increasing the compressed air flow rate to the nozzle by 0.1 *kg/hr*, was to reduce the mean particle size by 10*μm* for each batch. This was also found in the atomization study. For slurry rate deviations, it was found that increasing the slurry rate by 1 *kg/hr*, resulted in an increase of 15*μm*. With the gains known for the effect of air flow and slurry rate changes, the additional dynamics of the control loops used to manipulate them had to be included. The time constants were found to be 30 and 45 seconds respectively.

Transport and sampling delays have been introduced to reflect the residence time of the dryer, and the time taken to transport the powder to the CAMSIZER via the conveyor belt in order to make a measurement. This was estimated to be two minutes, as once the air flow or slurry rate was manipulated, no significant change was observed for two to three measurements of the MPS. Measurement of the PSD normally takes about a minute depending on the cleaning stage between samples. The two final additions to the model are the effect of blockages and noise. One of the typical problems that materialised on the spray dryer, was that it was common for the feed tray to the sampler to block, preventing powder from reaching the sampler. This was caused by the combined effect of high flow rates of powder leaving the dryer, and wet product sticking to the feeder. This blockage prevented newly produced powder from reaching the sampling point leading to inaccurate measurements of MPS. Noise was added to the estimated mean particle size, as when running under constant conditions experimentally, the MPS tended to fluctuate around its expected value. During everyday operation of the dryer, when a blockage is evident, the MPS can suddenly change by a significant amount. The operator then unblocks the feeder and waits for another measurement. This is easily achieved with manual control as the operator simply ignores the measurement. However, an automatic control strategy would make an unnecessary control action to correct for the sudden change in MPS. If the operator

does not observe that there is a blockage, then the loop will continue to change the air flow to try and correct the error causing the actual MPS to deviate away from set point. Once all the various elements depicted in Figure 53 were accounted for, the process was simulated with disturbances to the slurry rate, so the cascade loop could be auto tuned in SIMULINK®. The simulation diagram is depicted in Figure 54 with additional annotation. The slurry rate effect has been highlighted, including the source signal with white noise, and the process dynamics. A signal builder was used to show the impact of various changes in the slurry rate, and a first order time delayed transfer function was fitted from the historical data. Another signal builder has been used to replicate the effect of a blockage along with additional noise related to measurements of the MPS. The sampling and transport delays highlight a zero order hold, which holds the MPS measurement made every minute, and a transport delay for getting the powder to the analyser. The rest of the simulation diagram consists of the feedback loop, which uses the error in the MPS to change the air flow rate. There is a transfer function to relate the effect of a change in the air flow, and two constant values for the initial value of the MPS and the air flow from when the cascade loop is implemented. It is assumed that the cascade loop is only switched on when enough powder has reached the Camsizer, so the initial stages should be set manually by the operator. With everything set up, the controller can be tuned using an inbuilt algorithm in the software that allows the settings to be changed once results are analysed.
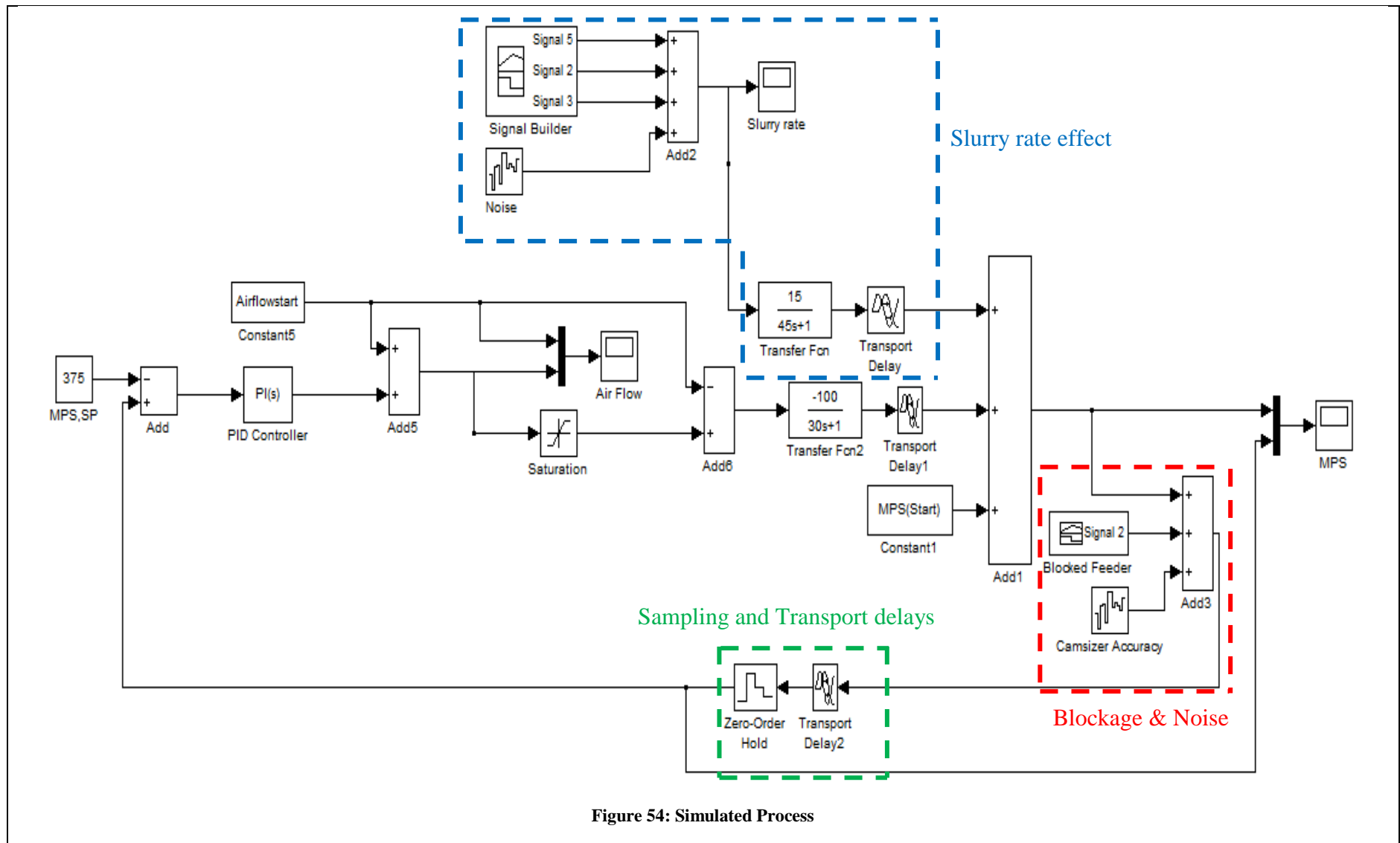
Figure 54: Simulated Process

Figure 55 to Figure 57 show the simulation of the MPS, the change in the atomizing air-flow rate to control the MPS and the disturbance produced from the slurry rate respectively. Figure 55 illustrates the assumed difference between the actual MPS and what is measured in the simulation. It shows the delay in the measurement due to the residence time of the dryer system, and that the MPS signal is being sampled and held, as only one measurement is made every minute. At 1700 seconds, an inaccurate measurement was introduced to simulate a blocked feed tray and to investigate by how much the control loop would cause the MPS to deviate from its set point by changing the air-flow rate to react to the disturbance before it was corrected. In this case, the controller reacted slowly so as not to affect the MPS when a blockage occurs. If the blockage is significant and leads to a large error in the particle size measurement, then this could have significant consequences in a matter of minutes if unattended.

Figure 56 shows the manipulation of the atomizer air-flow by the cascade loop. This is considered to ensure that the control loop does not cause any unnecessary action, and provides stable manipulation of the air-flow. As can be seen, there were no oscillation or sharp changes in the air-flow rate whilst it was manipulated to deal with the disturbance from the slurry rate. The drop at 1700 seconds was caused by a blocked feed measurement and was quickly rectified once a subsequent measurement had been recorded. The speed of response for the controller was reduced so that the operator had enough time to sort out the blockage. Figure 57 shows the changes in slurry rate from steady state. The slurry rate is a useful measurement when aiming to control moisture content and so is changed during a batch. By including it in the simulation, the controller was tuned so that it could deal with any changes that might occur during normal operation.
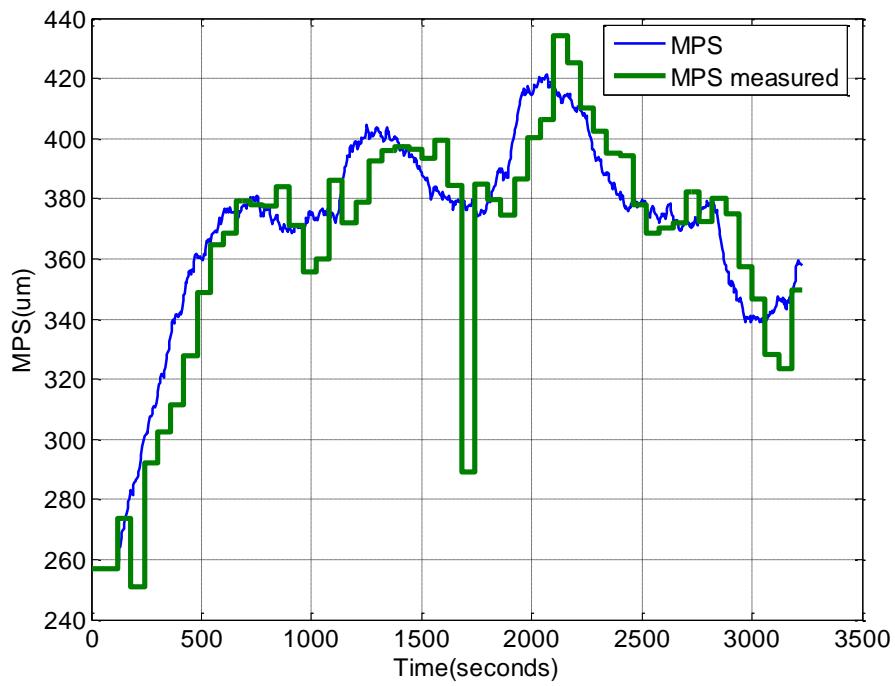
Figure 55: Simulated MPS controlled at 375μm and subject to disturbances
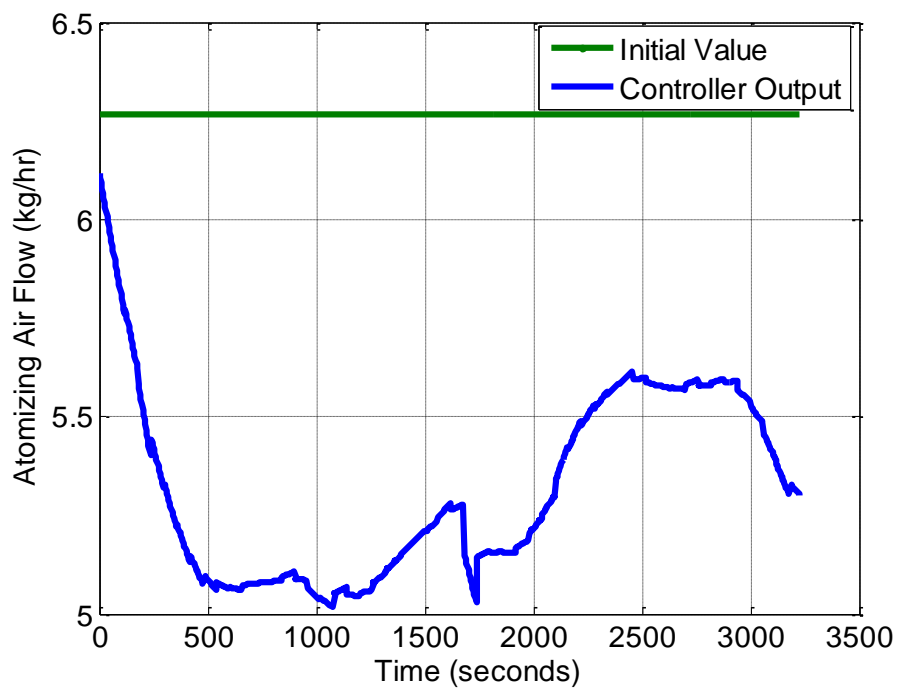
Figure 56: Simulated change in atomizing air flow to control MPS
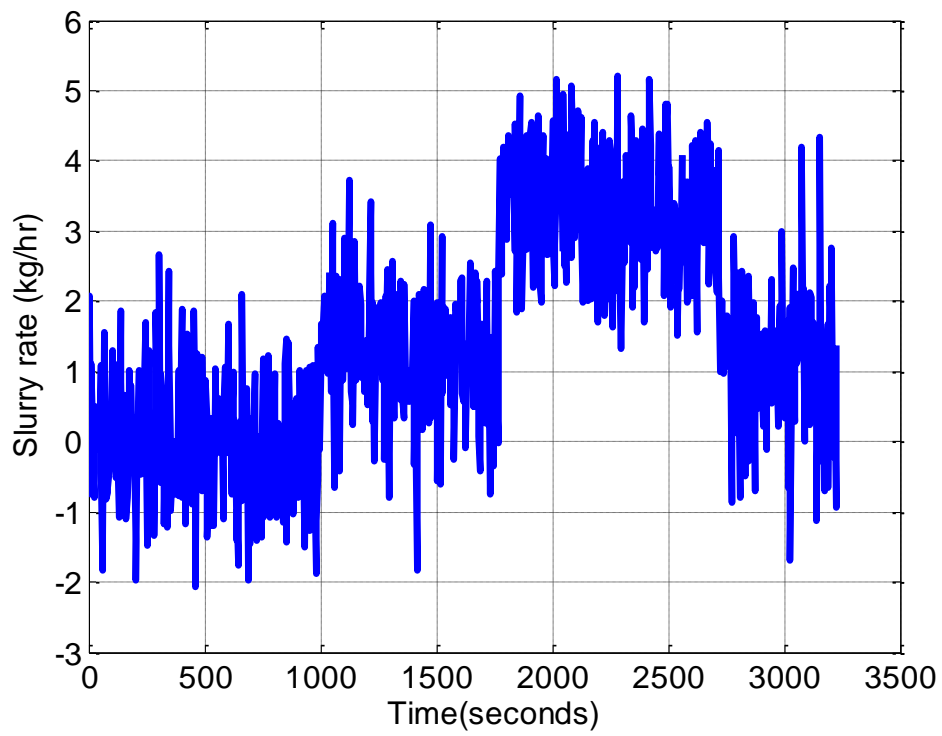
Figure 57: Simulated change in slurry rate with additional noise from steady state

3.2   Performance of Control Schemes

Slurry to air mass ratio control is currently utilised to operate the spray dryer unit. To assess the spray dryer's performance, 15 batches were run and analysed, where the sole goal for the operator was to attain set points for the powder quality as determined by the moisture content, density and particle size distribution. The 15 batches were conducted on 3 different formulations that typified the range of detergents manufactured. Figure 58 shows the average performance of the 15 batches and the associated variability, captured in terms of one standard error of the mean. By assuming a normal distribution, the probability that a measurement falls in this range was 68.2%. This allows for the consistency of the control strategy to be analysed on a batch to batch basis. Although the measurements of MPS are made once a minute, a moving average determined over 3 measurements was used to reduce the noise in the signal. By implementing this control strategy, it can be seen that the mean particle size did not reach its target until approximately 45 minutes. The average remains within $40\mu m$ of the target MPS after 15 minutes, however, considering the standard error of the measurements, there remains significant variation around the desired value of MPS. It can be seen that the range is $\pm50\mu m$, indicating that the best achievable control in these batches would produce a particle size between $325\mu m$ and $425\mu m$. However, the moisture content distribution and density are dependent on the PSD, and this variability can lead to inconsistent powder quality.

Figure 58: Average Error in Mean Particle Size for 15 batches using Ratio control ± σ
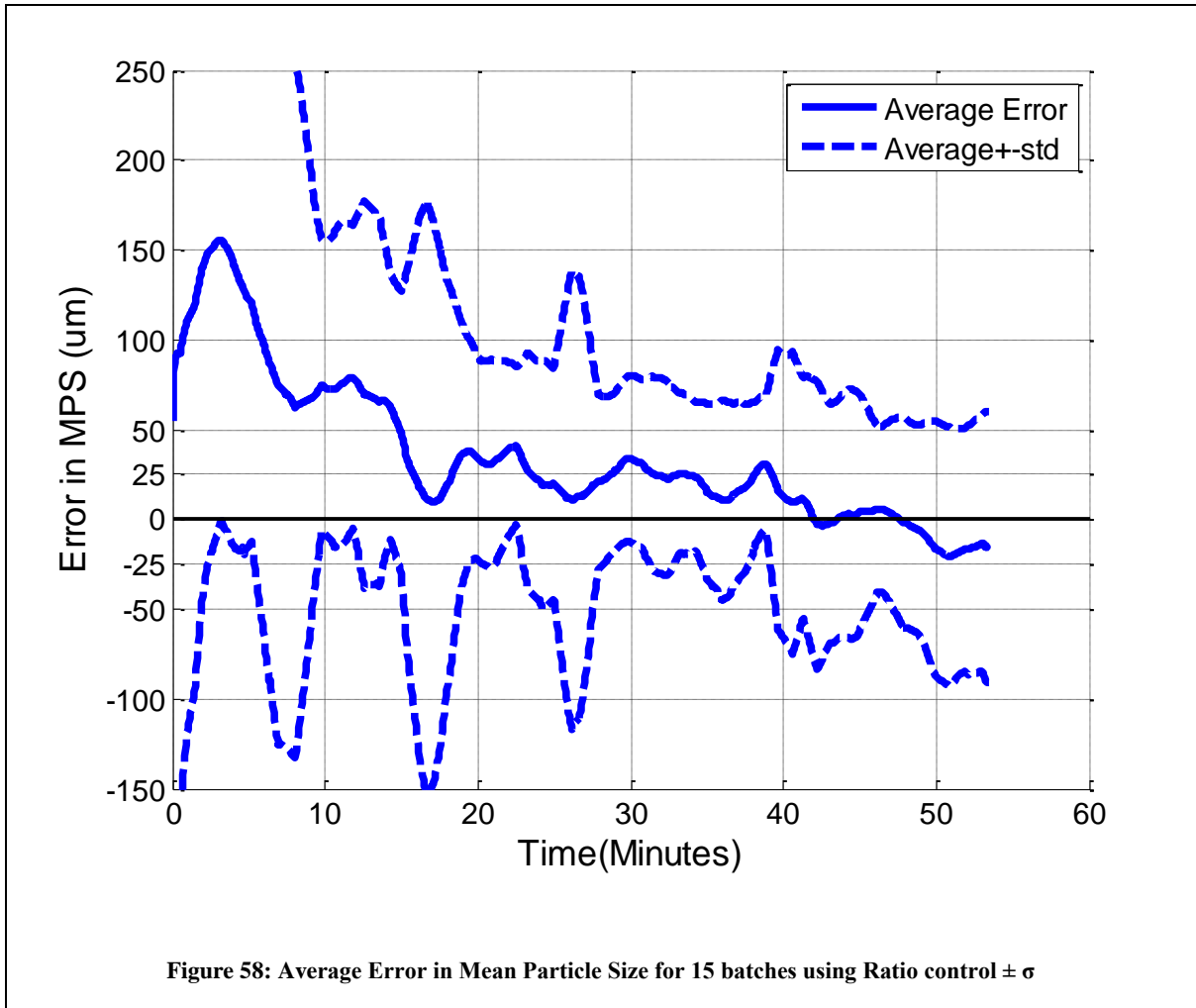
Figure 59 shows the average performance of 11 batches using the cascade control strategy. The 11 batches covered a range of formulations produced in the spray dryer. Again for these batches, the operator's goal was to reach the desired product quality. However, for one batch, the set point of the mean particle size was changed to see whether the automatic control loop was able to change from one state to another. As can be observed, the average particle size reached the target in approximately 21 minutes, the average measurement was within $20\mu m$ of the target MPS, and the level of variability remained within $\pm 20\mu m$ from 12 minutes into the batch.

Figure 59: Average Error in Mean Particle Size for 15 batches using Cascade control ± σ
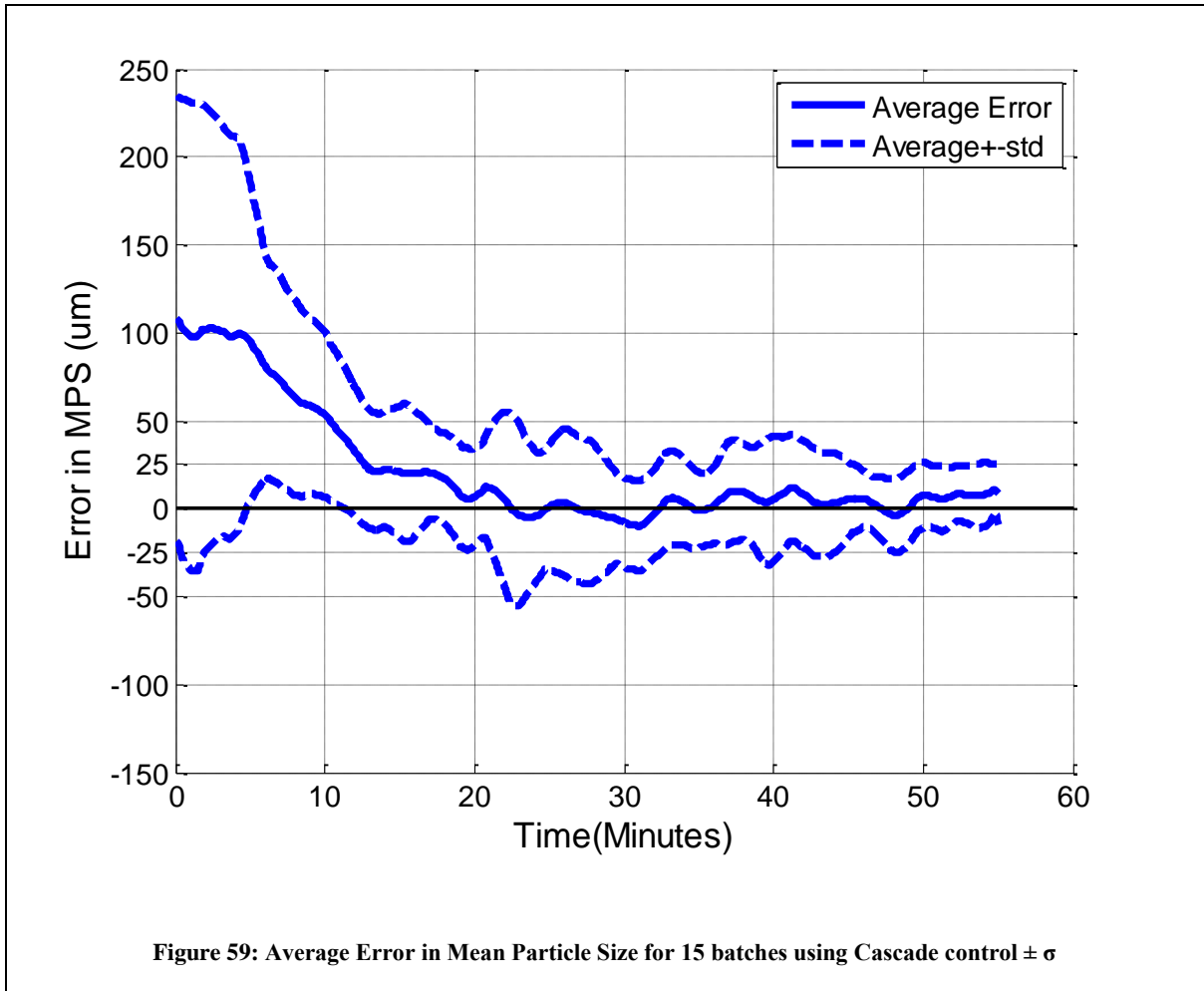
3.3 Control Comparison

The use of automatic cascade control has resulted in a significant improvement in the control of particle size distribution compared with manual ratio control. There are multiple reasons for this. Firstly, automatic control always reacts as soon as a change is recorded, and is self-regulating throughout the batch. More specifically, it is not dependent on the operator observing that the particle size has deviated from the target value. Secondly, it is not dependent on the slurry flow or properties. The ratio control theory indicates that if certain slurry to air ratios are maintained, then the mean droplet size will remain on target as long as the material properties are constant. The study of atomization was in agreement with this assumption, however, differences were noticed at different slurry rates. The atomization study also indicated the importance of maintaining the material properties as there was significant

134

variation in the atomization of the slurry. If material properties or slurry rates change, then the cascade loop makes corrections to stop any significant deviations. As for the ratio, if a slurry rate change is not recorded, then the ratio calculation is incorrect, and if the material properties change, the PSD associated with the ratio used also changes.

Slurries produced for the manufacture of detergents consist of a complex four phase suspension: Liquid electrolyte, liquid surfactant, air and undissolved solids phases. Depending on the rheology of the mixtures and the mixing conditions, their composition may vary with time due to aeration, sedimentation and creaming. Agitation and temperature control in the mixer are important factors ensuring consistent slurry is fed to the dryer. In a R&D environment, new formulations are tested which can result in mixing problems. The likelihood of segregation, aeration and sedimentation of the slurry is increased, thereby affecting the value of the Ohnesorge number and potentially causing the mass slurry rate to change over time. This scenario would not be captured by the empirical pump correlation, and would result in the calculated ratio being incorrect. An example of changes in flow properties resulting in an incorrect measurement of slurry rate on this unit is illustrated in Figure 60. This depicts an example of the effect of poorly mixed slurries. In this case, the pump speed was kept constant causing the empirical relationship to predict a mass flow rate of 55*kg/hr*. Although there is a significant amount of noise in the load cell measurement of the slurry rate, it shows a clear downward trend, and as the pump speed was constant, this could only be caused by changes in the material properties of the slurry. The slurry rate used in the mass ratio calculation could be up to 10 *kg/hr* away from its actual value by the end of the batch
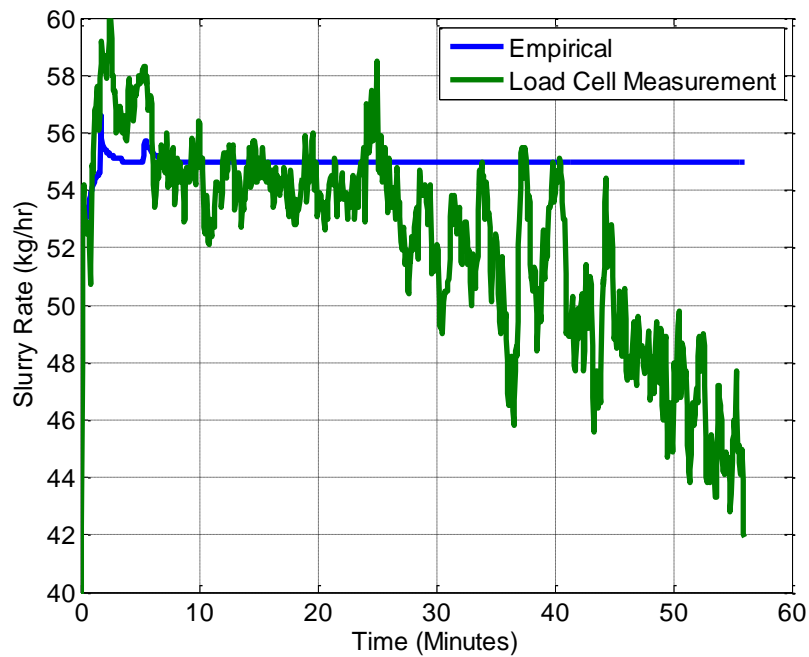
Figure 60: Changes in Slurry rate mass flow at a constant pump speed

To study the effect of these material property changes, the pressure at the nozzle was also analysed. The change in pressure is directly linked to changes in properties such as density and viscosity, as the slurry becomes easier or more difficult to pump. Two situations from historical data highlighted the impact of a change in pressure on the MPS produced from the spray dryer process. To show the effect, a ratio of the pressure difference in the slurry and the air flow has been compared with the mass ratio. Both have been used to fit a linear model to predict the particle size according to the theoretical relationships stated. With the resulting MPS known, an optimization function was used to reduce the root mean squared error (RMSE) of the linear fitting, the results are shown in Figure 61 and Figure 62.
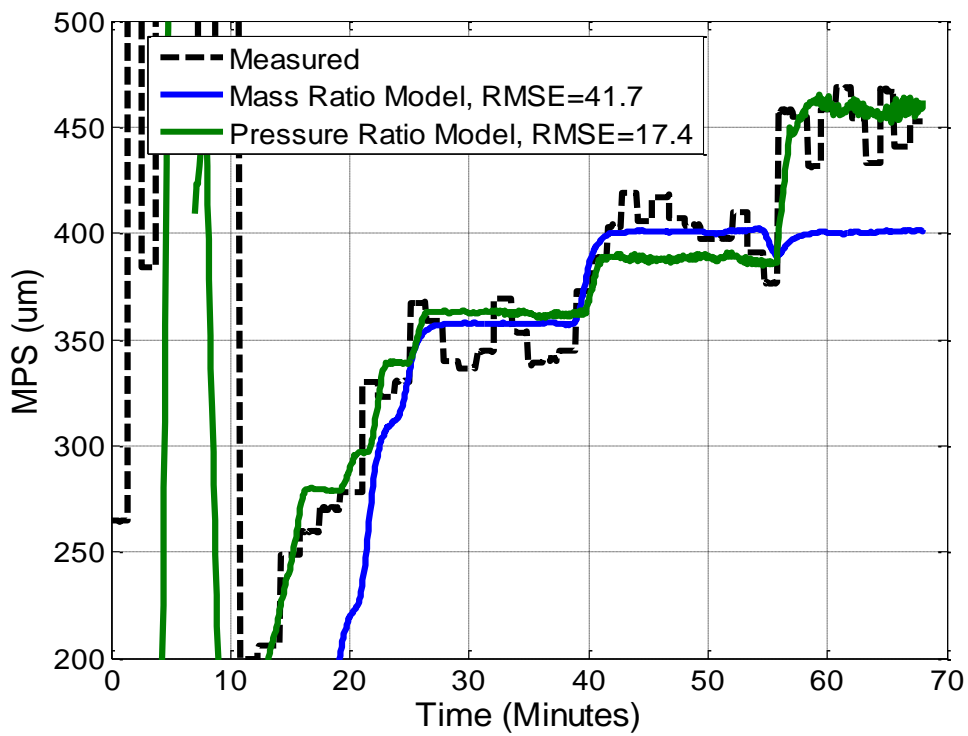
Figure 61: Deviation in MPS in relation to Mass ratio and Pressure ratio changes with slurry rate change
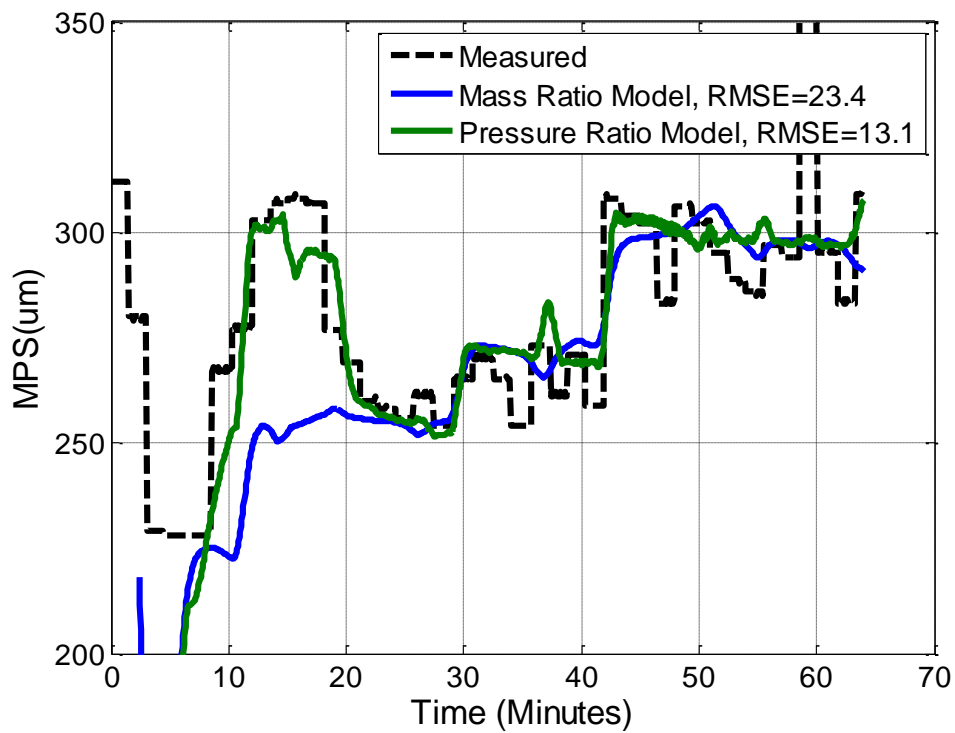
Figure 62: Deviation in MPS in relation to Mass ratio and Pressure ratio changes with change in slurry flow properties

In both cases, a pressure ratio model would provide a more accurate fit, with no extra information on the material properties known. However, the linear fitting values vary significantly between batches and formulations where the effect of a small change can have a large or minimal effect on the PSD. This is due to entrained air in the slurry that may change the flow characteristics and therefore the nozzle pressure significantly. This modelling method is useful in post processing to distinguish why the PSD changed, but would require calibration if used for prediction. During the batches depicted, the change in pressure is the only variable measured that could help explain the change in the MPS when no changes to the mass ratio have been made. Figure 61 shows that on the 56th minute, the MPS has increased due to a change in the pressure. This change in pressure occurred as a result of a slurry rate change. The air flow was adjusted to maintain the mass ratio, but MPS still increased, leading to a new steady state. In Figure 62 there was a large change in nozzle pressure at the start of the batch which led to much larger particle sizes being produced at low mass ratios. Eventually the pressure dropped and the particle size dropped by $50\mu m$, but none of this was captured by a mass ratio model, and the operator could not intervene until 30 minutes into the batch. It is clear that if these processing issues occur, then reliance on ratio control alone, without estimation of changes in the material properties, will not enable control of the particle size.

Another issue relating to the ratio control scheme, is that changes to the process dynamics caused by the change in atomization were not taken into consideration. As the slurry rate is changed by the operator, the air-flow is altered to maintain the ratio. The slurry rate is used to control the moisture content of the powder, so variations in the slurry rate are likely to occur during a batch. According to the research discussed, it is proposed that the MPS can be maintained as long as the slurry to air mass ratio is constant. However, there is no measurement of the amount of fines recycling in the process or of the effect of changing the concentration of particles inside the dryer as a result of changing the slurry rate. Figure 63 and Figure 64 show

that by increasing or decreasing the slurry rate, an increase in the particle size can result. In both cases, the mass slurry to air ratio was maintained but the particle size increased. This highlights that the other transformations in the process still play a role in the final PSD of the powder and steps should be taken to increase understanding of their influence.
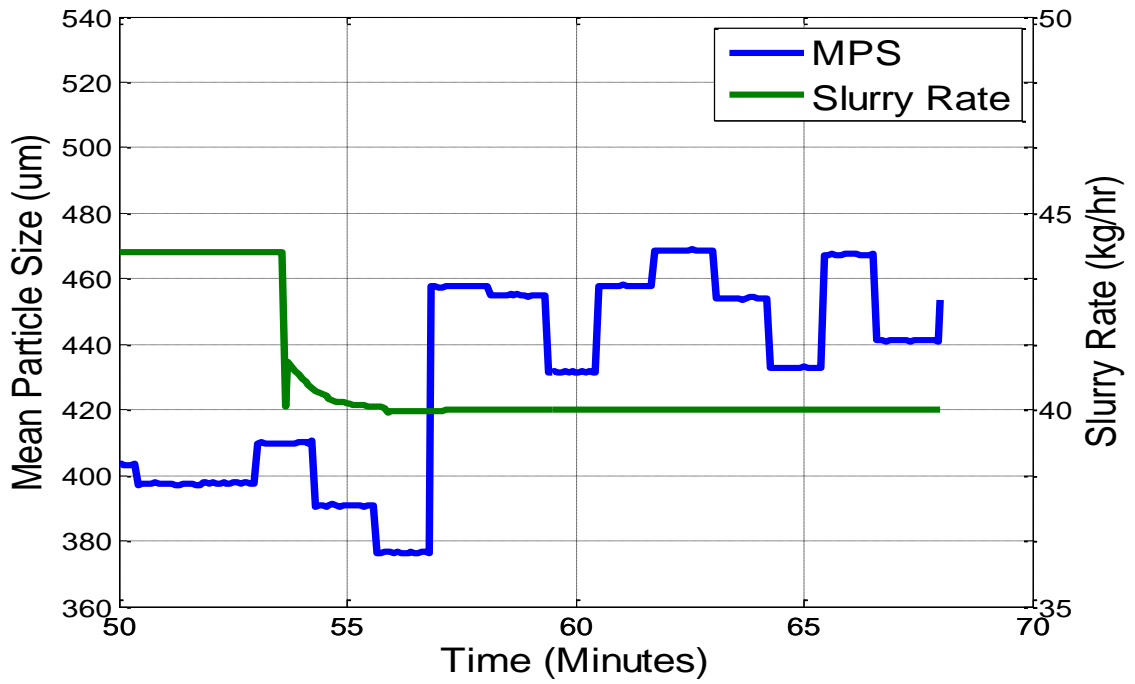
Figure 63: Positive change in MPS to a decrease in slurry rate
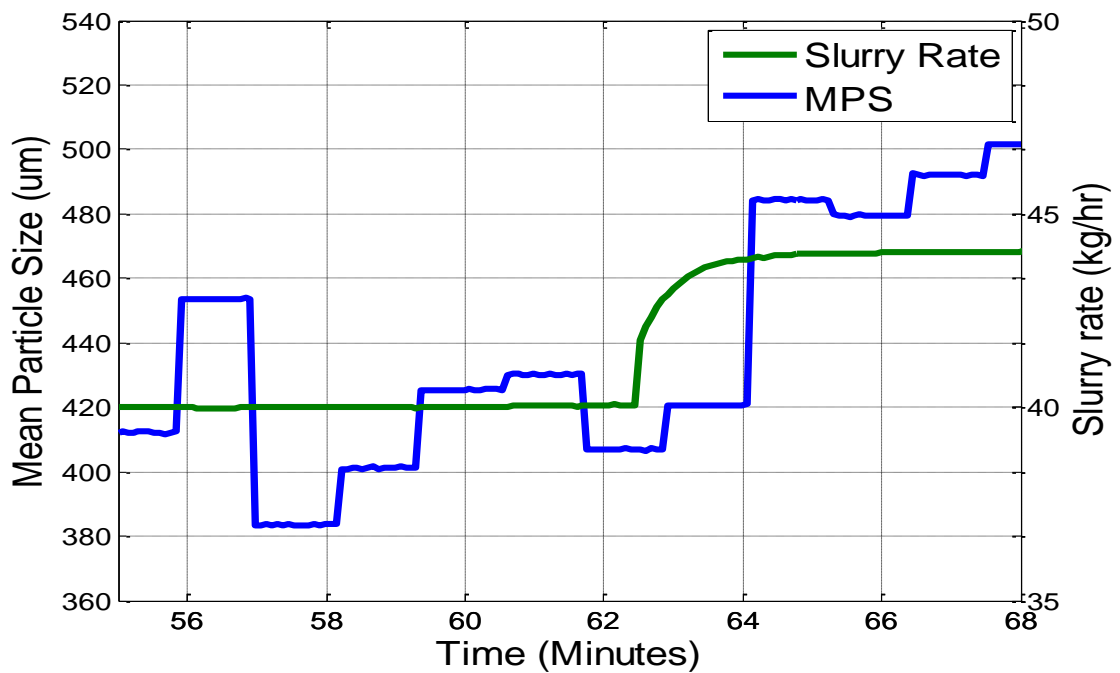
Figure 64: Positive change in MPS to an increase in Slurry rate

140

4   Conclusions

Cascade control of air flow rate provides more effective automatic control of mixed flow spray dryers than manually controlling the slurry to air mass ratio for the manufacture of detergent. This is as a consequence of the fact that cascade control relates only to the effect of air-flow changes, adjusting the air-flow to deal with any unmeasured disturbances in the slurry rate, slurry properties and any other impacts in the process that affect particle size. Ratio control failed to provide suitable control for this dryer system, as an accurate estimate of the slurry rate was not achieved, and the assumptions made about the effect of ratio changes being constant under different flow rates was not valid. Automatic control using the mass ratio is not feasible, as the effect of ratio changes differs for different slurry rates, with different material properties and different formulations. For ratio control to be suitable, constant manual changes to the ratio would be necessary to control the mean particle size to its target value. This is unrealistic as it would take too much of the operator's time during a batch. With the current portfolio of products, the cascade loop implemented on the pilot scale spray dryer provided more reliable, consistent control of the MPS and relieved a significant amount of pressure on the operator to control numerous variables at the same time.

6. BULK DENSITY

1 Introduction

The bulk density of a powder is recognised as a very important property highlighted for control in the scope of this project. It is directly related to particle porosity which influences product attributes such as dissolution rate and liquid loading capability. In terms of costs, bulk density dictates the mass of product per box of detergent on the shelf (Huntington, 2004). The filling of boxes can be volume or mass based, with the target amount recorded on the outside of the box. If the density is too low, there may be issues with packing the boxes. If the density is too high, then the box could look empty. The dosage of the product is also carried out on a volume basis, so accurate control of density is critical to ensure that consumer demands, needs and expectations of the product are met.

The bulk density of a powder is defined as the ratio of the weight of a freely poured powder to the total volume it occupies. The volume occupied is linked to the density of the powder particles and their spatial arrangement in the vessel, which leads to gaps between them. The gaps between particles, known as the inter-particle porosity, or voidage, can change depending on the vessel shape, the stickiness of powder particles, their shape and size distribution, and how the powder was poured. Small disturbances can lead to changes in bulk density, as the packing of the particles becomes altered, filling voids and making the measurement difficult to reproduce. Individual powder particles also contain pores in which air is entrained within the particle. This is defined as the intra-particle porosity and is dependent on the conditions in which the powder was dried and the formulation.

Bulk density is in reference to the "bulk" product and must incorporate all the properties of the powder, as it is dependent on key properties such as moisture content and particle size distribution, which are also controlled on the process. The product density is reduced from a slurry liquid density of 1300-1700 *g/l* to a powder bulk density between 350-550 *g/l* in the

drying process. For a significant part of the drying process (falling rate-period), water is removed, whilst maintaining the particle volume, which reduces the mass and therefore the density.

Moisture Content and PSD are control variables with their own targets, these should not be jeopardized in order to reach a target density value, so the best method available for control of the density is to modify the intra-particle porosity. To do this, air can be injected into the slurry before entering the drying chamber. By injecting air, the density of the liquid slurry transported through the pipes to the atomizer is changed. This will lead to a change in the atomization process and therefore the final PSD of the powder. However, the proposed PSD cascade control loop has proven disturbance rejection, and is capable of maintaining the PSD during changes to the air injection rate.

Manipulation of the air injection rate can lead to reductions in the bulk density of up to 100 *g/l*. The drop in density tends not to surpass this value, as a finite amount of air can be entrained, dependent on the formulation. As the rate of air injection is increased, the remaining air that wasn't entrained will simply escape during atomization. During atomization, no more air can be encapsulated in the pores of the droplet, limiting the impact. If the target density cannot be reached using this method, then the drying conditions, determined by the inlet air temperatures and flow rates in the process, can be manipulated. The impact of such changes on the moisture content of the powder will be more severe. If this approach was adopted, then the effect on both moisture content and particle size distribution would need to be quantified in order to select the most appropriate condition**s.**

2   Density Control

Manipulation of the air injection rate can be used to control the slurry liquid density entering the process, not the bulk density of the exiting powder. The bulk density is dependent on the slurry liquid density, but numerous other factors which are not measured inside the drying process, need to be taken into account. In order to provide a control strategy for the bulk density of the powder, it is beneficial to provide a model that quantifies the impact of each contributor. This will help determine whether the reduction in the slurry liquid density via air injection is sufficient to control the density without changing the drying conditions. To build this model, historical batches that were run on the spray dryer process for a range of formulations can be used for validation.

A density model needs to include the effects of the following:

- Slurry liquid density without air

- Air entrainment

- Drying conditions

- Powder properties & Packing

2.1   Slurry liquid density

Slurry liquid density can be estimated using the density and mass fraction of each component in the formulation. A single measurement of the slurry density is also made at the start of a batch, from the slurry line after the mixing process. However, as air is entrained into the slurry during the mixing process, its density could differ from the estimated value. There is also a risk that over time sedimentation can occur along with a change in the aeration, so this measurement may become invalid.

2.2   Air entrainment

The amount of air that can be entrained is finite depending on the formulation. Therefore, if more air is entrained in the mixer, less can be injected in the slurry line. This plays a key role in determining the limitations of using air injection to control the slurry liquid density.

2.3   Drying Conditions

The drying conditions determine how the droplets evolve during the process. Slow drying rates ensure that moisture can be transported to the surface of the droplets, leading to a reduction in volume as the water is removed. As the drying rates are increased, water could be removed internally, leaving internal pores in the particle and maintaining its volume. If the conditions are too severe, the droplet may puff, expanding the particle in a similar fashion to the production of popcorn.

Studies of the drying of milk droplets in a similar co current tower, highlighted that the shrinkage of the droplets changed significantly with droplet temperature (Fu, Woo, Selomulya, & Chen, 2013). The temperature differences represented the change in drying conditions in the dryer. As the drying rates increased, the amount of shrinkage decreased. The amount of droplet shrinkage could be related to the Peclet dimensionless number. This relates the external drying conditions, which change with temperature, to the internal water transport rates, which depend on the diffusion coefficients of the formulation. Therefore, shrinkage of the particles is a function of the temperature of the air and characteristics of the formulation.

2.4   Particle Properties & Packing

The bulk density leaving the dryer is dependent on the moisture content of the powder, its PSD, and how it packs during measurement. The removal of moisture has a clear impact on the density, as it reduces the mass of the particles. The impact of PSD is more difficult to quantify. It effects how the particles pack, which will change the voidage in the vessel used to measure

146

the bulk density. In the literature, the voidage of a packed bed or any cylinder filled with nearly spherical particles is typically assumed to be 0.4 (Towler & Sinnott, 2013). Many studies conclude that the voidage may decrease slightly with increases in particle size, but this is related to fluidized systems (Geldart, 1971). A distributed size range, leads to lower void fractions, due to smaller particles filling voids between the larger particles. If the span remains approximately the same, changes in voidage would be minimal with increasing particle size. According to some findings in the literature from the study of distributions of particles in packed beds (Caulkin, Fairweather, Jia, & Williams, 2005), the voidage has been found to range from 0.35 to 0.5. The results of previous work in modelling at P & G on this unit, suggest the voidage was closer to the upper limit, ranging from 0.45 to 0.5 for the detergents analysed. There is variance in the value of this because it has been used as a fitting parameter for the models suggested.

3   Density Model

The first step in creating a density model, is to use the slurry liquid density to determine the density of the solids (ρ_{Solids}). To do this, the mass fractions and densities of each component in the formulation are used to estimate the unaerated slurry liquid density ($\rho_{unaerated}$). This is then related to the density of solids by using the initial water content (*SMM*) and density (ρ_{water}) in Equation 63.

$$\frac{1}{\rho_{unaerated}} = \frac{SMM}{\rho_{water}} + \frac{(1 - SMM)}{\rho_{Solids}}$$

Equation 63

By rearranging the equation, the density of the solids can be calculated in Equation 64, assuming the slurry behaves as an ideal mixture.

$$\rho_{Solids} = \frac{(1-SMM)}{\dfrac{1}{\rho_{unaerated}} - \dfrac{SMM}{\rho_{water}}}$$

The unaerated density is also used to calculate the mass fraction of the air entrained in the slurry in the mixer ($m_{f,Air}$), by combining it with the measured value of the density of the slurry ($\rho_{Slurry,Initial}$).

$$\frac{1}{\rho_{Slurry,Initial}} = \frac{1-m_{f,Air}}{\rho_{unaerated}} + \frac{m_{f,Air}}{\rho_{Air}}$$

As the mass fraction of air is negligible, a further simplification is made as: $1 - m_{f,Air} \approx 1$. The effect of entrained air on the slurry density is large due to the significant difference in density between the air and the slurry. With additional air from the air injection, the final slurry density estimated is equivalent to Equation 66, where the total mass fraction of air in the slurry ($m_{f,AirTotal}$) is used.

$$\frac{1}{\rho_{Slurry}} = \frac{1}{\rho_{unaerated}} + \frac{m_{f,AirTotal}}{\rho_{Air}}$$

Equation 66 provides a specific volume for the slurry. Density changes are caused by changes in the volume and/or mass of the particles. To include the impact of drying conditions on density, it has been assumed that shrinkage is the main transformation. The percentage of shrinkage in the diameter of the particles has been introduced into the model and is a function of the temperature measured in the process. To relate the shrinkage in diameter to the reduction in volume, the shrinkage percentage is cubed in the model, assuming the droplets are spherical. The shrinkage impacts the volume of the particle, but as the moisture is removed, the mass also decreases. Assuming only water is removed, the change in mass is represented by the change

in water content. Equation 67 relates the change in mass to the change in volume in the drying process, in order to estimate the density of the particles ($\rho_{particles}$).

$$\rho_{Particles} = \frac{\dfrac{1-SMM}{1-X}}{(1-shrinkage(T_{Exhaust}))^3\left(\dfrac{1}{\rho_{Slurry}}\right)}$$

Equation 67

The final addition to the model, relates the bulk measurement of density (ρ_{Bulk}) to the density of the particles ($\rho_{particles}$) in Equation 68. This introduces the voidage term (ε) into the model, which represents how the particles pack during the bulk measurement.

$$\rho_{Bulk} = \rho_{Particles}(1-\varepsilon)$$

Equation 68

Taking all factors into account, the bulk density can be estimated using the density model expressed in Equation 69.

$$\rho_{Bulk} = \frac{(1-\varepsilon)\left(\dfrac{1-SMM}{1-X}\right)}{(1-shrinkage(T))^3\left(\dfrac{1}{\rho_{unaerated}} + \dfrac{m_{f,AirTotal}}{\rho_{Air}}\right)}$$

Equation 69

Using historical batch data, the models parameters can be fitted to predict the bulk density. To use the model, an expression is needed to relate shrinkage to temperature, and the impact of PSD on voidage is required. As previously mentioned, there is a finite mass fraction of air that

can be entrained in the slurry. This limits the value of the mass fraction in the model, and also needs to be taken into account when fitting the model.

4   Density Model Fitting

The derived density model provides flexibility in the representation of many possible scenarios. This flexibility is needed because the model is required to estimate the change in density for different formulations, which may entrain different amounts of air in the slurry and be more sensitive to the drying conditions. Because of this, the batches used to fit the model contain different levels of air injection, different particle sizes and different process conditions. It is ideal to have a universal model for all formulations so more emphasis was given to reaching a best fit model rather than individual fittings. The properties of each formulation used in the batches are listed in Table 3.

Table 3: Formulation Properties

Formulation	SMM(%)	Unaerated Density (kg/m^3)
1	34.75	1480
2	32.75-33.33	1545-1538
3	28.5	1655

A key problem, highlighted in the Materials and Methods chapter and the Particle Size Control chapter, is that in some batches, the load cell measurement deviated from the estimated slurry rate using the volumetric flow from the pump. This indicates a change in slurry density during the batch, which could be a result of sedimentation and/or a change in aeration over time. Sedimentation would lead to multiple other issues related to the change in composition of the slurry, so it has been assumed that the deviation can be described solely by the amount of entrained air during the mixing process. Using the measurement of the slurry density at the

start of the trial, and the difference between the slurry rate estimates, the slurry density before air injection can be estimated over time in Equation 70.

$$\rho_{Slurry}(t) = \rho_{Slurry,Initial}\left(\frac{m_{Slurry,Loadcell}(t)}{m_{Slurry,Pump}(t)}\right)$$

<div align="right">**Equation 70**</div>

This enables the use of Equation 65 to obtain an estimate for the mass fraction of air entrained in the mixer over time.

Previous studies on this unit with these formulations, suggest that as the mass fraction of air in the slurry increases, it becomes more difficult to entrain the air. This has been related to total mass flow of air via an efficiency term, which trends to zero as more air is entrained. The study concluded that the efficiency was 100% up to a certain mass fraction, and then reduced towards zero. The study also found that the impact of changing formulation could not be quantified obtaining a single model that fitted the formulations. The efficiency is expressed in Equation 71 where the efficiency (e) is 100% up to the critical mass fraction ($m_{Air,critical}$) and reduces logarithmically as the mass ratio of air to slurry increases. The value of the critical mass fraction ($m_{Air,critical}$) was found to be 0.000127 in previous work at *P & G*.

$$e = a \cdot \ln\left(\frac{m_{AirTotal}(t)}{m_{Slurry}(t)} - m_{Air,critical}\right) + b$$

<div align="right">**Equation 71**</div>

Using batches where the mass fraction of air is below the critical mass fraction, ie efficiency (e) is known to be 100%, the influence of packing, voidage and shrinkage can be assessed. Once obtained, the parameters a and b can be fitted for the remaining batches where the mass fraction is higher.

151

Previous studies have suggested voidage was between 0.45 and 0.5 for the formulations produced in this spray dryer. Analysis of the density in batches with 100% efficiency of air entrainment provided no visual trends to suggest that the voidage or shape changes with PSD. This is most likely due to lack of change in the span of the distribution which would be the main contributor to variance in the packing. This implies that a constant value could be used, one that lies in between 0.45 and 0.5 for all the formulations. To determine its value, the target shrinkage has been used. The target shrinkage values were calculated using manual measurements of bulk density and moisture content, and the range of values for the voidage in the density model. To ensure that the target shrinkage for all measurements in these batches was greater than zero, a value of 0.5 for the voidage was necessary. This means that the particles always shrank in the process rather than expanding.

The target shrinkage changed considerably in the batches. Using an empirical relationship, the change in shrinkage can be estimated to enable the prediction of future values of shrinkage in a batch. Using the batches with 100% air entrainment efficiency, Equation 72 was fitted to represent changes in shrinkage throughout a batch. This has been used for all formulations, despite the shrinkage also being dependent on the diffusion coefficient, which is formulation dependent. Therefore, it assumes that the diffusion coefficient does not change dramatically for the formulations produced.

$$\frac{\partial Shrinkage(t)}{\partial T_{Exhaust}(t)} = -0.00125 \qquad \text{Equation 72}$$

The remaining batches, with higher mass flows of air in the slurry line, were then used to fit the efficiency of air entrainment equation. The value of a and b in Equation 71 was found to be -0.025 and 0.1 respectively.

4.1 Density model performance

The density model predicted bulk density with a %RMSE of 4.77. Each measurement made in all the batches is compared to the prediction in Figure 65. The range in densities especially for Formulas 2 and 3 show how much the density can change in the process. In its current condition, the model predicts the bulk density to a high level of accuracy. Additional work could be carried out to assess the impact of formulation and the span of the product on voidage, but this is not necessary for the current application. The shrinkage in the batches ranged from 0 to 15% and the air entrainment efficiency reduced to 38%.

Figure 65: Density Prediction accuracy
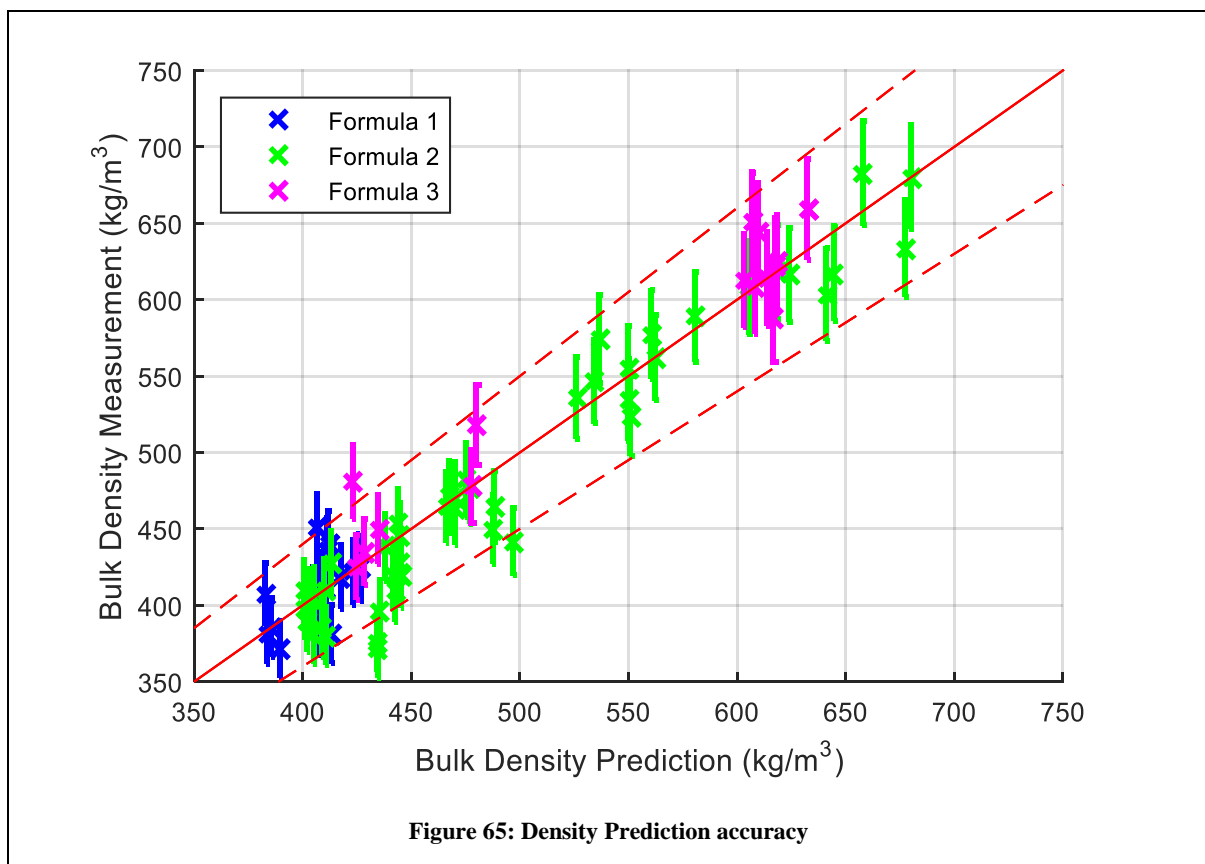
5 Conclusions

The proposed density model highlights the impact of inlet and process conditions on the powder bulk density. Prediction of density is very complex, relying heavily on the initial conditions of the slurry and on process conditions which are regularly manipulated. The effect of changing particle size on the packing voidage has been assumed to be negligible during the batches analysed. However, this density model is still reliant on PSD, as it affects the drying rates in the process, which determine the exhaust temperature, which is used to calculate the shrinkage. With the exhaust temperature measured, the density model can be used to provide a target mass fraction of air, which will provide a target air injection rate, in order to maintain the density at its target value. This target could then be used in an automatic loop, similar to the particle size control approach. However, the model can only be used with an estimated moisture value and should therefore be used in conjunction with a moisture control model. If the density target cannot be achieved, there may be integral windup causing an unstable signal to be sent to the air injection actuator. This would require operator intervention, and, in this case, the operator would simply set the air injection at its maximum value.

In its current state, the model can only be used online to control density. With the addition of a model to estimate how the drying conditions change, the models could be used to simulate the process and obtain optimized targets for the process parameters.

7. DRYING MODEL

1 Introduction

The individual projects have shown that it is possible to control particle size as a single objective. Control of the density of the powder is a more complex problem. The density can be manipulated by varying the initial slurry density via air injection, but the final density is very much dependent on particle size, moisture content and the drying conditions. The control of moisture content is hindered by sampling frequency, which makes its dependence on the other properties difficult to determine. By using overall heat and mass balances on the process, the exiting moisture content can be estimated in a more frequent manner, but it is reliant on calibration. When operating the process, the drying conditions play a critical role in the evolution of the particles in the spray dryer. These conditions are reliant on the initial conditions and the formulation that is being dried in the process. An estimate of moisture is now available, but knowledge of the sensitivity of this to changes in the inlet conditions is not known. In order to understand which initial conditions should be changed, the spray dryer system needs to be compartmentalised into its three different sections: the drying chamber, the inner fluid bed and the outer fluid bed.

Application of rate based models for each compartment can aid understanding of the impact of the changes in the initial conditions, and of how formulation plays a role in the process. In order to utilise these models, more information is needed, such as the residence time of the particles for each compartment. A previous internal study at P & G in 2007 on the spray dryer, estimated the overall particle residence time of the spray dryer using a tracer approach. This method dyed the slurry and measured the colour change of the powder using a colorimeter. The residence time was found to be approximately 107 seconds, with an additional 30 seconds before the powder was transported to the measuring points. During the study for particle size control, particle size changes were measured 2 or 3 samples after a change to the atomization. This equated to between 2 and 3 minutes, and agreed with this estimation of the residence time.

However, the tracer experiment was based on one single slurry rate of one formulation and the residence time is likely to change with volumetric flow, which depends on the mass flow rate and density of the slurry.

The rate based models are also reliant on accurate estimation of the flow properties of the particles and the surrounding air, in order to estimate heat and mass transfer coefficients. Each compartment provides different environments where the interaction of particles with surrounding air varies. It is common to use the Ranz-Marshall correlations which require estimated measurements of the relative velocity between the particles and the air.

2   Compartmental Heat & Mass balances

The spray dryer can be split into compartments by using the internal measurements in the process. These measurements can be used to produce mass and heat balances for each compartment by making a few assumptions. For each compartment, an additional two mass balances are available for the liquid and gas phases and a heat balance. This provides a total of 12 equations including 8 mass balances and 4 heat balances. Figure 66 depicts the mass flows in and out of each compartment and the heat losses, where *A* represents air flow, *S* is for slurry flow and *H* is for heat flow. Assuming only water is transferred between the liquid and gas phase, each flow contains 3 variables: the total mass flow, the water content and the temperature. This assumption also applies to the flow of fines in the exhaust air flow, which is assumed negligible. In reference to the figure, there are a total of 20 unknown variables. These include all the variables in the flow streams *S2, S3, S4*, *A6* and *A7*, the mass flow and water content of the exhaust, *A5* and the heat losses from each compartment. With 12 heat and mass balances available, a further 8 equations or assumptions are needed to close the system. These equations are produced using the following assumptions:

1. Each fluid bed is well mixed

2. Particles exit the chamber at $100 \, ^oC$

3. There is zero heat loss from the fluid bed

4. Heat losses from the outer fluid bed occur via convection

Figure 66: Process Flows in Mixed Flow spray Dryer
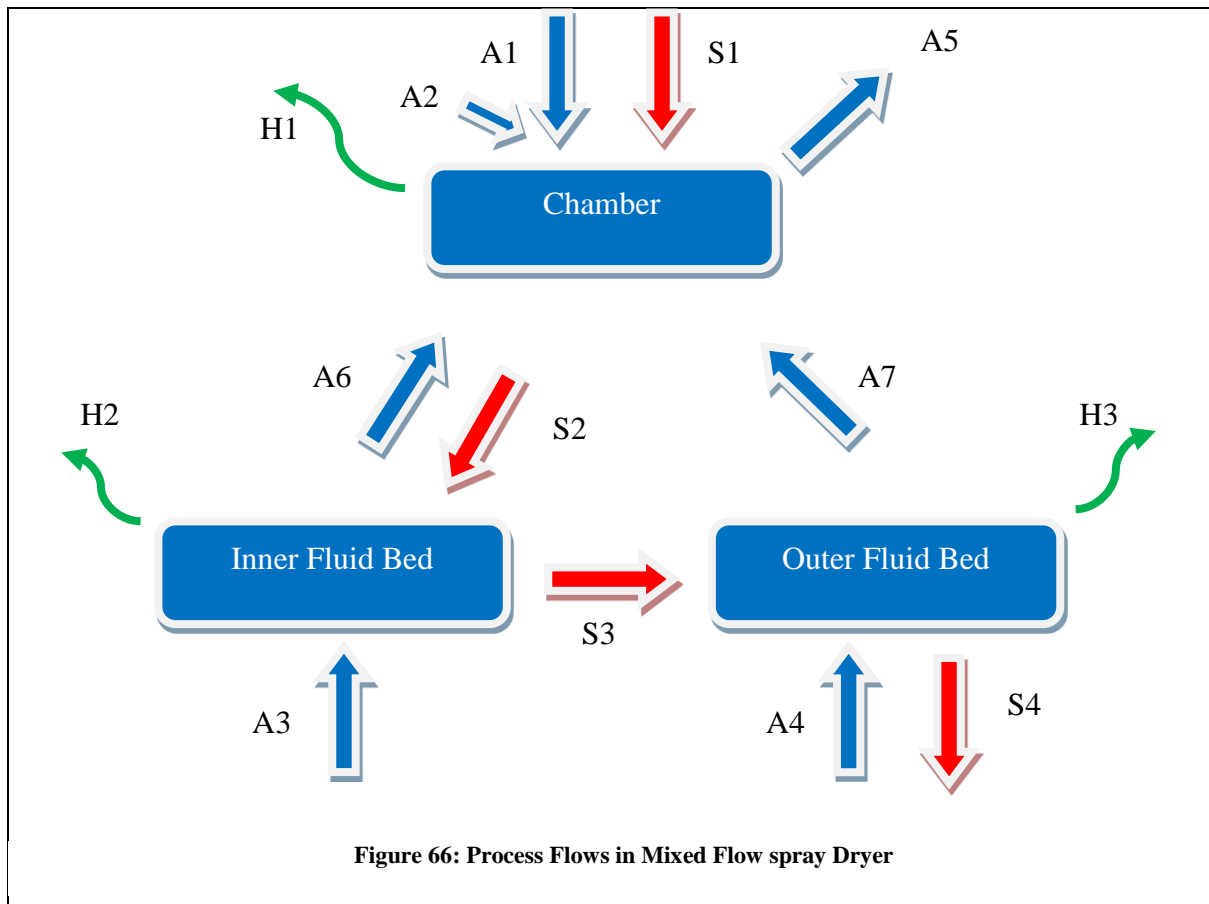
Assumption 1: Well Mixed Fluid bed

The assumption that the fluid bed is well mixed means that the temperature measurement from inside the fluid bed can be used to represent the temperatures of *A5*, *A6*, *S3* and *S4*. This is a common assumption as fluid beds are normally described by CSTR models.

Assumption 2: Particles exit at 100 °C

The temperature of the particles exiting the chamber should lie in between the inlet slurry temperature and the temperature of the particles now set in the inner fluid bed. In the batches analysed, the inner fluid bed temperature never dropped below the boiling point of pure water, 100^0C. If a significant amount of drying occurs in the chamber, the particles should have entered the "falling rate period" and the temperature should be at or approaching their boiling point. The particles are expected to be in the "falling rate period" as it is expected that most of the drying occurs in the chamber. Because of this, it is likely that the particle temperature is very close to 100^0C.

Assumption 3: No Heat losses in the Inner fluid bed

The inner fluid bed is surrounded by the outer fluid bed in the mixed flow spray dryer. Because of this, the heat losses to the surroundings have been assumed to be negligible.

Assumption 4: Heat loss from the Outer fluid bed occur via convection

The total heat losses from the process can be retrieved once the offset in the air humidity is accounted for, by using a manual measurement of the moisture content of the powder flow, *S4*. The distribution of these heat losses between the chamber and the fluid beds is unknown. By assuming the heat losses from the fluid bed are convective, it can be expressed by Equation 73 which is a function of the temperature difference between the outer fluid bed and the surroundings.

$$Heatloss_{OFB} = hA(T_{OFB} - T_{Ambient})$$

Equation 73

The convective heat transfer coefficient (h) and surface area (A) would both be constant for every historical batch so their contribution can be fitted. The heat losses must be low enough

to ensure that drying takes place in the outer fluid bed, but the amount of drying should also be considerably less than the chamber and the inner fluid bed, as the drying rate is slower at lower moisture contents. Using the historical data, hA was fitted to a value of 4 WK^{-1} which ranged from 10% to 30% of the total heat losses for each batch.

Table 4 lists how each equation was used to find unknown variables in the process. This can be carried out for every manual measurement of moisture to obtain the mass flow (M), water content (W) and temperature (T) of each stream in the process.

<div align="center">Table 4: Equations used to retrieve unknown Variables</div>

Equation	Unknown Variable
$T_{IFB} = A6(T)$	A6(T)
$T_{IFB} = S3(T)$	S3(T)
$T_{OFB} = A7(T)$	A7(T)
$T_{OFB} = S4(T)$	S4(T)
Liquid Mass Balance$_{Chamber}$	S2(M)
Gas Mass Balance$_{Chamber}$	A5(M)
Liquid Mass Balance$_{IFB}$	S3(M)
Gas Mass Balance$_{IFB}$	A6(M)
Liquid Mass Balance$_{OFB}$	S4(M)
Gas Mass Balance$_{OFB}$	A7(M)
Liquid Mass Balance$_{Overall}$	S2(W)
Gas Mass Balance$_{Overall}$	A5(W)
$S4(W) = X_{manual}$	S4(W)
Heat Loss$_{OFB = UA(T_{OFB} - T_{AMB})}$	H3

$Heat\ Loss_{IFB} = 0$	H2
$Heat\ Loss_{Chamber} = Heat\ Loss_{Total} - Heat\ Loss_{OFB}$	H1
$S2(T) = 100$	S2(T)
$Heat\ Balance_{Chamber}$	A6(W)
$Heat\ Balance_{IFB}$	S3(W)
$Heat\ Balance_{OFB}$	A7(W)

This compartmental approach allows further analysis of the drying process as a much larger insight into the system is provided. The amount of drying in each compartment is now modelled based on fundamental equations and can be used further to fit drying models. As reviewed in the literature, to fit these models, the size distribution and particle motion in each compartment needs to be represented in order to fit the rate based models. It is very important to understand the amount of time the particles spend in the dryer and the conditions they are subject to. Accurate representation of the process will enable comparison between batches, and enable analysis of the relationship between the powder properties and the process variables that can be manipulated.

3 Residence time study of the Compartments

Compartmental heat and mass balances are used to provide an estimation of the total amount of drying and energy transfer in each compartment. In order to use rate based models, it is necessary to estimate the rate of drying from the total amount of drying, and the residence time in each compartment. This highlights the importance of the estimation of the residence time of particles in the dryer. To use traditional methods such as the tracer approach, a sample point would be needed at the exit of each compartment. As the only sample point is at the exit of the process, the method could only be used to estimate the overall residence time. This would provide no insight into the influence of each compartment on the residence time and their sensitivity to changes in processing conditions. In order to estimate the residence time for each compartment, assumptions have been made in order to use modelling techniques applied in the literature for co current spray chambers and fluid beds.

3.1 Residence time of the Chamber

Depending on the complexity of the drying models, estimations of the residence time in co current towers vary between studies in the literature. The simplest method is to assume that the mean residence time of the particles is equivalent to the residence time of the air, which is calculated by dividing the volume of the spray dryer by the volumetric flow of the air (Birchal, Huang, Mujumdar, & Passos, 2006). This is applied to dryer processes where the air and powder exit at the same point. In these cases, the relative velocity of the particles and the air is assumed to be null, meaning that the heat and mass transfer coefficient estimation is simplified. With no relative velocity, the Reynolds number defaults to zero so using the Ranz Marshall equation, the Nusselt and Sherwood numbers are equivalent to their lower limit of 2. In more complex systems or scenarios where more detail about each particle is needed, CFD is used. This can provide the necessary detail needed to fit any rate based model, provided that the user

inputs the necessary equations. CFD has been used frequently to simulate drying of individual particle streams throughout the complex system (Huang, Kumar, & Mujumdar, 2006; Mezhericher, Levy, & Borde, 2009; Oakley, Scroll, & For, 2007; Wai et al., 2008a; Woo et al., 2008).

The mixed flow spray dryer system provides a more complex situation, where the air flow enters and exits at the top and bottom of the chamber. The air does not exit with the powder so the residence time of air should not be used. To understand the impact of a mixed flow regime on the residence time, CFD has been used to model the chamber.

3.1.1 CFD of the Chamber

ANSYS Fluent CFD software was used to simulate the chamber. To do this the following steps are taken:

1. Create the geometry of the chamber and apply suitable meshing technique

2. Set boundary conditions & Material properties

3. Simulate with single phase using Eulerian approach

4. Simulate with multiple phases using Eulerian-Lagrangian approach

5. Provide drying model and select correct settings for simulation

6. Analyse particles properties exiting chamber and validate with finding from experiments

Create the geometry of the chamber and apply suitable meshing technique

The geometry was produced using the dimensions expressed in section 2.1 of the Material and Methods chapter. The meshing of the chamber was carried out by the modelling department at P & G. The tetrahedron mesh consisted of 1.2 million cells with a minimum orthogonal quality reported to be 0.21. The max orthogonal skewness was 0.72 and the aspect ratio was reported to be 3.43.

Set Boundary conditions & Material properties

The boundary conditions are dependent on the scenario to be run. To ensure the CFD provides an accurate representation of the process, 5 scenarios have been chosen for simulation. These scenarios are based on experimental results recorded from 3 batches run continuously after each other on the same day with the same formulation. The settings are listed in Table 5, which details the flows, temperatures and sauter mean diameter of the distributions for each scenario. The flows in from the bottom of the chamber were assumed to be a well-mixed combination of the air flows from both the inner and outer fluid beds. There flows have been summed and the temperature and moisture content have been averaged. During normal operation, the temperature of the main air flow into the chamber is rarely manipulated and the air flow is kept constant. The size distributions entering the dryer and slurry rate are the main variables manipulated in the chamber, so these 5 scenarios have been chosen as they represent a range of distributions and slurry flows.

Table 5: Scenario Settings

Scenario	$m_{Air,Chamber}$ (kg/hr)	$T_{Air,Chamber}$ (^0C)	$m_{Air,Fluidbeds}$ (kg/hr)	$m_{water,Fluidbeds}$ (kg/hr)	$T_{Air,Fluidbeds}$ (^0C)	m_{Slurry} (kg/hr)	$D_{3,2}$ (μm)
1	180	300	200	4.8	107	44	245
2	180	300	200	5	107	44	268
3	180	300	200	5.3	103	44	286
4	180	300	200	5.8	100	50	304
5	180	300	200	6.5	108	40	315

Further boundary conditions are related to the walls of the chamber. The setting for the walls of the chamber was chosen as follows: coefficient of restitution or the discrete phase reflection

coefficient was set at 0.4. The roughness height was $0.002m$ and roughness constant was 0.5. It was assumed that heat losses were convective and a heat transfer coefficient of 5 $Wm^{-2}K^{-1}$ was fitted to produce the expected heat losses from the compartmental heat balance for all scenarios. The wall thickness was set at a value of $0.008m$. The free stream temperature was set to room temperature of 20^0C.

With the boundary conditions set, the material properties are needed before the simulation is carried out. For the material properties of air, empirical correlations were used to estimate the changes in respect to temperature. Hese were fitted to tabulated data online (The Engineering toolbox 2010). The correlations were needed to estimate density, specific heat, thermal conductivity and viscosity. The equations used are listed below, where change in viscosity is represented by Sutherland's law.

$$\rho_{Air}(T) = 2.4719 - 0.0056T + 4e^{-6}T^2$$

Equation 74

$$Cp_{Air}(T) = 1002.64 + 0.07114T + 2.14e^{-4}T^2$$

Equation 75

$$\lambda_{Air}(T) = 0.0241 + 7e^{-5}T$$

Equation 76

$$\mu_{Air}(T) = 1.716e^{-5}\left(\frac{T}{273.11}\right)^{\frac{3}{2}}\frac{273.11 - 110.4}{T + 110.4}$$

Equation 77

For slurry, the specific heat was set to 2000 $J\ Kg^{-1}K^{-1}$ the latent heat was assumed to be 2260 $kJ\ Kg^{-1}$ and the density was approximately 1300 $Kg\ m^{-3}$.

Converge simulation with single Eulerian phase

Before injecting the distribution, the scenarios must be converged with a single phase. To do so, the boundary conditions are needed, along with choice of models and methods for CFD to use. Following recommendation from the P & G modelling department, the Reynolds stress, seven equations viscous model was used and in solution methods, PISO and PRESTO were used for spatial discretization of the pressure. For all other methods, the first order upwind methods were used, apart from H_2O which used second order upwind.

The simulation was run with one phase in steady state until it converged after approximately 800 iterations, with most residuals ranging from 0.01 to 0.001. The residual for energy was around $1e^{-7}$. Figure 67 and Figure 68 illustrate the temperature and velocity profiles in the chamber once the simulation had converged. As you can see from the figures, the profile is close to symmetrical, as would be expected in a steady state system.

Figure 67: Contour of Temperature in Chamber (*K*)

Figure 68: Contour of Air Velocity in Chamber (*m/s*)
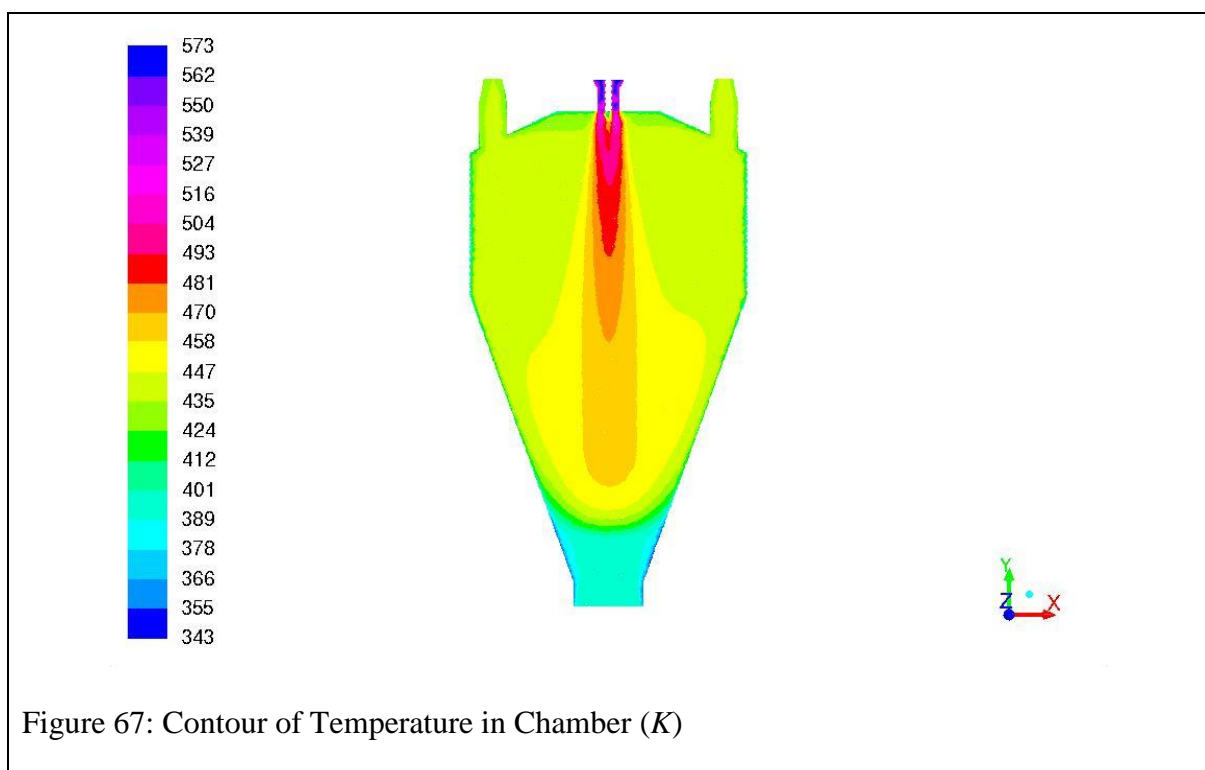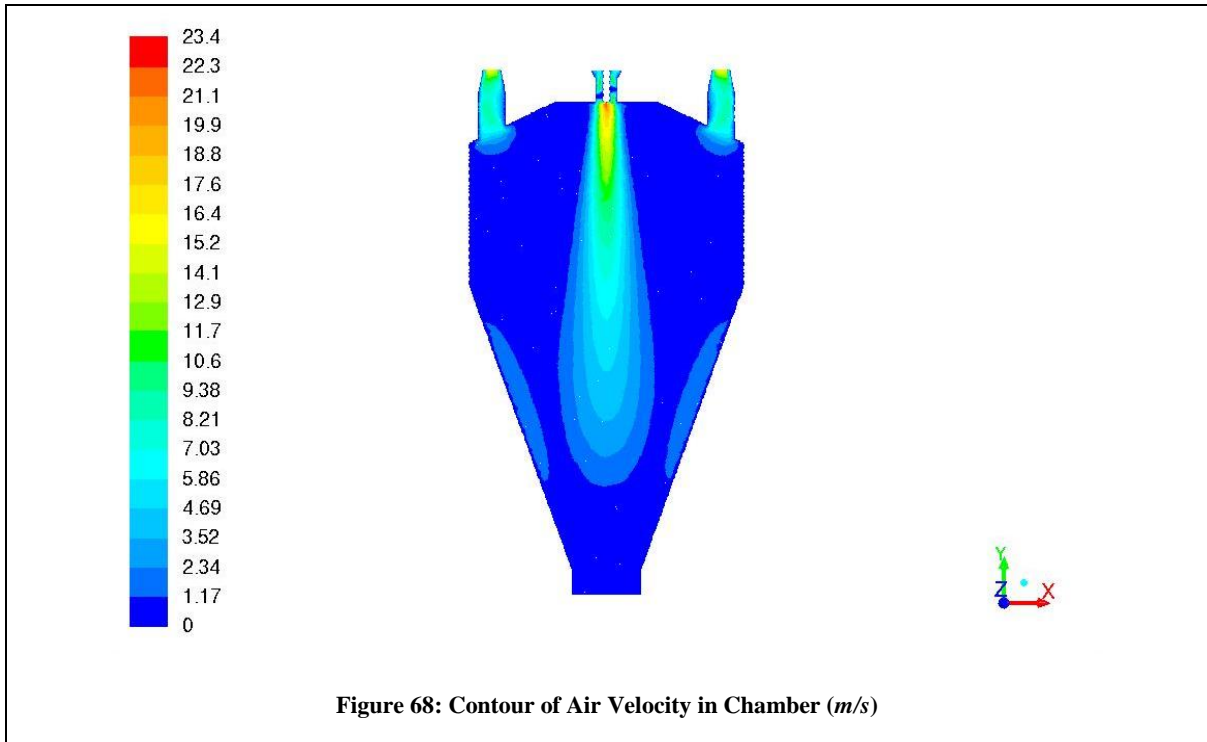
Simulate with multiple phases using Eulerian-Lagrangian approach

Once converged, the discrete phase can be introduced to the process. The introduction of particles into the CFD was carried out using a discrete phase method. The location of the nozzle tip was in the centre of the mesh, approximately 13cm down from the top of the chamber outlets. In order to inject the particles, the distribution has to be expressed along with the initial velocity and spray angle. The preferred option for modelling the distribution in the modelling department is described using a Rosin-Rammler distribution as expressed in Equation 78 where the parameters n and D_m need to be defined to obtain the cumulative distribution function.

$$R_{CDF} = 1 - \exp\left[-\left(\frac{D}{D_m}\right)^n\right]$$

Equation 78

Additional information on the spray type, direction, velocity and angle are also needed for the injection. The spray type is set as a full cone which sprays directly downwards into the chamber. The initial velocity and spray angle are dependent on the nozzle. Recommendations

167

for the initial velocity varied in literature. In some studies, where the particle size was low ($<50\mu m$) the initial velocity was very high (towards the velocity of air) and varied with size, but dropped off significantly in a short space of time (Gauvin, Katta, & Knelman, 1975). More recent studies have suggested that the initial droplet velocity is equivalent to the velocity of the liquid through the nozzle tip (Fritsching, 2005). The typical cone angle for a two fluid nozzle has been reported to range from 15 to 60 degrees (from centre to edge of spray), and depends on the characteristics and geometry of the nozzle used (Shafaee, Banitabaei, Esfahanian, & Ashjaee, 2012). The cone angle plays a vital role in the trajectory of the particles along with the initial velocity. To ensure that the correct settings were used, a high speed camera was utilised to analyse the initial velocity and spray angle using the atomization rig. Water was sprayed at 40 *kg/hr* with the typical air flows used with the nozzle. Setting the frame rate to 4000 frames per second and the exposure to 247µs, the approximate velocity could be quantified along with the angle. A typical frame is illustrated in Figure 69 where the nozzle tip is located on the left hand side and was used as a reference to calculate the distance travelled. The distance between the nozzle and the edge of the frame was 29mm and the velocity estimated in this distance was assumed to be equivalent to the initial velocity. After careful consideration of multiple frames, the spray angle was estimated as 30 degrees (from centre of spray to edge) and the droplet velocity was equivalent to roughly 3.5 *m/s*. This velocity was equivalent to the calculated liquid velocity exiting through the 2*mm* nozzle tip using a water flow rate of 40 *kg/hr*. The spray produced had a droplet size in the desired range and so the angle was assumed to be the same with slurry. Because of this, for simulation purposes, the angle has been assumed to be roughly 30 degrees and the initial velocity can be calculated based on slurry rate, slurry density and area of the nozzle tip for a given scenario. Any change in angle at lower or higher velocities could not be seen as significant so the angle was assumed to be constant.

Figure 69: Typical Frame of atomization from nozzle
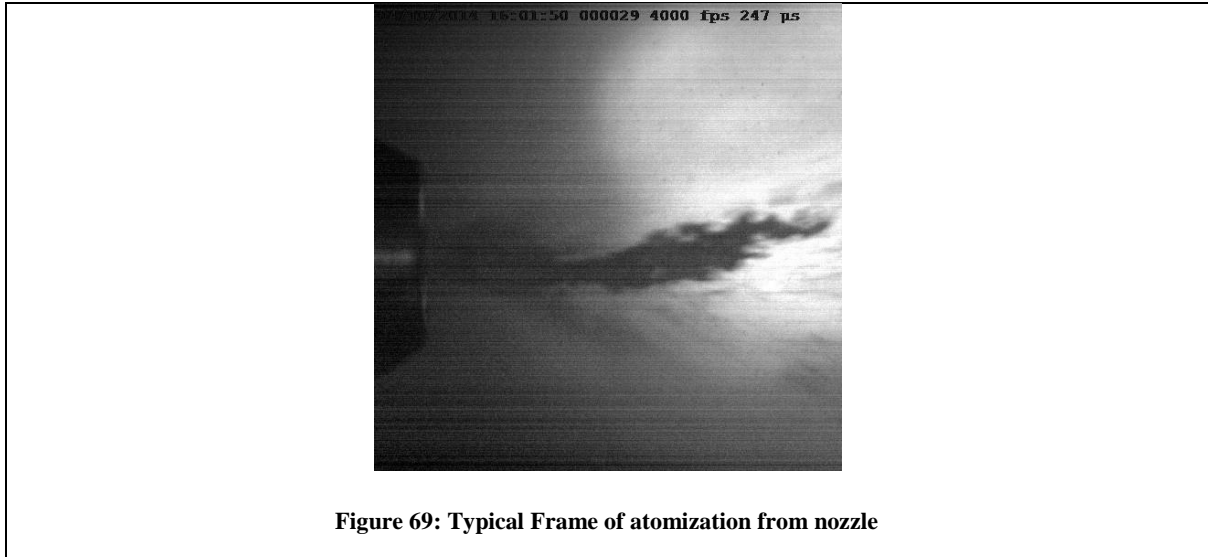
With the initial velocity and spray angle known, the final task is to fit the distributions for each scenario. In each scenario, the PSD of the powder was recorded and used to estimate the initial particle size. Using the values of $D_{3,2}$, $D_{v,10}$, $D_{v,50}$ and $D_{v,90}$ for each distribution, the Rosin-Rammler parameters were fitted for the particle injection. For this formulation shrinkage was minimal and so it was assumed the particle size does not change. The fittings use a set amount of particle sizes that are linearly spaced between a minimum and maximum particle size defined by the user. The correct sizes should be chosen to ensure the distribution is correctly represented in the simulation. Because of this, a total of 30 different particle sizes have been chosen. From the study of atomization of the slurry it was found that the particle sizes rarely exceeded $700\mu m$. The drying rate of droplets above this size is very low so any contact with the wall of the dryer would result in build up as it sticks. As I have assumed that this phenomenon does not occur, the maximum size was capped at 700. The powder does have $D_{v,90}$'s of greater values so it is also assumed that these measurements are a result of agglomeration in the process and are not produced at the nozzle. Because of this, the influence of $D_{v,90}$ on the fitting of the Rosin-Rammler distribution was reduced. The minimum size was

set at 50 μm. The fittings parameters for each distribution are listed in Table 6 given the limits of 50 to 700 μm. The resulting fits are expressed in Table 7.

Table 6: Rosin-Rammler parameters

Scenario	D_m	N
1	374	2.2
2	438	2.11
3	486	2.11
4	500	2.25
5	596	2.1

Table 7: Rosin-Rammler fittings

Scenario	$D_{3,2}$ (μm)		$D_{v,10}$ (μm)		$D_{v,50}$ (μm)		$D_{v,90}$ (μm)	
	Measured	Estimate	Measured	Estimate	Measured	Estimate	Measured	Estimate
1	245	244	148	129	268	306	643	520
2	268	268	162	139	312	343	767	577
3	286	286	172	150	331	368	884	600
4	304	304	173	165	373	384	1025	607
5	315	315	176	169	405	409	1072	629

The fitting process has focussed on reproducing the $D_{3,2}$ of the distribution, as this is the most characteristic of the spray for heat transfer purposes. The $D_{v,10}$ and $D_{v,50}$ values are also important, but have larger errors associated. The errors were still below 10% despite being limited to using 2 parameters in the Rosin-Rammler fitting. The size cap at 700μm and the

reduced influence of the $D_{v,90}$ measurement result in its high error values. This was necessary for the model as discussed on the previous page.

Provide drying model and select correct settings for simulation

With the initial conditions set for the simulation, the next step was to define a drying model and set processing parameters that estimate the heat losses and trajectories of the particles. The drying model used in this analysis was an internal model produced by P&G and based on three drying modes: surface drying, diffusion drying and puffing. A detailed description of the model can be found in the literature (Ali et al., 2014). The compartmental heat and mass balance was used on the experimental data for each scenario listed in Table 5. This provided a drying rate for the chamber and its associated exhaust temperature for each scenario. The drying rate in the model was modified to match the experimental drying rate. From analysis the dominant drying mode was diffusion drying. Knowing this, the parameters in the algebraic equation for this mode were modified. Equation 79 provides the model stated in the literature(Hecht., 2014)

$$-\frac{dm_{Droplet}}{dt} = 10^6 \, r_p \exp\left(-A\left(\frac{t-t_{sd}}{10^6 \, r_p}\right)^B - C\right) \qquad \textbf{Equation 79}$$

where t and t_{SD} represent time and the surface drying mode time period and r_p is the radius of the particle.

The exhaust temperatures produced by the simulation for each scenario were then compared to the experimental measurement to validate the simulation. The results are listed in Table 8. The temperature of the exhaust in the simulation was estimated by the area weighted average of the air temperature exiting the exhausts, and the water content was the mass-weighted average of the water content in the air exiting the exhaust, minus the water content in from the fluid bed. The results indicate that the simulation represents the process and captures the effects of changing the distribution and slurry rate. The results are very promising as there is a clear

change in the total drying carried out depending on slurry rate and distribution. The largest error in temperature is associated with scenario 4, which differs from the other scenarios due to its flow rate of 50kg/hr. However, the error is still less than 5% which is very low considering the number of assumptions made to estimate the process conditions from the experimental data. The largest error in the total drying carried out was found in scenario 1, with the smallest particle size. The error again is below 5% and is likely to be a result of the accuracy of the single Rosin-Rammler fitting. The single drying model applied for all scenarios provides an accurate simulation of the drying rate and temperature change of the air in the chamber.

Table 8: Simulation results vs Experimental results

Scenario	$D_{3,2}$ (μm)	Exhaust Temperature ($^o C$)		Drying rate (kg/hr)	
		Batch	CFD	Batch	CFD
1	245	111.5	111.2	9.0	9.3
2	268	113.8	114.8	8.5	8.5
3	286	114.4	114.7	8.0	8.0
4	304	114.5	110.5	9.0	9
5	315	121	121.8	6.8	6.6

Analyse particles properties exiting spray chamber and validate with findings from experiments

As the simulations matched the exit conditions for each scenario, details of the particle properties were analysed. Figure 70 illustrates the particle tracks inside the spray dryer chamber for a given simulation. The tracks are coloured using their overall residence time in the chamber. Every 10th particle size was omitted to prevent overcrowding of particle tracks in the figure. Most tracks have the colour blue, as the residence time for all particles greater than 200 μm was generally less than 1 second. More detailed information on the particle tracks was

obtained by making samples at the nozzle tip, the bottom outlet and the exhaust. The mesh height was used to filter the particle tracks so that only particles closest to the outlets and the nozzle were recorded. For the nozzle inlet, the first value recorded for each particle ID was used and for the outlets, the final value was used. The recorded data for each particle, to be used for analysis, included its particle size, moisture content and residence time. Any particles stuck in the simulation could also be highlighted by comparing the particle identification number's in the inlet to the outlets.

Figure 70: Particle tracks residence time (seconds) in simulated spray dryer chamber, Scenario 1
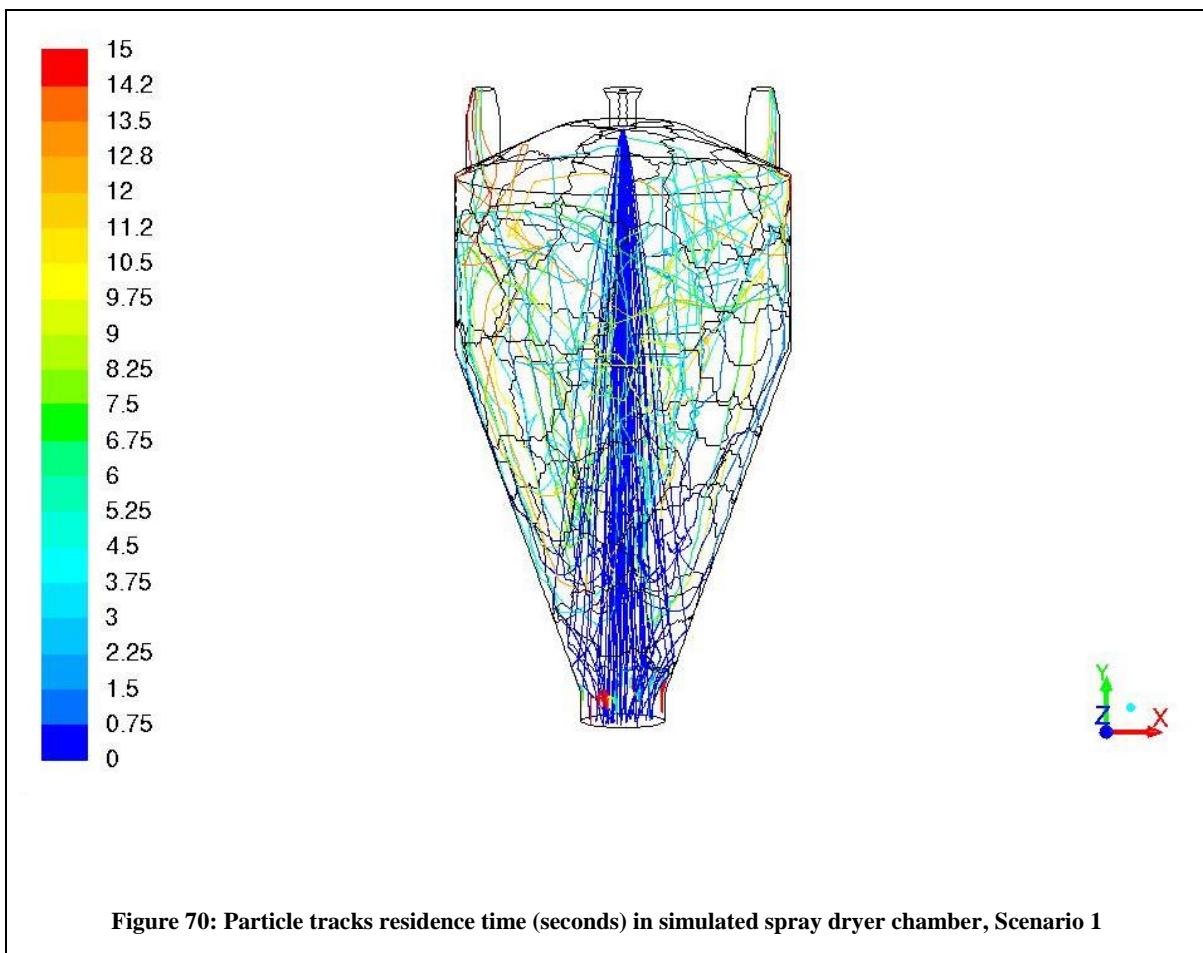
Figure 71 shows how the powder outlet distribution leading to the fluid beds differs to the inlet in scenario 2. This is a result of shrinkage and loss of fines in the exhaust stream. The shrinkage effect can be seen by the shift of the data points to the left, and the loss of fines clearly occurs with particle sizes less than 100 μm. The fines distribution was dominated by a peak for the

particles beginning at 50 μm. The 95 μm particle size tracks tended to get stuck in the simulation and not exit the system even after 50,000 iterations. Out of all 5 simulations, only 3 of the 250 particles sized 95 μm exited through the chamber outlets. This seems to be the result of an equilibrium in the particle speed. The particles are too heavy to be lifted out of the chamber and too light to exit the bottom past the fluid bed air flow. Therefore, no matter how long you run the simulation, the particle will stay in the same place. Particle sizes starting at 72 and 117 μm also tended to get stuck in the simulation, with a total of 29 and 22 out of 250 particles exiting for each size respectively.

Figure 71: Inlet distribution vs Powder Outlet, Scenario 2
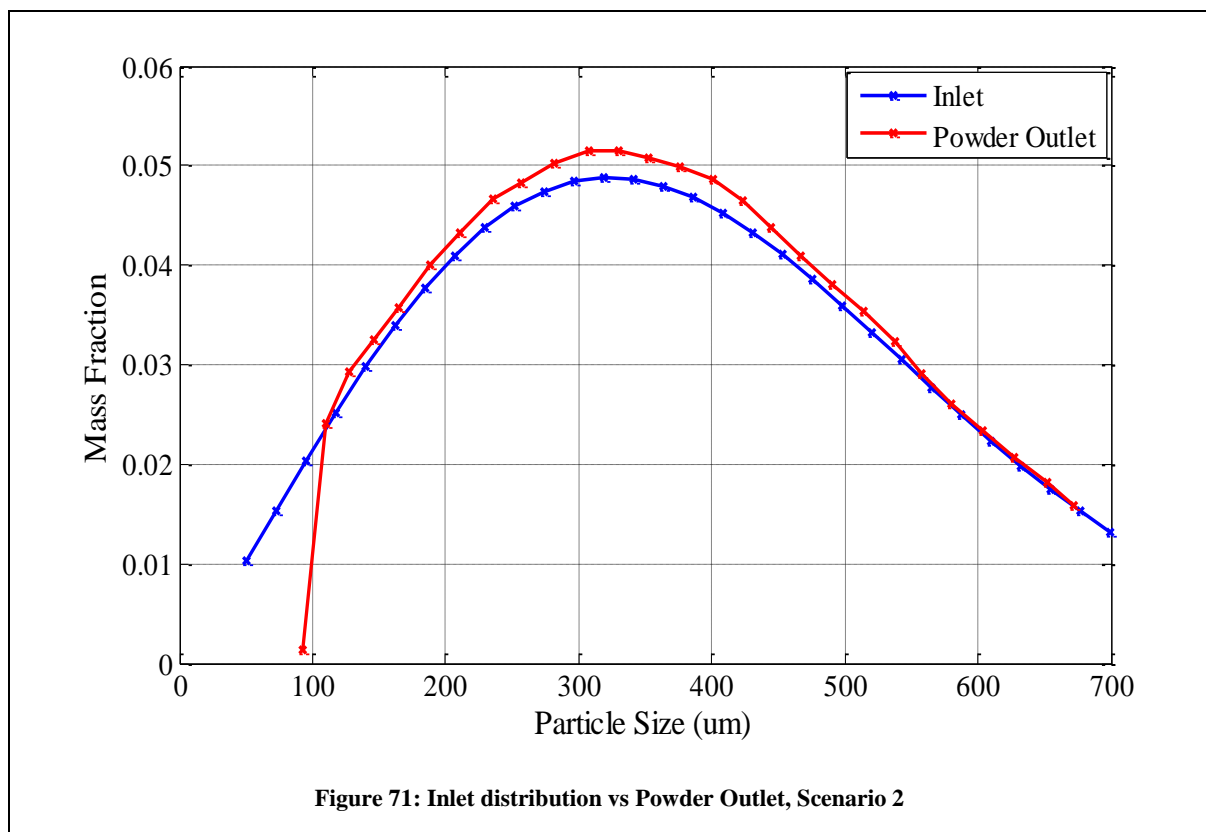
Figure 72 shows the average moisture content based on mass distribution for each particle size exiting the bottom outlet of the chamber. All particles below 150 μm exiting the bottom dried to 0% moisture in the chamber. These particles would have significantly shorter residence times than those that were stuck in the simulation, which means that all stuck particles in the

174

simulation would be fully dried. This means that the moisture removed is independent of the amount of stuck particles below 150 *μm*. The initial moisture content for each particle was 0.3275, and as particle size increases, the amount of drying reduces; this is likely to be related to the residence time of the particles, as drying rates increase with particle surface area.

Figure 72: Moisture content of Particles, Scenario 2
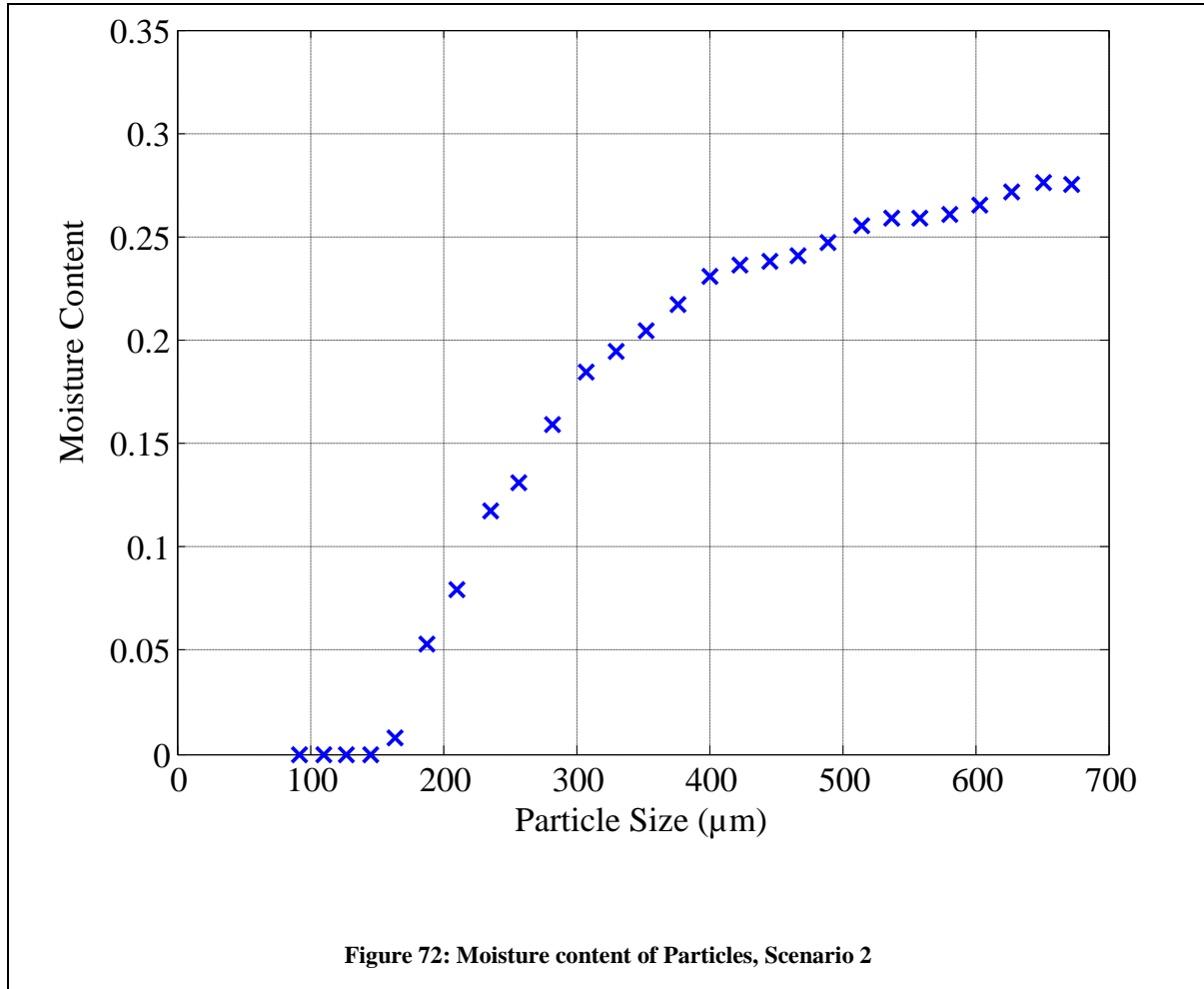
The residence time for individual particle sizes and for the entire distribution, can be calculated in a number of ways. It can be done by taking the average residence time per particle size cut in the distribution. This would treat the process like a plug flow reactor, as each particle size or the entire distribution are be assumed to spend an exact amount of time in the chamber. The most appropriate method involves the distribution of residence time per particle size. Figure 73 to Figure 75 illustrate the distribution of residence time for each particle size in each of the 5

scenarios simulated. The initial particle sizes are stated as 50 μm, 184μm and 431μm for the relevant figure. The first 3 scenarios are expected to yield the same results. The only difference in the inlet conditions is the particle distribution and the particle tracks do not interact with each other.
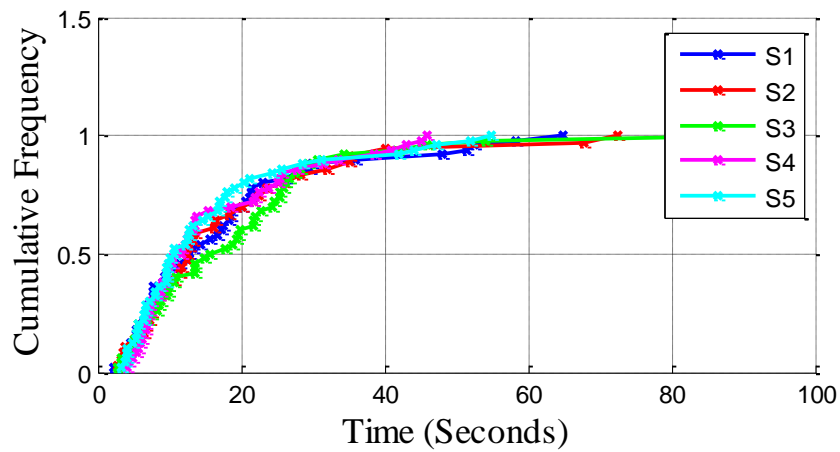

Figure 73: Residence time distribution for Particle Size of 50 *μm*
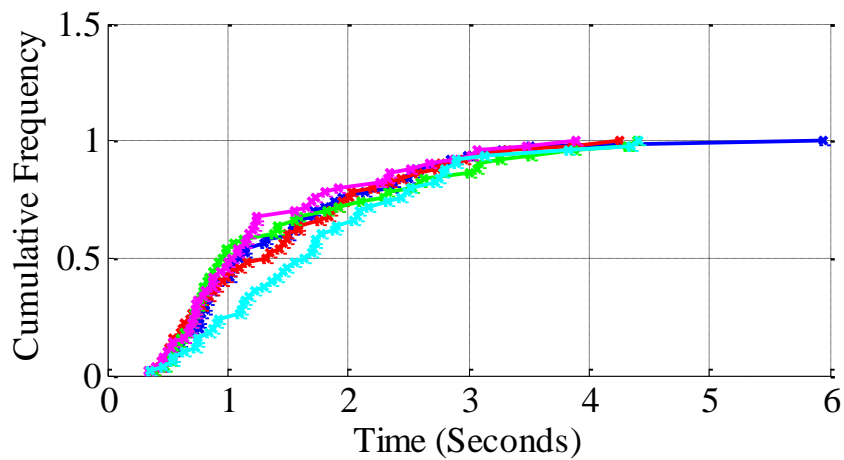
Figure 74: Residence time distribution for Particle Size of 184 *μm*

176
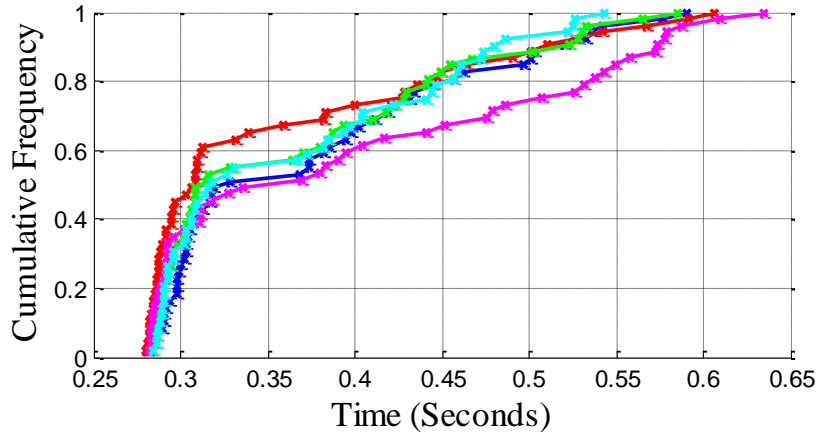
Figure 75: Residence time distribution for Particle Size of 431 _μm_

The slurry rates of the 4th and 5th scenario are 40 and 50 _kg/hr_. This provides an initial velocity of 2.28 _m/s_ and 2.85 _m/s_. However, the air flow velocity around the nozzle is 10 times greater, at around 28m/s, which could explain why the impact of changing slurry rate seems to be minimal according to the figures. It is clear that the residence time of different particle sizes is significantly different, with the 50 _μm_ having residence times spread over 60 seconds, and all particles of size 431 _μm_ leaving within 0.65 seconds. The minimum time for a particle to exit is always greater than 0.27 seconds for all particle sizes. This would mean a CSTR fit to the residence time would not be accurate, as CSTR assumes particles can exit straight away. Particles below 200 _μm_ have a minimum time greater than this depending on size, but all sizes above have a minimum time ranging from 0.27 to 0.3 seconds independent of size. The remaining particles all follow a trend similar to a CSTR. By combining a CSTR and PFR equations, the distributions can be represented by Equation 80. This combines a time delay variable, θ to represent the plug flow residence time, and a CSTR model with residence time, τ.

$$M_{CDF} = 1 - \exp\left(-\left(\frac{t + \theta}{\tau}\right)\right)$$

Equation 80

As there is no obvious effect of changing the slurry rate on the residence time, all 5 scenarios have been used to fit the residence time distribution function. An example of this is shown in Figure 76, where $\theta = 0.26$ and $\tau = 0.12$. The mean residence time results for all particle sizes in the distribution are displayed in Figure 77. The mean residence time initially increases as the first two particle sizes exit the exhaust, where it is beneficial to be smaller. The mean residence time of particle sizes from 70 to 200 μm then rapidly reduces from around 47 seconds to 0.4 seconds, where all the remaining particle sizes exit in approximately the same length of time.

The residence time distribution can now be used along with the particle size distribution to fit any rate based drying models. However, this method makes it necessary to have the entire size distribution. For simplification, it has been assumed that given the $D_{3,2}$, the characteristic particle size correlations fitted to the distributions should be robust enough to represent the PSD's for the operation of this unit. The characteristic residence time of the entire distribution is then simply the summation of the product of the average residence time and particle size distribution on a mass basis. The resulting characteristic residence times for a distribution are shown in Figure 78. The red line indicates a fitting to the data expressed in Equation 81.

$$\overline{\tau}_{Chamber} = 99677 \cdot D_{3,2}^{-1.943}$$

Equation 81

178
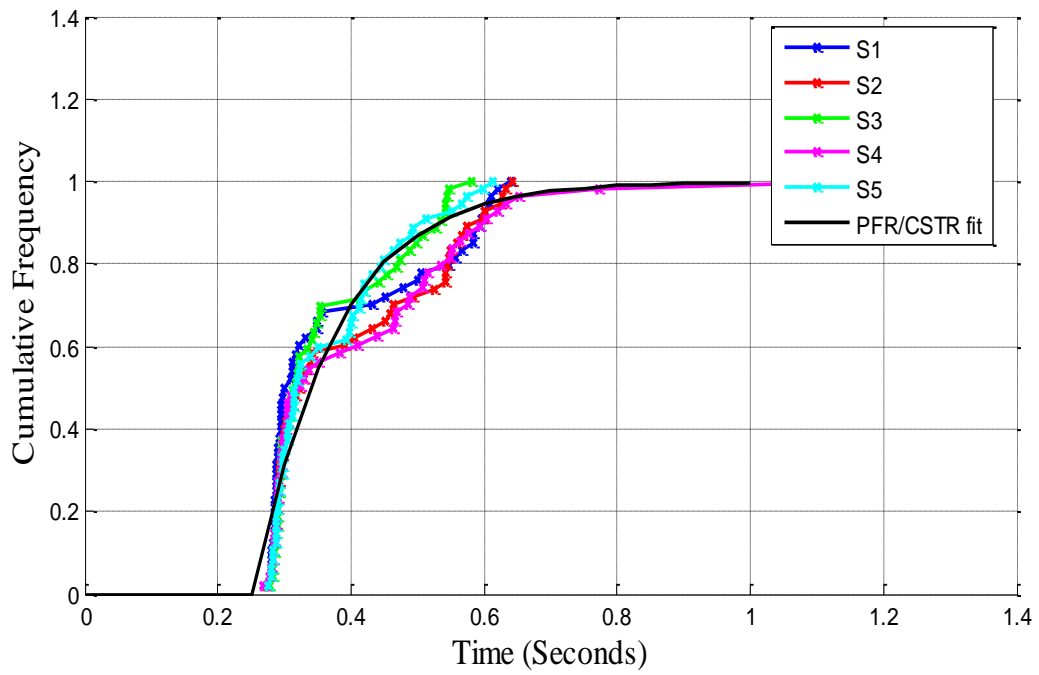
Figure 76: Fitting PFR/CSTR fit to distribution, 319 *μm*
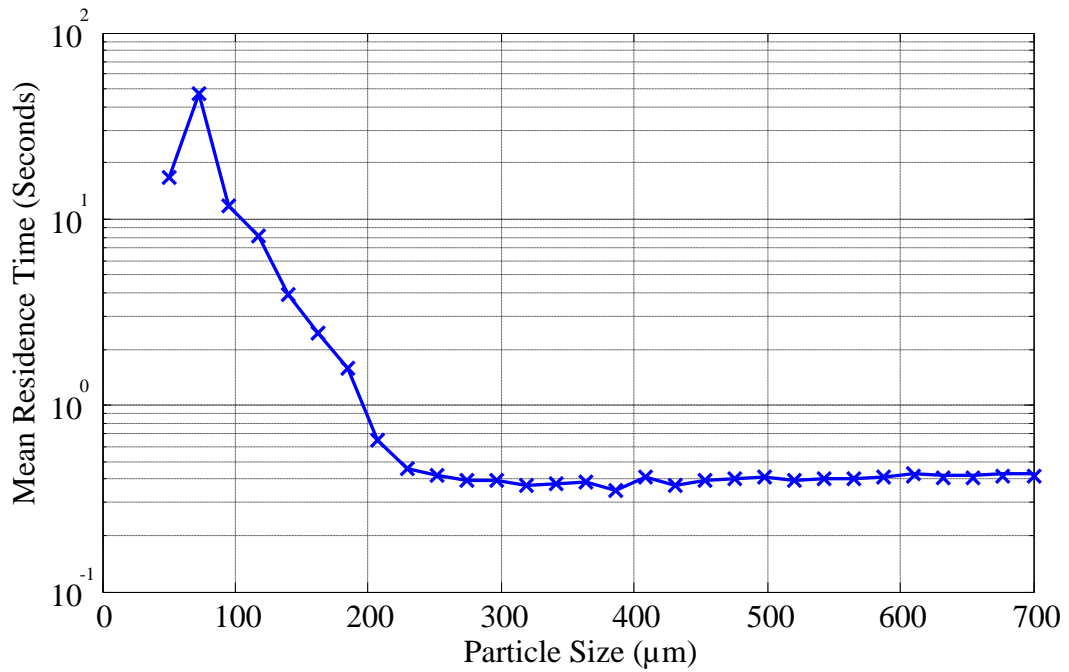
Figure 77: Residence time Distribution of each Particle Size

Figure 78: Change in CharacteristicResidence time with $D_{3,2}$
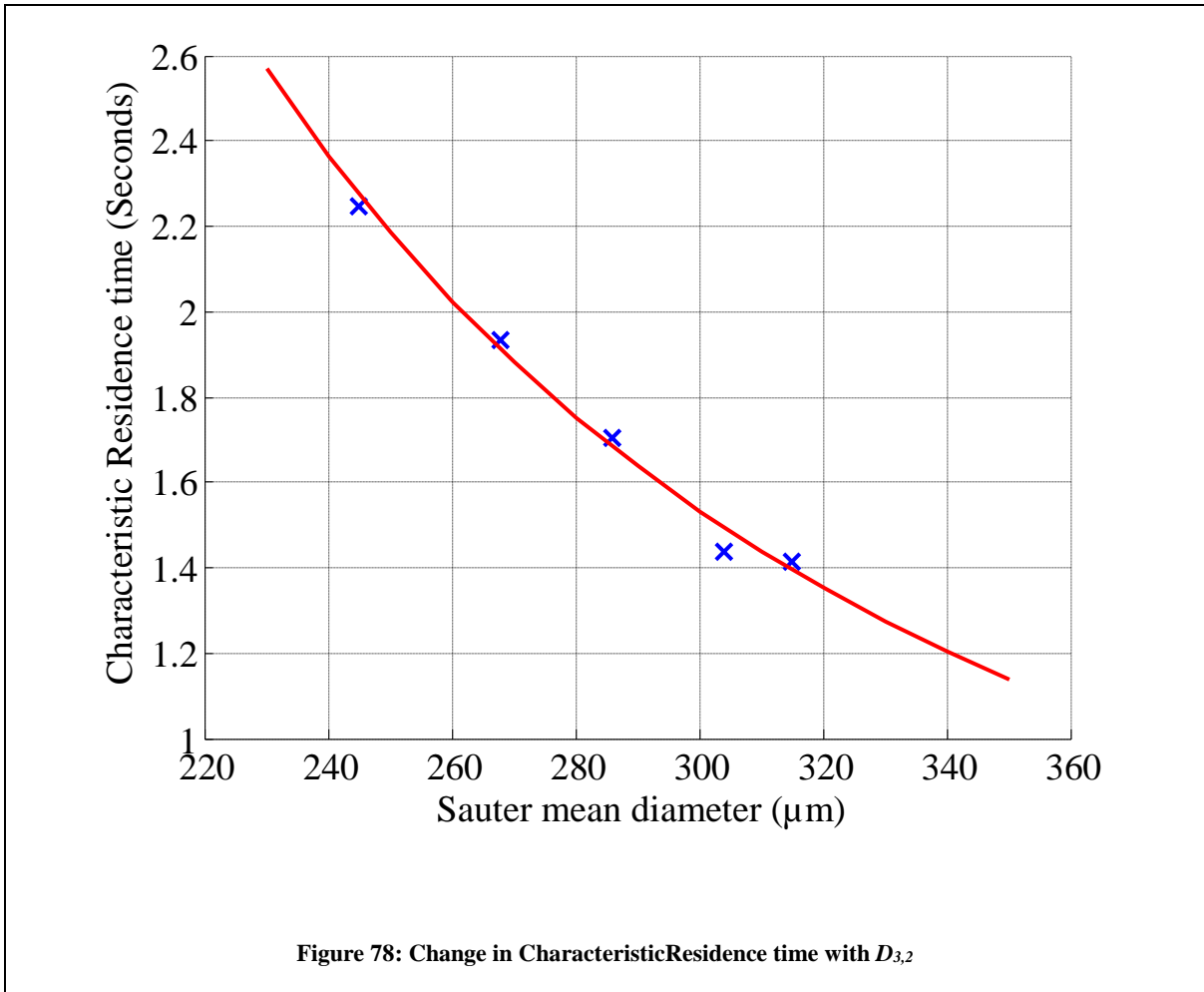
3.2 Residence time of the fluid beds

The fluid bed in the mixed spray dryer system is split into two compartments. For the outer fluid bed, the powder flow out of the system is controlled by the systematic opening of a valve to release the powder from the dryer. To reduce air leakage, this valve opens into a contained volume for the powder which is eluted once the valve used to release the powder is shut. The valve opening follows a systematic cycle. It remains closed for 9 seconds and then opens for 6 seconds, providing an average residence time for the powder of 7.5 seconds. The inner compartment can be assumed to behave like a typical fluid bed. The powder enters from the top of the bed and is eventually elutriated over a weir into the outer compartment. Air makes

contact with the powder flow via a perforated plate at the bottom of the fluid bed. Detail on the dimensions of the fluid bed is expressed in the Material and Methods chapter.

Fluid beds and fluidization have been researched extensively in order to understand the dynamics of the process (Pell, 2008; Richardson J.F., 2002; Wen-Ching Yang, 2003). This research has led to a common set of equations that can be utilised to model the fluid bed in order to estimate the residence time and heat transfer rates. For residence time, it is necessary to estimate or measure the bed height, cross sectional area, bulk density, voidage of the fluid bed and the mass flow rate. Firstly the total volume occupied by particles in the fluid bed is calculated by Equation 82

$$Volume_{Particles} = (1 - \varepsilon) A_{IFB} H_{BED}$$

<div align="right">**Equation 82**</div>

The fluid bed in the spray dryer process has a fixed height depending on how high the weir is located. By having a fixed height, the volume of particles is dependent only on the voidage in the fluid bed. To obtain the mean residence time, it has been assumed that the fluid bed behaves like a CSTR, and so the mean residence time (τ_{IFB}) is equivalent to the total volume in which the particles travel in the bed, divided by the volumetric flow rate of the slurry in the fluid bed.

$$\tau_{IFB} = \frac{Volume_{Particles}}{V_{Slurry,IFB}}$$

<div align="right">**Equation 83**</div>

where

$$V_{Slurry,IFB} = \frac{m_{Slurry,IFB}}{\rho_{Bulk,IFB}}$$

<div align="right">**Equation 84**</div>

By assuming the fluid bed behaves like a *CSTR*, the system is assumed to be fully mixed. In this case, the mass of slurry and density is equivalent to their value as the powder exits the fluid

bed. To calculate the density, the density model expressed in the bulk density modelling chapter is utilized assuming that all shrinkage occurred in the chamber. This means that changes in density after the chamber are a result of the change in mass of the droplets due to drying.

Voidage is highly dependent on the velocity of the fluid phase in the fluid bed. The air flow rate is set at 100*kg/hr* for all batches. According to technical drawings of the fluid bed, the inner compartment represented 37.1% of the total cross sectional area. Using the cross sectional area of the fluid bed expressed below in Equation 85, the air velocity was found to be around 100*cm/s* depending on the temperature of the air.

$$A_{IFB} = 0.371\left(\frac{\pi D^2}{4}\right)$$

Equation 85

Estimation of the effect of air velocity on voidage above the minimum fluidization velocity is difficult to predict. Research suggests that high levels of voidage around 0.75 occur for air velocities close to 100cm/sec and a bed height of 10cm (Bakker & Heertjes, 1959), but this was for fluidized beds of a larger diameter. With the measurements available, it is not possible to estimate the voidage value. The value from the literature provides an estimation for the residence time according to the overall residence time expected, so the voidage has been assumed to be 0.75.

The same approach was taken to model the residence time of the outer fluid bed. The bed height was assumed constant for both beds. As the area of the outer fluid bed was greater, so was the volume. As the mass flow of powder remained the same, the voidage would increase in the larger compartment. In this case, with increased air velocity and less powder, a value of 0.95 for the voidage was used. This value provided the desired overall residence time and followed the trends seen in literature as the voidage increased with a sharp gradient in relation to air velocity(Bakker & Heertjes, 1959).

4 Obtaining Heat and Mass Transfer Coefficients

With the total drying in each compartment known, along with the residence time, the rate based drying models can be fitted. When using rate based models for spray dryer processes, the heat and mass transfer coefficients are routinely estimated using Ranz-Marshall correlations (Chen, 2008; Mezghericher, Levy, & Borde, 2008; Seydel, Blömer, & Bertling, 2006; Wai et al., 2008b). These correlations are used in fluid beds (Kiel, Prins, & van Swaaij, 1993; Papadakis, Bahu, McKenzie, & Kemp, 1993), but there have been some extensive studies carried out to obtain a number of different correlations for these numbers, yielding very different results depending on the particle size and bed dimensions (Balakrishnan & Pei, 1979; Barker, 1965; Molerus & Mattmann, 1992). However, after using multiple, these correlations are expressed below in Equation 86 and Equation 87 were found to provide the expected results.

$$Nu = 2 + 0.6 \cdot \mathrm{Re}^{\frac{1}{2}} \cdot \mathrm{Pr}^{\frac{1}{3}}$$

Equation 86

$$Sh = 2 + 0.6 \cdot \mathrm{Re}^{\frac{1}{2}} \cdot Sc^{\frac{1}{3}}$$

Equation 87

The Reynolds number used in these correlations plays a significant role, but is reliant on an estimation of the relative velocity between the air and the particles. Currently this relative velocity is unknown, but can be estimated using an analysis carried out for each compartment. If the correlations don't produce the expected heat transfer coefficients for fluid beds of similar sizes, then other correlations may be utilized.

4.1 Relative Air velocity in Chamber

According to the particle tracks, the majority of particles travel down the centre of the chamber. Five lines were produced in CFD to understand the velocity profiles in this area. The first was

located in the centre, and the remaining four started in the centre and deviated to the edge of the powder outlet. These four lines represent the outer boundaries of the area in which the particles travel, and are assumed to represent the route taken with the slowest air flow. The centre line represents the route in which the air velocity is expected to be at its greatest value. The outer lines are evenly spread to capture the "cone" of particles. The lines are roughly presented in Figure 79. Two lines cannot be seen as they are in line with the central line, 90 degrees to the lines depicted at the edge of the cone. The average air velocity down the centre of the chamber from the nozzle to the powder outlet was 6.3 *m/s* according to analysis from CFD. The average velocity from the nozzle to the edge of the powder outlet was 5.7 *m/s* for all cases, leading to an overall average air velocity of 6 *m/s*.

By assuming the majority of particles travel down the centre, the velocity of the particles can be estimated. The velocity is equivalent to the distance from the nozzle to the powder outlet divided by the residence time. This distance is approximately 2.1m and the residence time can be chosen based on the sauter mean diameter using Equation 81. The relative velocity in the chamber is expressed in Equation 88.

$$V_{R,Chamber} = 6 - \frac{2.1}{\overline{\tau}_{Chamber}}$$

Equation 88

Figure 79: Particle tracks with trajectory lines(--), Scenario 1
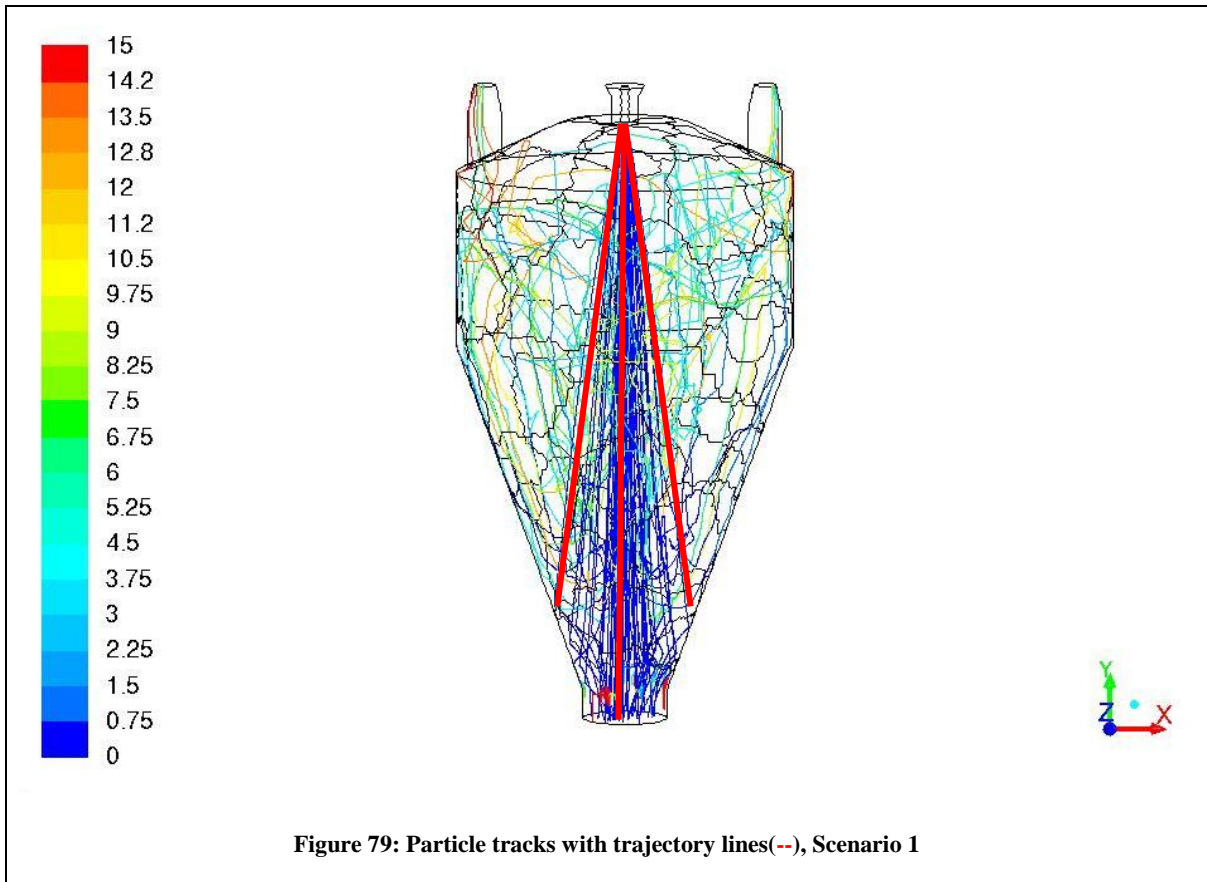
4.2 Relative Velocity in the Inner Fluid bed

The inner fluid bed has been assumed to behave like a typical fluid bed system. As such, the apparent air velocity can be expressed simply by relating the mass flow of air and the cross-sectional area of the fluid bed in Equation 89.

$$V_{Air,IFB} = \frac{\left(\dfrac{m_{Air,IFB}}{\rho_{Air,IFB}}\right)}{A_{IFB}}$$

Equation 89

The difficulty in modelling fluid beds lies with the estimation of the particle velocity. As the air velocity increases past the minimum fluidization point, the air begins to bubble through the fluid bed. These bubbles of air are assumed to be a separate phase that does not interact with

185

the mixture of air and particles in the bed. The floating particles in the bed are assumed to remain at the minimum fluidization velocity, which has the same physical meaning as the free fall velocity of a particle. This velocity is related to the pressure drop in the fluid bed according to Equation 90, but the pressure drop isn't measured.

$$\Delta P = (1 - \varepsilon_{mf})(\rho_P - \rho_{Air})gH_{BED}$$

<div align="right">**Equation 90**</div>

The Ergun relationship for fixed beds can also be used to describe the pressure drop in Equation 91 (Ergun & Orning, 1949).

$$\Delta P = H_{BED}\frac{150(1-\varepsilon)^2}{\varepsilon^3}\frac{\mu_{Air}V_{Air}}{(\Phi_s D_p)^2} + H_{BED}\frac{1.75(1-\varepsilon)}{\varepsilon^3}\frac{\rho_{Air}V_{Air}^2}{\Phi_s D_p}$$

<div align="right">**Equation 91**</div>

By combining the two empirical relationships, the Reynolds number at minimum fluidization can be estimated without needing the pressure drop in the Wen and Yu relationship expressed in Equation 92 (Wen & Yu, 1966).

$$\text{Re}_{mf} = \left(33.7^2 + 0.0408Ar\right)^{0.5} - 33.7$$

<div align="right">**Equation 92**</div>

where

<div align="right">**Equation 93**</div>

$$Ar = \frac{gD_P\rho_{Air}(\rho_P - \rho_{Air})}{\mu_{Air}^2}$$

With the Reynolds number at minimum fluidization known, a Ranz-Marshall correlation can be used for the inner fluid bed. The heat transfer coefficients were around $250\frac{W}{m^2K}$ which is in the range expected for this type of fluid bed and particle size (Molerus & Mattmann, 1992).

4.3 Relative Velocity in the Outer Fluid bed

The outer fluid bed was assumed to behave in the same way as the inner fluid bed.

5 Rate based drying models

The compartmental model involves 3 sections in the dryer in which a drying model can be applied. Using the measurements and estimations for each section, the evolution of the particles throughout the process can be modelled according to a rate based equation. This model can then be used to predict how the process will react to changes and provide insight to aid operation of the dryer in the most efficient manner. CDRC and REA models described in the literature review were used to fit the experimental data.

5.1 Governing Equations

Each model has a set of governing equations that enable fitting of the drying model. The first step in all cases is to estimate the heat transfer coefficient or mass transfer coefficient depending on the drying rate model.

5.1.1 CDRC model

The fraction of the maximum drying rate, f is represented by Equation 94.

$$f = \frac{-\dfrac{dm_{Droplet}}{dt}\lambda}{h_c A_{Droplet}(T_{air} - T_{WB})}$$

Equation 94

The drying rate, $\frac{dm_{Droplet}}{dt}$ can be represented by the change in moisture content in a mass basis over time in Equation 95.

$$-\frac{dm_{Droplet}}{dt} = m_{slurry,dry}\frac{dX}{dt}$$

<div align="right">Equation 95</div>

The surface area for all droplets, $A_{Droplet,}$ can be calculated from the sauter mean diameter ($D_{3,2}$). Equation 96 shows how this is derived, in terms of the slurry flow and the density exiting the compartment.

$$A_{Droplet} = 6\frac{V_{Droplet}}{D_{3,2}} = 6\frac{m_{slurry,out}}{\rho_{slurry,out}D_{3,2}} = 6\frac{m_{slurry,dry}(1+X_{Out})}{\rho_{slurry,out}D_{3,2}}$$

<div align="right">Equation 96</div>

The exiting density uses the density model derived in the Bulk Density chapter, with the moisture content in the mass basis. This is expressed in Equation 97 where the shrinkage is assumed to occur in the chamber and all of the air that was entrained in the slurry remains in the particles.

$$\rho_{Slurry,out} = \frac{\left(\dfrac{1+X_{Out}}{1+X_{In,Chamber}}\right)}{(1-shrinkage(T_{Exhaust}))^3\left(\dfrac{1}{\rho_{Slurry}}\right)}$$

<div align="right">Equation 97</div>

By substituting this into the surface area equation, Equation 98 can be derived.

$$A_{droplet} = 6\frac{m_{slurry,dry}\left(1+X_{In,Chamber}\right)(1-shrinkage(T_{Exhaust}))^3}{D_{3,2}\rho_{Slurry}}$$

<div align="right">Equation 98</div>

Determination of the fraction of the maximum drying rate, f now depends on the treatment of the change in moisture over time. This treatment varies when using a PFR and CSTR model. For the CSTR, the well mixed assumption presupposes that the moisture content is evenly distributed inside and is equivalent to the exit moisture content. In this case Equation 99 can be used.

$$\frac{dX}{dt} = \left(\frac{X_{In} - X_{Out}}{\tau} \right)$$

<div align="right">**Equation 99**</div>

For the plug flow, the moisture evolves as it travels through the reactor. As f is a function of the moisture content it must be integrated.

$$\int_{X_{Out,PFR}}^{X_{In}} \frac{1}{f} dX = \int_{0}^{\tau_{PFR}} \frac{h_c A_{Droplet}(T_{air} - T_{WB})\lambda}{\lambda} dt$$

<div align="right">**Equation 100**</div>

where

$$f = 1 \qquad \text{if} \qquad \overline{X} > X_{Cr} \quad \text{and}$$

$$f = \phi^n = \left(\frac{\overline{X} - X_{eq}}{X_{Cr} - X_{eq}} \right)^n \qquad \text{if} \qquad \overline{X} < X_{Cr}$$

To fit the parameters in the function, every manual measurement from the historical batches was used. The fitting of X_{Cr}, X_{eq} and n can be done in several ways, depending on the need for the model. It can be calculated with one manual measurement or multiple manual measurements across a batch. It can also be fitted to all manual measurements made for a formulation, assuming batch to batch variations in the mixing process have no impact on the drying rate.

5.1.2   REA model

For the REA approach, the importance lies with the estimation of the vapour concentration at the surface of the droplets, $\rho_{v,s}$ in Equation 101.

<div align="right">189</div>

$$\rho_{v,s} = \rho_{v,\infty} + \frac{-\dfrac{dm_{Droplet}}{dt}}{k_g A_{Droplet}}$$

Instead of creating a fraction of the maximum drying rate, the REA model uses a fraction of the maximum surface concentration. This is expressed in Equation 102 where the fully saturated vapour concentration at the droplets temperature is used to represent the maximum value. As stated in the literature review, the value of K_V at 1 atm was estimated as 2.62236×10^5 kg m^{-3} and E_V was 40.207×10^3 J mol^{-1} (Keey, 1991).

$$\phi = \frac{\rho_{v,s}}{\rho_{v,sat}(T_{Droplet})} = \frac{\rho_{v,s}}{K_v \exp\left(-\dfrac{E_v}{RT_{Droplet}}\right)}$$

The fractions can now be calculated for each compartment, however, the fraction still needs to be related to the powder's properties. In the REA approach, the evaporation of water is assumed to be an activation process having to overcome an energy barrier. Consequently, the fraction can be expressed by Equation 103, which provides an estimate for a correction factor, ΔE_v for the apparent activation energy.

$$\phi = \exp\left(-\frac{\Delta E_v}{RT_{Droplet}}\right)$$

The correction factor's maximum value should occur when the temperature of the droplet is equivalent to the surrounding air, T_∞. At this point, the vapour concentration will be equivalent to the bulk concentration in the air, $\rho_{v,\infty}$ for that compartment. The maximum values can be calculated using Equation 104.

$$\Delta E_{v,\infty} = RT_\infty \ln\left(\frac{\rho_{v,\infty}}{\rho_{v,sat}(T_\infty)}\right)$$

The value of the correction factor should begin at zero, when liquid fully covers the surface, and then increase with decreasing moisture content as it becomes more difficult to dry. The scaling of the correction factor versus its maximum value is used to fit a function of the average moisture content in Equation 105. As for the CDRC model, in the plug flow model this expression needs to be integrated in respect of X, once substituted in Equation 101.

$$\frac{\Delta E_v}{\Delta E_{v,\infty}} = \exp\left(- A\left(\overline{X} - X_{eq}\right)^B\right)$$

One concern with this approach is the use of the droplet temperature, which is not measured. It is assumed that the slurry exits the chamber at 100 degrees and leaves each fluid bed at the same temperature as the air, for the heat balances. For the CDRC approach, the wet bulb temperature has been used to calculate the maximum drying rate for each compartment and the temperature of the droplet has not been used. The wet bulb temperature is estimated from the airs relative humidity and temperature, but no estimate of how the temperature of the droplets change over time has been implemented.

5.2 Fitting the models

The number of points used for the fittings is dependent on the strategy and implementation of the model. Possible methods are listed below:

- Create new fittings for every manual measurement
- Create a fitting based on all manual measurements recorded during a batch
- Use a fitting based on the average from the previous batch
- Use a set fitting for a formulation from previous batches

Each of these methods can be used to provide a model to predict how the process will behave during a batch and can be implemented for both rate based model approaches.

5.2.1 CDRC Model

A single batch has been used to demonstrate the performance of the different fittings applied to the data. Each manual measurement in the batch provides an estimate for the exit moisture content of the chamber, inner fluid bed and outer fluid bed using the compartmental heat balance. These are listed in Table 9 along with the *SMD* to help aid discussion.

<div align="center">

Table 9: Measurements during batch

</div>

Measurement	Time (*min*)	SMD (*µm*)	$X_{Chamber}(\%)$	$X_{IFB}(\%)$	$X_{OFB}(\%)$
1	7	253	15.7	3.4	1.9
2	23	311	20.6	5.3	2.4
3	32	313	22.3	7.8	5.0
4	46	323	20.7	5.4	2.9
5	55	330	22.9	8.4	3.9
6	63	346	22.8	8.9	4.2

The first measurement estimates that significantly more drying occurs in the chamber as the droplets/particles exit, with average moisture content of 15.7%. This measurement took place when the PSD was represented by a $D_{3,2}$ of $253\mu m$ compared to the remaining measurements with a $D_{3,2} >310 \ \mu m$. This shows how much the change in the initial PSD can have on the drying rates in the process. The inlet and exit conditions for each compartment were used to estimate the fraction of maximum drying rate, *f*. The fluid beds are assumed to behave like a CSTR so the fully mixed characteristic means the exit moisture content is constant throughout the fluid bed. For the chamber, the characteristic moisture content is modelled to change as the droplet travels through the chamber. Therefore, the *f* function has to be integrated during the

fitting process. Table 10 lists the fitted parameters for each measurement made in this batch. The X_{Cr} ranged from 40 to 60, however, measurements 2 to 5 were between 43 and 46. It is possible that the initial measurement taken early, and the final measurement that was taken later into the batch, were impacted by non steady state conditions. In these cases, the transient nature of the process during start up and the drop off in flow at the end of the batch can have an effect on the mass and heat balances. It is important therefore to choose sampling times wisely, ensuring that a measurement is taken under steady state conditions.

Table 10: Fitting Parameters for each measurement for the CDRC model

Measurement	X_{Cr}(%)	n
1	60	1.8
2	46	2.2
3	45	2.7
4	44	2.2
5	43	2.8
6	39	3

Figure 80 demonstrates the differences graphically, where each manual measurement is used separately to fit the drying model. Studying the remaining measurements, there is also a difference between the 2nd and 4th and the 3rd, 5th and 6th. This is the impact of the parameter n on the model. They result in two separate regions of moisture contents exiting the inner fluid bed. No changes in the inlet conditions relate to this change in drying performance.
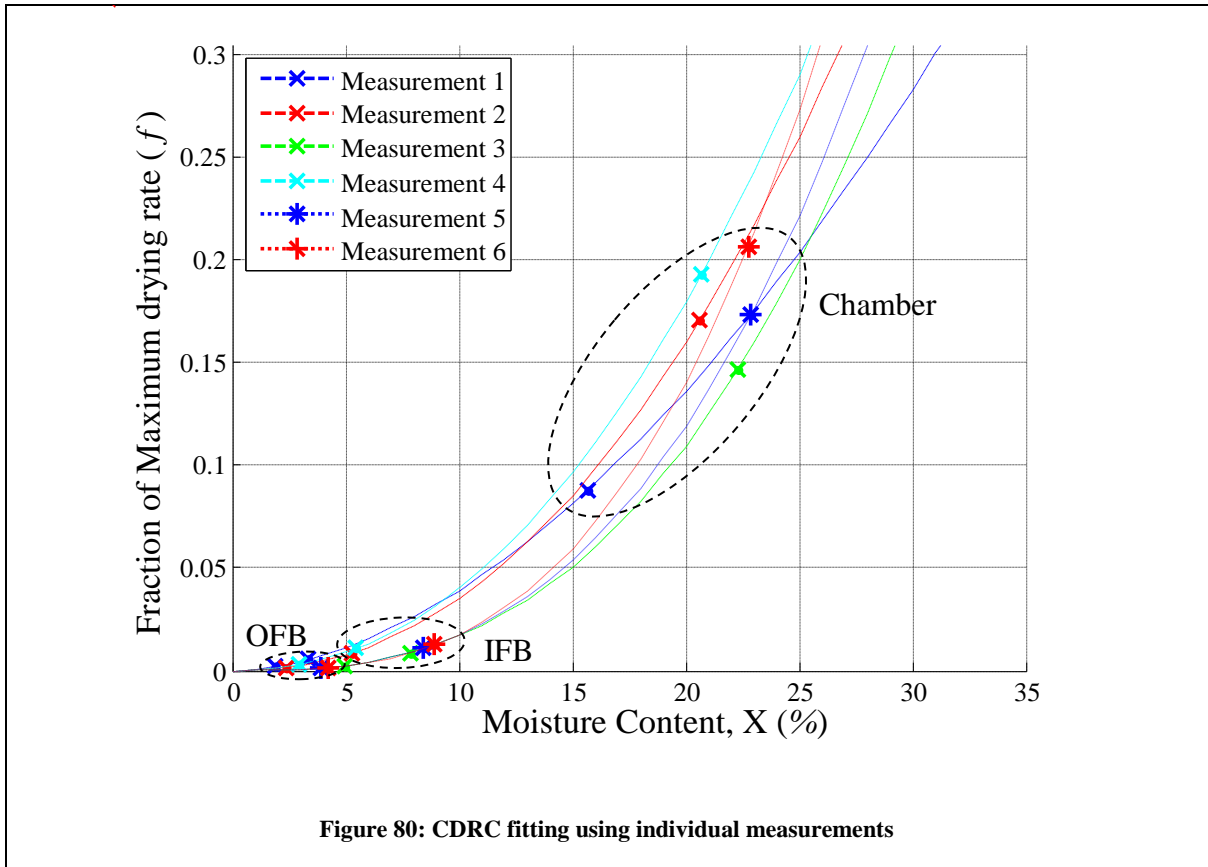
Figure 80: CDRC fitting using individual measurements

Figure 81 displays the fittings when using every measurement available at that point in the batch. This creates an average fitting to the results. As more measurements are made, the influence of less accurate estimations is reduced, and the fitting converges on a set drying profile. The critical moisture content reduced from the initial measurement to a value of 45 as seen in Table 11. In all cases the equilibrium moisture content converged to zero.

Table 11: Fitting Parameters when using every measurement for the CDRC model

Measurement	$X_{Cr}(\%)$	n
1	60	1.8
2	55	2.0
3	48	2.4
4	49	2.3
5	47	2.4
6	45	2.5

194

As seen in the graph, by using this method the variance in the drying profile produced is reduced. The final fitting from this batch could be used further in other batches of this formulation and would provide an estimate before measurements are made and enable the prediction of the correct inlet conditions to meet powder specification criteria.

Figure 81: CDRC fitting using every measurement available during a batch
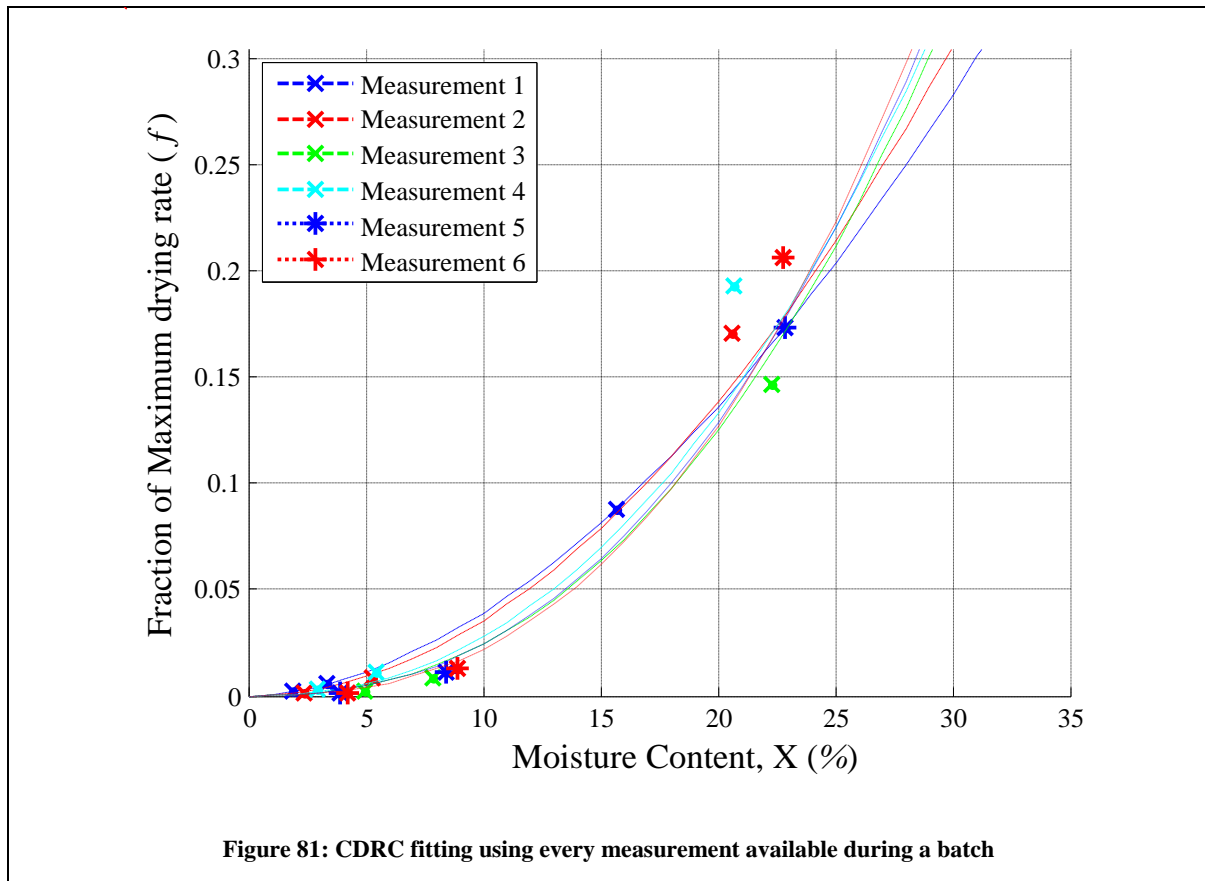
Multiple batches were run for each formulation. Using the measurements made in each batch, a fitting can be established to estimate how a formulation performs on the spray dryer process. This enables comparison between formulations and provides insight into how their drying profiles differ. Figure 82 shows the fitting for each of the 3 formulations. To show the variance in the fittings for the fluid beds, a log scale has been used for the y axis. Confidence intervals have also been calculated to assess the performance of the fit. They represent 95% of the data. The biggest issue with the fittings is related to formulation 1. The gradient of change in the drying rate is not captured well by the model, leading to an offset for the outer fluid bed. In this

case, the model fails to capture the dynamics, assuming the measurements and assumptions made are valid. For the other formulations, the drop off is well captured using this model, and the range of moisture contents seen show that it is capable to model different scenarios. This highlights how much the drying can change for every batch.

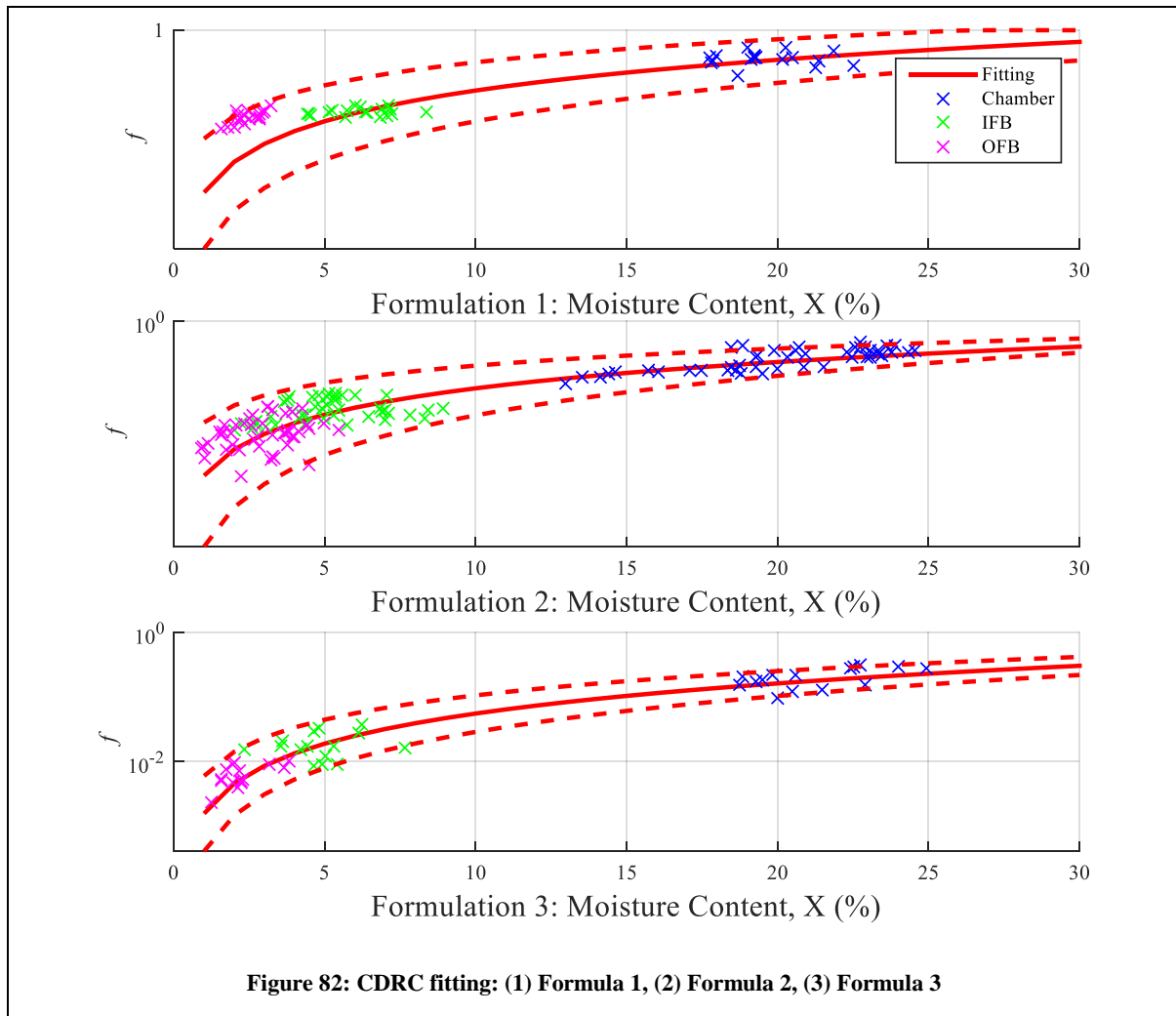**Figure 82: CDRC fitting: (1) Formula 1, (2) Formula 2, (3) Formula 3**

Table 12 lists the fitting parameters, and their confidence intervals, used for each formulation. The equilibrium moisture content in each case converged to zero. The table shows that the range of values for *Xcr* and *n* suggest that the first formulation has a significantly different drying profile to formulations 2 & 3 which dry in a similar manner.

Table 12: Fitting Parameters CDRC model

Formulation	X_{Cr}(%)	n
1	39.0±7.8	2.31±0.60
2	58.2±6.1	1.92±0.42
3	63.8±4.0	1.55±0.3

Figure 83 shows the fitted drying profile from the initial moisture content for each formulation. According to the fittings, only formulation 1 has a constant drying rate period, as its initial moisture content is greater than the critical moisture content. This leads to a greater amount of drying in the chamber. Eventually the drying becomes more difficult for this formulation at lower moisture contents (<8% for formulation 2 & <14% for formulation 3) however as can be seen for formulation 1 in Figure 82, the model fits lower values of *f* than the cluster of outer fluid bed estimations. Formulation 3 seems to be easier to dry than formulation 2. This is due to its lower initial moisture content and reduced gradient of change. For this formulation, the main contributor to drying in the process will be the fluid beds, as higher drying rates are maintained for a longer period of time at the lower moisture contents. This leads to the conclusion that different approaches should be taken for different formulations, to maximise the impact of the process changes.
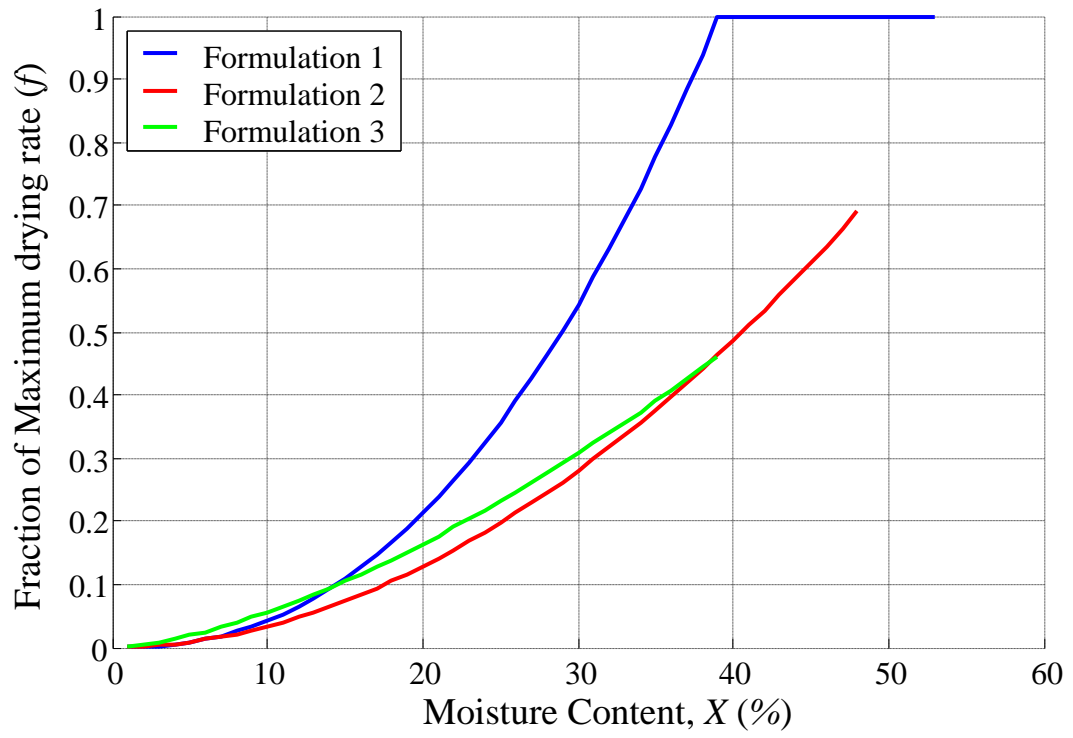
Figure 83: CDRC fittings to formulations

5.2.2 REA Model

Table 13 lists the parameters fitted for the REA model for the same batch. For this model the equilibrium moisture content has a greater impact since the value converged to zero for the CDRC model in every case. As the batch continues the values of *A* decrease and increase for *B*. As these parameters are set for this model it is important that the equilibrium moisture content is below the target moisture content. With no model implemented to estimate changes in this equilibrium with the surrounding air properties, it makes it difficult to use this drying model. If the drying model fitting from measurement 3 was used, then the target moisture content could not be achieved. If this was used in a control loop, the manipulated variable would be changed indefinitely.

Table 13: Fitting parameters for each measurement for the REA model

Measurement	A	B	X_{eq}
1	1.7	0.05	1.9
2	1.5	0.11	2.1
3	1.6	0.10	4.8
4	1.6	0.11	2.7
5	1.2	0.19	1.4
6	1	0.27	0

Figure 84 depicts the REA fittings for individual measurements. Using the graph it becomes clear again that the first measurement is different to the remaining measurements. For measurements 2 to 4 it would appear that the equilibrium moisture content has been reached as the slope of the lines become vertical. For 5 and 6 it seems that more drying could have taken place in the outer fluid bed giving more flexibility to the operator under these conditions.

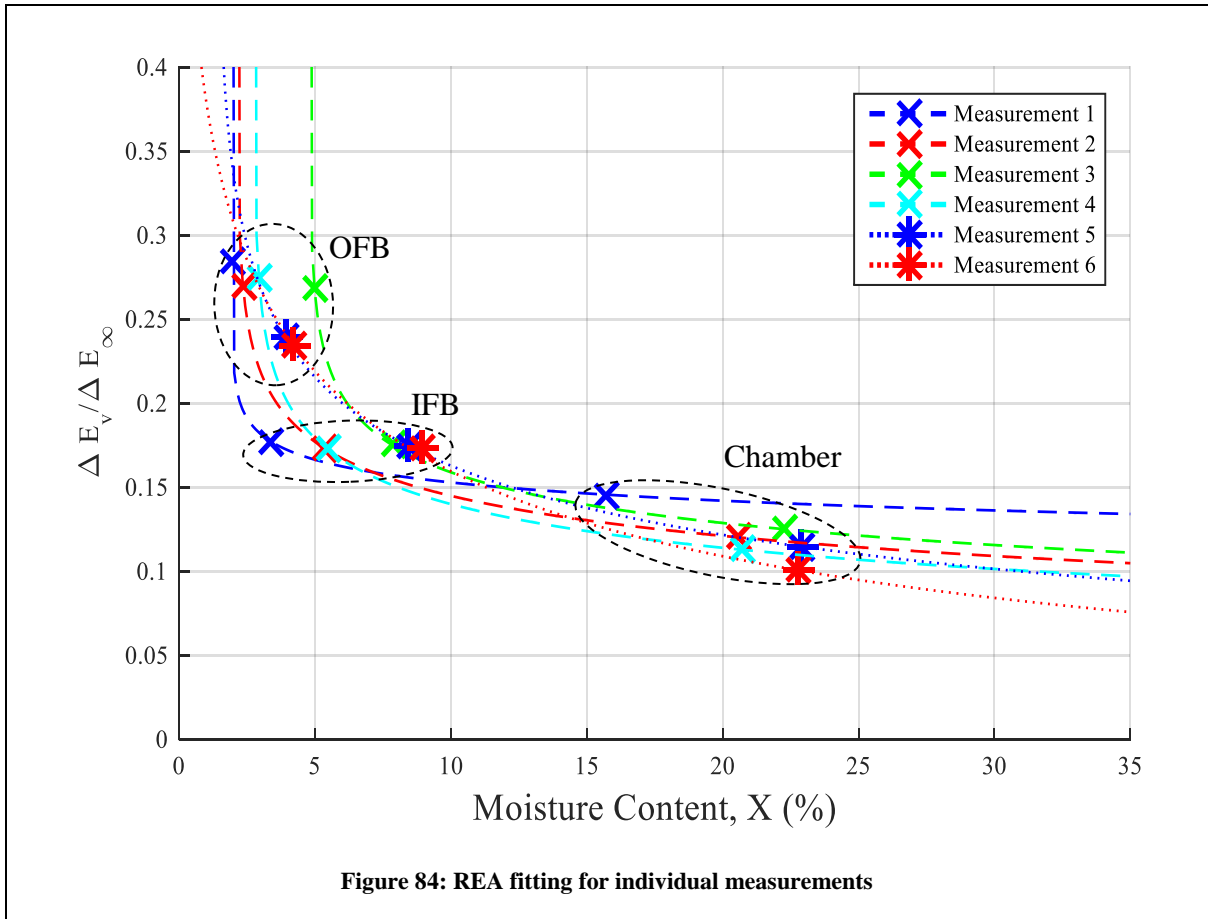**Figure 84: REA fitting for individual measurements**

Figure 85 depicts the fitting taking into account all measurements up to that point. The fittings equilibrium moisture content still varies, as would be expected with different properties of the air and powder for each measurement. Table 14 provides a list of the fitted values. It becomes clear here that the latter fitted models have equilibrium moisture contents greater than some of the moisture contents at the exit of the outer fluid bed. This means that if the dryer was represented by these models the moisture content measured would not be achievable.

Table 14: Fitting parameters for every measurement for the REA model

Measurement	A	B	X_{eq}
1	1.7	0.05	1.9
2	1.7	0.8	1.9
3	1.5	0.10	3.4
4	1.3	0.16	2.9
5	1.4	0.14	2.3
6	1.4	0.14	2.3

Figure 85: REA fitting for every measurement
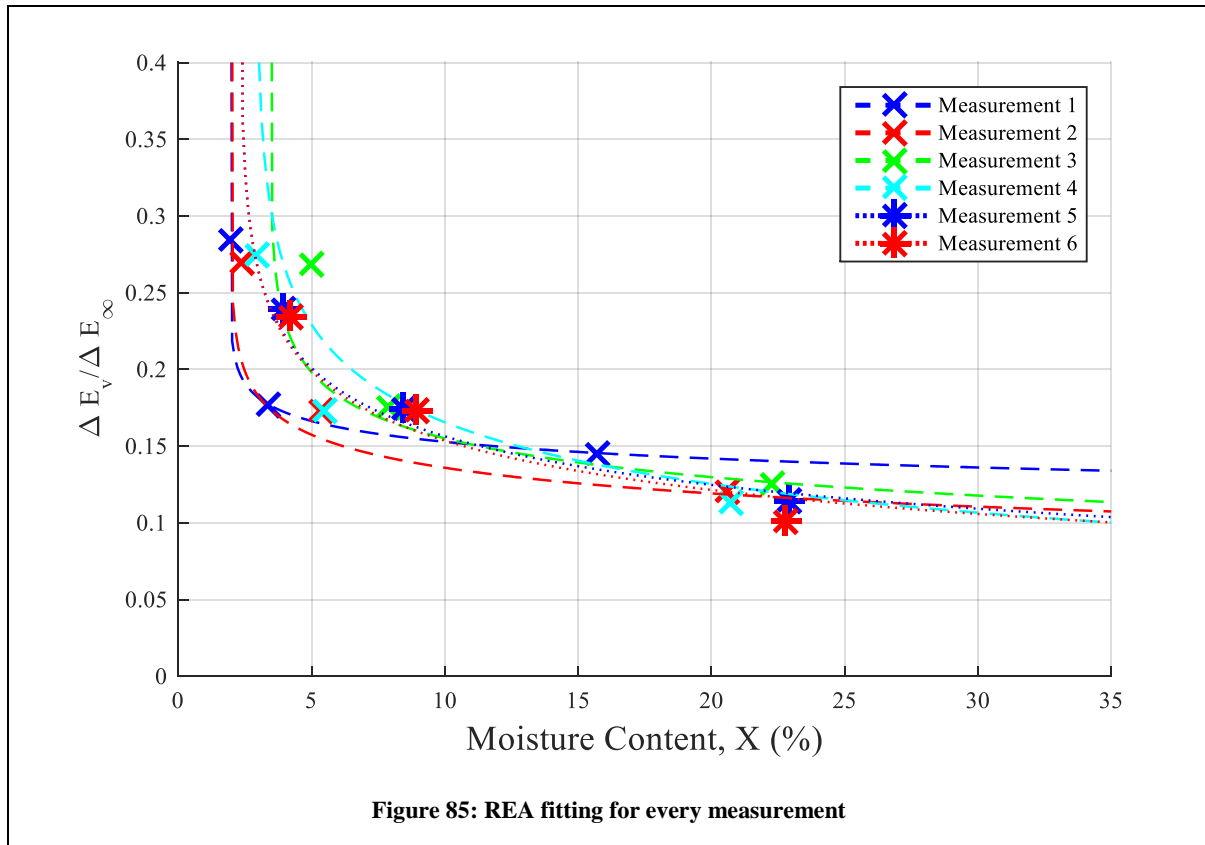
Figure 86 displays the fittings for each formulation. The model captures the change in drying rate for each formulation quite well. The main source of variance is associated with the inner fluid bed estimations. The fitting for Formulation 1 performs best, this seems to be as a result of the equilibrium moisture content not being reached. Table 15 lists the values for the fitted

parameters and their confidence intervals. Again the fitting for the first formulation is significantly different to the other two.

Table 15: Fitting parameters REA model

Formulation	A	B	X_{eq}
1	1.20∓0.06	0.22±∓0.02	0
2	1.51∓0.2	0.10∓0.01	2.41±1
3	1.63∓0.1	0.07∓0.01	1.78∓0.5

Figure 86: REA fitting: (1) Formula 1, (2) Formula 2, (3) Formula 3
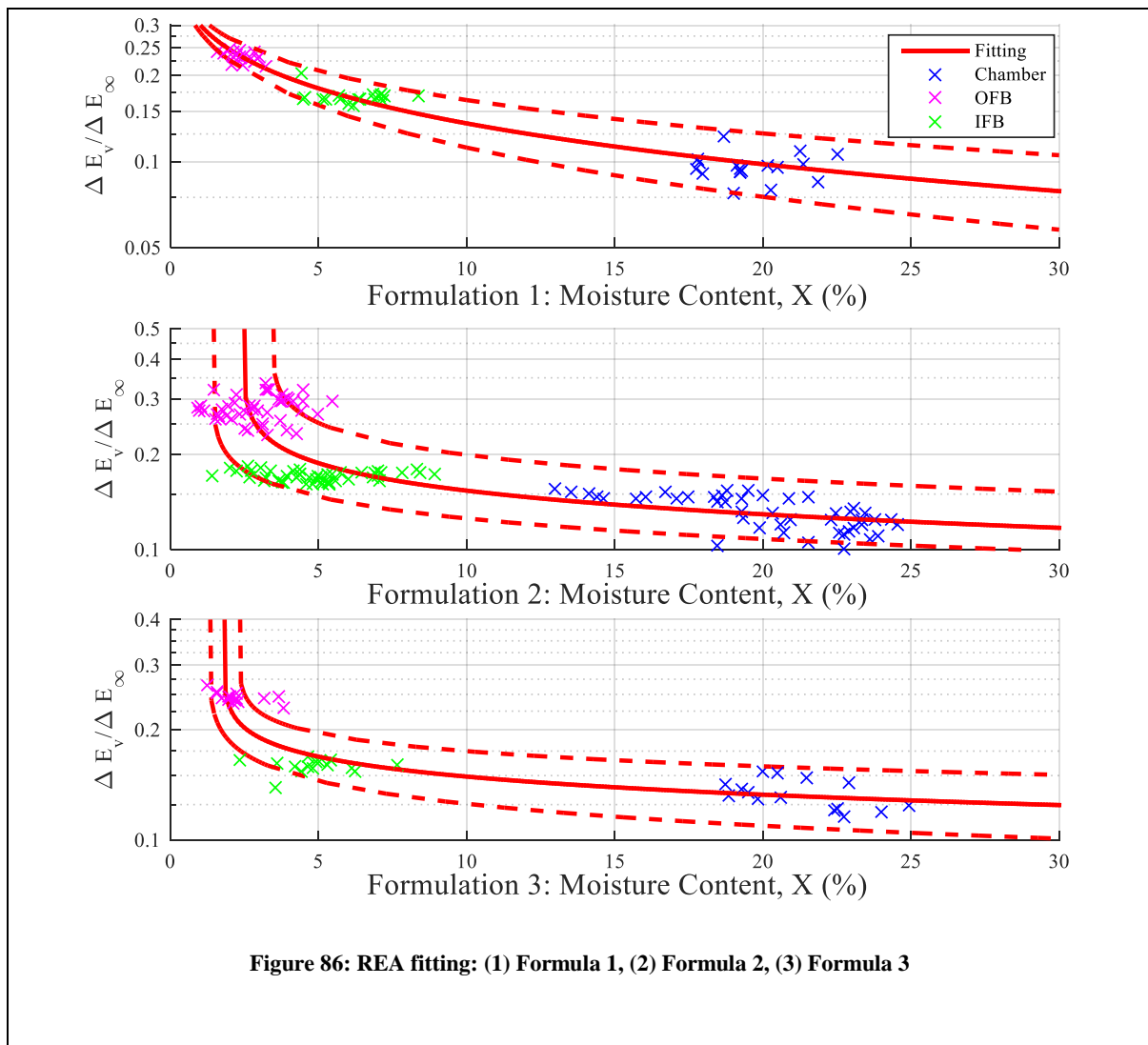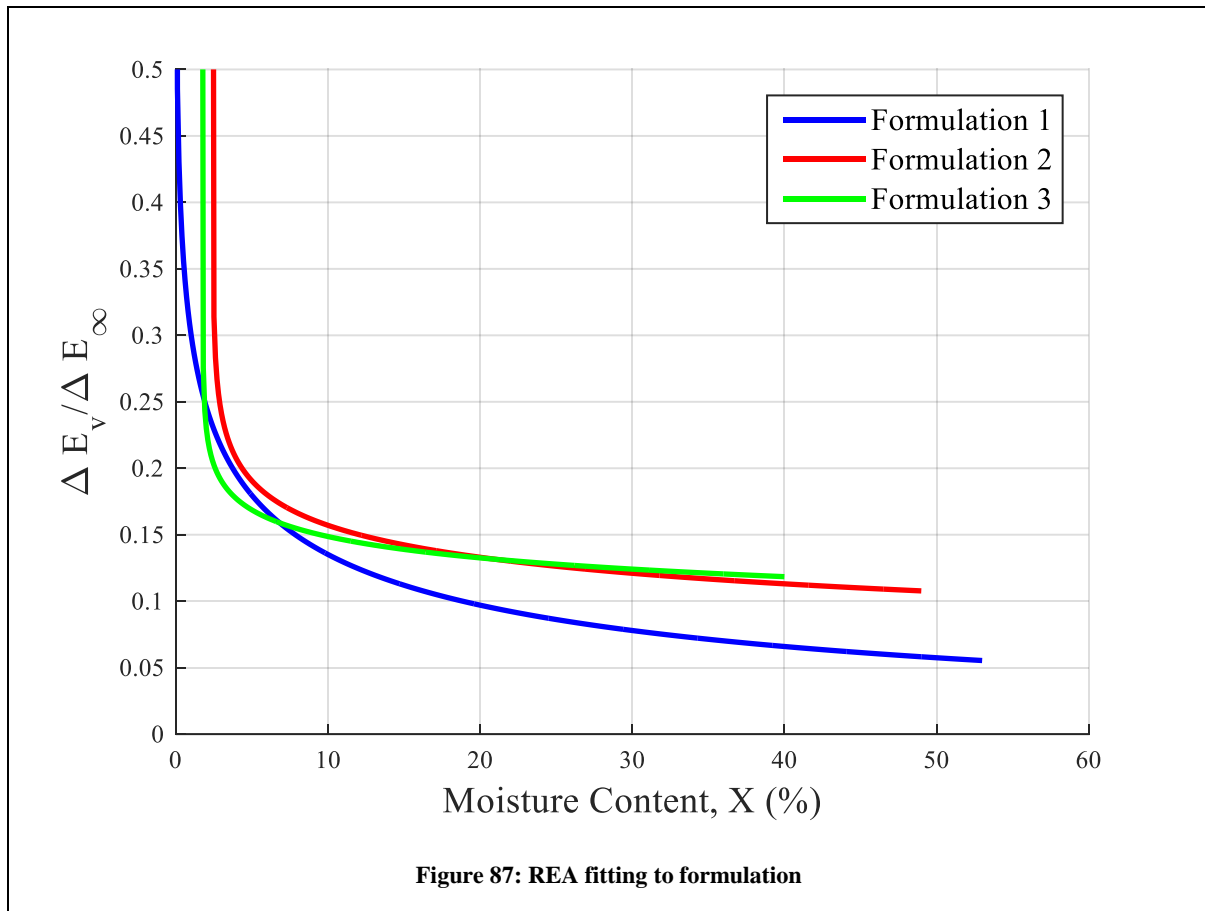
Figure 87 illustrates the difference between the formulations more clearly. In this scenario, the first formulation has less resistance to drying than formulation 2. Formulation 3 becomes easier to dry for a short period until the moisture content approaches the equilibrium moisture content.

Figure 87: REA fitting to formulation

5.2.3 Sigmoidal Model

When fitting the CDRC model, it is clear that an offset occurred for the first formulation. The change in drying rate followed a pattern closer to a sigmoidal curve as the gradient drops sharply and then plateaus. Because of this, an additional model has been implemented to provide a more accurate fitting to the measurements made. This approach also enables a smoother transition between the constant rate period and the falling rate period, with a more gradual drop off in drying rate which is more realistic than a sudden drop. This is a similar approach to the REA using the exponential curve based model described in Equation 106.

$$f = \frac{1}{1 + \exp(-A(X + B))} \qquad \text{Equation 106}$$

The fitting values are listed for each individual measurement for the batch in Table 16.

Table 16: Fitting Parameters for each measurement for the SIG model

Measurement	A	B
1	22.5	-0.30
2	17.8	-0.31
3	18.1	-0.33
4	19.1	-0.30
5	19.1	-0.32
6	21.0	-0.30

Figure 88 displays the fitting for the individual measurements on the same batch. In this case the fittings are very similar for each measurement showing less variability than the previous CDRC approach. From the table you can see the similarities in the fittings with the values changing significantly less than with the alternative CDRC and REA models.
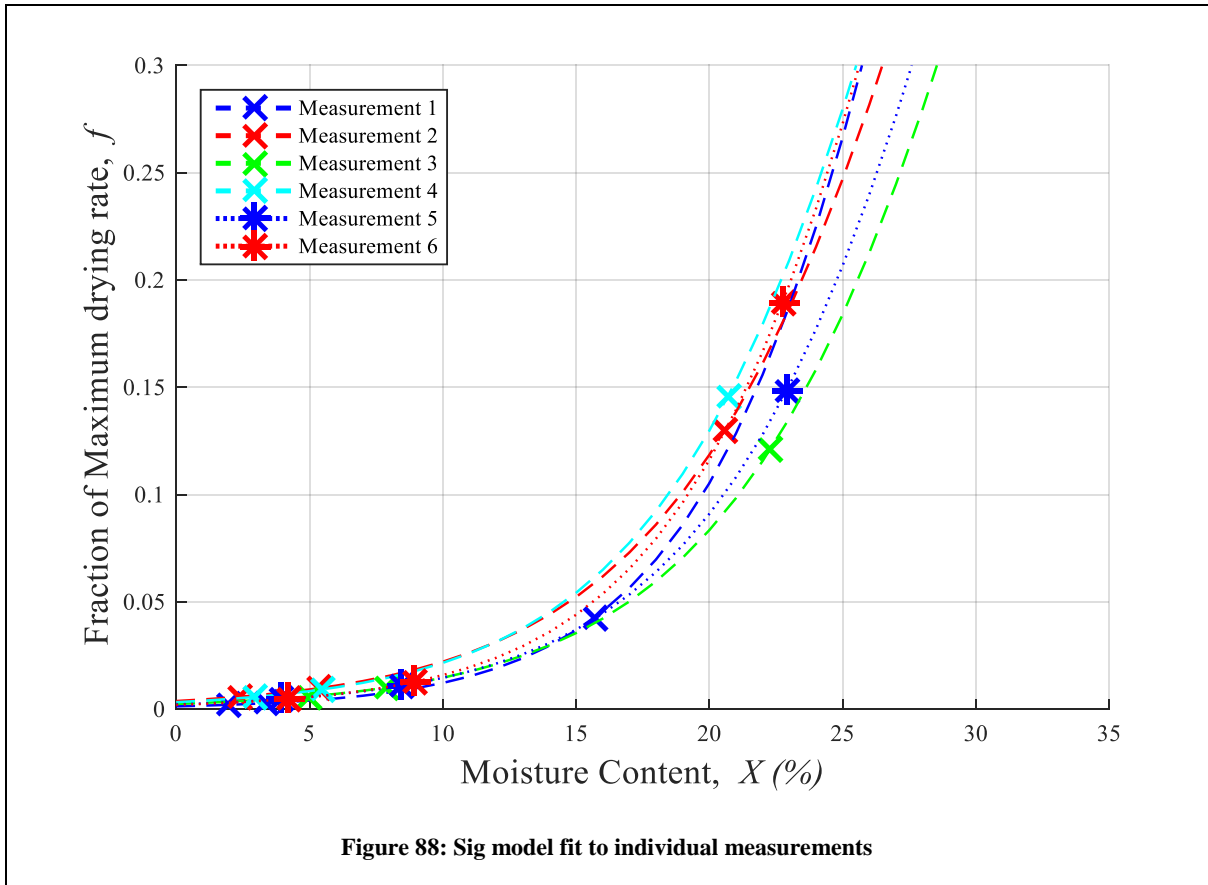
Figure 88: Sig model fit to individual measurements

Table 17 lists the fitting for every measurement up to that point. There is the continuous downward trend in parameter *A* which also occurred for CDRC but parameter *B* remains consistent.

Table 17: Fitting Parameters for every measurement in the SIG model

Measurement	A	B
1	22.5	-0.30
2	18.5	-0.31
3	19.2	-0.31
4	18.9	-0.31
5	18.6	-0.32
6	18.6	-0.31

Figure 89 illustrates the model fitting using every measurement available. Again, variation in the model is reduced, and every measurement fits along the single drying profile.

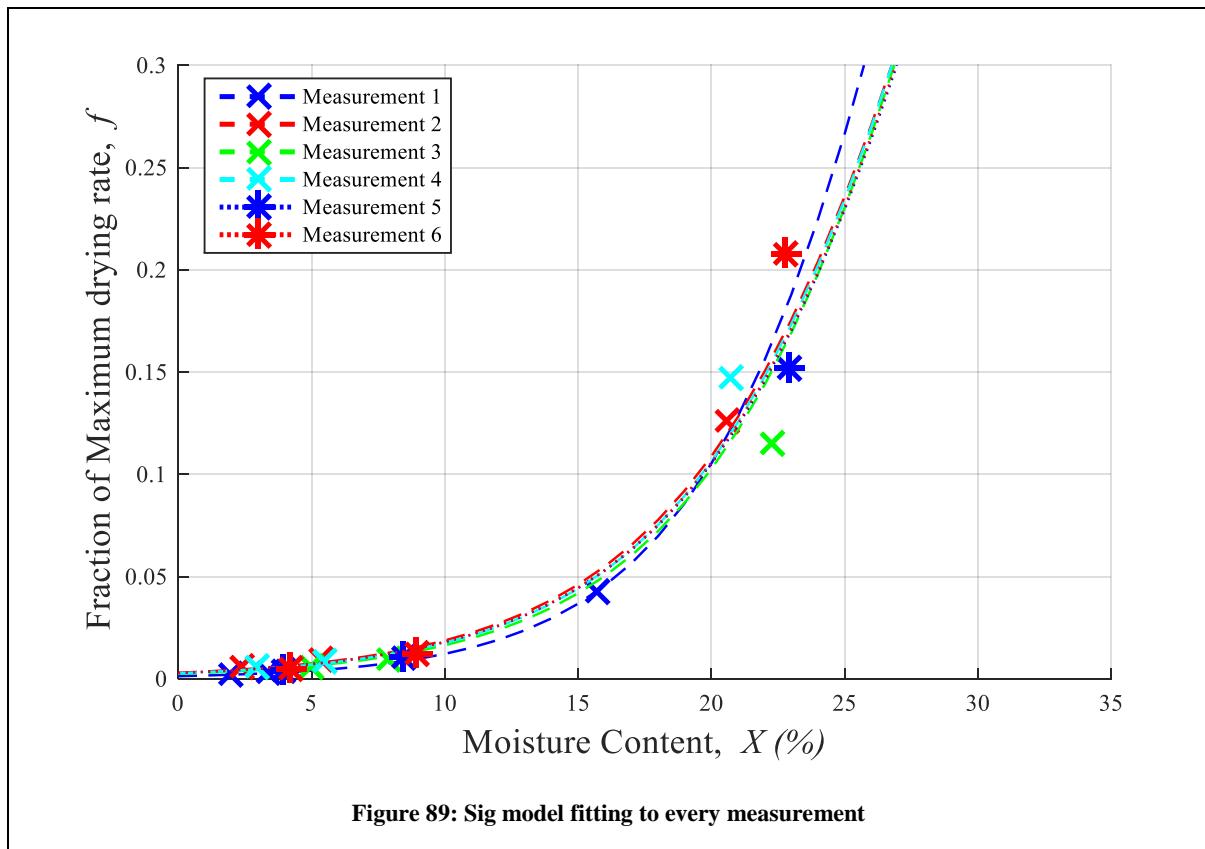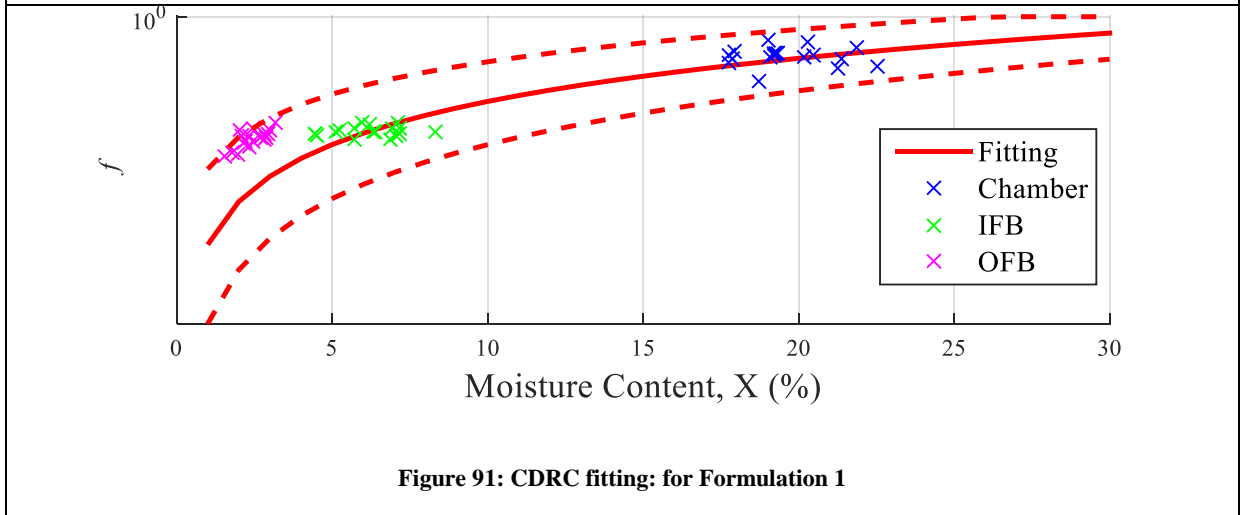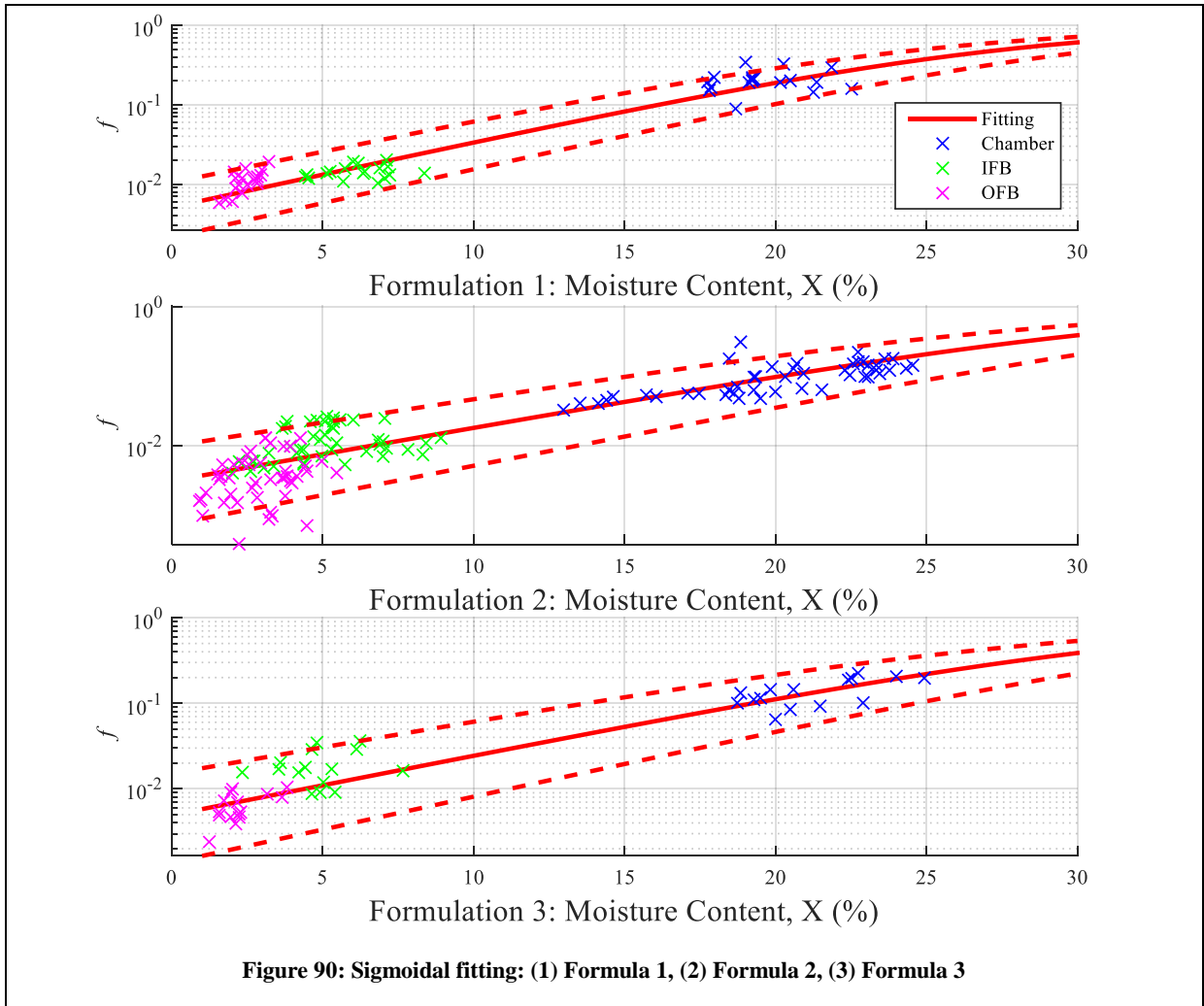**Figure 89: Sig model fitting to every measurement**

Figure 90 depicts the fitting of the sigmoidal curve to the data sets for each formulation. A log scale has been used to show the variations in the fluid bed estimations as well as the chamber. The model was implemented due to the offset observed for formulation 1 using the CDRC model. This fitting has been depicted again in Figure 91 for reference. The new model removes this and maintains the accuracy of the fittings for formulations 2 & 3. Table 18 lists the values of the fitted parameters with their confidence intervals. According to the confidence intervals, the fitting to the first formulation is more consistent, and again it seems this formulation can be separated from the others. To enable a better comparison to the CDRC approach, the critical moisture content was also estimated from the model.

Figure 90: Sigmoidal fitting: (1) Formula 1, (2) Formula 2, (3) Formula 3

**Figure 91: CDRC fitting: for Formulation 1**

The estimated critical moisture contents are very similar to those estimated using the previous CDRC model for formulations 2 & 3. The difference between formulation 1 and these formulations is reduced, as the estimate for the critical moisture content is much larger, suggesting that most of the drying cycle would be hindered for each formulation.

Table 18: Fitting parameters for Sigmoidal model

Formulation	A	B	$X_{Cr, SIG}$ (%)	$X_{Cr, CDRC}$ (%)
1	19.0±0.8	- (0.28±0.03)	52±2	39±8
2	17.7±1.8	- (0.33±0.04)	58±2	58±6
3	16.1±1.7	- (0.33±0.04)	60±2	64±4

Figure 92 shows how the drying rate changes from the initial moisture content to zero for each formulation. According to the sigmoidal model, the behaviour of the different formulations is very similar at lower moisture contents. The main differences between the formulations occur above a moisture content of 10%. The drying of formulation 2 and 3 are almost equivalent to each other but Formulation 3 starts with a lower moisture content.

Figure 92: Sig model fitting to formulations
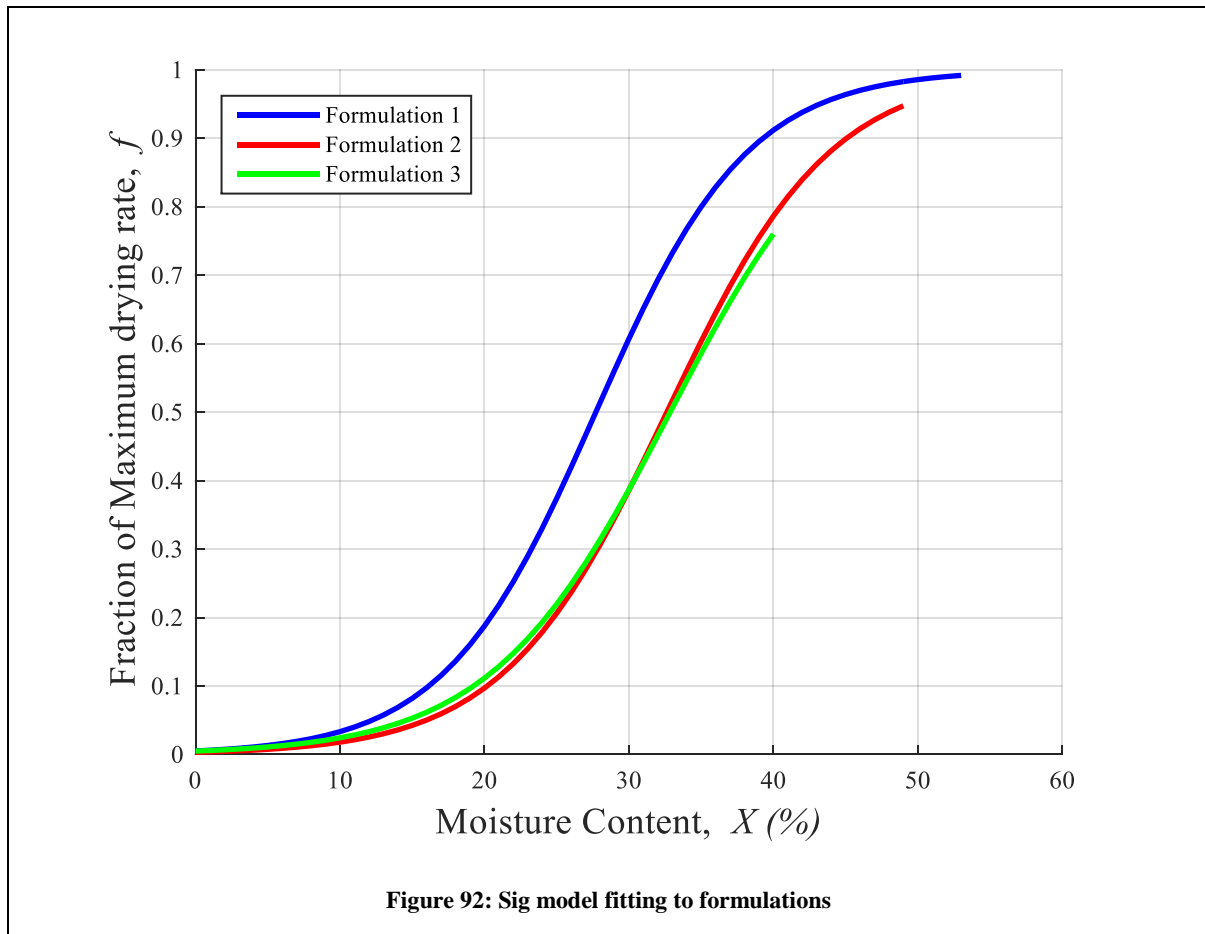
5.3   Drying Model Conclusions

Using the estimations provided for the compartmental heat and mass balances and the estimations for residence time and flow characteristics, drying models have been fitted to represent how the slurry dries in the process. The drying models are fitted with data collected at the time of manual measurements of the powder. This ensures that the correct calibration is used for the exiting air moisture content. A density model has also been applied for each compartment, assuming that all shrinkage occurred in the chamber. The drying models fit well to the data, however the fittings can vary significantly for the same formulation depending on the batch and the day of operation. Fittings can be applied to formulations for comparison, but it is likely that a fitting made on the day or during the batch would provide a more accurate representation. Both the CDRC approach and the REA approach could be used in a predictive model. However, the non-zero equilibrium moisture contents for the REA approach may cause convergence issues when trying to reach target moisture contents below this value. The CDRC model struggled to capture the change in drying rate for formulation 1. To correct this, a sigmoidal model was applied to enable modelling of a more reduced gradient at lower moisture contents. This improved the accuracy of the fitting for formulation 1 by removing the offset and it also maintained the accuracy for formulations 2 & 3. Comparison of the CDRC and REA approach is difficult as they are fitting separate parameters. Their performance in a predictive model will provide more insight into which one is best suited for the process.

8. MODEL PERFORMANCE

1 Introduction

The drying models fitted by experimental data on the small scale dryer system have a number of applications. For the mixed flow spray dryer process, they can be implemented online or as a simulation tool offline.

Their online implementation would provide a soft sensor for moisture content, which takes into account all aspects of the drying process including changes in the PSD and the density of the powder. Estimation of the moisture content will enable different control strategies to be implemented, and incorporation of the density model could provide target air injection levels for density control. The drying models also provide information about the influence of each compartment of the mixed flow spray dryer, and this knowledge could be used to aid operators in their choice of which process conditions to manipulate in order to control the process.

Using the drying model for simulation of the process provides an opportunity for the implementation of automatic control strategies on the small scale drying process without running the unit. Different control strategies can be tested off line first for validation and to identify the most optimal set up. Further insight into the drying profile would also help to assess the processing difficulty of different formulations, aiding the decision process on their suitability for scale up.

To run these models for a given formulation, one set of conditions is needed from the small scale dryer. The models could then provide estimates for the deviation in the process variables from this initial set of steady state conditions. It is best practise to use a manual measurement, so that the offset in the mass balance can be removed and the heat losses can be estimated. Details of the application of models as an online and simulation tool are described, along with their ability to represent the process.

2 Application as an online model

During start-up of a batch, the operator makes multiple changes in order to reach the specification criteria for the powder's properties. The purpose of the model produced is to increase understanding of how these properties are related, and how each is affected by the manipulation of process conditions, enabling the best strategy to be derived. From the studies carried out, it is clear that using an automatic control strategy, which manipulated the atomizing air flow rate, was the best method for the control of PSD. For density control, the best method is to manipulate the air injection. Derivation of the density model highlighted that the density of the powder is very sensitive to changes in the drying conditions. If the maximum air injection level fails to reach the target density, then the drying conditions can be manipulated to reduce the density further. For moisture control, the first goal was to provide regular measurements/estimations of the moisture. The second goal was to understand its dependence on the process conditions and the PSD and density in the process. The drying model provides a soft sensor for the moisture content and also quantifies the impact of changes in the process conditions, PSD and density on the drying rates and drying conditions throughout the process. This can help to provide the correct strategy for simultaneous control of the density and moisture during the entirety of the batch. A start-up strategy could also be derived during which the PSD is manipulated to reach its target value.

When running the models, updates from manual measurements caused convergence errors in the REA approach, which led to oscillations in the estimate. With the temperature measurement set, any error in the REA model fitting was transferred into the estimate of the moisture content. The main errors were associated with the fitting to the estimates from the inner fluid bed, which was the main cause for the oscillations. Because of this, the REA approach has been disregarded for online implementation. Typical performance of the CDRC and sigmoidal model approaches as a soft sensor are depicted for the estimation of moisture content in Figure

93, and the estimation of density is shown in Figure 94. These figures illustrate the performance when using a formulation fitting for the drying models. The figures begin 400 seconds after the first manual measurement, as this is the assumed time taken for the manual measurement to take place and be recorded in the PLC. For moisture, the update to the offset is clear for the first measurements. The first measurement was taken 9 minutes into the batch. It is likely that steady state had not been achieved, as the powder flow measurements described in the Material and Methods chapter showed that it could take up to 16 minutes from producing a sustained slurry flow to reach a constant powder flow. The Sigmoidal approach estimates that the moisture content would deviate more during the batch given the process conditions. This is a regular pattern leading to the loss of accuracy for the sigmodal approach as listed in Table 19. Analysis of the density model shows that there is little difference in accuracy, as it is mainly dependent on the air injection level and temperature in the chamber which is measured in this case. The slight difference seen is a result of the change in the moisture content estimate. Although it fits the data better, when applied to the online model, the sigmoidal model fails. Overall, the CDRC model outperforms the sigmoidal model when estimating the moisture content. In Table 19, use of a batch fitting led to a poorer performance. This is because the impacts of poor measurements such as the first one in this case, have a much larger influence causing greater errors in the estimation.

Table 19: Accuracy of Estimations

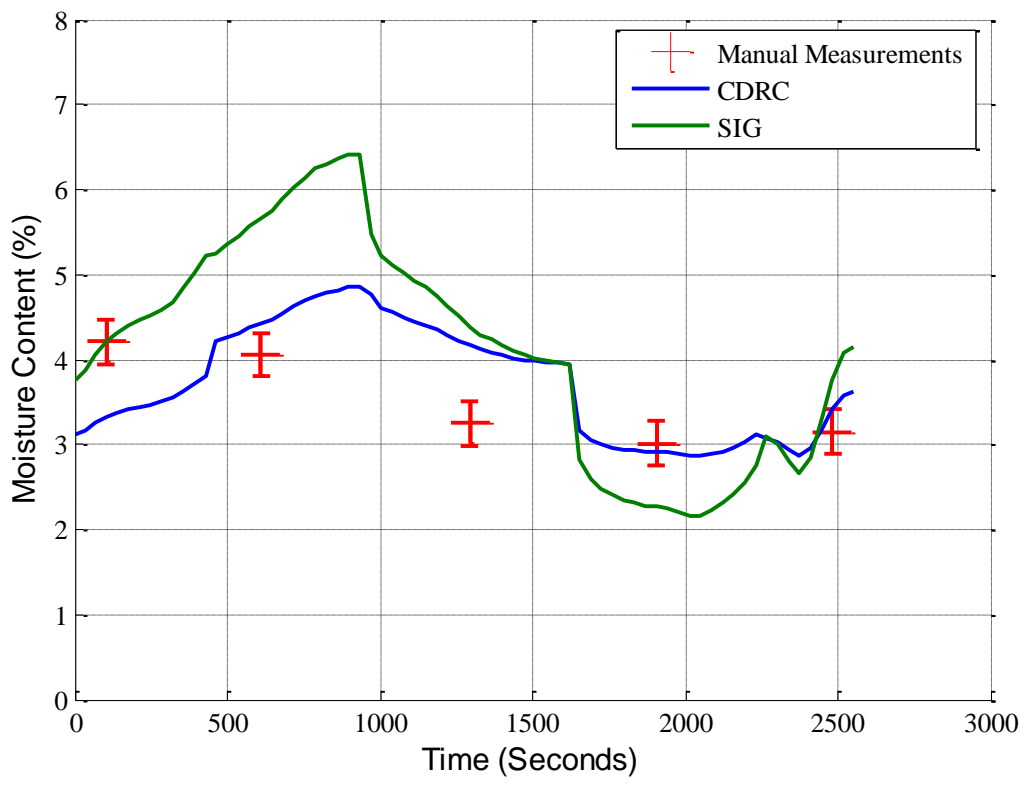| Model Fitting	RMSE	
	Moisture (%)	Density ($kg/m3$)
CDC Formulation	0.64	16
CDC Batch	0.89	18
SIG Formulation	0.97	17
SIG Batch	1.28	16

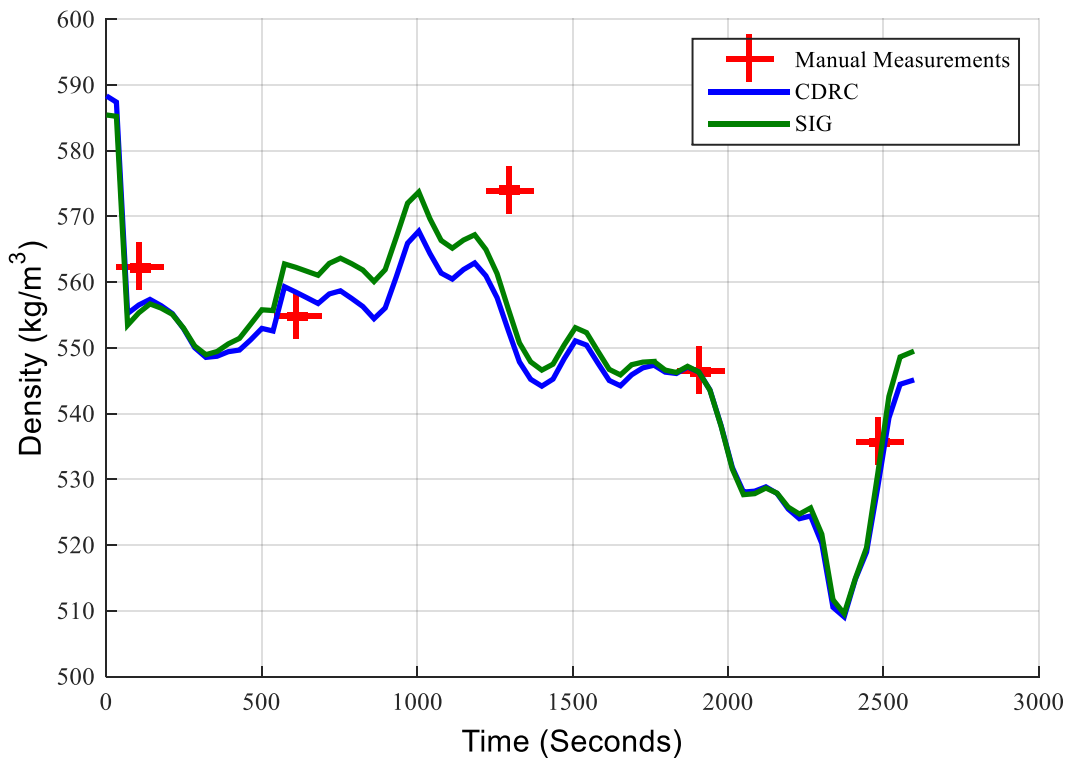**Figure 93: Typical performance of drying model estimation of moisture content**

Figure 94: Typical performance of drying model estimation of density

214

3   Application for Simulation

Simulation of the process provides a platform to implement and analyse multiple different strategies and to develop understanding of the process. However, it is very important that the simulation represents reality sufficiently. This will determine whether a proposed strategy from the simulated model will be relevant for the actual process. In order to simulate the process, the model needs to predict the outputs for each compartment in the process. This includes the temperatures which were previously measured inside each fluid bed and in the exhaust of the chamber. Changes in these temperatures are dependent on the drying rates, the initial conditions and the heat losses from the process. The initial conditions provide an estimate for the heat loss, but during start-up they are likely to be transient and not steady state. Also as the batch continues and the inlet conditions are manipulated, the state would change. To simulate how the heat loss changes, all manual measurements were analysed and compared to temperature gradients between the process and the environment. Possible areas of interest were determined to be the walls of the outer fluid bed, the chamber and the inlet piping. Assuming the heat losses occur mainly by convection, they can be represented by Equation 107 as they would be controlled by external convection and unit insulation. The UA terms for the outer fluid bed and chamber were negligible, with the biggest impact coming from the pipes when inlet air temperature changes are made. This provided a UA value of 15*W/K* for the pipes providing an RMSE of 17% for the heat loss. The heat losses changed significantly for the first batch of the day. This was due to its transient nature as heat is accumulated within the equipment. Without these batches, the RMSE was 9%. It should also be highlighted that the heat losses include all errors associated with the heat balance and assumptions made for the modelling of the process. This will lead to variations in the estimations used for the fitting, which don't necessary reflect a change in heat losses.

$$Q_{Heatloss} = \sum_{i=1}^{n} U_i A_i \Delta T_i$$

<div align="right">**Equation 107**</div>

In general, the transient nature of the first batch meant that the accuracy of the models was significantly reduced for the first batch of the day. When comparing the average performance of the different models, the first batches of the day have been disregarded. The impact of the first batch can still be seen in Figure 95, which illustrates the accuracy of the model when simulating the historical batches. For each model there is the option to use a fitting based on all measurements made for that formulation, and one for every measurement in the batch. In each case, the first batch measurements are illustrated. A proportion of the first batch measurements have accurate predictions which generally occur later in the batch when a steady state would have been achieved. The difference between each model is quantified in Table 20 and Table 21 which provides the RMSE of the measured outputs estimated at the manual measurement points for formulation and batch fittings.

Table 20: Performance using fittings for formulations

Model Fitting	RMSE				
	Moisture (%)	Density (*kg/m3*)	Exhaust (^{0}C)	IFBT (^{0}C)	OFBT (^{0}C)
CDC	0.48	28	3	8	4
REA	0.69	28	3	5	5
SIG	0.72	29	3	5	5

Table 21: Performance of fitting for individual batches

Model Fitting	RMSE				
	Moisture (%)	Density (*kg/m3*)	Exhaust (^{0}C)	IFBT (^{0}C)	OFBT (^{0}C)
CDC	0.45	28	3	8	5
REA	0.73	29	3	5	5
SIG	0.64	29	3	12	10

As can be seen, the CDRC provides the most accurate predictions for each output apart from for the inner fluid bed temperature. In this case the REA model is more accurate as the temperatures tend to be less sensitive to changes in the inlet conditions. However, without these temperature changes the moisture prediction is less accurate so the use of the model is dependent on the purpose. The sigmoidal model provides a better estimate with a formulation fitting, but when using the current batch fitting, the estimations for both the fluid bed temperatures were worse. This is a result of the gradient of the f curve at the lower moisture contents. If the fitting is inaccurate, the higher gradient means the estimated conditions will be further away from reality. The formulation fitting to the inner fluid bed estimations was more accurate using the sigmoidal model rather than the CDRC model. This means that the estimated gradient of the line is more accurate, so the change in temperature with varying moisture contents would be better represented. The formulation fitting also performed better for the sigmoidal model because the impact of the poor measurements is diluted, and their influence is reduced. The REA models matched the performance of the sigmoidal model but again are prone to oscillations in some instances.
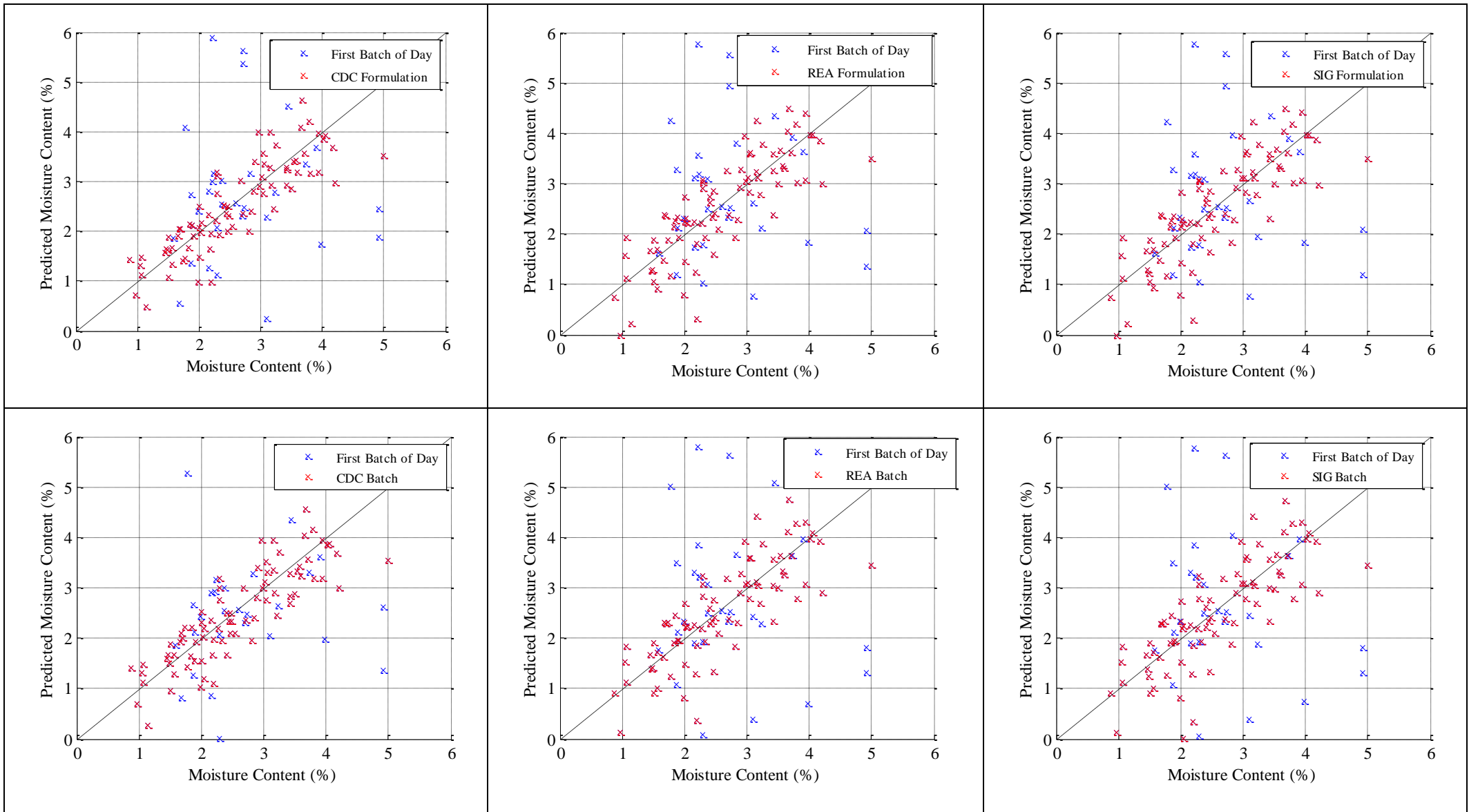
Figure 95: Predictions vs measurements for simulating batch with Formulation fittings and fittings based on every measurement made in the batch

218

It is noticeable that the moisture content exiting the chamber and fluid beds is very similar for all formulations. It is also apparent that the difference between using the current batch and the formulation fitting is quite small. Because of this, a fit was produced using all manual measurements made, assuming that there is little impact from changing formulation. Table 22 details the result which shows that the impact on the CDRC and REA models is minimal. The sigmoidal model's accuracy is poor using this fitting, as it clearly struggles to represent the drying conditions in the fluid beds.

Table 22: Performance of fitting for all measurements

Model Fitting	RMSE				
	Moisture (%)	Density ($kg/m3$)	Exhaust (^{0}C)	IFBT (^{0}C)	OFBT (^{0}C)
CDC	0.48	28	3	8	4
REA	0.72	29	3	5	5
SIG	1.31	31	3	15	9

The performance of these models for an entire batch is illustrated in Figure 96. In each case, the formulation fitting was used and the simulation starts from the first manual measurement of the batch. The graphs show the prediction of moisture content, density and the exhaust, inner fluid bed and the outer fluid bed temperature. The actual batch is represented by the individual measurement points or dashed lines for temperatures which were measured continuously. The trend for the CDRC and sigmoidal models are almost identical for moisture density and exhaust temperature. The main differences are related to the fluid bed temperature predictions. This is where the model fittings differ most, which leads to a difference in temperature prediction for the two models. This in turn leads to the slight difference seen in the exhaust temperature. Which estimate is closer to reality is difficult to say, as the measurement in the fluid beds can be impacted regularly by build up of powder on the temperature probes. For the REA approach,

in general the change in moisture content during a batch is much less than in the two other models. This is due to the influence of the fitting of the equilibrium moisture content. In this case, because the moisture content does not change significantly in the outer fluid bed, the model predicts that the temperature changes more, leading to the conclusion that this is the more inaccurate model.
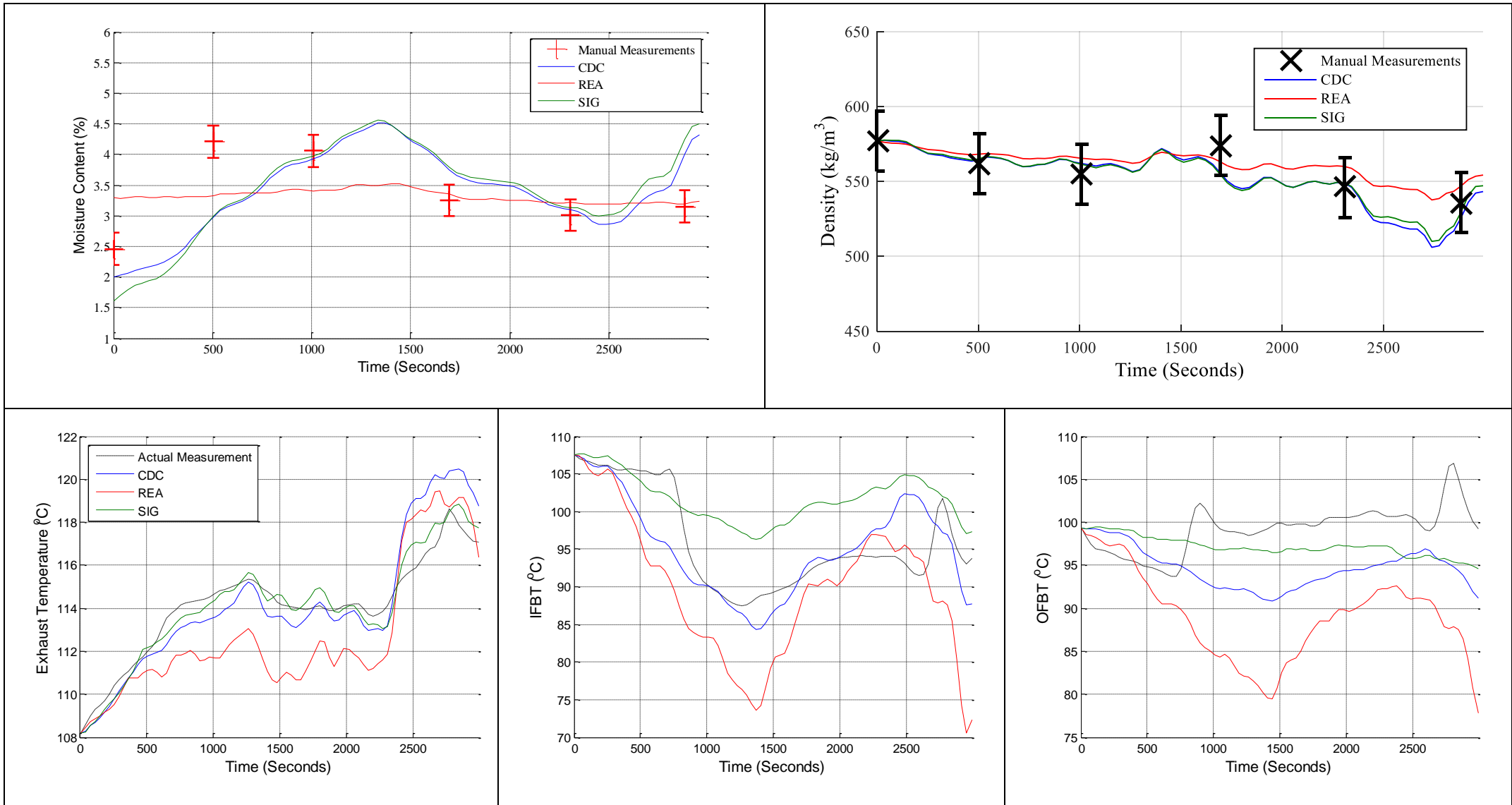
Figure 96: Simulation of a typical batch using the formulation fitting of the CDC, REA and Sigmoidal approach

4 Conclusions to drying model performance

The proposed models of the process demonstrate that they are capable of simulating the process, and provide an opportunity to use model based control techniques on the small scale dryer process. They also provide opportunities to carry out investigations into the process, in order to optimize the current operating procedures. Each model of the process can be used to identify how the process conditions should be changed to ensure that the target conditions are reached as soon as possible and are maintained, despite changes in the slurry inlet conditions or atomization.

In general, the CDRC model performs best for online use during a batch, and for simulation of the process. Using a general fitting to the manual measurements carried out for a formulation, leads to the best performance. The difference between formulations was found to have little impact on the drying curve. The amount of drying in each compartment varied for each formulation, this was due to the change in the initial moisture content. The REA approach is not well suited as an online model. If a measurement holds a value lower than the equilibrium moisture content fitted, then the model fails to converge. Failure is also caused by an inaccurate fitting to some estimates for the inner fluid bed moisture contents, which caused oscillations. The equilibrium moisture content fitted is constant, but in reality it changes with the external conditions, and this is the major flaw in the current model.

The Sigmoidal model provided the most accurate drying model fit to the data estimated from manual measurements and the compartmental heat balances. However, it failed to be a more accurate solution to the CDRC model. The models fluid bed estimations became more sensitive to temperature changes online expecting the moisture to change more as a result. This reduced its accuracy. When simulating it therefore predicted temperatures to change less for the same change in moisture content. This led to its loss in performance compared to the CDRC. The

fluid bed temperature probes were most sensitive to powder build up and could suggest temperature changes that do not occur uniformly over the fluid bed. The CDRC's less accurate fitting makes it less sensitive to this and could be the reason for why it outperforms the sigmoidal model.

The models produced provide opportunities for further development and understanding of the process. Modifications to the models would enable the simulation of individual particles through the process, rather than using a bulk value for their distribution. This would provide further distributions in residence time and moisture content which could be validated by making more measurements during a batch.

The simplifications used ensured that the computational time was kept to a minimum, as the model was for online implementation to represent trends during operation. The CDRC and Sigmoidal model successfully model the process and could be utilised as online tools to control the moisture and density of the powder in parallel to the automatic particle size control loop. The models could be used in a control loop or manually by providing set points for the air injection rate and temperatures of each air flow to the spray dryer.

An additional bonus is that the work has provided a standalone real time simulation tool. This is much more useful to a practical industrial engineer than a complex CFD model that takes days to converge. The work carried out has proven that these methods and simplifications can be used to model a spray dryer system. There has been no reason to suggest that this model isn't applicable at larger scales and that the learning made about the formulations could not be transferrable.

9. CONCLUSIONS

From the literature reviewed it was clear that in the current processing environment, advanced modelling was the way forward to achieve the goals set out in the objectives of this project. Fast response times were essential but it was important to have enough complexity to accurately represent the spray dryer process. To estimate the moisture content alone the best method was to use an empirical approach with an average error of 0.35% moisture content. However, this is dependent on a manual measurement that has to occur during steady state. It also gave the operator no advice on what to do in order to control the moisture.

An extensive study was made into the particle size distribution in the spray dryer. As a result an automatic control strategy for particle size was developed which halved the time to reach specification and maintained it at its target value. This control also provided benefits in density and moisture control as it reduced the variance for the entire spray dryer process by controlling the atomization. It also freed the operator of a time consuming role that required constant manipulation of the slurry to atomizing air flow ratio to alter the powder particle size.

A density model was produced that was clearly dependent on the moisture content and drying rate in the spray dryer. It estimated the impact of changes in the air injection rate on the density of the powder very accurately with a %RMSE of 4.77. This is more than sufficient to enable its use in a control strategy. However, if the target density is not feasible under the dryer current drying conditions it may need operator intervention to prevent the control loop from continually increasing the air injection rate.

 An important aspect of the project was to understand the process and to try and provide a scalable model. Although the simple empirical approach provided the best way to estimate moisture changes, it gave no insight into how the moisture content changes throughout the process. To gain this knowledge, the heat and mass balances were used further to compartmentalise the dryer and various methods were used to estimate the residence time of

particles in the dryer. Three drying models were applied to fit the data. This included the CDRC and REA approach and a novel sigmoidal approach produced for this project. It was found that the REA approach taken may struggle to converge without an additional model to vary the equilibrium moisture content. The sigmoidal approach provided a more accurate fitting to the same data used for the CDRC approach. This is because the model was derived to provide a more suitable drying profile for the data retrieved from the spray dryer.

The drying models produced incorporated the particle size and density changes in the process that were modelled in previous chapters. They were assessed as online and simulation tools for the spray dryer process. In general, the CDRC model performs best for online use during a batch, and for simulation of the process. It was also found that using a single fitting for all the measurements of a given formulation lead to the best performance of the model. The REA approach was not well suited as an online model. If a measurement holds a value lower than the equilibrium moisture content fitted, then the model failed to converge. Failure was also caused by an inaccurate fitting to some estimates for the inner fluid bed moisture contents, which caused oscillations in the predicted process outputs. The Sigmoidal model which provided the most accurate drying model failed to outperform the CDRC model. The area it struggled with was matching the fluid bed outlet conditions. By becoming more reliant on the process data it became more sensitive to its inaccuracies surrounding the fluid beds. This is the reason I believe it did not improve on the accuracy of the CDRC model.

The models produced provide opportunities for further development and understanding of the process. Modifications to the models would enable the simulation of individual particles through the process, rather than using a bulk value for their distribution. This would provide further distributions in residence time and moisture content which could be validated by making more measurements during a batch.

The simplifications used ensured that the computational time was kept to a minimum, as the model was for online implementation to represent trends during operation. The CDRC and Sigmoidal model successfully model the process and could be utilised as online tools to control the moisture and density of the powder in parallel to the automatic particle size control loop. The models could be used in a control loop or manually by providing set points for the air injection rate and temperatures of each air flow to the spray dryer.

An additional bonus is that the work has provided a standalone real time simulation tool. This is much more useful to a practical industrial engineer than a complex CFD model that takes days to converge. The work carried out has proven that these methods and simplifications can be used to model a spray dryer system. There has been no reason to suggest that this model isn't applicable at larger scales and that the learning made about the formulations could not be transferrable.

10. REFERENCES

Ali, M. et al., 2014. A one-dimensional plug-flow model of a counter-current spray drying tower. *Chemical Engineering Research and Design*, 92(5), pp.826–841. Available at: http://dx.doi.org/10.1016/j.cherd.2013.08.010.

Allen, R.M. & Bakker, H.H.C., 1994. Spray Dryer Control based on Online Particle Size Analysis. *Trans IChemE*, 72, Part A.Atkinson, D.S.F. & Strauss, W., 1978. Droplet Size and Surface Tension in Venturi Scrubbers. *Journal of the Air Pollution Control Association*, 28(11), pp.1114–1118.

Bakker, P. J., & Heertjes, P. M. (1959). Porosity distributions in a fluidized bed. *Chemical Engineering Science*, *12*, 260–271.

Balakrishnan, A.R. & Pei, D.C.T., 1979. Heat Transfer in Gas-Solid Packed Bed Systems. 1. A Critical Review. *Industrial & Engineering Chemistry Process Design and Development*, 18(1), pp.30–40. Available at: http://pubs.acs.org/doi/abs/10.1021/i260069a003.

Barker, J.J., 1965. Heat transfer in fluidized beds. , 57(5), pp.33–39.

Birchal, V.S. et al., 2006. Spray Dryers: Modeling and Simulation. *Drying Technology*, 24(3), pp.359–371. Available at: http://www.tandfonline.com/doi/abs/10.1080/07373930600564431 [Accessed April 9, 2012].

Bitron, M.D., 1955. Atomization of Liquids by Supersonic Air Jets. *Industrial & Engineering Chemistry*, 47(1), pp.23–28. Available at: http://pubs.acs.org/cgi-bin/doilookup/?10.1021/ie50541a019.

Burgschweiger, J. & Tsotsas, E., 2002. Experimental investigation and modelling of continuous fluidized bed drying under steady-state and dynamic conditions. *Chemical Engineering Science*, 57(24), pp.5021–5038.

Canals, A., Hernandis, V. & Browner, R.F., 1990. Experimental evaluation of the Nukiyama-Tanasawa equation for pneumatic nebulisers used in plasma atomic emission spectrometry. *Journal of Analytical Atomic Spectrometry*, 5(1), p.61.

Caulkin, R., Fairweather, M., Jia, X., & Williams, R. (2005). A numerical case study of packed columns. *Computer Aided Chemical Engineering*, *20*, 367–372.

Charlesworth, D.H., Marshall, W.R., 1960. Evaporation from droplets containing dissolved solids. *A.I.Ch.E. Journal, 6 (1)*, pp.9–23.

Chen, X.D., 2008. The Basics of a Reaction Engineering Approach to Modeling Air-Drying of Small Droplets or Thin-Layer Materials. *Drying Technology*, pp.627–639.

Chen, X.D. & Xie, G.Z., 1997. Fingerprints of the Drying Behaviour of Particulate or Thin Layer Food Materials Established using a Reaction Engineering Model. *Trans IChemE Part C*, 75, pp.213–222.

Cheong, H.W., Jeffreys, G. V. & Mumford, C.J., 1986. A receding interface model for the drying of slurry droplets. *AIChE Journal*, 32(8), pp.1334–1346. Available at: http://doi.wiley.com/10.1002/aic.690320811.

Chung, L.L. & Mujumdar, A.S., 2014. Fluidized Bed Dryers. In *Handbook of Industrial Drying*. New York: CRC Press, pp. 162–186.

Dlouhy, J. & Gauvin, W.H., 1960. Evaporation rates in spray drying. *The Canadian Journal of Chemical Engineering*, 38(4), pp.113–120. Available at: http://doi.wiley.com/10.1002/cjce.5450380405.

Ergun, S., & Orning, a. a. (1949). Fluid Flow through Randomly Packed Columns and Fluidized Beds. *Industrial & Engineering Chemistry*, *41*(6), 1179–1184. doi:10.1021/ie50474a011

Farid, M., 2003. A new approach to modelling of single droplet drying. *Chemical Engineering Science*, 58(13), pp.2985–2993. Available at: http://linkinghub.elsevier.com/retrieve/pii/S0009250903001611 [Accessed January 13, 2013].

Filkova, I., Huang, L. & Mujumdar, A.S., 2014. Industrial Spray Drying Systems. In A. . Mujumdar, ed. *Handbook of Industrial Drying*. New York: CRC Press, pp. 191–225.

Fogler, H.S., 2006. Distributions of Residence Times for Chemical Reactors. In *Elements of Chemical Reaction Engineering*. Pearson Education, Inc, pp. 867–941.

Francia, V., Martin de Juan, L. & Bayly, A., 2015. The Role of Wall Depositon and Re-Entrainment in Swirl Spray Dryers. *AIChE Journal*, 61(6), pp.1804–1821.

Fritsching, U., 2006. Spray Systems. In C. T. Crowe, ed. *Mulitphase Flow Handbook*. CRC Press, p. 50.

Fu, N., Woo, M. W., Selomulya, C., & Chen, X. D., 2013. Shrinkage behaviour of skim milk droplets during air drying. *Journal of Food Engineering*, 116(1), pp.37–44. Available at: http://linkinghub.elsevier.com/retrieve/pii/S0260877412005572 [Accessed March 3, 2015].

Gauvin, W.H., Katta, S. & Knelman, F.H., 1975. Drop trajectory predictions and their importance in the design of spray dryers. *International Journal of Multiphase Flow*, 1(6), pp.793–816. Available at: http://linkinghub.elsevier.com/retrieve/pii/0301932275900361.

GEA, N., 2013. Nozzle Atomizers. Available at: http://www.niro.com/NIRO/cmsdoc.nsf/WebDoc/webb8cshg5 [Accessed April 9, 2013].

Geldart, D. (1971). The Effect of Particle Size and Size Distribution on the Behaviour of Gas-Fluidised Beds. *Powder Technology*, *6*, 201–215.

Genskow, L., 2008. Psychrometry, evaporative cooling, and solids drying. *Control and ….* Available at: ftp://cpe-142-136-216-106.socal.res.rr.com/Elements/Documents/eBooks/Perry's Chemical Engineers' Handbook (8th Edition)/Section 12. Psychrometry, Evaporative Cooling, and Solids Drying.pdf [Accessed June 3, 2014].

Genskow, L.R. et al., 2007. Psychrometry, Evaporative Cooling, and Solids Drying. In *Perry's Chemical Engineers' Handbook*. McGraw Hill professional. McGraw-Hill Education. Available at: http://books.google.com/books?id=tH7IVcA-MX0C.

Gianfrancesco, A., Turchiuli, C. & Dumoulin, E., 2008. Powder agglomeration during the spray-drying process: measurements of air properties. *Dairy Science and Technology*, 88(1), pp.53–64.

Gosman, A.D., 1998. Developments in Industrial Computational Fluid Dynamics. *Trans IChemE Part A*, 76(February), pp.153–161.

Handscomb, C.S. & Kraft, M., 2010. Simulating the structural evolution of droplets following shell formation. *Chemical Engineering Science*, 65(2), pp.713–725. Available at: http://linkinghub.elsevier.com/retrieve/pii/S0009250909006198 [Accessed January 13, 2013].

Hecht, J.P., King, C.J.,2014. Personal Communication. P & G Technical Centres, UK

Huang, L., Kumar, K., & Mujumdar, a. (2006). A comparative study of a spray dryer with rotary disc atomizer and pressure nozzle using computational fluid dynamic simulations. *Chemical Engineering and Processing*, 45(6), 461–470. doi:10.1016/j.cep.2005.11.004

Huntington, D.H., 2004. The Influence of the Spray Drying Process on Product Properties. *Drying Technology*, 22(6), pp.1261–1287. Available at: http://www.tandfonline.com/doi/abs/10.1081/DRT-120038730 [Accessed September 18, 2014].

Keey, R.B., 1991. *Drying Of Loose And Particulate Materials*, New York: CRC Press.

Keshani, S. et al., 2015. CFD Modeling of Air Flow on Wall Deposition in Different Spray Dryer Geometries. *Drying Technology*, 33(7), pp.784–795. Available at: http://www.tandfonline.com/doi/full/10.1080/07373937.2014.966201.

Kiel, J.H. a., Prins, W. & van Swaaij, W.P.M., 1993. Mass transfer between gas and particles in a gas—solid trickle flow reactor. *Chemical Engineering Science*, 48(1), pp.117–125.

Kim, W.T. et al., 2003. A Predictive Model for the Initial Droplet Size and Velocity Distributions in Sprays and Comparison with Experiments. , 20.

Koç, B., Eren, I. & Kaymak Ertekin, F., 2008. Modelling bulk density, porosity and shrinkage of quince during drying: The effect of drying method. *Journal of Food Engineering*, 85(3), pp.340–349.

Kocamustafaogullari, G., Smits, S. & Razi, J., 1994. Maximum and mean droplet sizes in annular two-phase flow. *International Journal of Heat and Mass Transfer*, 37(6), pp.955–965. Available at: http://linkinghub.elsevier.com/retrieve/pii/0017931094902208.

Langrish, T.A.G., 2009. Multi-scale mathematical modelling of spray dryers. *Journal of Food Engineering*, 93(2), pp.218–228. Available at: http://linkinghub.elsevier.com/retrieve/pii/S0260877409000326 [Accessed March 7, 2011].

Langrish, T.A.G. & Kockel, T.K., 2006. The assessment of a characteristic drying curve for milk powder for use in computational fluid dynamics modelling. *Chemical Engineering*, 84(2001), pp.69–74.

Lefebvre, A., 1988. Drop Size Distributions of Sprays. In *Atomization and Sprays*. CRC Press, p. 87.

Lipp, C.W., 2000. Sprays. In *Kirk-Othmer Encyclopedia of Chemical Technology*. John Wiley & Sons, Inc. Available at: http://dx.doi.org/10.1002/0471238961.19161801130115.a01.pub2.

Lukasiewicz, S.J. (1989). Spray-drying ceramic powders. *Journal of the American Ceramic Society*, 72, pp. 617.

Masters, K., 1991. *Spray Drying Handbook* Fifth Edit., New York: Longman Scientific and Technocal, J. Wiley & Sons.

Meel, D. Van, 1958. Adiabatic convection batch drying with recirculation of air. *Chemical Engineering Science*, 9, pp.36–44. Available at: http://www.sciencedirect.com/science/article/pii/0009250958870050 [Accessed February 3, 2015].

Mezhericher, M., Levy, A. & Borde, I., 2008. Heat and mass transfer of single droplet / wet particle drying. , 63, pp.12–23.

Mezhericher, M., Levy, A., & Borde, I. (2009). Modeling of Droplet Drying in Spray Chambers Using 2D and 3D Computational Fluid Dynamics, 359–370. doi:10.1080/07373930802682940

Molerus, O. & Mattmann, W., 1992. Heat transfer mechanisms in gas fluidized beds. Part 3: Heat transfer in circulating fluidized beds. *Chemical Engineering & Technology*, 15(5), pp.291–294. Available at: http://doi.wiley.com/10.1002/ceat.270150502.

Mulhem, B. et al., 2004. IFPRI Project – Annual Report 2004 Control of Droplet Characteristics in Liquid Atomization with Suspended Particles 2 . Background and Project Overview. *Chemical Engineering Science*, pp.1–27.

Nukiyama, S. & Tanasawa, Y., 1939. An experiment on the atomization of liquid. *Trans. Soc. Mech. Engrs (Japan)*, 14, p.Summary Section.

Oakley, D.E., 2004. Spray Dryer Modeling in Theory and Practice. *Drying Technology*, 22(6), pp.1371–1402. Available at: http://www.tandfonline.com/doi/abs/10.1081/DRT-120038734 [Accessed April 26, 2012].

Oakley, D. E., Scroll, P., & For, D. (2007). Scale-up of Spray Dryers with the aid of Computational Fluid Dynamics; (January 2013), 37–41.

Ohnesorge, W., 1936. Application of a cinematographic high frequency apparatus with mechancial control of exposure for photographing the formation of drops and the break up of jets. *Z angew. Math. Mech*, 16, p.320.

Pakowski, Z. & Mujumdar, A.S., 2014. Basic Process Calculations and Simulations in Drying. In A. S. Mujumdar, ed. *Handbook of Industrial Drying*. New York: CRC Press, pp. 51–75.

Papadakis, S.E. et al., 1993. Correlations for the Equilibrium Moisture Content of Solids. *Drying Technology*, 11(3), pp.543–553. Available at: http://www.tandfonline.com/doi/abs/10.1080/07373939308916843 [Accessed October 3, 2014].

Pell, M. (2008). Fluidized-Bed Systems. In R. H. Perry & D. W. Green (Eds.), *Perry's Chemical Engineers' Handbook* (8th ed., pp. 2–17). New York: McGraw Hill.

Ranz, W.E. & Marshall, W.R., (1952). Evaporation from drops. *Chemical Engineering Progress*, *48*, 141–146.

Richardson, J.F. & Peacock, D.G., 1994. Flow Characteristics of Reactors- Flow Modelling. In *Coulson & Richardson's Chemical Engineering Volume 3 - Chemical and Biochemical Reactors and Process Control*. Elsevier, pp. 71–108.

Richardson J.F., H. J. H. B. J. R. (2002). Fluidisation. In *Coulson and Richardson's Chemical Engineering Volume 2 - Particle Technology and Separation Processes (5th Edition)* (pp. 292–319). Elsevier.

 Polynomial curve fits to Table 2.1. *R. R. Rogers; M. K. Yau (1989). A Short Course in Cloud Physics (3rd ed.). Pergamon Press. p. 16. ISBN 0-7506-3215-1.*

Sazhin, S., 2009. Modeling of sprays using computational fluid dynamics codes. *Pollack Periodica*, 4(1), pp.5–16.

Scherer, G.W., 1990. Theory of drying. *Journal of the American Ceramic Society,*73, pp.3–14.

Semião, V., 1996. Spray characterization: Numerical prediction of Sauter mean diameter and droplet size distribution. *Fuel*, 75(15), pp.1707–1714. Available at: http://linkinghub.elsevier.com/retrieve/pii/S0016236196001639.

Setty, Y.P. & Murthy, J.V.R., 2003. Development of a model for drying of solids in a continuous fluidized bed dryer. *Indian Journal of Chemical Technology*, 10(1), pp.477–482.

Seydel, P., Blömer, J. & Bertling, J., 2006. Modeling Particle Formation at Spray Drying Using Population Balances. *Drying Technology*, 24(2), pp.137–146. Available at: http://www.tandfonline.com/doi/abs/10.1080/07373930600558912.

Shafaee, M. et al., 2012. An investigation on effect of geometrical parameters on spray cone angle and droplet size distribution of a two-fluid atomizer. *Journal of Mechanical Science and Technology*, 25(12), pp.3047–3052. Available at: http://link.springer.com/10.1007/s12206-011-0901-2 [Accessed March 18, 2015].

Strutt, J.W. & Rayleigh, Lord, 1878. On the instability of jets. *Proceedings of the London mathematical society*, 10, pp.4–13.

The Engineering ToolBox. *Air Properties,* retrieved from

http://www.engineeringtoolbox.com/air-properties-d_156.html [Accessed March 12, 2009]

The Engineering ToolBox. *Water Properties,* retrieved from

http://www.engineeringtoolbox.com/water-properties-d_1508.html [Accessed March 12,

2009]

The Engineering ToolBox. *Water Vapor- Specific Heat ,* retrieved from

http://www.engineeringtoolbox.com/water-vapor-d_979.html [Accessed March 12, 2009]

Towler, G., & Sinnott, R. K. (2013). Specification and Design of Solids-Handling

Equipment. In *Chemical Engineering Design - Principles, Practice and Economics of Plant*

and Process Design (2nd Edition) (pp. 940–946). Elsevier.

Thybo, P. et al., 2008. Droplet size measurements for spray dryer scale-up. *Pharmaceutical
development and technology*, 13(2), pp.93–104. Available at:
http://www.ncbi.nlm.nih.gov/pubmed/18379901 [Accessed January 12, 2015].

Wai, M. et al., 2008. Comparative study of droplet drying models for CFD modelling.
Chemical Engineering Research and Design, 6(October 2007), pp.1038–1048.

Walton, D.E., 2004. The Evaporation of Water Droplets. A Single Droplet Drying
Experiment. *Drying Technology*, 22(3), pp.431–456.

Weber, C., 1931. Disintegration of Liquid Jets. *Z. Agnew Math. Mech.*, 11, pp.136–159.

Wen, C. Y., & Yu, Y. H. (1966). A generalized method for predicting the minimum
fluidization velocity. *AIChE Journal*, *12*(3), 610–612. doi:10.1002/aic.690120343

Wen-Ching Yang. (2003). *Handbook of Fluidization and Fluid-Particle Systems*. New York:
CRC Press.

Woo, M.W. et al., 2008. CFD Evaluation of Droplet Drying Models in a Spray Dryer Fitted
with a Rotary Atomizer. *Drying Technology*, 26(10), pp.1180–1198. Available at:
http://www.informaworld.com/openurl?genre=article&doi=10.1080/07373930802306953&m
agic=crossref||D404A21C5BB053405B1A640AFFD44AE3 [Accessed September 30, 2013].

Zbicinski, I., Piatkowski, M. & Fngineering, E., 2005. Determination of Spray-Drying
Kinetics in a Small Scale. , pp.1751–1760.